AD_____

Award Number: DAMD17-99-1-9465

TITLE: Combinatorial Approach for Novel Phosphatase Inhibitors

PRINCIPAL INVESTIGATOR: John S. Lazo

CONTRACTING ORGANIZATION: University of Pittsburgh
                           Pittsburgh, Pennsylvania   15260

REPORT DATE: March 2000

TYPE OF REPORT: Annual Summary

PREPARED FOR: U.S. Army Medical Research and Materiel Command
               Fort Detrick, Maryland 21702-5012

DISTRIBUTION STATEMENT: Approved for Public Release;
                        Distribution Unlimited

DTIC QUALITY INSPECTED 3

20010110 064

REPORT DOCUMENTATION PAGE

Public reporting burden for this collection of information is estimated to average 1 hour per response, including the time for reviewing instructions, searching existing data sources, gathering and maintaining the data needed, and completing and reviewing this collection of information. Send comments regarding this burden estimate or any other aspect of this collection of information, including suggestions for reducing this burden to Washington Headquarters Services, Directorate for Information Operations and Reports, 1215 Jefferson Davis Highway, Suite 1204, Arlington, VA 22202-4302, and to the Office of Management and Budget, Paperwork Reduction Project (0704-0188), Washington, DC 20503

1. AGENCY USE ONLY (Leave blank)	2. REPORT DATE March 2000	3. REPORT TYPE AND DATES COVERED Annual Summary Report (1 Mar 99 – 28 Feb 00)

4. TITLE AND SUBTITLE

Combinatorial Approach for Novel Phosphatase Inhibitors

5. FUNDING NUMBERS

DAMD17-99-1-9465

6. AUTHOR(S)
John Stephen Lazo

7. PERFORMING ORGANIZATION NAME(S) AND ADDRESS(ES)

University of Pittsburgh
Pittsburgh, Pennsylvania   15260

E-Mail: lazo+@pitt.edu

8. PERFORMING ORGANIZATION REPORT NUMBER

9. SPONSORING / MONITORING AGENCY NAME(S) AND ADDRESS(ES)

U.S. Army Medical Research and Materiel Command
Fort Detrick, Maryland 21702-5012

10. SPONSORING / MONITORING AGENCY REPORT NUMBER

11. SUPPLEMENTARY NOTES

12a. DISTRIBUTION / AVAILABILITY STATEMENT
Approved for Public Release; Distribution Unlimited

12b. DISTRIBUTION CODE

13. ABSTRACT (Maximum 200 Words)

We have synthesized more than 500 new small molecules in the Combinatorial Chemistry Center (CCC) using novel parallel approaches. We have examined the biochemical activity of these compounds as well as the Diverset, which are 2,000 compounds selected by the NCI from their 130,000+ compound library and that contain maximal chemical diversity. The 500 novel small molecules synthesized by the CCC were designed around the AC/SC pharmacophore and are based on Natural Products. Within this library, we have identified FY21-$\alpha\alpha$09 as the most potent inhibitor of the oncogene Cdc25. We also found that FY21-$\alpha\alpha$09 was an inhibitor of human malignant cell cycle transition in both G1 and G2/M phase consistent with its proposed ability to inhibit both Cdc25A, B and C. We also found that SC-$\alpha\alpha\delta$9 blocked G1 and G2/M transition and caused hyperphosphorylation of cyclin-dependent kinase 1 and 4. We have used a similar approach to identify a vitamin K analog, compound 5, which is also an inhibitor of Cdc25. We have identified 5 inhibitors of Cdc25 in the NCI Diverset each having a median inhibitory concentration below 1 μM. They may have the potential of being new platforms for future compounds.

14. SUBJECT TERMS	15. NUMBER OF PAGES 74
Protein Phosphatase; Cdc25; Natural Products; Cell cycle;combinatorial chemistry	16. PRICE CODE

17. SECURITY CLASSIFICATION OF REPORT Unclassified	18. SECURITY CLASSIFICATION OF THIS PAGE Unclassified	19. SECURITY CLASSIFICATION OF ABSTRACT Unclassified	20. LIMITATION OF ABSTRACT Unlimited

NSN 7540-01-280-5500

FOREWORD

Opinions, interpretations, conclusions and recommendations are those of the author and are not necessarily endorsed by the U.S. Army.

_____ Where copyrighted material is quoted, permission has been obtained to use such material.

_____ Where material from documents designated for limited distribution is quoted, permission has been obtained to use the material.

_____ Citations of commercial organizations and trade names in this report do not constitute an official Department of Army endorsement or approval of the products or services of these organizations.
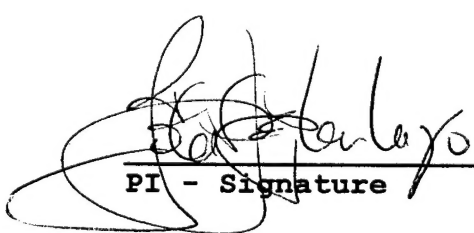
_____ In conducting research using animals, the investigator(s) adhered to the "Guide for the Care and Use of Laboratory Animals," prepared by the Committee on Care and use of Laboratory Animals of the Institute of Laboratory Resources, national Research Council (NIH Publication No. 86-23, Revised 1985).

N/A For the protection of human subjects, the investigator(s) adhered to policies of applicable Federal Law 45 CFR 46.

_____ In conducting research utilizing recombinant DNA technology, the investigator(s) adhered to current guidelines promulgated by the National Institutes of Health.

_____ In the conduct of research utilizing recombinant DNA, the investigator(s) adhered to the NIH Guidelines for Research Involving Recombinant DNA Molecules.

_____ In the conduct of research involving hazardous organisms, the investigator(s) adhered to the CDC-NIH Guide for Biosafety in Microbiological and Biomedical Laboratories.

PI - Signature   6/26/00
                                                    Date

TABLE OF CONTENTS

SUMMARY REPORT

Introduction

Prostate cancer continues to be a major lethal disease in American men and current treatment modalities produce only modest improvement in survival. New treatments must incorporate contemporary information about the molecular biology of prostate cancer. This grant adopts a multidisciplinary approach incorporating the most contemporary methodologies in bioorganic chemistry and integrating them with recent discoveries concerning the molecular biology and biochemistry of prostate cancer. We had proposed to create a library of compounds and to test these new compounds for their usefulness in the treatment of human prostate cancer. The targets for our study were the dual specificity phosphatases (DSPases) Cdc25A, B and C. Because Cdc25A and B are key oncogenes in many human prostate cancers, we believe inhibition of their threonine/tyrosine phosphatase activity will produce an agent that is useful for the treatment of prostate cancer. A secondary working hypothesis was that selective inhibitors of Cdc25A, B and C can be developed using a combinatorial chemistry approach with the basic pharmacophore of a threonine phosphatase inhibitor. Our technical objectives for the three year grant were to: (1) synthesize 3,000 novel compounds based on the calyculin A pharmacophore, (2) investigate the ability of the new synthesized compounds to inhibit Cdc25A, B, and C DSPases, (3) determine the specificity of phosphatase inhibition by examining the ability of the compounds to inhibit other phosphatases, (4) test the new synthesized compounds to inhibit the growth or cause apoptosis in human prostate PC-3 cells and primary prostate cancer cells and (5) to examine the specificity of the agents using mouse embryonic cells (MEC) transfected with H-RAS^{G12V} and Cdc25A or Cdc25B and in mouse embroyonic cells that are null for one or more of the Cdc25.

Body

Although the grant was only funded for one year, we have accomplished many of our original goals. Based on the structure activity studies of naturally occurring phosphatase inhibitors and following up on previously published research, we designed a new pharmacophore and synthesized new libraries. We also capitalized on a previous report suggesting that the vitamin K pharmacophore might be useful in the design of new Cdc25 inhibitors. We adopted an inexpensive, nonradioactive, and simple method to evaluate the activity of our combinatorial compounds. These recombinant methods with glutathione S-transferase fusion proteins allow for an almost unlimited source of easily purified enzymes. We used fluorescein monophosphate as the substrate and measured the fluorescein product (Ex. 485 nm; Em. 530 nm) with a Biosystems Cytofluor II. We also tested these compounds for antiproliferative activity against several malignant cell lines including a temperature sensitive mouse line useful for examining cell cycle control and human prostate cells.

We found two compounds of interest in our initial *in vitro* screen: FY3-αα09 and FY21-αα09. These compounds were partial competitive inhibitors against Cdc25 with K_i values of 7.6 ± 0.5 and 1.6 ± 0.2 µM, respectively. The rigidified *trans*-cyclohexyldiamine structure contained in FY21-αα09 possessed only moderate activity against PTP1B.

5

Consistent with its *in vitro* anti-phosphatase activity, FY21-$\alpha\alpha$09 inhibited growth of several human cells including PC-3 cells with an $IC_{50} < 15 \mu M$. FY21-$\alpha\alpha$09 also inhibited the G2/M transition in tsFT210 mouse cells, consistent with Cdc25B and C inhibition and G1 transition consistent with inhibition of Cdc25A. We found hyperphosphorylation of Cdk1, Cdk2 and Cdk4 after synchronized cells were treated for with FY21-$\alpha\alpha$09. The structure of FY21-$\alpha\alpha$09 provides a useful platform from which additional potent and more highly selective phosphatase inhibitors might be generated.

We have examined a small focused library of synthetic vitamin K analogs and identified one, 2-(2-mercaptoethanol)-3-methyl-1,4-napthoquinone or Compound 5, which arrested cell cycle progression at both G1 and G2/M. We demonstrated that Compound 5 was a potent, selective, and partially competitive inhibitor of Cdc25 phosphatases. Furthermore, Compound 5 caused time-dependent, irreversible enzyme inhibition, consistent with arylation of the catalytic cysteine in Cdc25. Treatment of tsFT210 cells with Compound 5 blocked dephosphorylation of the Cdc25C substrate, Cdk1, and its kinase activity. Compound 5 enhanced tyrosine phosphorylation of two potent regulators of G1 transition, namely Cdk2 and Cdk4, and decreased the phosphorylation of Rb, an endogenous substrate for Cdk4 kinase. Furthermore, close chemical analogs that lacked *in vitro* Cdc25 inhibitory activity failed to block cell cycle progression and Cdk1 kinase activity. Compound 5 did not alter the levels of p53 or the endogenous cyclin dependent kinase inhibitors, p21 and p16. Our results support the hypothesis that the disruption in cell cycle transition caused by Compound 5 was due to intracellular Cdc25 inhibition. This novel thioalkyl K vitamin analog could be useful for cell cycle control studies and may provide a valuable pharmacophore for the design of future therapeutics.

We have also begun to examine the NCI's compound library for new potential pharmacophores. We have evaluated their Diverset, which contains 2,000 compounds selected for maximal diversity. We screened these compounds for anti-phosphatase activity and identified at least 5 compounds with median inhibitors activities below 1 μM for Cdc25. Selectivity studies against other protein phosphatases are proceeding. These compounds could form the basis for future analog design and development.

APPENDIX

Key accomplishments

- Synthesize 500 new compounds in three distinct libraries.
- Identified two compounds, namely FY21-αα09 and Compound 5, that are potent inhibitors of Cdc25A,B and C. These are the most potent inhibitors of Cdc25 reported to date.
- FY21-αα09 and Compound 5 caused G1 and G2/M phase arrest consistent with their ability to inhibit Cdc25.
- FY21-αα09 and Compound 5 blocked the cell proliferation of human prostate cells.
- One of our lead compounds, SC-ααδ9, induced insulin-like growth factor-1-resistant apoptosis
- SC-ααδ9 also had modest antitumor activity in one in vivo model.
- We identified FY21-αα09 as a partial competitive inhibitor of Cdc25. This is a new pharmacophore for use in the design of additional libraries.
- FY21-αα09 caused hyperphosphorylation of Cdk1, Cdk2 and Cdk4.

Reportable Outcomes

Manuscripts

1. Tamura, K., Southwick, E.C., Kerns, J., Rosi, K., Carr, B., Wilcox, C. and Lazo, J.S. Cdc25 inhibition and cell cycle arrest by a synthetic thioalkyl vitamin K analogue. Cancer Res. 5:1317-1325, 2000.

2. Vogt, A., Wang, A.S., Johnson, C.S, Fabisiak, J.P., Wipf, P. and Lazo, J.S. In vivo antitumor activity and induction of insulin-like growth facor-1-resistant apoptosis by SC-ααδ9. J. Pharmacol. Exp. Therap. 292:530-537, 2000.

3. Lazo, J.S. and Wipf. P. Combinatorial chemistry and contemporary pharmacology. J. Pharmacol. Exp. Therap. 293:705-708, 2000.

4. Ducruet, A.P., Rice, R.L., Tamura, K., Yokokawa, F., Yokokawa, S., Wipf, P. and Lazo, J.S. Identification of new Cdc25 dual specificity phosphatase inhibitors in a targeted small molecule array. Bioorg. Med. Chem. In Press.

5. Wipf, P., Jung, J.-K., Rodriguez, S. and Lazo, J.S. Synthesis and biological evaluation of deoxypreussomerin A and palmarumycin CP1 and related naphthoquinone spiroketals. Tetrahedron. In Press.

Abstracts

1. Tamura, K., Rice, R.L., Wipf, P. and Lazo, J.S. Dual G1 and G2/M phase inhibition by SC-ααδ9, a Cdc25 phosphatase inhibitor identified in a novel combinatorial library. Proc. Amer. Assoc. Cancer Res. 40:4782, 1999.

2. Pestell, K., Southwick, E.C., Wilcox, C. and Lazo, J.S. Vitamin K analogs inhibit Cdc25B and disrupt Cdc25B2 subcellular distribution. Proc. Amer. Assoc. Cancer Res. 41:371, 2000.

3. Ducruet, A.P., Rice, R.L., Tamura, K., Yokokawa, F., Yokokawa, S., Wipf, P. and Lazo, J.S. Identification of Cdc25 dual specificity phosphatase inhibitors in a targeted small molecule array. Proc. Amer. Assoc. Cancer Res. 41:2998, 2000.

Cdc25 Inhibition and Cell Cycle Arrest by a Synthetic Thioalkyl Vitamin K Analogue[1]

Kenji Tamura, Eileen C. Southwick, Jeffrey Kerns, Katherine Rosi, Brian I. Carr, Craig Wilcox, and John S. Lazo[2]

Departments of Pharmacology [K. T., E. C. S., J. S. L.], Chemistry [J. K., K. R., C. W.], and Surgery [B. C.], University of Pittsburgh, Pittsburgh, Pennsylvania 15261, and Second Department of Internal Medicine [K. T.], Hiroshima University School of Medicine, Hiroshima 734, Japan

ABSTRACT

A synthetic vitamin K analogue, 2-(2-mercaptoethanol)-3-methyl-1,4-naphthoquinone or compound 5 (Cpd 5), was found previously to be a potent inhibitor of tumor cell growth. We now demonstrate that Cpd 5 arrested cell cycle progression at both G_1 and G_2-M. Because of the potential arylating activity of Cpd 5, it might inhibit Cdc25 phosphatases, which contain a cysteine in the catalytic site. To test this hypothesis, we examined the inhibitory activity of Cpd 5 against several cell cycle-relevant protein tyrosine phosphatases and found that Cpd 5 was a potent, selective, and partially competitive inhibitor of Cdc25 phosphatases. Furthermore, Cpd 5 caused time-dependent, irreversible enzyme inhibition, consistent with arylation of the catalytic cysteine in Cdc25. Treatment of cells with Cpd 5 blocked dephosphorylation of the Cdc25C substrate, Cdc2, and its kinase activity. Cpd 5 enhanced tyrosine phosphorylation of both potent regulators of G_1 transition, *i.e.*, Cdk2 and Cdk4, and decreased the phosphorylation of Rb, an endogenous substrate for Cdk4 kinase. Furthermore, close chemical analogues that lacked *in vitro* Cdc25 inhibitory activity failed to block cell cycle progression and Cdc2 kinase activity. Cpd 5 did not alter the levels of p53 or the endogenous cyclin-dependent kinase inhibitors, p21 and p16. Our results support the hypothesis that the disruption in cell cycle transition caused by Cpd 5 was attributable to intracellular Cdc25 inhibition. This novel thioalkyl K vitamin analogue could be useful for cell cycle control studies and may provide a valuable pharmacophore for the design of future therapeutics.

INTRODUCTION

The vitamin K family of molecules comprises the natural forms vitamin K_1 (phylloquinone) and vitamin K_2 (menaquinones) and the synthetic form vitamin K_3 (menadione). These naphthoquinone-containing molecules inhibit tumor cell growth in culture, with vitamin K_3 being more potent than either vitamin K_1 or K_2 (1). Vitamin K_3 exhibits low toxicity to animals (2, 3) and can enhance the antiproliferative effects of other clinically used anticancer agents (4), although it is toxic to humans (5). The growth-inhibitory actions of vitamin K_3 have been ascribed to both sulfhydryl arylation and oxidative stress because of redox cycling (6, 7). We previously synthesized and characterized a thioalkyl K vitamin analogue, Cpd 5[3] (Fig. 1), with superior growth-inhibitory activity that also rapidly enhances cellular protein tyrosine phosphorylation and causes apoptosis (8). The antiproliferative and antiphosphatase activity of Cpd 5 is antagonized by exogenous thiols but not by nonthiol antioxidants,

suggesting that unlike vitamin K_3, its inhibition is mediated by sulfhydryl arylation rather than oxidative stress (8). One proposed site for interaction is the catalytic cysteine(s) found in protein tyrosine phosphatases that regulate cell proliferation (2).

Protein tyrosine phosphatases that have an essential role in cell cycle progression include the Cdc25 phosphatases, which activate Cdks. In mammalian cells, Cdc25 phosphatases are encoded by a multigene family consisting of Cdc25A, Cdc25B, and Cdc25C (9–11). Each Cdc25 homologue controls distinct aspects of cell cycle progression. Cdc25C dephosphorylates and activates the mitotic kinase Cdc2/cyclin B, which is required for entry into mitosis (12). Cdc25A is important for entry into S-phase (13), whereas Cdc25B is essential for preinitiating G_2-M transition and S-phase progression (14). Cdc25A and Cdc25B have oncogenic properties in cells that have mutated Ha-*ras* or loss of *Rb1*, the Rb susceptibility gene (15). Cdc25A and Cdc25B are transcriptional targets of the c-*myc* oncogene (16) and are overexpressed in several tumor types and may reflect poor prognosis (15, 17–19). Unfortunately, potent and selective inhibitors of Cdc25 phosphatases are currently unavailable but would be attractive candidates as potential anticancer agents.

In human hepatoma cells, vitamin K_3 induces hyperphosphorylation of $p34^{cdc2}$ (Cdc2) kinase and decreases the protein tyrosine phosphatase activity in cell lysates (20). Vitamin K_3 and other naphthoquinone analogues inhibit Cdc25A *in vitro*, and one of these analogues has been shown to cause G_1 arrest (21). The mechanism by which the potent redox-deficient thioalkyl K vitamin analogue Cpd 5 inhibits cell growth is not known, although inhibition of Cdc25 has been hypothesized (2). Thus, we have examined the actions of Cpd 5 and two other vitamin K analogues on protein tyrosine phosphatases, including Cdc25A, Cdc25B, and Cdc25C, as well as their antiproliferative and cell cycle checkpoint activity.

MATERIALS AND METHODS

Materials and Antibodies. tsFT210 cells were a generous gift from Dr. Chris Norbury (Oxford University, Oxford, United Kingdom) and were maintained for no longer than 30 passages as described elsewhere (22). The anti-Cdc2 (SC 54), anti-Cdk2 (SC 163G), anti-Cdk4 (SC 601G), anti-cyclin D1 (SC 6281), anti-cyclin E (SC 481), anti-p53 (SC 1312), anti-p21 (SC 3976), and anti-p16 (SC 1207) antibodies were purchased from Santa Cruz Biotechnology (Santa Cruz, CA). Agarose conjugate of each antibody was used for immunoprecipitation. Anti-cyclin A antibody was purchased from Oncogene Research Product (Cambridge, MA). Anti-phosphotyrosine antibody was purchased from Upstate Biotechnology (Lake Placid, NY). Phospho-Rb antibody and Rb antibody were purchased from New England Biolabs, Inc. (Beverly, MA), and anti-GAPDH antibody was purchased from Chemicon International, Inc. (Temecula, CA). Histone H1 was obtained from Boehringer Mannheim Co. (Indianapolis, IN). $[\gamma\text{-}^{32}\text{P}]\text{ATP}$ (10 mCi/ml) was from Amersham Life Science, Inc. (Arlington Heights, IL).

Chemical Syntheses. To synthesize Cpd 5, we added 1,8-diazabicyclo[5.4.0]un-dec-7-ene (0.07 ml, 0.7 mmol) dropwise to a solution of menadione (5.154 g, 29.9 mmol) and 2-mercaptoethanol (2.10 ml, 29.9 mmol) in 150 ml ether at room temperature. Stirring was maintained at room temperature for 23 h, and then 20 ml of 3.6 M HCl were added. The organic and aqueous phases were separated, and the aqueous layer was extracted with ether. The combined organic layers were dried over magnesium sulfate,
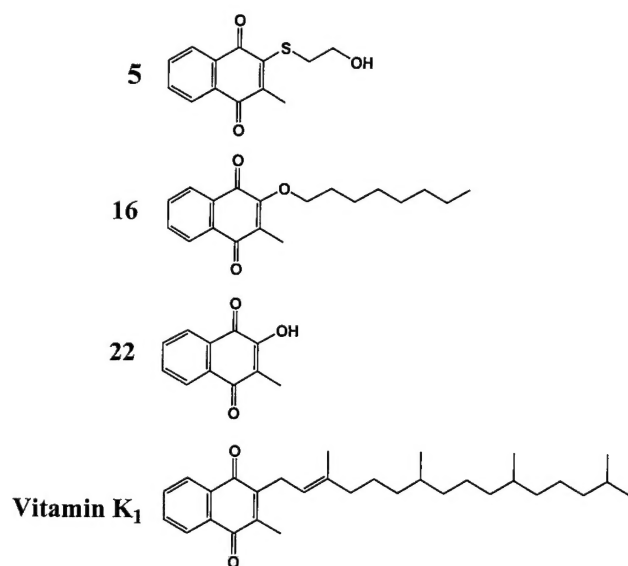
5

16

22

Vitamin K₁

Fig. 1. Chemical structures of vitamin K₁ and several analogues.

filtered, and concentrated to give 8.223 g of a dark brown viscous liquid. Purification by flash chromatography using 30% ethyl acetate/hexanes to elute the first two bands, followed by 50% ethyl acetate/hexanes, gave 2.698 g (36%) of an orange solid: melting point 78–80°C. ^{1}H NMR (CDCl₃) δ 8.08–8.03 (m, 2H), 7.71–7.68 (m, 2H), 3.80 (t, J = 5.7, 2H), 3.34 (t, J = 5.8, 2H), 2.50 (s, 1H), 2.38 (s, 3H); ^{13}C NMR (CDCl₃) 182.10, 181.42, 147.85, 145.87, 133.74, 133.41, 132.61, 131.86, 128.78, 126.55, 62.02, 37.11, 15.40; IR (KBr) cm^{-1} 3292 (m), 1657 (s), 1585 (s), 1554 (s); UV (ethanol) λmax (log ε) 204 (4.21), 260 (4.22), 408 (3.33); MS (m/z): 248 (2), 230 (63), 221 (100), 197 (73); high resolution MS: calculated for C₁₃H₁₀O₂S: 230.0412, found: 230.0405.

To synthesize Cpd 22, we used Fieser's method. A solution of sodium

carbonate (2.40 g, 22.6 mmol) and 30% hydrogen peroxide (10 ml, 97.9 mmol) in water (50 ml) was added together to a solution of menadione (10.168 g, 59.1 mmol) in warm ethanol (110–135 ml). The yellow quinone color disappeared, and the flask was then cooled in ice. Water was added (300 ml) to give 16.334 g of a white solid; melting point 87°C. 1.076 g of this solid was dissolved in concentrated sulfuric acid (6 ml), giving a deep red solution. The flask was swirled intermittently for 10 min, and then water (20 ml) was added slowly to give a yellow precipitate. The mixture was filtered, and the filtercake was washed with water until the filtrate was no longer acidic. This procedure afforded 0.724 g (67%) of Cpd 22; melting point 170–171°C. ^{1}H NMR (CDCl₃) δ 8.15–8.07 (m, 2H), 7.79–7.66 (m, 2H), 7.3 (s, 1H), 2.12 (s, [³H]); ^{13}C NMR (CDCl₃) 185.08, 181.23, 153.21, 134.89, 132.96, 129.47, 126.78, 126.18, 120.60, 8.74; IR (KBr) cm^{-1} 3312 (brs), 1643 (s), 1579 (m); UV (ethanol) λmax (log ε) 206 (4.54), 242 (4.48), 252 (4.47), 276 (4.65); MS (m/z): 188 (100), 160 (30), 132 (42), 105 (33), 77 (35); high resolution MS: calculated for C₁₁H₈O₃: 188.0473442, found: 188.049347.

To synthesize Cpd 16, we added a solution of Cpd 22 (0.713 g, 3.793 mmol) in dry THF (4 ml) via cannula to a suspension of potassium hydride (0.229 g, 5.711 mmol) in dry THF (10 ml) at 0°C. The resulting dark brown mixture was stirred for 5–10 min when a solution of 18-Crown-6 (1.542 g, 5.841 mmol) in dry THF (4 ml) was added. In some reactions, we used supplemental THF to aid in the stirring of the solution. The resulting burgundy mixture was stirred for 20 min, and then 1-iodooctane (0.68 ml, 3.768 mmol) was added. The mixture was refluxed for 21 h and then stirred at room temperature for 24 h. The reaction was quenched with saturated ammonium chloride and extracted with ether. The organic and aqueous phases were separated, and the aqueous layer was extracted with ether. The combined organics were dried over magnesium sulfate, filtered, and concentrated to give 1.704 g of a dark brown liquid. Purification by flash chromatography using 5% ethyl acetate/hexanes gave 1.11 g (98%) of a yellow solid: melting point, 38°C. ^{1}H NMR (CDCl₃) δ 7.85–7.80 (m, 2H), 7.53–7.46 (m, 2H), 4.22 (t, J = 6.6, 2H), 1.94 (s, 3H), 1.68–1.59 (m, 2H), 1.35–1.16 (m, 10H), 0.77 (t, J = 6, 3H). ^{13}C NMR (CDCl₃) 185.26, 180.90, 157.20, 133.33, 132.84, 131.70, 131.40, 131.22, 125.81, 73.51, 31.67, 30.42, 29.18, 29.12, 25.69, 22.52, 13.97, 9.15; IR (KBr) cm^{-1} 1668 (s), 1620 (s) 1593 (s); UV (ethanol) λmax (log ε) 208 (4.20), 248 (4.29), 276

Fig. 2. Inhibition of tsFT210 cell cycle progression at G₂-M by Cpd 5 tsFT210 cells cultured at the permissive temperature of 32.0°C (A) and then incubated for 17 h at the nonpermissive temperature of 39.4°C (B). Cells were released from cycle arrest by shifting to the 32.0°C medium. The cells were then incubated for 6 h in the presence of DMSO vehicle (C), 1 μM nocodazole (D), 10 μM Cpd 5 (E), 20 μM Cpd 5 (F), 20 μM Cpd 16 (G), 20 μM Cpd 22 (H), or 100 μM SC-αα∂9 (I). Vertical bars, fluorescence corresponding to 2C and 4C DNA content. Results are representative of at least three independent experiments.
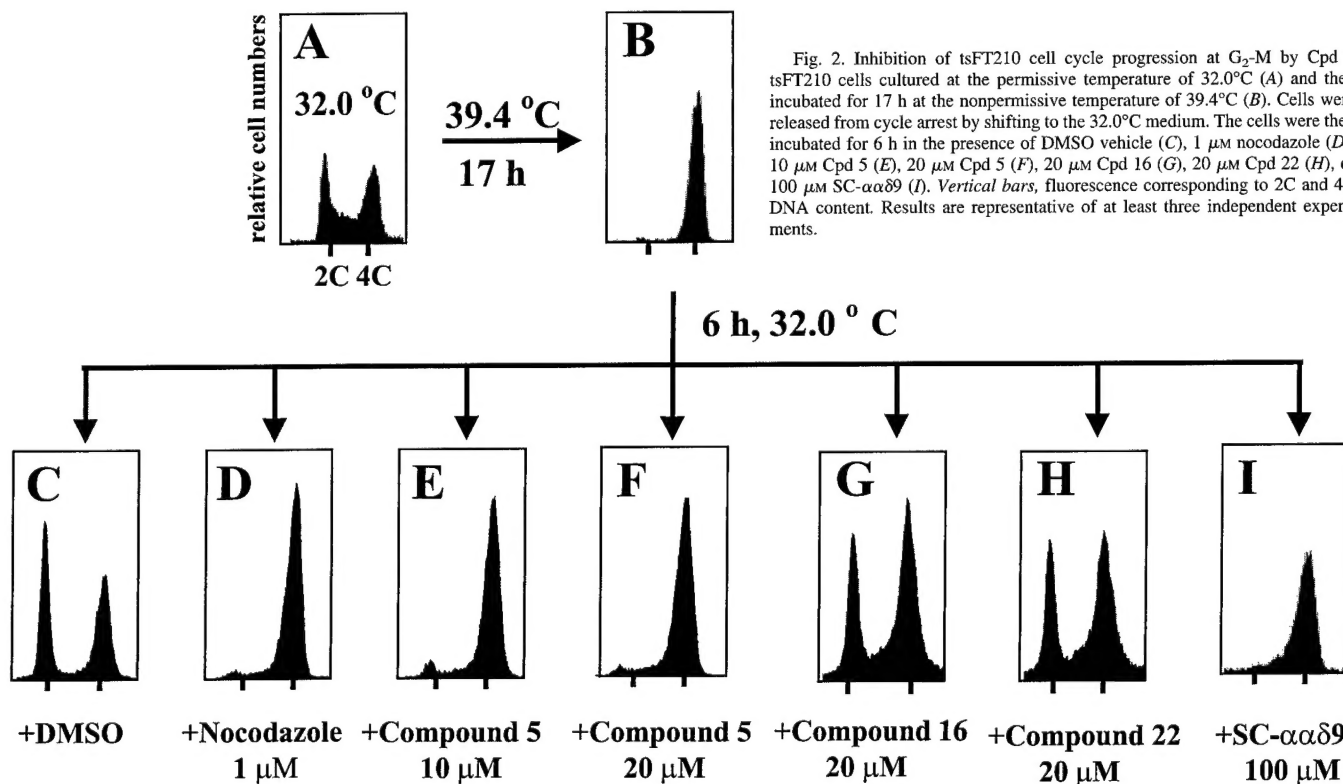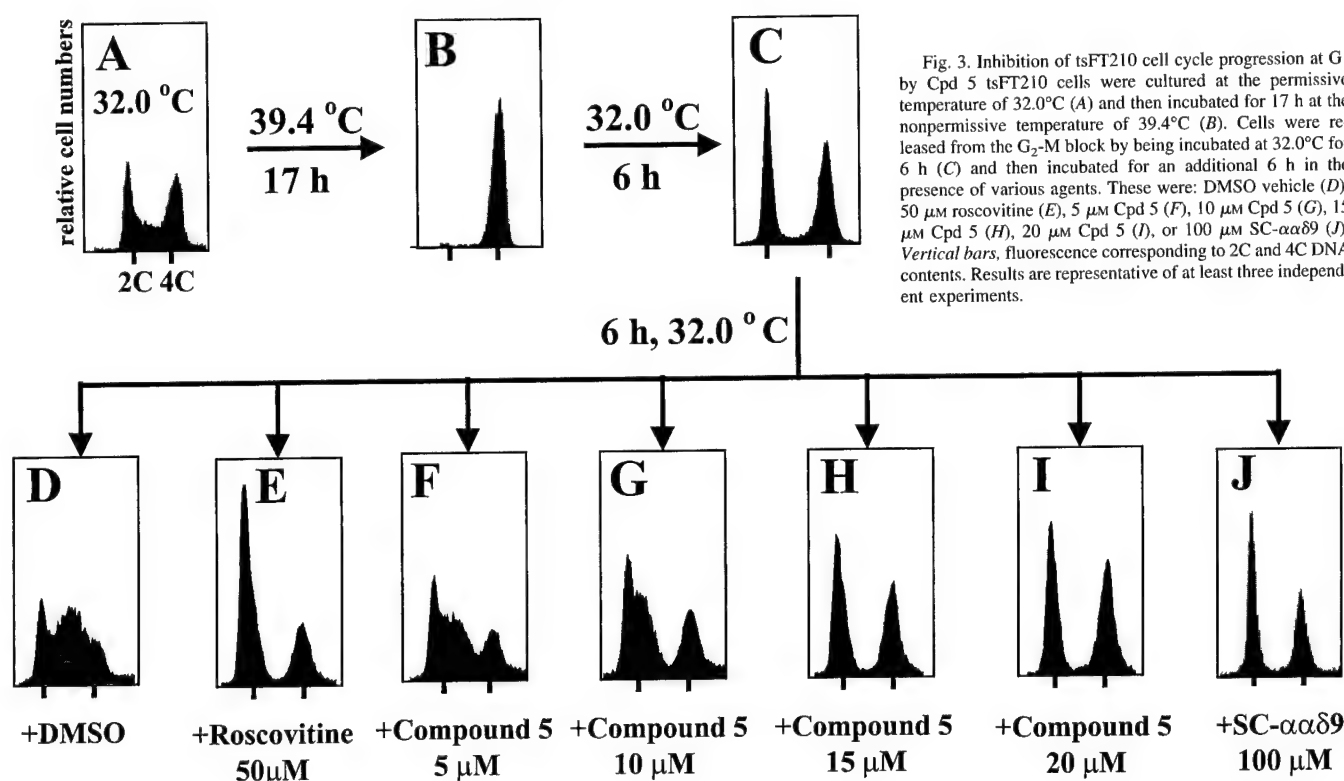
Fig. 3. Inhibition of tsFT210 cell cycle progression at G_1 by Cpd 5 tsFT210 cells were cultured at the permissive temperature of 32.0°C (A) and then incubated for 17 h at the nonpermissive temperature of 39.4°C (B). Cells were released from the G_2-M block by being incubated at 32.0°C for 6 h (C) and then incubated for an additional 6 h in the presence of various agents. These were: DMSO vehicle (D), 50 μM roscovitine (E), 5 μM Cpd 5 (F), 10 μM Cpd 5 (G), 15 μM Cpd 5 (H), 20 μM Cpd 5 (I), or 100 μM SC-$\alpha\alpha\delta$9 (J). Vertical bars, fluorescence corresponding to 2C and 4C DNA contents. Results are representative of at least three independent experiments.

(4.07), 334 (3.51); MS (m/z): 316 (15) 201 (30), 188 (100), 172 (45), 160 (30); high resolution MS: calculated for $C_{19}H_{24}O_3$: 300.1725, found: 300.1745.

Flow Cytometric Analysis. tsFT210 cells were plated at 2×10^5 cells/ml and maintained at 32.0°C as described previously (22). Cell proliferation was blocked at G_2 phase by incubation at 39.4°C for 17 h. The synchronized cells were then released by reincubating at 32.0°C and treated immediately with Cpd 5, Cpd 16, Cpd 22, or SC-$\alpha\alpha\delta$9, respectively, to probe for G_2-M arrest. Cells were treated 6 h after G_2-M release to determine G_1 arrest. For both G_2-M and G_1 blockage studies, treated cells were incubated at 32.0°C for an additional 6 h after each drug exposure and then harvested with PBS at 5×10^5 cells/ml. The harvest cells were stained with a solution containing 50 μg/ml propidium iodide and 250 μg/ml RNase A. Flow cytometry analysis was conducted with a Becton Dickinson FACS Star (Franklin Lakes, NJ). Each compound was tested at least three independent times. A final concentration of 0.5% DMSO was used for all compounds and as a negative control. For positive controls, we used 100 μM SC-$\alpha\alpha\delta$9 (for both G_2-M and G_1), 1 μM nocodazole (for G_2-M), or 50 μM roscovitine (for G_1).

Enzyme Assays. The preparation of plasmid DNA and GST-fusion proteins has been described previously (23). The activities of the GST-fusion Cdc25A, Cdc25B$_2$, Cdc25C, and VHR, as well as human recombinant PTP1B, were measured as described previously (23) in a 96-well microtiter plate using the substrate OMFP (Molecular Probes, Inc., Eugene, OR), which is readily metabolized to the fluorescent o-methyl fluorescein. OMFP concentrations approximating the K_m were used: Cdc25A, Cdc25B$_2$ and Cdc25C, 40 μM; VHR, 10 μM; and PTP1B, 200 μM. Inhibitors were resuspended in DMSO, and all reactions including controls were performed at a final concentration of 7% DMSO. The final incubation mixture (150 μl) was optimized for enzyme activity and comprised 30 mM Tris (pH 8.5 for Cdc25 phosphatases; pH 7.5 for VHR and PTP1B), 75 mM NaCl, 1 mM EDTA, 0.033% BSA, and 1 mM DTT. Reactions were initiated by adding 1 μg of Cdc25 phosphatases, 0.025 μg of VHR, or 0.25 μg of PTP1B phosphatase. Fluorescence emission from the product was measured over a 20–60 min reaction period at ambient temperature with a multiwell plate reader (PerSeptive Biosystems Cytofluor II; Framingham, MA; excitation filter, 485/20; emission filter, 530/30). For all enzymes, the reaction was linear over the time used in the experiments and was directly proportional to both the enzyme and substrate concentration. Best curve fit for Lineweaver-Burk plots and K_is was determined by using the curve-fitting programs Prism 3.0 (GraphPad Software, Inc., San Diego, CA) and EZ-Fit 5.03 (Perrella Scientific, Inc., Amherst, NH).

Western Blotting and Immunoprecipitation Studies. tsFT210 cells were harvested and sonicated in the lysis buffer using the same procedure for cell synchronizing and drug exposure as described above for the G_1 flow cytometric analysis. For the phospho-Rb study, we harvested the cells at each time point: -6 h (releasing point from the G_2-M synchronizing); and -3, 0, 1.5, 3, and 6 h after treatment with 20 μM Cpd 5. The protein lysates were analyzed by Western Blot for phospho-Rb, Rb, GAPDH, p53, p21, and p16. Immunoprecipitation assays were performed essentially as described previously (24), except we replaced 0.1% Tween 20 for 1% Triton X-100 in the lysis buffer. We incubated 2 mg of protein lysate on a rocker platform with 10 μg of anti-Cdk2 or anti-Cdk4 agarose conjugate for 4 h at 4°C. The immunocomplexes were washed four times with the same lysis buffer. After the final wash, the immunocomplexes were suspended with SDS-electrophoresis loading buffer and analyzed by Western blotting for Cdk2, tyrosine phosphorylated Cdk2, Cdk4, tyrosine phosphorylated Cdk4, cyclin A, cyclin E, and cyclin D1 as described above. To quantify the phosphorylation level of Cdk2 or Cdk4, we scanned X-ray films and analyzed band intensity on a Molecular Dynamics personal SI densitometer and analyzed them using the Image Quant software package (Ver. 4.1; Molecular Dynamics, Sunnyvale, CA). The phosphorylation level (pCdk2/Cdk2) was calculated by using the formula; pCdk2/Cdk2 = (a)/(b), where a was the intensity of the phosphorylated Cdk2 band and b was the intensity of the Cdk2 band, respectively. Statistical significance was analyzed using Student's unpaired t test.

Cdc2 Assays. tsFT210 cells were synchronized, exposed to drugs, and harvested as described above for the G_2-M flow cytometric analysis. The protein lysates were analyzed by Western blot for Cdc2 as described previously (25). Cdc2 kinase activity assay was performed as described previously (26). Briefly, the Cdc2 immunoprecipitates were incubated in 20 μl of kinase reaction buffer (26) for 30 min at 37°C, with 3 μg of histone H1, 20 mM Tris-HCl, 10 mM MgCl$_2$, 5 μM cold ATP, and 10 μCi of [γ-^{32}P]ATP. The proteins were separated by SDS-PAGE and analyzed with a Molecular Dynamics STORM 860 PhosphorImager (Sunnyvale, CA).

RESULTS

Cpd 5 Arrested Synchronous tsFT210 Cell Cycle Progression at G_2-M. We initially determined whether Cpd 5 blocked cell cycle progression through checkpoints using murine tsFT210 cells, because
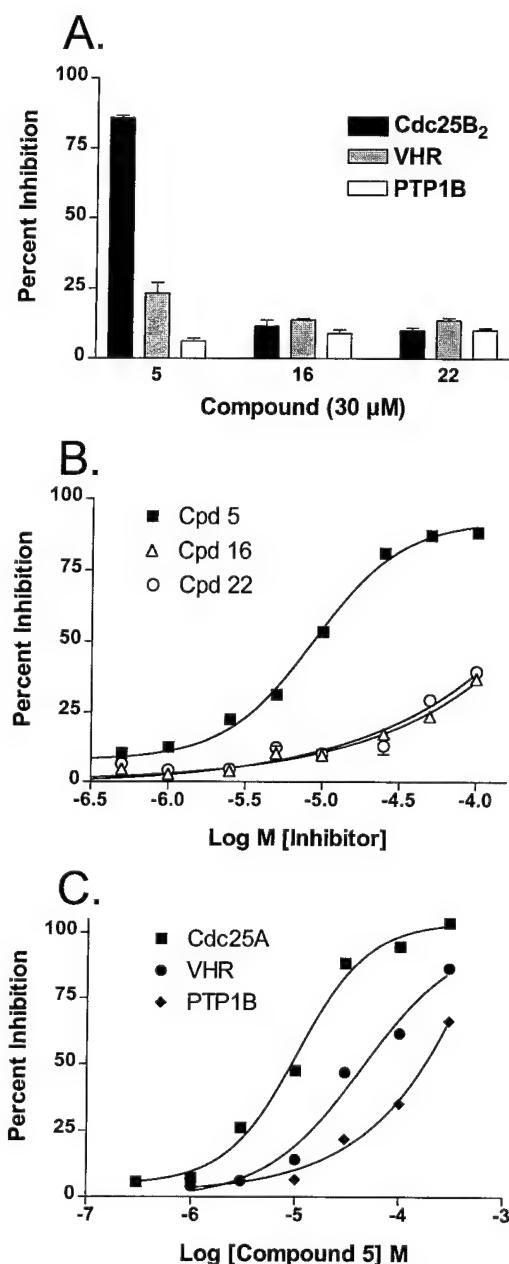
Fig. 4. Inhibition of recombinant human phosphatases by vitamin K analogues. *A*, human recombinant Cdc25B$_2$, VHR, or PTP1B was incubated with each vitamin K$_3$ analogue (30 μM) at room temperature for 0–60 min, and inhibition was determined as described in "Materials and Methods." ■, Cdc25B$_2$; ▨, VHR; □, PTP1B ($n = 3$). *Bars*, SE. *B*, Cdc25B$_2$ was incubated at room temperature with each compound at 0.1–100 μM for 0–60 min. The percentage of inhibition by Cpd 5 (■), Cpd 16 (△), or Cpd 22 (○; $n = 3$) is shown. *C*, selectivity of inhibition. The concentration-dependent inhibition profile for inhibition of GST fusion proteins Cdc25B$_2$ (■), VHR (●), and PTP1B (◆) is shown. Activities of GST fusion phosphatases were assayed as described in "Materials and Methods." Each value is the mean of three independent experiments.

2*D*). To determine the effect of Cpd 5 on G$_2$-M cell cycle transition, we treated cells with either 10 or 20 μM Cpd 5 for 6 h after releasing cells at 32.0°C. As indicated in Fig. 2, *E* and *F*, both concentrations of Cpd 5 significantly arrested cells at G$_2$-M phase. This G$_2$-M inhibition was selective to Cpd 5 and not seen with two structural analogues, *i.e.*, Cpd 16 and Cpd 22 (Fig. 1, *G* and *H*). The G$_2$-M inhibition was similar to that seen with another inhibitor of the Cdc25 family of phosphatases, SC-$\alpha\alpha\delta$9, which is structurally unrelated (Refs. 23 and 27; Fig. 2*I*).

Cpd 5 Arrested Synchronous tsFT210 Cell Cycle Progression at G$_1$. We next examined whether Cpd 5 caused G$_1$ arrest in tsFT210 cells. To investigate the mechanism of G$_1$ cell cycle block by Cpd 5, we arrested tsFT210 cells at G$_2$-M by shifting to the nonpermissive temperature, then released them into G$_1$ by shifting to the permissive temperature, and subsequently added either Cpd 5 or DMSO vehicle 6 h later. Cells that were treated with the DMSO vehicle passed through G$_1$ phase as expected and produced the broad S-phase peak (Fig. 3*D*), whereas cells exposed continuously to 50 μM roscovitine were blocked and did not pass through G$_1$ (Fig. 3*E*). As illustrated in Fig. 3, *F–I*, cells treated with 5 or 10 μM Cpd 5 were delayed, whereas cells treated with 15 or 20 μM Cpd 5 were fully blocked at G$_1$. In contrast, neither Cpd 16 nor Cpd 22 at 20 μM blocked G$_1$ transition (data not shown). As expected from our previous studies (Fig. 2), Cpd 5 not only caused a G$_1$ block but also prevented cells that were in the G$_2$ phase from progressing through G$_2$-M, which resulted in two prominent cell cycle peaks (Fig. 3, *H* and *I*). This dual G$_1$ and G$_2$-M inhibition was similar to that seen with a much higher concentration
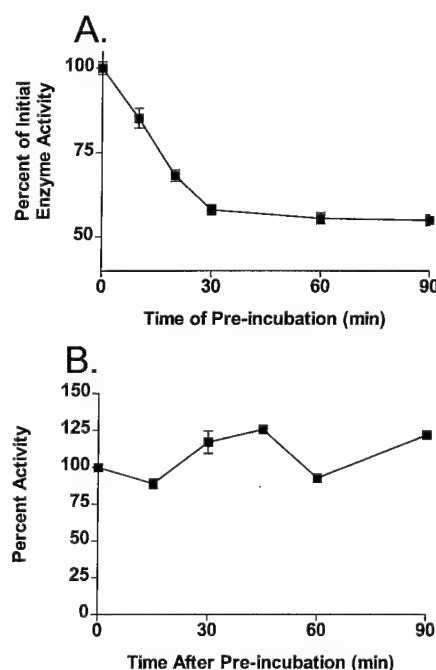

Fig. 5. Time- and concentration-dependent phosphatase inhibition by Cpd 5. *A*, time-dependent inhibition of GST-Cdc25B$_2$. The enzymes were either preincubated at room temperature with either 0.5% DMSO or 2 μM Cpd 5 for 0, 10, 20, 30, 60, or 90 min. The reaction was initiated by addition of substrate OMFP. Activities of GST fusion phosphatases were assayed as described in "Materials and Methods." The percentage of inhibition was determined by comparison to the DMSO control at each time point. Each value is the mean of three independent experiments and the SEs are indicated by *bars* unless they are less than the symbol size. *B*, irreversibility of Cdc25B$_2$ inhibition. GST-Cdc25B$_2$ was incubated with 2 μM Cpd 5 at room temperature for 30 min. The reaction mixture was centrifuged in a Centricon 30 concentrator (Amicon, Inc., Bedford, MA), then washed three times with assay buffer to remove Cpd 5 from the enzyme. At time points 0, 15, 30, 45, 60, and 90 min after Cpd 5 removal, the enzyme solution was assayed for phosphatase activity by the addition of substrate OMFP, as described in "Materials and Methods."

they can be readily synchronized with exogenous compounds because of a ts Cdc2 (22). When tsFT210 cells were incubated at the permissive temperature of 32.0°C, they had a normal cell cycle distribution (Figs. 2*A* and 3*A*); when cells were incubated at the nonpermissive temperature of 39.4°C, they arrested at G$_2$-M, because of Cdc2 inactivation (Ref. 22; Figs. 2*B* and 3*B*). When G$_2$-M arrested cells were cultured at the permissive temperature for 6 h with DMSO vehicle alone, we saw clear evidence of entry into G$_1$ (Fig. 2*C*). In contrast, 1 μM nocodazole blocked cell passage through G$_2$-M (Fig.
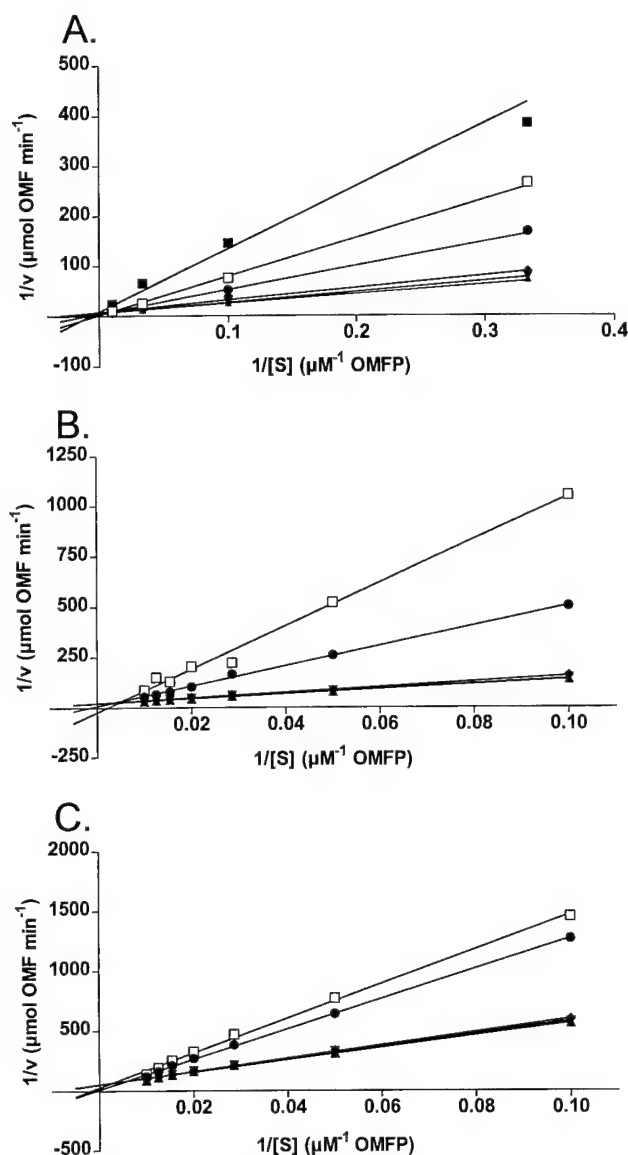
A.

B.

C.

Fig. 6. Kinetic analyses of Cdc25A, Cdc25B$_2$, and Cdc25C inhibition by Cpd 5. Inhibitor concentrations: ▲, 0 μM; ▼, 0.3 μM; ◆, 1 μM; ●, 3 μM; □, 10 μM; ■, 30 μM. Double-reciprocal plots of inhibition by Cpd 5 of Cdc25A (A), Cdc25B$_2$ (B), and Cdc25C (C) are shown. Enzyme activities were determined as outlined in "Materials and Methods." Best curve fit for Lineweaver-Burk plots and K_is were determined by using the curve-fitting programs Prism 3.0 (GraphPad Software, Inc.) and EZ-Fit 5.03 (Perrella Scientific, Inc.).

of the structurally unrelated and less potent Cdc25 inhibitor, SC-$\alpha\alpha\delta 9$ (Fig. 3J).

Cpd 5 Is a Selective Inhibitor of Cdc25. Because of the dual G$_1$ and G$_2$-M blockage with Cpd 5 and previous speculation concerning possible phosphatase inhibitory activity (8), we examined the inhibitory activity of Cpd 5, Cpd 16, and Cpd 22 (Fig. 1) against the dual specificity phosphatases Cdc25B$_2$ and VHR and the tyrosine phosphatase PTP1B. At 30 μM, Cpd 5 caused >75% inhibition of recombinant human Cdc25B$_2$ activity with only a small effect on VHR and no inhibition of PTP1B (Fig. 4A). In contrast, identical concentrations of the close structural analogues, Cpd 16 and Cpd 22, did not inhibit any of these protein phosphatases, indicating the essential nature of the β-mercaptoethanol moiety for enzyme inhibition. A more extensive study revealed that the Cdc25B$_2$ IC$_{50}$ for Cpd 5 was 3.8 ± 0.6 μM compared with >150 μM for the close analogues Cpd 16 and Cpd 22 (Fig. 4B). Thus, Cpd 5 was 40-fold more active than Cpd 16 or Cpd

22. The selectivity of Cpd 5 is illustrated in Fig. 4C; the IC$_{50}$s for VHR and PTP1B were 45 and 3200 μM, respectively. We also found that 40 and 80 μM Cpd 5 lacked any significant inhibitory activity against recombinant human mitogen-activated protein kinase (data not shown).

The inhibition of Cdc25B$_2$ was dependent on the length of enzyme exposure to Cpd 5; a 30-min preincubation with 2 μM Cpd 5 caused almost 50% more inhibition in enzyme activity than in samples that were exposed to Cpd 5 at the time of substrate addition (Fig. 5A). Preincubation longer than 30 min did not produce greater inhibition, possibly because Cpd 5 became inactivated. No reduction in enzyme activity was seen when Cdc25B$_2$ was preincubated with 0.5% DMSO for 90 min or less. The time-dependent inhibition was irreversible; a 90-min incubation in Cpd 5-free buffer did not restore the lost enzyme activity (Fig. 5B). Similar results were seen with both Cdc25A and VHR (data not shown). A kinetic analysis of the inhibition indicated a partial competitive inhibition for full-length human Cdc25A, Cdc25B$_2$, and Cdc25C (Fig. 6). The K_is for Cdc25A, Cdc25B$_2$, and Cdc25C were 15, 1.7, and 1.3 μM, respectively.

Cpd 5 Increased the Phosphorylation Level of Cdc2 in Synchronous tsFT210 Cells. One of the putative, endogenous, cellular substrates for both Cdc25B and Cdc25C is the mitotic inhibitor Cdc2, which must be dephosphorylated to allow entry into mitosis (14, 22, 28). Thus, we reasoned that an effective Cdc25 inhibitor would not only cause a G$_2$-M cell cycle block but would also prevent Cdc2 dephosphorylation. We, therefore, performed Western blotting on tsFT210 cell extracts to determine the Cdc2 phosphorylation levels in the presence or absence of Cpd 5. Protein lysates of tsFT210 cells arrested at the G$_2$-M boundary were harvested and analyzed by SDS-PAGE. Approximately 50% of Cdc2 was in the mitotic-inactive, hyperphosphorylated form, as reflected by a slower migrating Cdc2 (Fig. 7A). The phosphorylation of Cdc2 decreased gradually after cells were released from G$_2$-M block, and most of the Cdc2 was dephosphorylated 6 h after G$_2$-M release, even in the presence of the DMSO vehicle (Fig. 7A). When we incubated cells with 1 μM nocodazole, which caused a G$_2$-M arrest, no hyperphosphorylation of Cdc2 was seen (Fig. 7B), consistent with its proposed inhibitory activity after Cdc2 activation. In contrast, Cdc2 dephosphorylation was partially blocked (~70%) with 10 μM Cpd 5 and completely blocked (94%) with 20 μM (Fig. 7C). The Cdc2 phosphorylation status after 6 h with DMSO alone was similar in Fig. 7, A and C. SC-$\alpha\alpha\delta 9$ at 50 μM also caused hyperphosphorylation of Cdc2 (Fig. 7B). Because the phosphorylation status of Cdc2 determines its enzymatic activity (29), we examined the kinase activity of immunoprecipitated Cdc2 by measuring histone H1 phosphorylation *in vitro*. We found that the Cdc2 kinase activity in cells treated with 1 μM nocodazole was significantly increased, which was consistent with a previous study using tsFT210 cells (26). The Cdc2 kinase activity in cells treated with 10–20 μM Cpd 5 was markedly reduced (Fig. 7D). The congeners, Cpd 16 and Cpd 22, however, did not block this kinase activity as expected by their lack of effect on Cdc25 activity (Fig. 4A). Similar amounts of Cdc2 were immunoprecipitated in cells treated with Cpd 5 (Fig. 7E).

Cpd 5 Increased Cdk2 and Cdk4 Tyrosine Phosphorylation in Synchronous tsFT210 Cells. Cdk4 plays a central role in regulating the G$_1$ transition by its association with cyclin D1 (30). This complex remains inactive until Cdc25A dephosphorylates it. Cdk2 is also involved in regulating the G$_1$-S transition by its association with cyclin E or cyclin A. The Cdk2/cyclin E complex has been shown to be dephosphorylated at Thr-14 and Tyr-15 and, thereby, activated by Cdc25A treatment *in vitro* (31). To clarify the mechanism of G$_1$ cell cycle block by Cpd 5, we treated tsFT210 cells with ≤20 μM Cpd 5 for 6 h, immunoprecipitated Cdk2 or Cdk4 from the cell lysates, and then determined tyrosine phosphorylation by Western blotting, using
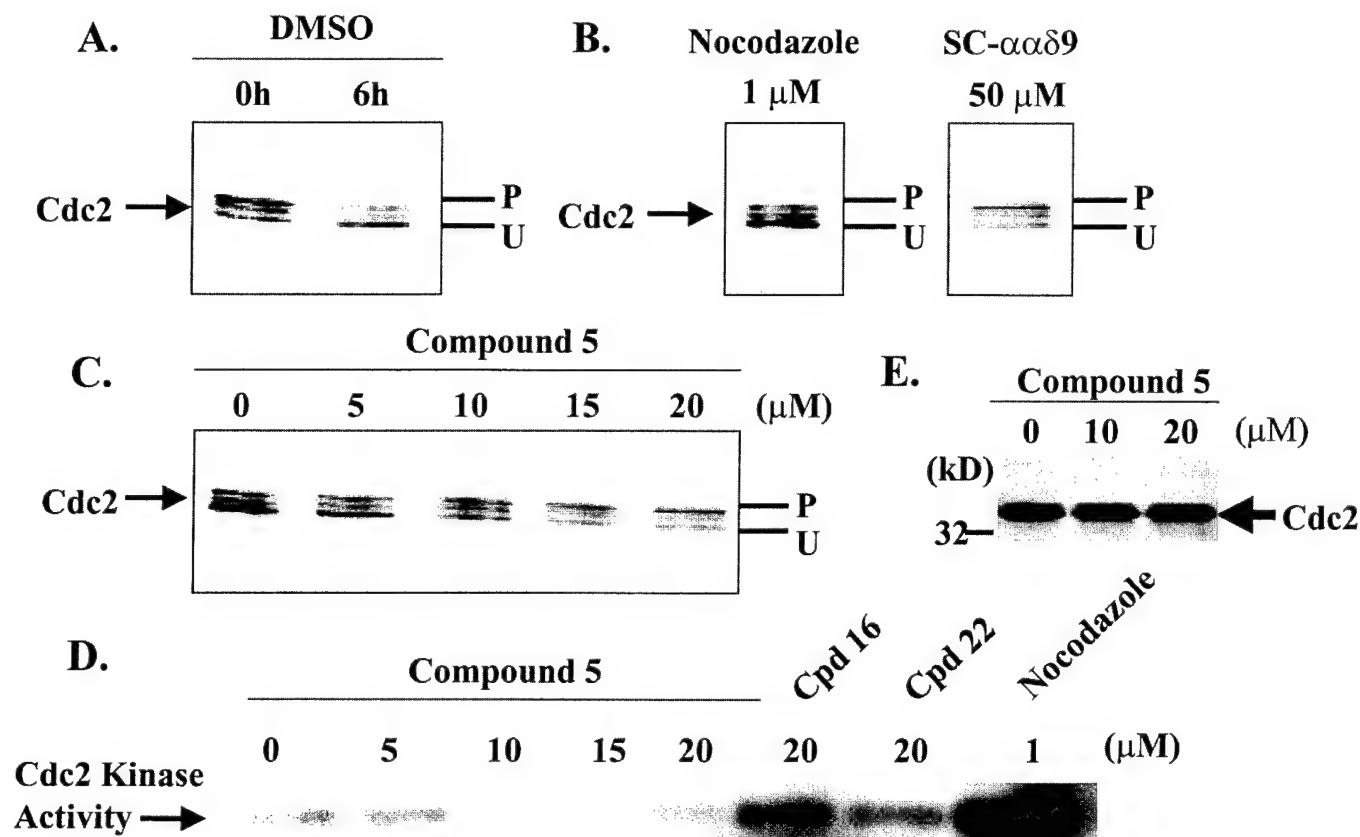
Fig. 7. Inhibition of Cdc2 dephosphorylation and kinase activity by Cpd 5 in synchronous tsFT210 cells. G_2-M synchronous tsFT210 cells were treated with vehicle or various compounds and permitted to reenter the cell cycle by culturing at 32.0°C. We isolated protein lysates from cells that were not incubated (*0h*) or from cells incubated for 6 h at the permissive temperature in the presence of a compound or vehicle. The protein lysate were analyzed by Western blotting for Cdc2 or Cdc2 kinase activity assay as described in "Materials and Methods." *A*, DMSO control. *B*, nocodazole (1 μM) and SC-$\alpha\alpha\delta9$ (50 μM) at 6 h. *C*, Cpd 5 or DMSO control at 6 h. *D*, Cdc2 kinase activity with histone H1 as a substrate. *E*, Cdc2 content in immunoprecipitates from Cpd 5-treated cells. *P*, phosphorylated; *U*, unphosphorylated.

anti-phosphotyrosine monoclonal antibody. As illustrated in Fig. 8, the phosphorylation of both Cdk2 and Cdk4 increased after Cpd 5 treatment. We confirmed that there was equivalent loading of Cdk2 or Cdk4 with anti-Cdk2 or anti-Cdk4 antibody, respectively (Fig. 8). To quantify the phosphorylation level of Cdk2 or Cdk4, we determined the intensity of the bands by densitometer and calculated a phosphorylation level as described in "Materials and Methods." Both Cdk2 and Cdk4 tyrosine phosphorylation increased in a concentration-dependent manner after Cpd 5 treatment, with a >5-fold increase being seen after exposure to 20 μM Cpd 5.

Cpd 5 Does Not Affect Cyclin Interactions with Cdk2 or Cdk4. Cdk requires noncovalent interactions with cyclins to be functional. To exclude the possibility that Cpd 5 simply blocked such an intracellular interaction, we treated tsFT210 cells with Cpd 5 for 6 h, immunoprecipitated Cdk2 from cell lysates with an anti-Cdk2 antibody, and then examined the immunoprecipitate for cyclin A and E content by Western blotting. We also immunoprecipitated Cdk4 from cell lysates with anti-Cdk4 and determined cyclin D1 protein levels. Cyclin A or E association with Cdk2 was unchanged after Cpd 5 treatment (Fig. 9A). Similarly, Cdk4 association with cyclin D1 was unaffected by the Cpd 5 treatment (Fig. 9B). For both analyses, we loaded equivalent amounts of Cdk2 or Cdk4 as detected with anti-Cdk2 or anti-Cdk4, respectively (Fig. 9).

Cpd 5 Decreases the Phosphorylation of Rb. The phosphorylation of Rb, which is a critical regulator of the G_1 checkpoint, is controlled in part by Cdk2. Thus, we examined the phosphorylation status of Rb in synchronous tsFT210 cells at various times after addition of 20 μM Cpd 5 (Fig. 10). As expected, the Rb phosphoryl-

ation increased with passage into G_1 phase (Fig. 10). Within 1.5 h after exposure of cells to Cpd 5, however, there was a marked inhibition of Rb phosphorylation with no alteration of Rb protein levels. Equivalent loading was confirmed by measuring GAPDH (Fig. 10). Thus, our results support the hypothesis that Cpd 5 blocked cell cycle progression through the G_1 checkpoint by disruption of functional Cdk activity through inhibition of Cdc25A activity.

Cpd 5 Did Not Alter p53, p21, or p16 Levels. To ensure that the inhibition of Cdk4 kinase activity and cell cycle arrest were not secondary to p53 induction or increased Cdk inhibitors, we measured p53, p21, and p16 levels in tsFT210 cells after Cpd 5 treatment (Fig. 11). tsFT210 cells, which had been treated with an equitoxic etoposide concentration, displayed elevated p53 levels, whereas Cpd 5 produced no increase (Fig. 11A). We also saw no increase in p21 or p16 with Cpd 5 (Fig. 11, *B* and *C*), suggesting that the dual cell cycle phase arrest was not due simply to nonspecific cell stress or DNA damage.

DISCUSSION

The Cdc25 dual-specific phosphatases have an essential role in controlling cell proliferation by regulating the activities of Cdks (14, 31). In higher eukaryotes, Cdc25A is responsible for governing G_1 transition into S phase, Cdc25B probably initiates cell cycle movement through the G2 phase, and Cdc25C is required for entry into mitosis, because of its ability to dephosphorylate and activate Cdc2. Because Cdc25A and Cdc25B have also been reported to be oncogenic (15) and to be overexpressed in several tumor types (17, 18),

A

Compound 5

1   2   3

←pCdk2

← Cdk2
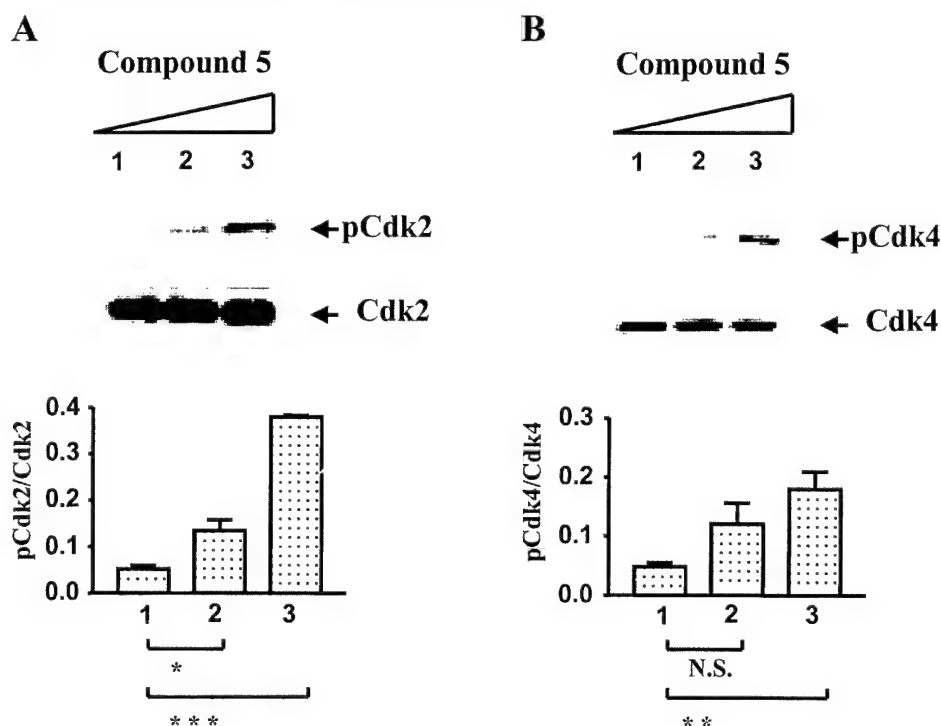
B

Compound 5

1   2   3

←pCdk4

← Cdk4

Fig. 8. Effect of Cpd 5 on Cdk4 or Cdk2 tyrosine phosphorylation in tsFT210 cells. Synchronized tsFT210 cells were cultured for 6 h at 32.0°C and then incubated for an additional 6 h in the presence of 0 μM (*Lane 1*), 10 μM (*Lane 2*), or 20 μM (*Lane 3*) of Cpd 5. The cells were harvested and sonicated in lysis buffer and probed for tyrosine phosphorylation and total Cdk by Western blot as described in "Materials and Methods." *A,* Cdk2 protein content and phosphorylation. *B,* Cdk4 protein content and phosphorylation. *, $P < 0.05$; **, $P < 0.01$; ***, $P < 0.005$. *N.S.,* not significant. *Bars,* SE.

Cdc25 is an attractive therapeutic target. Although the Cdc25 family members appear to have distinct biological functions and possibly substrates, the amino acids comprising their active site $HC(X_5)R$ region are identical, suggesting that inhibitors with specificity to all three Cdc25s are feasible. Moreover, significant structural differences exist among the other protein tyrosine phosphatases and Cdc25 (32). Thus, it may be possible to identify selective inhibitors of this family of enzymes.

Except for the widely used broad-spectrum protein phosphatase inhibitor vanadate (33), few dual-specificity protein phosphatase inhibitors have been reported (34, 35). Moreover, these analogues are generally in limited supply, and the effects of these compounds on cell cycle transition or other enzymes are not known. We have previously synthesized and evaluated a small molecule, SC-$\alpha\alpha\delta9$, that was among the most potent of the known synthetic inhibitors of the Cdc25 dual-specificity phosphatases (23). As noted in our current studies and elsewhere (27), this competitive inhibitor of Cdc25 caused both G_2-M and G_1 inhibition.

Previously, we reported that the thioether vitamin K analogue Cpd 5 was a more potent inhibitor of hepatoma cell proliferation than other K vitamins (8). Hepatoma cells normally only arrest in G_1. Moreover, we found that growth-inhibitory concentrations of Cpd 5 caused a rapid increase in protein tyrosine phosphorylation that could be blocked by elevating intracellular stores of thiols, such as cysteine (36, 39). Although we proposed sulfhydryl arylation of protein phosphatases as a potential mechanism for enhanced phosphorylation and growth inhibition, no experimental examination of the effects of Cpd 5 on specific phosphatases was performed previously. We now report that Cpd 5 inhibited Cdc25 in a partially competitive manner that was time dependent and ultimately irreversible. The Cdc25 enzymes share a conserved COOH-terminal catalytic domain containing the Cys-$(X)_5$-Arg motif. In Cdc25A and presumably other Cdc25 enzymes, Cys-430 forms a disulfide bond with Cys-384 that may be self-inhibiting and redox sensitive (32). In contrast to other K vitamins, however, Cpd 5 lacks significant redox activity (8). Thus, we hypothesize that arylation, possibly of Cys-430 or Cys-384, is responsible for

A.

Compound 5

(kD)   1   2   3

73.0—

43.5—

73.0—

43.5—

32.0—

←Cyclin A

←Cyclin E

←Cdk2

B.

Compound 5
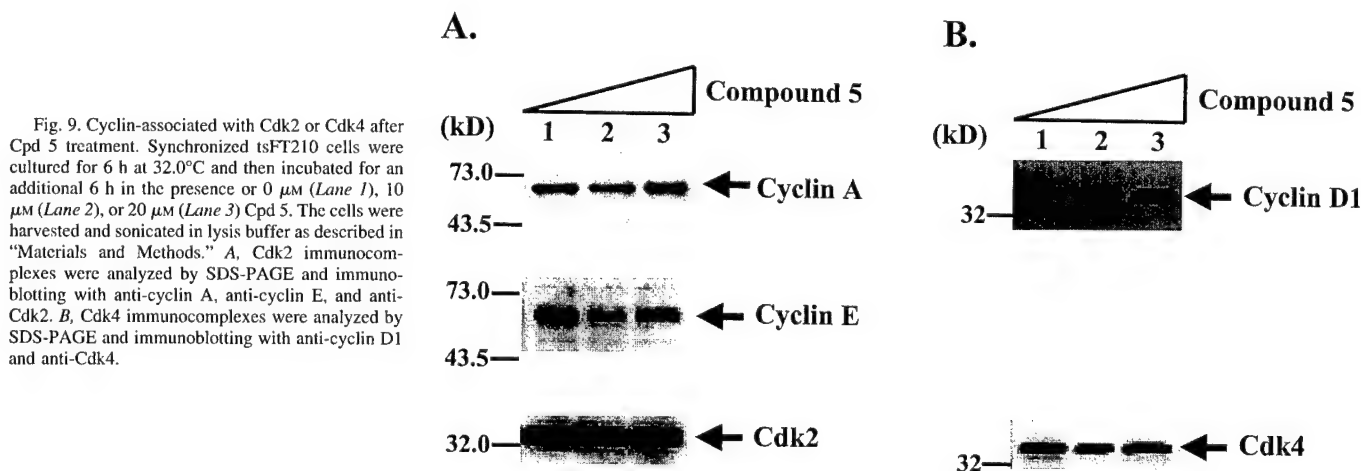
(kD)   1   2   3

32—

32—

←Cyclin D1

←Cdk4

Fig. 9. Cyclin-associated with Cdk2 or Cdk4 after Cpd 5 treatment. Synchronized tsFT210 cells were cultured for 6 h at 32.0°C and then incubated for an additional 6 h in the presence or 0 μM (*Lane 1*), 10 μM (*Lane 2*), or 20 μM (*Lane 3*) Cpd 5. The cells were harvested and sonicated in lysis buffer as described in "Materials and Methods." *A,* Cdk2 immunocomplexes were analyzed by SDS-PAGE and immunoblotting with anti-cyclin A, anti-cyclin E, and anti-Cdk2. *B,* Cdk4 immunocomplexes were analyzed by SDS-PAGE and immunoblotting with anti-cyclin D1 and anti-Cdk4.

the enzyme inhibition. This will require additional experimental studies to establish.

We used the well-studied tsFT210 cell system, because the cells can be synchronized without any exogenous agents or drugs. Both Cpd 16 and Cpd 22, which are close congeners of Cpd 5, failed to block cell cycle progression. Neither Cpd 16 nor Cpd 22 had inhibitory activity against Cdc25 phosphatases *in vitro*. By contrast, Cpd 5 inhibited both cell cycle progression and Cdc25 phosphatase activity *in vitro*. These data revealed a close correlation between Cdc25 inhibition *in vitro* and disruption of cell cycle regulation. The observed elevated Cdc2 phosphorylation and the loss of Cdc2 kinase activity provided additional biochemical evidence for intracellular Cdc25 inhibition. Cpd 5, but not the other closely related but biochemically inactive analogues, decreased Cdc2 kinase activity in the intact cells. These concentration-response studies showing that Cpd 5 induced Cdc2 phosphorylation and inhibited its kinase activity suggest that Cpd 5 had an inhibitory effect on Cdc25B and Cdc25C within the cell and provide a mechanistic basis for the blockage at G_2-M.

We hypothesized that inhibition of Cdc25A might mediate the G_1 block caused by Cpd 5, because Cdc25A seems to be important for entry into S phase (13, 31). The tyrosine phosphorylation status of both Cdk2 and Cdk4 was markedly increased by the actions of Cpd 5. Both of these Cdks have a central role in regulating the G_1-S transition (30). Cdc25A dephosphorylates Cdk2 at Thr-14 and Tyr-15 and activates the functional Cdk2/cyclin E complex required for progression through the S phase of the cell cycle (31). Cdc25A also controls the tyrosine phosphorylation status of Cdk4, which regulates G_1 arrest by agents such as UV irradiation (37). Furthermore, the activity of Cdc25A determines the phosphorylation status of Rb through its effects on Cdk4 kinase. Our data show that Cpd 5 increased Cdk4 tyrosine phosphorylation, thereby decreasing kinase activity against Rb. Thus, the dephosphorylated Rb might cause the G_1 block in tsFT210.

We cannot, however, formally exclude that Cpd 5 acts on other cell cycle control mechanisms or on other protein phosphatases. Indeed, in hepatoma cells, Cpd 5 transiently enhanced the phosphorylation of a number of proteins (36, 39). Nonetheless, we found that differences exist in the *in vitro* sensitivity of several classes of protein phosphatases and that Cpd 5 induced persistent inhibition of one class of protein phosphatases, *i.e.*, Cdc25. Furthermore, we have established that cell cycle arrest resulted from the cellular effects of Cpd 5 consistent with
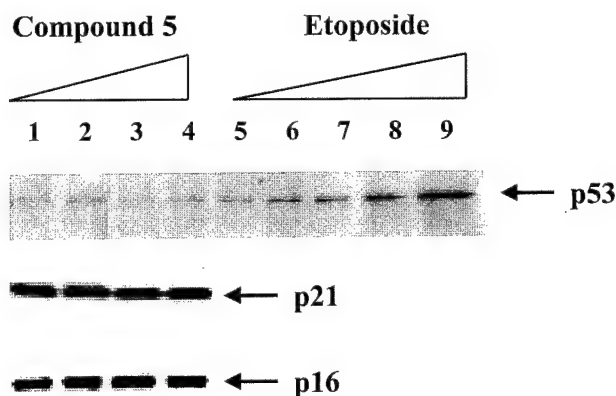

Fig. 11. Western blot of p53, p21, and p16. Synchronized tsFT210 cells were cultured for 6 h at 32.0°C and then incubated for an additional 6 h in the presence of 0 µM (Lane 1), 10 µM (Lane 2), 15 µM (Lane 3), or 20 µM (Lane 4) Cpd 5. Cells were also incubated in the presence of 0 µM (Lane 5), 3 µM (Lane 6), 10 µM (Lane 7), 30 µM (Lane 8), or 50 µM (Lane 9) of etoposide. Cells were harvested and analyzed by Western blotting for p53, p21, or p16 expression by Western blotting methods.

intracellular inhibition of the catalytic activity of Cdc25. It is well established that DNA damage, such as that induced by ionizing radiation, produces a p53 induction and blocks the cell cycle at both G_1 and G_2-M (38). Our results indicate, however, that exposure of tsFT210 cells to Cpd 5 for 6 h did not produce p53, p21, or p16 induction (Fig. 11). These data suggest that the main pathway causing the dual cell cycle arrest by Cpd 5 is different from p53 (p21) or p16 induction pathways.

In summary, we demonstrated that the potent K vitamin analogue, Cpd 5, inhibited an important class of growth-regulatory, dual-specificity phosphatases and arrested cells in both G_1 and G_2-M phases. We suggest that small molecule inhibitors derived from the Cpd 5 pharmacophore will be useful for furthering our understanding of the role of Cdc25 in regulating G_1 and G_2 transition and may contribute to a further development of novel anticancer agents.

ACKNOWLEDGMENTS

REFERENCES

1. Ngo, E. O., Sun, T-P., Chang, J-Y., Wang, C. C., Chi, K-H., and Nutter, L. M. Status of glutathione and glutathione-metabolizing enzymes in menadione-resistant human cancer cells. Biochem. Pharmacol., 42: 1961–1968, 1991.
2. Kerns, J., Naganathan, S., Dowd, P., Finn, F. M., and Carr, B. Thioalkyl derivatives of vitamin K_3 and vitamin K_3 oxide inhibit growth of Hep3B and HepG2 cells. Bioorg. Chem., 23: 101–108, 1995.
3. Chlebowski, R. T., Dietrich, M., Akman, S., and Block, J. B. Vitamin K3 inhibition of malignant murine cell growth and human tumor colony formation. Cancer Treat. Rep., 85: 527–532, 1985.
4. Nutter, L. M., Cheng, A. L., Hung, H. L., Hsieh, R. K., Ngo, E. O., and Liu, T. W. Menadione: spectrum of anticancer activity and effects on nucleotide metabolism in human neoplastic cell lines. Biochem. Pharmacol., 41: 1283–1292, 1991.
5. Akman, S., Carr, B. I., Leong, L., Margolin, K., Odujinrin, O., and Doroshow, J. Phase I trial of menadiol sodium diphosphate in advance cancer. Proc. Am. Soc. Clin. Oncol. Annu. Meet., 7: 290, 1988.
6. Nutter, L. M., Ngo, E. O., Fisher, G. R., and Gutierrez, P. L. DNA strand scission and free radical production in menadione-treated cells. Correlation with cytotoxicity and role of NADPH quinone acceptor oxidoreductase. J. Biol. Chem., 267: 2474–2479, 1992.
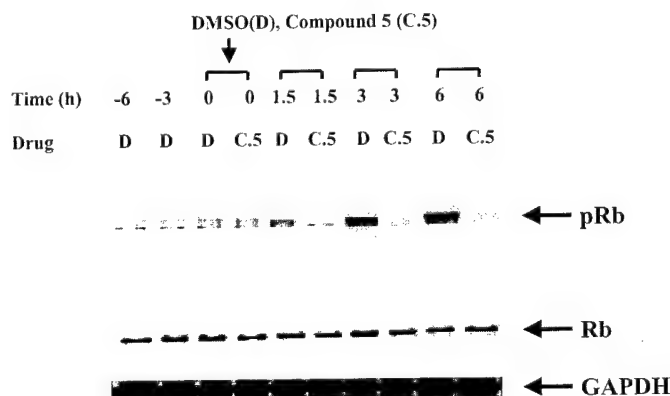
Fig. 10. Rb phosphorylation after treatment with Cpd 5. G_2-M synchronous tsFT210 cells were cultured for 6 h at 32.0°C and treated with DMSO (D) or 20 µM Cpd 5 (C.5). The cells were then reincubated at 32.0°C. The times from protein lysate generation were determined from the time of compound or vehicle addition. Thus, the -6 determination was at the time of G_2-M block, the -3 determination was taken 3 h after release from G_2-M block, and the 0 determination was taken 6 h after the release and at the time either DMSO or Cpd 5 was added. The 1.5-, 3-, and 6-h determinations were taken 7.5, 9, and 12 h after the initial release from G_2-M block and 1.5, 3, and 6 h after compound or vehicle addition.

7. Rossi, L., Moore, G. A., Orrenius, S., and O'Brien, P. J. Quinone toxicity in hepatocytes without oxidative stress. Arch. Biochem. Biophys., 251: 25–31, 1986.

8. Nishikawa, Y., Carr, B. I., Wang, M., Kar, S., Finn, F., Dowd, P., Zheng, Z. B., Kerns, J., and Naganathan, S. Growth inhibition of hepatoma cells induced by Vitamin K and its analogs. J. Biol. Chem., 47: 28304–28310, 1995.

9. Sadhu, K., Reed, S. I., Richardson, H., and Russell, P. Human homolog of fission yeast Cdc25 mitotic inducer is predominantly expressed in G2. Proc. Natl. Acad. Sci. USA, 87: 5139–5143, 1990.

10. Galaktionov, K., and Beach, D. Specific activation of Cdc25 tyrosine phosphatases by B-type cyclins: evidence for multiple roles of mitotic cyclins. Cell, 67: 1181–1194, 1991.

11. Nagata, A., Igarashi, M., Jinno, S., Suto, K., and Okayama, H. An additional homolog of the fission yeast *cdc25+* gene occurs in humans and is highly expressed in some cancer cells. New Biol., 3: 959–968, 1991.

12. Millar, J. B., Blevitt, J., Gerace, L., Sadhu, K., Featherstone, C., and Russell, P. p55CDC25 is a nuclear protein required for the initiation of mitosis in human cells. Proc. Natl. Acad. Sci. USA, 88: 10500–10504, 1991.

13. Jinno, S., Suto, J., Nagata, A., Igarashi, M., Kanaoka, Y., Nojima, H., and Okayama, H. Cdc25A is a novel phosphatase functioning early in the cell cycle. EMBO J., 13: 1549–1556, 1994.

14. Lammer, C., Wagerer, S., Saffrich, R., Mertens, D., Ansorge, W., and Hoffmann, I. The cdc25B phosphatase is essential for G2/M phase transition in human cells. J. Cell Sci., 111: 2445–2453, 1998.

15. Galaktionov, K., Lee, A. K., Eckstein, J., Draetta, G., Meckler, J., Loda, M., and Beach, D. CDC25 phosphatases as potential human oncogenes. Science (Washington DC), 269: 1575–1577, 1995.

16. Galaktionov, K., Chen, X., and Beach, D. Cdc25 cell-cycle phosphatase as a target of c-myc. Nature (Lond.), 382: 511–517, 1996.

17. Gasparotto, D., Maestro, R., Piccinin, S., Vukosavljevic, T., Barzan, L., Sulfaro, S., and Boiocchi, M. Overexpression of Cdc25A and Cdc25B in head and neck cancers. Cancer Res., 57: 2366–2368, 1997.

18. Hernandez, S., Hernandez, L., Bea, S., Cazorla, M., Fernandez, P. L., Nadal, A., Muntane, J., Mallofre, C., Montserrat, E., Cardesa, A., and Campo, E. Cdc25 cell cycle-activating phosphatases and c-myc expression in human non-Hodgkin's lymphomas. Cancer Res., 58: 1762–1767, 1998.

19. Wu, W., Fan, Y-H., Kemp, B. L., Walsh, G., and Mao, L. Overexpression of *cdc*25A and *cdc*25B is frequent in primary non-small cell lung cancer but is not associated with overexpression of c-*myc*. Cancer Res., 58: 4082–4085, 1998.

20. Juan, C-C., and Wu, F-Y. H. Vitamin K3 inhibits growth of human hepatoma HepG2 cells by decreasing activities of both p34cdc2 kinase and phosphatase. Biochem. Biophys. Res. Commun., 190: 907–913, 1993.

21. Ham, S. W., Park, J., Lee, S. J., Kim, W., Kang, K., and Choi, K. H. Naphthoquinone analogs as inactivators of cdc25 phosphatase. Bioorg. Med. Chem. Lett., 8: 2507–2510, 1998.

22. Th'ng, J. P., Wright, P. S., Hamaguchi, J., Lee, M. G., Norbury, C. J., Nurse, P., and Bradbury, E. M. The FT210 cell line is a mouse G2 phase mutant with a temperature-sensitive *CDC2* gene product. Cell, 63: 313–324, 1990.

23. Rice, R. L., Rusnak, J. M., Yokokawa, F., Yokokawa, S., Messner, D. J., Boynton, A. L., Wipf, P., and Lazo, J. S. A targeted library of small molecule, tyrosine and dual specificity phosphatase inhibitors derived from a rational core design and random side chain variation. Biochemistry, 36: 15965–15974, 1997.

24. Kakeya, H., Onose, R., Liu, C-C. P., Onozawa, C., Matsumura, F., and Osada, H. Inhibition of Cyclin D1 expression and phosphorylation of retinoblastoma protein by phosmidosine, a nucleotide antibiotic. Cancer Res., 58: 704–710, 1998.

25. Vogt, A., Rice, R. L., Settineri, C. E., Yokokawa, F., Yokokawa, S., Wipf, P., and Lazo, J. S. Disruption of insulin-like growth factor-1 signaling and down-regulation of Cdc2 by SC-ααδ9, a novel small molecule antisignaling agent identified in a targeted array library. J. Pharmacol. Exp. Ther., 287: 806–813, 1998.

26. Yu, L., Orlandi, L., Wang, P., Orr, M. S., Senderowicz, A. M., Sausville, E. A., Silvestrini, R., Watanabe, N., Piwnica-Worms, H., and O'Connor, P. M. UCN-01 arrogates G2 arrest through a Cdc2-dependent pathway that is associated with inactivation of the Wee1Hu kinase and activation of the Cdc25C phosphatase. J. Biol. Chem., 273: 33455–33464, 1998.

27. Tamura, K., Rice, R. L., Wipf, P., and Lazo, J. S. Dual G1 and G2/M phase inhibition by SC-ααδ9, a combinatorially derived Cdc25 phosphatase inhibitor. Oncogene, 18: 6989–6996, 2000.

28. Strausfeld, U., Labbe, J. C., Fesquet, D., Cavadore, J. C., Picard, A., Sadhu, K., Russell, P., and Doree, M. Dephosphorylation and activation of a p34^{cdc2}/cyclin B complex *in vitro* by human CDC25 protein. Nature (Lond.), 351: 242–245, 1991.

29. Morgan, D. O. Principles of CDK regulation. Nature (Lond.), 374: 131–134, 1995.

30. Hunter, T., and Pines, J. Cyclins and cancer II: cyclin D and CDK inhibitors come of age. Cell, 79: 573–582, 1994.

31. Hoffman, I., Draetta, G., and Karsenti, E. Activation of the phosphatase activity of human cdc25A by a cdk2-cyclin E dependent phosphorylation at the G1/S transition. EMBO J., 13: 4302–4310, 1994.

32. Fauman, E. B., Cogswell, J. P., Lovejoy, B., Rocque, W. J., Holmes, W., Montana, V. G., Piwnica-Worms, H., Rink, M. J., and Saper, M. A. Crystal structure of the catalytic domain of the human cell cycle control phosphatase, Cdc25A. Cell, 93: 617–625, 1998.

33. Baratte, B., Meijer, L., Galaktionov, K., and Beach, D. Screening for antimitotic compounds using the cdc25 tyrosine phosphatase, an activator of the mitosis-inducing p34^{cdc2}/cyclin B^{cdc13} protein kinase. Anticancer Res., 12: 873–880, 1992.

34. Peng, H., Zalkow, L. H., Abraham, R. T., and Powis, G. Novel CDC25A phosphatase inhibitors from pyrolysis of 3-α-azido-B-homo-6-oxa-4-cholesten-7-one on silica gel. J. Med. Chem., 41: 4677–4680, 1998.

35. Horiguchi, T., Nishi, K., Hakoda, S., Tanida, S., Nagata, A., and Okayama, H. Dnacin A1 and Dnacin B1 are antitumor antibiotics that inhibit cdc25B phosphatase activity. Biochem. Pharmacol., 48: 2139–2141, 1994.

36. Ni, R., Nishikawa, Y., and Carr, B. I. Cell growth inhibition by a novel vitamin K is associated with induction of protein tyrosine phosphorylation. J. Biol. Chem., 272: 9906–9911, 1998.

37. Terada, Y., Tatsuka, M., Jinno, S., and Okayama, H. Requirement for tyrosine phosphorylation of Cdk4 in G1 arrest induced by ultraviolet irradiation. Nature (Lond.), 376: 358–362, 1995.

38. Hermeking, H., Lengauer, C., Polyak, K., He, T. C., Zhang, L., Thiagalingam, S., Kinzler, K. W., and Vogelstein, B. 14-3-3σ is a p53-regulated inhibitor of G2/M progression. Mol. Cell, 1: 3–11, 1997.

39. Nishikawa, Y., Wang, Z., Kerns, J., Wilcox, C. S., and Carr, B. I. Inhibition of hepatoma cell growth *in vitro* by arylating and non-arylating K vitamin analogs. J. Biol. Chem., 274: 34803–34810, 1999.

In Vivo Antitumor Activity and Induction of Insulin-Like Growth Factor-1-Resistant Apoptosis by SC-ααδ9[1]

ANDREAS VOGT, ANGELA S. WANG, CANDACE S. JOHNSON, JAMES P. FABISIAK, PETER WIPF, and JOHN S. LAZO

Departments of Pharmacology (A.V., A.S.W., C.S.J., J.P.F.), Chemistry (P.W., J.S.L.), Environmental and Occupational Health (J.P.F.), and the University of Pittsburgh Cancer Institute (C.S.J., P.W., J.S.L.), University of Pittsburgh, Pittsburgh, Pennsylvania

Accepted for publication September 20, 1999   This paper is available online at http://www.jpet.org

ABSTRACT

We previously showed that SC-ααδ9 {4-(benzyl-(2-[(2,5-diphenyl-oxazole-4-carbonyl)-amino]-ethyl)-carbamoyl)-2-decanoylamino butyric acid} is a novel antiphosphatase agent that selectively inhibits the growth of transformed cells in culture and affects elements of insulin-like growth factor-1 (IGF-1) signaling. We now show that SC-ααδ9 induces IGF-1-resistant apoptosis and kills tumor cells in vivo. In cultured murine 32D cells, SC-ααδ9 induced concentration-dependent apoptosis that was blocked by ectopic Bcl-2 expression. No apoptosis was detected in 32D cells treated with the congener SC-α109, which lacks the ability to disrupt IGF-1 signaling. After interleukin-3 withdrawal or etoposide treatment, exogenous IGF-1 prevented apoptosis and elevated levels of Cdc2, a biochemical indicator of a functional IGF-1 receptor pathway. In contrast, exogenous IGF-1 did not prevent apoptosis or loss of Cdc2 expression caused by SC-ααδ9. Furthermore, IGF-1 receptor overexpression failed to protect cells against SC-ααδ9-induced apoptosis. Kinetic analyses demonstrated that Cdc2 down-regulation after SC-ααδ9 treatment preceded both apoptosis and loss of the IGF-1 receptor, indicating that loss of Cdc2 was a direct effect of SC-ααδ9 treatment and not secondary to cell death. IGF-1 receptor autophosphorylation studies indicated that SC-ααδ9 did not interact directly with the IGF-1 receptor nor bind to the growth factor itself, suggesting a site of action distal to the IGF-1 receptor. In the SCCVII murine tumor model, a single i.p. injection of SC-ααδ9 caused a dose-dependent decrease in clonogenic cell survival. The IC_{50} of SC-ααδ9 was 35 mg/kg, comparable to 25 mg/kg carboplatin. The ability to induce IGF-1-resistant apoptosis distinguishes SC-ααδ9 from other apoptosis-inducing agents and suggests compounds of this class deserve further study as potential anticancer agents.

Growth factors and their receptors are key regulators of cell growth and survival. Growth factor involvement in carcinogenesis is common and includes overexpression of growth factor receptors (Baselga and Mendelsohn, 1994), enhanced kinase activity (Resnik et al., 1998), or stimulation of cancer cell growth by autocrine/paracrine mechanisms (Yee et al., 1989).

It has been postulated that cells require constant activation of survival pathways; among a variety of growth factors, insulin-like growth factor-1 (IGF-1) is the most effective protector against programmed cell death (apoptosis) induced by c-myc (Harrington et al., 1994). The antiapoptotic effects of IGF-1 have been reported to be more pronounced in vivo than in vitro (Resnicoff et al., 1995a,b). High levels of circulating IGF-1 have been found in prostate (Chan et al., 1998) and breast cancer patients (Peyrat et al., 1993). IGF-1 has been shown to protect cells against a variety of noxious stimuli, including cytokine withdrawal (Rodriguez-Tarduchy et al., 1992), overexpression of interleukin-1 β-converting enzyme (Jung et al., 1996), or clinically used anticancer agents (Sell et al., 1995; Dunn et al., 1997). The mechanism by which IGF-1 and its receptor protect cells from apoptosis involves elements of the mitogen-activated protein kinase and phosphoinositide 3-OH kinase [PI(3)K] pathways (Parrizas et al., 1997). Recent studies have identified a linear survival cascade consisting of IGF-1, the IGF-1 receptor, PI(3)K, and the serine/threonine kinase Akt (also termed protein kinase B or PKB) (Kulik and Weber, 1997). Activated Akt phosphorylates Bad, a proapoptotic member of the Bcl-2 family, thereby abolishing Bad's apoptotic properties (Datta et al., 1997; del Peso et al., 1997). An IGF-1 dependent, but PI(3)K and Akt-independent survival pathway also has been described (Kulik and Weber, 1998). The role of the IGF-1 receptor in cellular transformation has been studied extensively (Sell et al., 1994; Baserga, 1995), and controlling IGF-1 receptor function has become a target for anticancer therapy (Baserga, 1996). Despite the large body of evidence linking IGF-1 and its recep-

ABBREVIATIONS: IGF-1, insulin-like growth factor-1; PI(3)K, phosphoinositide 3-OH kinase; SC-ααδ9, 4-(benzyl-(2-[(2,5-diphenyl-oxazole-4-carbonyl)-amino]-ethyl)-carbamoyl)-2-decanoylamino butyric acid; IL-3, interleukin-3; FBS, fetal bovine serum; PAGE, polyacrylamide gel electrophoresis; SC-α109, 4-{(2-[(5-methyl-2-phenyl-oxazole-4-carbonyl)-amino]-ethyl)-carbamoyl}-2-decanoylamino butyric acid.

tor to the establishment of the transformed phenotype, however, therapies based on specific inhibition of IGF-1 receptor function are just beginning to emerge. Although several small molecules inhibiting various downstream targets of the IGF-1 receptor have been identified, few agents have been described that selectively inhibit IGF-1 receptor signaling.

Recent work from our laboratory has identified a novel antiproliferative agent, SC-$\alpha\alpha\delta$9 {4-(benzyl-(2-[(2,5-diphenyl-oxazole-4-carbonyl)-amino]-ethyl)-carbamoyl)-2-decanoylamino butyric acid}, from a combinatorial library modeled after natural product phosphatase inhibitors (Rice et al., 1997; Wipf et al., 1997; Vogt et al., 1998). Studies of SC-$\alpha\alpha\delta$9 in cultured mouse embryonic fibroblasts transformed with the simian virus large T antigen (SV40 MEF) showed selective inhibition of transformed cell growth and suggested that SC-$\alpha\alpha\delta$9 affected elements of IGF-1 signaling (Vogt et al., 1998). Because these studies involved long-term (48 h) exposure to the drug, however, the functional significance of these observations remains unclear. In addition, we were unable to unambiguously determine whether SC-$\alpha\alpha\delta$9 induced programmed cell death in these cells.

In the current study, we have extended our previous observations by investigating the induction of apoptosis by SC-$\alpha\alpha\delta$9 in 32D mouse myeloid progenitor cells, a well studied and convenient model for programmed cell death (Nunez et al., 1990). Not only did we demonstrate that SC-$\alpha\alpha\delta$9 caused apoptosis but also in contrast to interleukin-3 (IL-3) withdrawal or treatment with the clinically used antineoplastic agent etoposide, SC-$\alpha\alpha\delta$9-induced apoptosis was resistant to both an overabundance of IGF-1 and to overexpression of the IGF-1 receptor. Furthermore, although exogenous IGF-1 was able to maintain or elevate levels of Cdc2, a biochemical indicator of a functional IGF-1 receptor pathway, in IL-3-deprived and etoposide-treated cells, exogenous IGF-1 was unable to maintain Cdc2 expression after SC-$\alpha\alpha\delta$9 treatment. Finally, we demonstrated in vivo antitumor activity of SC-$\alpha\alpha\delta$9 against a murine small cell squamous carcinoma that is positive for the IGF-1 receptor. Taken together, our data suggest SC-$\alpha\alpha\delta$9 has potential for the treatment of IGF-1-dependent tumors.

Materials and Methods

Chemical Compounds. The synthesis of compounds SC-$\alpha\alpha\delta$9 and 4-[(2-[(5-methyl-2-phenyl-oxazole-4-carbonyl)-amino]-ethyl)-carbamoyl]-2-decanoylamino butyric acid (SC-α109) has been previously described (Rice et al., 1997; Wipf et al., 1997; Vogt et al., 1998). Compounds were isolated as racemic mixtures by chromatography on SiO$_2$ and characterized by NMR and high-resolution mass spectrometry.

Cell Culture. Four murine cell lines were used to probe the pharmacological effects of SC-$\alpha\alpha\delta$9. All cells were grown in a humidified atmosphere of 5% CO$_2$ at 37°C. 32D/neo and 32D/Bcl-2 (clone 23) cells were a kind gift from Dr. Daniel Johnson (University of Pittsburgh Cancer Institute). The IGF-1 receptor overexpressing line 32D/GR15 and the empty vector control 32D/mscv were a kind gift from Dr. Renato Baserga (Kimmel Cancer Center, Philadelphia, PA). These cells were established from 32D cells (clone 3) by transfection with wild-type human IGF-1 receptor cDNA subcloned into the mscv retroviral vector (Romano et al., 1999; Valentinis et al., 1999). All 32D subclones were maintained as previously described (Fabisiak et al., 1997) in RPMI 1640 medium containing 10% fetal bovine serum (FBS), 1% penicillin/streptomycin, 2 mM glutamine, 1.25 μg/ml fungizone, and 10% WEHI-3B conditioned medium as a source of IL-3,

an essential survival factor for 32D cells. LISN C4 cells, an NIH 3T3 cell line overexpressing human IGF-1 receptors (Kaleko et al., 1990) were obtained from Dr. Daniel Altschuler (University of Pittsburgh) and cultured in Dulbecco's modified Eagle's medium supplemented with 5% bovine calf serum as described (Altschuler et al., 1994). Murine SCCVII/SF squamous cell carcinoma tumors were produced by s.c. inoculation of 5×10^5 exponential growing tumor cells from culture in the right flank of 6- to 10-week-old female C3H/HeJ mice. SCCVII/SF cells were generated from these tumors by routine dissection and resuspension in Dulbecco's minimum essential medium containing 20% FBS supplemented with 1% penicillin/streptomycin (Johnson et al., 1993).

Antiproliferative and Antitumor Activity of SC-$\alpha\alpha\delta$9. The in vitro antiproliferative activity of SC-$\alpha\alpha\delta$9 was determined by our previously described 3-[4,5-dimethylthiazol-2-yl]-2,5-diphenyltetrazolium bromide (MTT) assay with 48 h of continuous drug exposure (Vogt et al., 1998). The in vivo effect of SC-$\alpha\alpha\delta$9 was evaluated and compared with other clinically used anticancer agents with the in vivo excision clonogenic cell survival assay (Johnson et al., 1993). Briefly, animals (three to four mice per treatment group) with established tumors (day 14 postimplant) were treated with a single i.p. dose of either vehicle (Cremophor EL/ethanol), SC-$\alpha\alpha\delta$9, cis-diamminedichloroplatinum (cisplatin), or cis-diammine(1,1-cyclobutane-dicarboxylato)platinum (carboplatin) at varying doses. After 24 h, tumors were harvested and single cell preparations generated as previously described (Johnson et al., 1993). Viable tumor cells as determined by trypan blue exclusion were plated at various dilutions and after 7 days of incubation, colonies were counted and numbers of clonogenic cells per gram of tumor were enumerated. The surviving fraction per gram of tumor was defined as the number of clonogenic tumor cells per gram of treated tumor divided by the number of clonogenic tumor cells per gram of control (untreated) tumor.

Nuclear Morphology. Exponentially growing 32D cells were treated with drug or vehicle for 24 h and collected by centrifugation (400g, 2 min). Cells were washed in PBS, fixed with 2% paraformaldehyde in PBS, and stained with Hoechst 33342 fluorescent dye (1 μg/ml) as described (Fabisiak et al., 1997). For quantitation of apoptosis, at least 300 cells were examined by fluorescence microscopy. Apoptotic cells were identified by condensed, bright-staining nuclei, usually very rounded, and sometimes fragmented into distinct sections.

Western Blotting. 32D cells were seeded at 1.5×10^5 cells/ml and treated 2 days later with drug or vehicle for various periods of time. Cell pellets were treated with lysis buffer (30 mM HEPES, pH 7.5, 1% Triton X-100, 10% glycerol, 5 mM MgCl$_2$, 25 mM NaF, 1 mM EGTA, 10 mM NaCl, 2 mM Na$_3$VO$_4$, 10 μg/ml trypsin inhibitor, 10 μg/ml aprotinin, 25 μg/ml leupeptin, 2 mM PMSF, and 6.4 mg/ml Sigma-104 phosphatase substrate). Cleared lysates were electrophoresed on 4 to 20% gradient gels (NOVEX, San Diego, CA), transferred to nitrocellulose, and immunoblotted with antibodies against Cdc2 (17) or the IGF-1 receptor β subunit (C-20; both from Santa Cruz Biotechnology, Santa Cruz, CA). Positive antibody reactions were visualized with peroxidase-conjugated secondary antibodies (Jackson ImmunoResearch, West Grove, PA) and an enhanced chemiluminescence detection system (Renaissance; NEN, Boston, MA) according to manufacturer's instructions. For quantitation of protein expression levels, X-ray films were scanned on a Molecular Dynamics personal SI densitometer and analyzed with the ImageQuant software package (version 4.1; Molecular Dynamics, Sunnyvale, CA). Band intensities were normalized to untreated control samples harvested at the same time.

IGF-1 Protection Experiments. As described above, 32D cells were treated with vehicle, SC-$\alpha\alpha\delta$9, or etoposide. For IL-3 withdrawal experiments, the cells were centrifuged for 5 min at 400g, washed five times in cold PBS, and resuspended in medium containing 10% FBS. Exogenous human recombinant IGF-1 (Sigma Chemical Co., St Louis, MO) was added to drug treated or IL-3-deprived

cells at the time of treatment. The percentage of cells with apoptotic nuclei was determined after 24 h as described above.

IGF-1 Receptor Tyrosine Phosphorylation Assay. For receptor autophosphorylation experiments, LISN C4 cells were grown to near confluency and growth arrested in 1% fetal calf serum for 24 h. SC-$\alpha\alpha\delta9$ or vehicle was included during the last 4 h of starvation, and cells were stimulated with IGF-1 (50 ng/ml) for 15 min. Monolayers were rinsed once with PBS and lysed in 50 mM HEPES, pH 7.5, 150 mM NaCl, 1.5 mM MgCl$_2$, 1 mM EGTA, 10% glycerol, 1% Triton X-100, 100 mM NaF, 10 mM sodium pyrophosphate, 0.2 mM Na$_3$VO$_4$, 1 mM 4-(2-aminoethyl)benzenesulfonyl fluoride, and 10 μg/ml aprotinin. Lysates were cleared by centrifugation for 2 min at 3000g. Then 250 to 500 μg of protein lysate were brought up to 1 or 2 volumes with washing buffer [20 mM HEPES, pH 7.5, 150 mM NaCl, 0.1% Triton X-100, 10% glycerol, 0.2 mM Na$_3$VO$_4$, 0.2 mM 4-(2-aminoethyl)benzenesulfonyl fluoride, and 2 μg/ml aprotinin] and immunoprecipitated overnight at 4°C with 1 μg of anti-IGF-1 receptor α-subunit antibody (IR-3, AB-1; Oncogene, Cambridge, MA) along with whole mouse IgG conjugated to agarose (Sigma Chemical Co.) as a carrier. Immunoprecipitates were collected by centrifugation at 13,000g for 4 min., washed three times with washing buffer, and boiled in SDS-polyacrylamide gel electrophoresis (PAGE) sample buffer. Supernatant proteins (25 μl) were separated on 4 to 12% Tris-glycine gradient gels and immunoblotted with a horseradish peroxidase-conjugated anti-phosphotyrosine antibody (PY20-HRP; Transduction Laboratories, Lexington, KY). Duplicate gels were blotted with a rabbit polyclonal anti-IGF-1 receptor β-subunit antibody (C-20; Santa Cruz Biotechnology) followed by a horseradish peroxidase-conjugated secondary antibody (Jackson ImmunoResearch, West Grove, PA) to confirm the presence of the receptor.

Results

SC-$\alpha\alpha\delta9$-Induced Apoptosis in 32D/neo But Not 32D/Bcl-2 Cells. The antiproliferative activity of SC-$\alpha\alpha\delta9$ against human MDA-MB-231 breast cancer and mouse embryonic cells has been reported previously (Wipf et al., 1997; Vogt et al., 1998). To more precisely probe mechanisms of SC-$\alpha\alpha\delta9$ antiproliferative activity, we used 32D cells as a convenient and well established model of programmed cell death (apoptosis) (Nunez et al., 1990). Cells were treated continuously with SC-$\alpha\alpha\delta9$ for 24 h and three different parameters indicative of apoptosis were measured. With Hoechst fluorescent dye staining, we found that SC-$\alpha\alpha\delta9$ caused concentration-dependent nuclear morphology changes characteristic of apoptosis in 32D cells (Figs. 1 and 2) with an IC$_{50}$ value of 15 μM. Apoptotic death was further confirmed by analysis of cellular DNA by agarose gel electrophoresis and by flow cytometry. Cells treated with SC-$\alpha\alpha\delta9$ also displayed internucleosomal DNA fragments ("ladders") as well as a population of cells with <2 N DNA content (data not shown). In contrast, SC-$\alpha109$, a congeneric analog of SC-$\alpha\alpha\delta9$, which we previously described and that differs from SC-$\alpha\alpha\delta9$ only in the lack of a phenyl and benzyl moiety (Vogt et al., 1998), did not induce changes in nuclear morphology or degradation of DNA into internucleosomal fragments (Fig. 2 and data not shown). Overexpression of the antiapoptosis gene product Bcl-2 protected 32D cells against SC-$\alpha\alpha\delta9$-induced apoptosis (Figs. 1 and 2), indicating that SC-$\alpha\alpha\delta9$ specifically affected signaling mechanisms leading to programmed cell death.

IGF-1 Protects against IL-3 Withdrawal and Etoposide But Not against SC-$\alpha\alpha\delta9$. To investigate whether IGF-1 survival pathways were functionally involved in the apoptotic properties of SC-$\alpha\alpha\delta9$, we first assessed whether
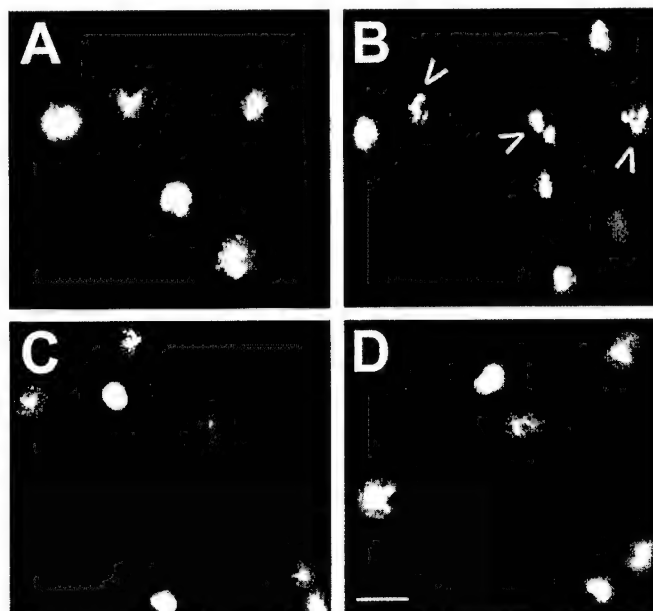

Fig. 1. SC-$\alpha\alpha\delta9$ induces apoptosis in 32D/neo but not 32D/Bcl-2 cells. 32D/neo (A, B) and 32D/Bcl-2 (C, D) cells were exposed to vehicle (A, C) or 30 μM SC-$\alpha\alpha\delta9$ (B, D) for 24 h, centrifuged, fixed, stained with Hoechst 33342 fluorescent dye, and photographed. Arrows denote apoptotic nuclei that show chromatin condensation and bright micronuclei. Bar = 3 μm.
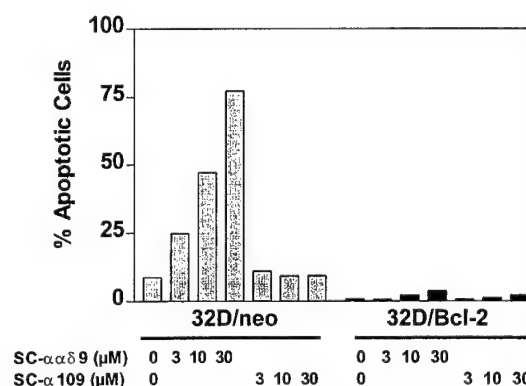

Fig. 2. A closely related analog of SC-$\alpha\alpha\delta9$ did not alter nuclear morphology and Bcl-2 expression blocked apoptosis induced by SC-$\alpha\alpha\delta9$. 32D/neo and 32D/Bcl-2 cells were treated with the indicated concentrations of either SC-$\alpha\alpha\delta9$ or SC-$\alpha109$ for 24 h, and stained with Hoechst 33342 fluorescent dye. Approximately 300 nuclei were scored for apoptotic morphology as described in the legend to Fig. 1. Apoptosis is expressed as the percentage of apoptotic cells in the entire cell population.

SC-$\alpha\alpha\delta9$-induced apoptosis could be overcome by high concentrations of IGF-1. To demonstrate that these cells, which lack insulin receptor substrate-1 and insulin receptor substrate-2 (Wang et al., 1993; Myers et al., 1996) responded to IGF-1 with increased cell survival, we treated IL-3-deprived cells with IGF-1. Withdrawal of IL-3 resulted in 57% apoptosis after 24 h and IGF-1 (100 ng/ml) reduced apoptosis in cytokine-deprived cells by 40% (Fig. 3). Cells were then treated with SC-$\alpha\alpha\delta9$ in the presence or absence of exogenous IGF-1 for 24 h and analyzed for apoptotic morphology. In contrast to IL-3 withdrawal, addition of IGF-1 did not significantly reduce apoptosis by SC-$\alpha\alpha\delta9$ (Fig. 3). IGF-1 did, however, cause a statistically significant decrease in the apoptosis induced by the clinically used antineoplastic agent etoposide, consistent with previous reports (Sell et al., 1995).
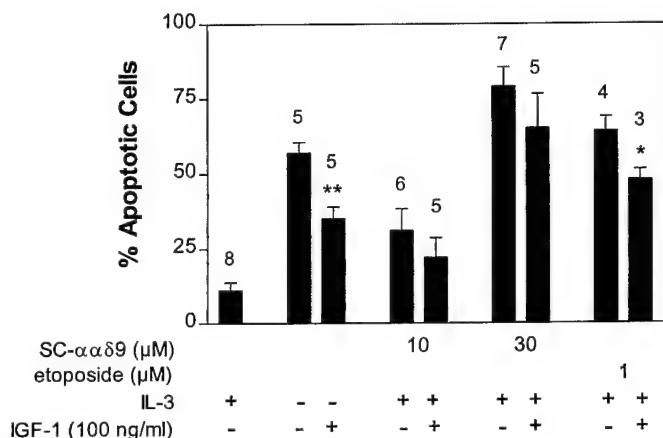
Fig. 3. IGF-1 protects against IL-3 withdrawal and etoposide but not against SC-ααδ9. 32D/neo cells were treated with SC-ααδ9 (10 or 30 μM), etoposide (1 μM), or were deprived of IL-3 for 24 h in the presence or absence of exogenously added IGF-1 (100 ng/ml). Data are means ± S.E. from the indicated numbers of independent experiments. Statistical analysis was by a two-tailed Student's t test assuming unequal variances compared with samples that did not receive IGF-1. $^{*}P < .05$, $^{**}P < .01$.

IGF-1 Prevents Down-Regulation of Cdc2 in Response to IL-3 Withdrawal, Partially after Etoposide, But Not after SC-ααδ9.

We next asked whether exogenous IGF-1 was able to maintain Cdc2 levels, a biochemical indicator of a functional IGF-1 receptor pathway, during SC-ααδ9 treatment. 32D/neo cells were treated with SC-ααδ9 or etoposide, or deprived of IL-3 for 24 h in the presence or absence of 100 ng/ml IGF-1. Western blotting of cellular lysates with an anti-Cdc2 antibody showed that IGF-1 prevented down-regulation of Cdc2 by cytokine withdrawal, but not by SC-ααδ9 (Fig. 4, top). An equitoxic concentration of etoposide (1 μM) did not appreciably decrease Cdc2. In contrast to SC-ααδ9, addition of IGF-1 to etoposide-treated cells resulted in elevated Cdc2 expression. Because there is no known involvement of etoposide in IGF-1 receptor signaling, our data support the hypothesis that SC-ααδ9 counteracted the ability of IGF-1 to maintain Cdc2 levels, presumably by affecting a target in the IGF-1 receptor pathway. Immunoblot analysis with an anti-IGF-1 receptor β-subunit antibody confirmed the presence of the IGF-1 receptor in all cases, although a significant loss of receptor occurred with 30 μM SC-ααδ9 and, to a lesser extent, with 1 μM etoposide (Fig. 4, middle).

IGF-1 Receptor Overexpression Did Not Protect Cells against SC-ααδ9.

Having demonstrated the inability of IGF-1 to rescue cells from apoptosis by SC-ααδ9, we next asked whether protection from SC-ααδ9 could be conferred by overexpression of the IGF-1 receptor. Three 32D subclones were examined for IGF-1 receptor expression by Western blot analysis and subjected to treatment with SC-ααδ9 for 24 h. As shown in Fig. 5A, 32D/neo cells had detectable IGF-1 receptor levels, whereas the 32D/mscv, which is a clonally derived cell line used as a control for the 32D/GR-15 cells, had very low IGF-1 receptor levels. As expected, the transfected 32D/GR-15 cells had the highest growth factor receptor levels. Figure 5B shows that SC-ααδ9 was equally active in three 32D cell lines despite the considerable difference in IGF-1 receptor levels Thus, we concluded that the apoptotic activity of SC-ααδ9 was independent of IGF-1 receptor density, which is consistent with a downstream target that is limiting in the pathway.

Kinetics of SC-ααδ9-Induced Cdc2 and IGF-1 Receptor Down-Regulation in 32D Cells.

Having demonstrated an involvement of IGF-1 survival mechanisms in SC-ααδ9-induced apoptosis, we next probed potential sites of action for SC-ααδ9 in the IGF-1 receptor pathway. First, to exclude the possibility that the effects of SC-ααδ9 on Cdc2 and the IGF-1 receptor were a result of cell death rather than a direct consequence of compound treatment, we examined the temporal relationships between apoptosis, Cdc2 levels, and IGF-1 receptor levels in 32D cells after exposure to SC-ααδ9. 32D/neo and 32D/Bcl-2 cells were treated with SC-ααδ9 (30 μM), harvested at various times, and assayed for nuclear morphology and expression of Cdc2 and IGF-1 receptor as described in *Materials and Methods*. A 12- to 24-h exposure to SC-ααδ9 was required to reduce protein levels of Cdc2 in
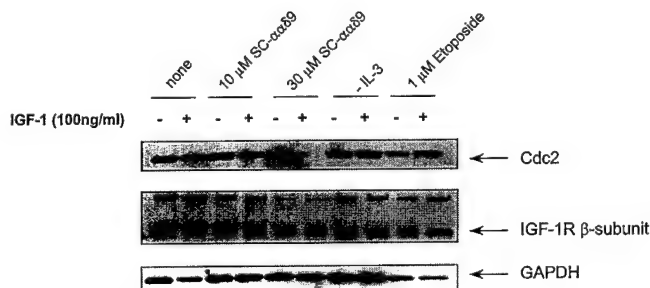

Fig. 4. IGF-1 prevents down-regulation of Cdc2 by IL-3 withdrawal, but not by SC-ααδ9. Cells were deprived of IL-3 (-IL-3) or treated with 1 μM etoposide, or 10 μM and 30 μM SC-ααδ9 in the presence or absence of exogenous IGF-1 (100 ng/ml). After 24 h, lysates were separated on SDS-PAGE and immunoblotted with anti-Cdc2 (top) or anti-IGF-1 receptor (middle) antibodies. Identical results were obtained in a second independent experiment. GAPDH, loading control.

Fig. 5. IGF-1 receptor overexpression does not protect against SC-ααδ9-induced apoptosis. A, three subclones of 32D cells (neo, mscv, GR-15) were analyzed for expression of the IGF-1 receptor by Western blotting with an anti-IGF-1 receptor β-subunit antibody. B, cells were treated with vehicle or SC-ααδ9 (30 μM) for 24 h and apoptotic nuclei were scored as described in *Materials and Methods*. Data are the average from two independent experiments ± range.

both cell lines (Figs. 6 and 7B). In contrast to Cdc2, however, loss of IGF-1 receptor was more pronounced in the 32D/neo cells and occurred earlier than in the Bcl-2 transfectants (Figs. 6 and 7C). Almost 50% of the IGF-1 receptor remained in Bcl-2-expressing cells 24 h after a 30-μM treatment with SC-$\alpha\alpha\delta$9, whereas only 15% remained in the 32D/neo cells. Nonspecific toxicity, presumably due to growth and survival factor deprivation, was observed in both cell lines after 2 days in culture and resulted in a loss of Cdc2 and IGF-1 receptor even in the absence of SC-$\alpha\alpha\delta$9 (Fig. 6). In 32D/neo cells, apoptosis showed some correlation with a loss of Cdc2, whereas in 32D/Bcl-2 cells loss of Cdc2 clearly preceded apoptosis (Fig. 7, A and B). For example, 32D/Bcl-2 cells treated with SC-$\alpha\alpha\delta$9 showed a near complete loss of Cdc2 at 24 h, a time when only 10% of cells were undergoing apoptosis (Fig. 7, A and B). After 12 h, when loss of Cdc2 became first apparent (Fig. 7B), IGF-1 receptor levels were essentially unchanged in both cell lines (Fig. 7C). These data suggest that reduction of Cdc2 levels was likely to be a direct effect of SC-$\alpha\alpha\delta$9, whereas loss of IGF-1 receptor may be a secondary effect.

Effects of SC-$\alpha\alpha\delta$9 on IGF-1 Receptor Autophosphorylation. To test the hypothesis that SC-$\alpha\alpha\delta$9 affected IGF-1 signaling at the receptor level, we attempted to detect IGF-1 receptor tyrosine phosphorylation as previously described (Vogt et al., 1998). Unfortunately, due to low phosphotyrosine levels, Western blot analysis of either lysates or IGF-1 receptor immunoprecipitates from 32D cells failed to indicate the presence of tyrosine-phosphorylated IGF-1 receptors in exponentially growing cells. Thus, we used LISN C4 cells, an NIH 3T3 cell line engineered to ectopically express high levels of the human IGF-1 receptor (Altschuler et al., 1994). IGF-1 stimulation of serum-starved cells resulted in increased IGF-1 receptor tyrosine phosphorylation (data not shown). Inclusion of a pharmacologically relevant concentration of SC-$\alpha\alpha\delta$9 at 4 h before IGF-1 stimulation did not inhibit tyrosine phosphorylation in response to IGF-1, indicating that SC-$\alpha\alpha\delta$9 did not directly interact with the IGF-1 receptor or the growth factor itself (data not shown). We have, however, seen inhibition of IGF-1 receptor autophos-
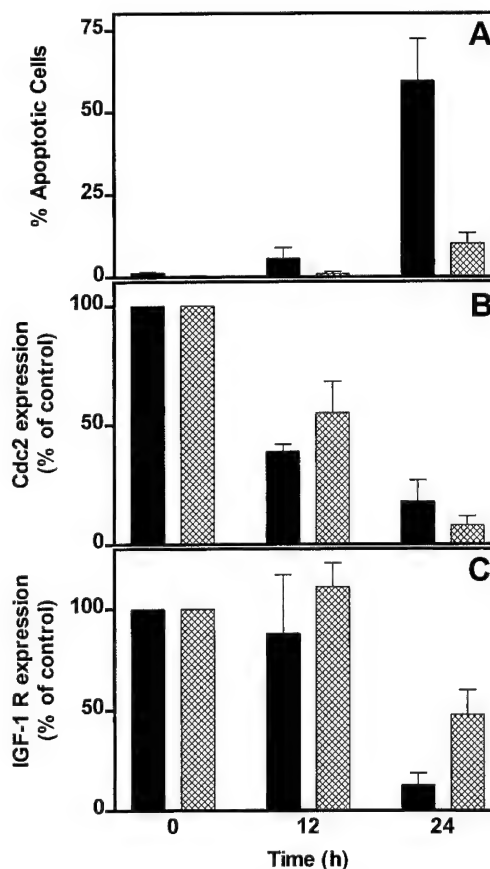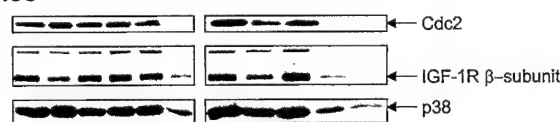

A. 32D/neo

B. 32D/Bcl-2

Fig. 6. Effects of SC-$\alpha\alpha\delta$9 on Cdc2 and IGF-1 receptor levels in 32D/neo and 32D/Bcl-2 cells. Exponentially growing 32D/neo (A) or 32D/Bcl-2 (B) cells were exposed to 30 μM SC-$\alpha\alpha\delta$9 or vehicle. At the indicated time points, cells were collected by centrifugation, lysed, and lysates separated on SDS-PAGE. Western blot analysis was performed with antibodies against Cdc2 and the IGF-1 receptor β-subunit. Equal protein loading was confirmed by immunoblotting the identical lysates with an anti-p38 mitogen-activated protein kinase antibody.

Fig. 7. Cdc2 down-regulation precedes apoptosis and loss of IGF-1 receptor. 32D/neo (■) and 32D/Bcl-2 (▨) cell suspensions were treated with vehicle or SC-$\alpha\alpha\delta$9 and divided into two aliquots at the time of harvesting. A, quantitation of apoptotic nuclei. Expression of Cdc2 (B) and IGF-1 receptor (C). Lysates were immunoblotted with anti-Cdc2 and anti-IGF-1 receptor antibodies as described in *Materials and Methods*. Protein bands were quantitated by densitometric scanning of the X-ray films, normalized to band intensity in untreated control samples, and expressed as percentage of control for each time point. Data are the averages of at least three independent experiments. Vertical bars represent S.E.M.

phorylation at higher concentrations of SC-$\alpha\alpha\delta$9 (100 μM) or after a 6-h exposure (data not shown).

SC-$\alpha\alpha\delta$9 Has In Vivo Antitumor Activity. Because SC-$\alpha\alpha\delta$9 has apoptotic activities that are independent of IGF-1, a property not shared with other apoptosis-inducing agents, we examined the antitumor effects of SC-$\alpha\alpha\delta$9 in a whole animal model. We used the in vivo excision clonogenic SCC-VII tumor cell survival assay because of the relatively small amount of drug required for antitumor studies and because it permits a quantitative estimation of in vivo cell kill (Johnson et al., 1993). We first determined that the murine SCCVII squamous cell carcinoma tumor cells grown in culture were sensitive to SC-$\alpha\alpha\delta$9. Figure 8A shows that SC-$\alpha\alpha\delta$9 inhibited SCCVII cell proliferation with an IC$_{50}$ value of 20 μM, which is similar to the IC$_{50}$ value observed in mouse embryonic fibroblasts transformed with simian virus 40 large T antigen but lower than that seen with human breast cancer cells (Vogt et al., 1998). We then examined the antitumor activity of SC-$\alpha\alpha\delta$9 in mice bearing established SCCVII tumors. A single i.p injection of SC-$\alpha\alpha\delta$9 decreased tumor cell viability in a dose-dependent manner (Fig. 8B). The IC$_{50}$ value for SC-$\alpha\alpha\delta$9 was 35 mg/kg; the maximum cell kill was a 60% decrease at 45 mg/kg (Fig. 8B). In comparison, a single
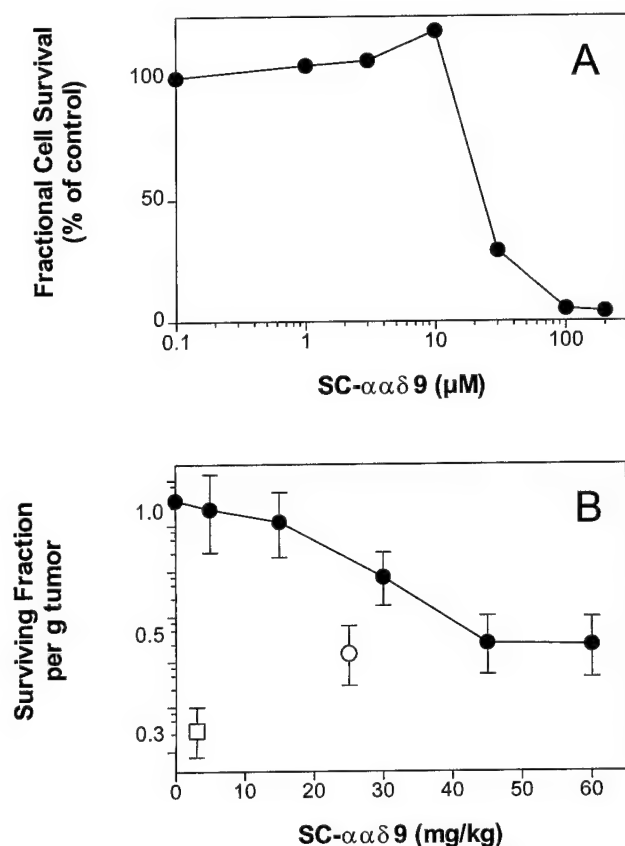
Fig. 8. Growth inhibition and antitumor activity of SC-$\alpha\alpha\delta$9 against SCCVII mouse small cell squamous carcinoma. A, growth inhibition assay. SCCVII cells were plated at 2000 cells/well in 96-well plates and treated with SC-$\alpha\alpha\delta$9 for 48 h. Cell survival was determined by the 3-[4,5-dimethylthiazol-2-yl]-2,5-diphenyltetrazolium bromide assay as described in *Materials and Methods*. B, tumor excision clonogenic assay. Mice bearing SCCVII murine small cell carcinomas were treated with a single dose of SC-$\alpha\alpha\delta$9 (●), cisplatin (□), or carboplatin (○). After 24 h, tumors were excised, and a single cell suspension was prepared. Cell survival was scored with a clonogenic assay and expressed in surviving fraction per gram of tumor. There were three or four mice in each group with points representing means ± S.D.

dose of ~2.5 mg/kg *cis*-diamminedichloroplatinum (cisplatin) or 25 mg/kg carboplatin was required for a 50% reduction in SCCVII tumor clonogenicity. Thus, SC-$\alpha\alpha\delta$9 had significant antitumor activity and was ~70% as potent as the clinically used carboplatin.

Discussion

SC-$\alpha\alpha\delta$9 is a simple, nonelectrophilic, small-molecule antiproliferative agent that was identified in a targeted array library modeled after complex natural product phosphatase inhibitors. This novel agent has antiproliferative activity against cancer cell lines in culture and is selective for the transformed phenotype. SC-$\alpha\alpha\delta$9 is a potent inhibitor of Cdc25 and PTP1B in vitro (Rice et al., 1997). SC-$\alpha\alpha\delta$9 also decreased Cdc2 protein levels (Vogt et al., 1998), a downstream event in the IGF-1 receptor-signaling cascade (Surmacz et al., 1992). The antiproliferative effects of SC-$\alpha\alpha\delta$9, however, have not yet been directly linked to any of these actions. In this report, we demonstrate that SC-$\alpha\alpha\delta$9, which is structurally unrelated to any known anticancer agent, caused Bcl-2 sensitive, but IGF-1 insensitive apoptosis in a

well established model cell system and effectively sacrificed murine tumor cells in vivo. Furthermore, we have extended our investigations of the IGF-1-related effects of SC-$\alpha\alpha\delta$9 to prove a functional involvement of IGF-1-mediated survival in SC-$\alpha\alpha\delta$9-induced apoptosis.

Numerous recent reports have established a role for IGF-1 and its receptor in the establishment of the transformed phenotype (for review, see Resnicoff and Baserga, 1998). Auto/paracrine stimulation by IGF-1 is thought to play a major role in transformation by viral oncogenes (Baserga, 1993). High levels of circulating IGF-1 have been associated with an increased risk of prostate cancer (Chan et al., 1998). Studies in cultured cells have demonstrated that IGF-1 was able to protect cells from a variety of apoptotic stimuli, including the clinically used antineoplastic agents camptothecin, 5-fluorouracil, tamoxifen, and methotrexate (Dunn et al., 1997), as well as cisplatin and doxorubicin (Geier et al., 1995), suggesting that IGF-1 also may play a role in resistance to cancer chemotherapy.

Several approaches aimed at IGF-1 receptor inactivation have been shown to reverse the transformed phenotype, among them treatment with antisense oligonucleotides (Resnicoff et al., 1995b), deletion of the IGF-1 receptor gene by homologous recombination (Sell et al., 1994), or peptide analogs that interfere with autocrine IGF-1 receptor stimulation (Pietrzkowski et al., 1993; Hayry et al., 1995). Despite the large body of evidence that IGF-1 and the IGF-1 receptor are rational targets for anticancer drug design, few small-molecule-, cell-permeable-, specific disrupters of IGF-1 signaling have been identified to date. There are, however, examples of agents that specifically inhibit PI(3)K, a downstream event in the IGF-1 signaling pathway, some of which have shown promising antitumor activity (Norman et al., 1996).

In contrast to other growth factors, IGF-1 is also a potent antiapoptotic factor. To investigate a functional role of IGF-1 or its receptor in SC-$\alpha\alpha\delta$9 toxicity, we chose 32D mouse myeloid progenitor cells as a well established model for apoptotic death, and found that SC-$\alpha\alpha\delta$9 caused concentration-dependent apoptosis in these cells. Consistent with previous reports (Rodriguez-Tarduchy et al., 1992), IGF-1 protected 32D cells against apoptosis induced by cytokine withdrawal, but did not rescue cells from SC-$\alpha\alpha\delta$9-induced apoptosis. IGF-1 also afforded protection against the apoptotic effects of etoposide, an agent whose mechanism of action is not known to involve inhibition of growth factor signaling. Furthermore, IGF-1 maintained or elevated expression levels of Cdc2 in the absence of IL-3 and during etoposide treatment, but not after treatment with equitoxic concentrations of SC-$\alpha\alpha\delta$9. It should be noted, however, that IGF-1 protection from apoptosis was not complete and was only observed at high concentrations of IGF-1, perhaps because IGF-1 delays apoptosis rather than prevents it. Although all IGF-1 protection experiments were scored 24 h after exposure to apototic stimuli, it is possible that the antiapoptotic effects of IGF-1 could be more pronounced at earlier time points. We then examined whether overexpression of the IGF-1 receptor rendered cells less sensitive to SC-$\alpha\alpha\delta$9 and found that SC-$\alpha\alpha\delta$9-induced apoptosis was independent of IGF-1 receptor levels. The cells were, however, protected from apoptosis by SC-$\alpha\alpha\delta$9 by overexpression of the antiapoptotic gene product Bcl-2. Bcl-2 has been shown to protect against a number of apoptotic stimuli

such as chemotherapeutic drugs, irradiation, or growth factor deprivation but it does not prevent cell death by complement-mediated lysis, tumor necrosis factor-α, or hydrogen peroxide, which often induce necrotic rather than apoptotic cell death (Reed, 1994). Bcl-2 prolongs cell survival without inducing proliferation, presumably by blocking a final common pathway in the execution of programmed cell death. Bcl-2 protection against SC-$\alpha\alpha\delta9$ suggests that the compound acts on a specific intracellular target which, in turn, triggers the apoptotic machinery. Furthermore, although ectopic expression of Bcl-2 prevented apoptosis, it did not prevent down-regulation of Cdc2 in the presence of SC-$\alpha\alpha\delta9$, indicating that the decrease in Cdc2 levels was a direct result of compound treatment and not secondary to cell death. Because Cdc2 is a biochemical indicator of IGF-1 signaling, these data suggest that SC-$\alpha\alpha\delta9$ perturbs the IGF-1 receptor pathway. Whether the decrease in Cdc2 levels is important for programmed cell death by SC-$\alpha\alpha\delta9$ is currently not known. Future experiments should focus on this issue.

The most obvious explanation for the above-mentioned results would be that SC-$\alpha\alpha\delta9$ acts at the level of the IGF-1 receptor itself. Receptor autophosphorylation studies in NIH 3T3 cells, however, indicated that a short-term exposure to SC-$\alpha\alpha\delta9$ did not affect IGF-1 tyrosine phosphorylation, but that concentrations higher than those inducing apoptosis or prolonged exposure times were required for a decrease in receptor autophosphorylation. Several important conclusions can be drawn from these data. First, SC-$\alpha\alpha\delta9$ does not bind to or inactivate the growth factor itself, as is the case with suramin (Middaugh et al., 1992). Second, SC-$\alpha\alpha\delta9$ does not bind to the extracellular portion of the IGF-1 receptor. Third, it is unlikely that SC-$\alpha\alpha\delta9$ directly inhibits receptor tyrosine kinase activity. This is consistent with its lack of in vitro inhibition of Cdc2 (Rice et al., 1997), or c-Src tyrosine kinase (data not shown). Thus, it seems most likely that the molecular target of SC-$\alpha\alpha\delta9$ is intracellular and distal to the IGF-1 receptor.

In summary, SC-$\alpha\alpha\delta9$ is a novel inducer of apoptosis whose effects, in contrast to etoposide or IL-3 withdrawal, could not be overcome by high levels of exogenous IGF-1 or by overexpression of the IGF-1 receptor. Unlike IL-3 withdrawal, SC-$\alpha\alpha\delta9$ also compromised the ability of IGF-1 to maintain levels of Cdc2, a downstream effector of an intact IGF-1 receptor pathway. These data suggest a functionally significant involvement of the IGF-1 receptor pathway in SC-$\alpha\alpha\delta9$-induced apoptosis. The ability of SC-$\alpha\alpha\delta9$ to counteract IGF-1 action in whole cells is apparently not due to inhibition of the IGF-1 receptor tyrosine kinase, but more work is needed to more precisely determine the molecular target(s) of SC-$\alpha\alpha\delta9$. Even though SC-$\alpha\alpha\delta9$'s mechanism of action is not completely understood, its independence from growth factor-mediated survival sets SC-$\alpha\alpha\delta9$ apart from other structurally and mechanistically unrelated antineoplastic agents such as antimetabolites (methotrexate), anthracyclines (doxorubicin), antiestrogens (tamoxifen), or topoisomerase inhibitors (camptothecin, etoposide), all of which are sensitive to the survival effects of IGF-1 or the IGF-1 receptor. Coupled with SC-$\alpha\alpha\delta9$'s selective in vitro activity for transformed cells and promising antitumor activity in an in vivo tumor model that is positive for the IGF-1 receptor, our data suggest that SC-$\alpha\alpha\delta9$ or related compounds warrant further study as potential agents for the treatment of growth factor-dependent tumors.

References

Altschuler D, Yamamoto K and Lapetina EG (1994) Insulin-like growth factor-1-mediated association of p85 phosphatidylinositol 3-kinase with pp 185: Requirement of SH2 domains for in vivo interaction. *Mol Endocrinol* **8:**1139–1146.

Baselga J and Mendelsohn J (1994) Receptor blockade with monoclonal antibodies as anti-cancer therapy. *Pharmacol Ther* **64:**127–154.

Baserga R (1993) Gene regulation by IGF-I. *Mol Reprod Dev* **35:**353–356.

Baserga R (1995) The insulin-like growth factor I receptor: A key to tumor growth? *Cancer Res* **55:**249–252.

Baserga R (1996) Controlling IGF-receptor function: A possible strategy for tumor therapy. *Trends Biotechnol* **14:**150–152.

Chan JM, Stampfer MJ, Giovannucci E, Gann PH, Ma J, Wilkinson P, Hennekens CH and Pollak M (1998) Plasma insulin-like growth factor-I and prostate cancer risk: A prospective study. *Science (Wash DC)* **279:**563–566.

Datta SR, Dudek H, Tao X, Masters S, Fu H, Gotoh Y and Greenberg ME (1997) Akt phosphorylation of BAD couples survival signals to the cell-intrinsic death machinery. *Cell* **91:**231–241.

del Peso L, Gonzalez-Garcia M, Page C, Herrera R and Nunez G (1997) Interleukin-3-induced phosphorylation of BAD through the protein kinase Akt. *Science (Wash DC)* **278:**687–689.

Dunn SE, Hardman RA, Kari FW and Barrett JC (1997) Insulin-like growth factor 1 (IGF-1) alters drug sensitivity of HBL100 human breast cancer cells by inhibition of apoptosis induced by diverse anticancer drugs. *Cancer Res* **57:**2687–2693.

Fabisiak JP, Kagan VE, Ritov VB, Johnson DE and Lazo JS (1997) Bcl-2 inhibits selective oxidation and externalization of phosphatidylserine during paraquat-induced apoptosis. *Am J Physiol* **272:**C675–C684.

Geier A, Beery R, Haimsohn M and Karasik A (1995) Insulin-like growth factor-1 inhibits cell death induced by anticancer drugs in the MCF-7 cells: Involvement of growth factors in drug resistance. *Cancer Invest* **13:**480–486.

Harrington EA, Bennett MR, Fanidi A and Evan GI (1994) c-Myc-induced apoptosis in fibroblasts is inhibited by specific cytokines. *EMBO J* **13:**3286–3295.

Hayry P, Myllarniemi M, Aavik E, Alatalo S, Aho P, Yilmaz S, Raisanen-Sokolowski A, Cozzone G, Jameson BA and Baserga R (1995) Stabile D-peptide analog of insulin-like growth factor-1 inhibits smooth muscle cell proliferation after carotid ballooning injury in the rat. *FASEB J* **9:**1336–1344.

Johnson CS, Chang MJ, Yu WD, Modzelewski RA, Grandis JR, Vlock DR and Furmanski P (1993) Synergistic enhancement by interleukin-1 alpha of cisplatin-mediated antitumor activity in RIF-1 tumor-bearing C3H/HeJ mice. *Cancer Chemother Pharmacol* **32:**339–346.

Jung Y, Miura M and Yuan J (1996) Suppression of interleukin-1 beta-converting enzyme-mediated cell death by insulin-like growth factor. *J Biol Chem* **271:**5112–5117.

Kaleko M, Rutter WJ and Miller AD (1990) Overexpression of the human insulinlike growth factor I receptor promotes ligand-dependent neoplastic transformation. *Mol Cell Biol* **10:**464–473.

Kulik G, Klippel A and Weber MJ (1997) Antiapoptotic signalling by the insulin-like growth factor I receptor, phosphatidylinositol 3-kinase, and Akt. *Mol Cell Biol* **17:**1595–1606.

Kulik G and Weber MJ (1998) Akt-dependent and -independent survival signaling pathways utilized by insulin-like growth factor I. *Mol Cell Biol* **18:**6711–6718.

Middaugh CR, Mach H, Burke CJ, Volkin DB, Dabora JM, Tsai PK, Bruner MW, Ryan JA and Marfia KE (1992) Nature of the interaction of growth factors with suramin. *Biochemistry* **31:**9016–9024.

Myers MG Jr, Zhang Y, Aldaz GA, Grammer T, Glasheen EM, Yenush L, Wang LM, Sun XJ, Blenis J, Pierce JH and White MF (1996) YMXM motifs and signaling by an insulin receptor substrate 1 molecule without tyrosine phosphorylation sites. *Mol Cell Biol* **16:**4147–4155.

Norman BH, Shih C, Toth JE, Ray JE, Dodge JA, Johnson DW, Rutherford PG, Schultz RM, Worzalla JF and Vlahos CJ (1996) Studies on the mechanism of phosphatidylinositol 3-kinase inhibition by wortmannin and related analogs. *J Med Chem* **39:**1106–1111.

Nunez G, London L, Hockenbery D, Alexander M, McKearn JP and Korsmeyer SJ (1990) Deregulated Bcl-2 gene expression selectively prolongs survival of growth factor-deprived hemopoietic cell lines. *J Immunol* **144:**3602–3610.

Parrizas M, Saltiel AR and LeRoith D (1997) Insulin-like growth factor 1 inhibits apoptosis using the phosphatidylinositol 3'-kinase and mitogen-activated protein kinase pathways. *J Biol Chem* **272:**154–161.

Peyrat JP, Bonneterre J, Hecquet B, Vennin P, Louchez MM, Fournier C, Lefebvre J and Demaille A (1993) Plasma insulin-like growth factor-1 (IGF-1) concentrations in human breast cancer. *Eur J Cancer* **29:**A492–A497.

Pietrzkowski Z, Mulholland G, Gomella L, Jameson BA, Wernicke D and Baserga R (1993) Inhibition of growth of prostatic cancer cell lines by peptide analogues of insulin-like growth factor 1. *Cancer Res* **53:**1102–1106.

Reed JC (1994) Bcl-2 and the regulation of programmed cell death. *J Cell Biol* **124:**1–6.

Resnicoff M, Abraham D, Yutanawiboonchai W, Rotman HL, Kajstura J, Rubin R, Zoltick P and Baserga R (1995a) The insulin-like growth factor I receptor protects tumor cells from apoptosis in vivo. *Cancer Res* **55:**2463–2469.

Resnicoff M and Baserga R (1998) The role of the insulin-like growth factor I receptor in transformation and apoptosis. *Ann NY Acad Sci* **842:**76–81.

Resnicoff M, Burgaud JL, Rotman HL, Abraham D and Baserga R (1995b) Correla-

tion between apoptosis, tumorigenesis, and levels of insulin-like growth factor I receptors. *Cancer Res* **55:**3739–3741.

Resnik JL, Reichart DB, Huey K, Webster NJ and Seely BL (1998) Elevated insulin-like growth factor I receptor autophosphorylation and kinase activity in human breast cancer. *Cancer Res* **58:**1159–1164.

Rice RL, Rusnak JM, Yokokawa F, Yokokawa S, Messner DJ, Boynton AL, Wipf P and Lazo JS (1997) A targeted library of small-molecule, tyrosine, and dual-specificity phosphatase inhibitors derived from a rational core design and random side chain variation. *Biochemistry* **36:**15965–15974.

Rodriguez-Tarduchy G, Collins MK, Garcia I and Lopez-Rivas A (1992) Insulin-like growth factor-I inhibits apoptosis in IL-3- dependent hemopoietic cells. *J Immunol* **149:**535–540.

Romano G, Prisco M, Zanocco-Marani T, Peruzzi F, Valentinis B and Baserga R (1999) Dissociation between resistance to apoptosis and the transformed phenotype in IGF-I receptor signaling. *J Cell Biochem* **72:**294–310.

Sell C, Baserga R and Rubin R (1995) Insulin-like growth factor I (IGF-I) and the IGF-I receptor prevent etoposide-induced apoptosis. *Cancer Res* **55:**303–306.

Sell C, Dumenil G, Deveaud C, Miura M, Coppola D, DeAngelis T, Rubin R, Efstratiadis A and Baserga R (1994) Effect of a null mutation of the insulin-like growth factor I receptor gene on growth and transformation of mouse embryo fibroblasts. *Mol Cell Biol* **14:**3604–3612.

Surmacz E, Nugent P, Pietrzkowski Z and Baserga R (1992) The role of the IGF1 receptor in the regulation of cdc2 mRNA levels in fibroblasts. *Exp Cell Res* **199:**275–278.

Valentinis B, Romano G, Peruzzi F, Morrione A, Prisco M, Soddu S, Cristofanelli B, Sacchi A and Baserga R (1999) Growth and differentiation signals by the insulin-like growth factor 1 receptor in hemopoietic cells are mediated through different pathways. *J Biol Chem* **274:**12423–12430.

Vogt A, Rice RL, Settineri CE, Yokokawa F, Yokokawa S, Wipf P and Lazo JS (1998) Disruption of insulin-like growth factor-1 signaling and down-regulation of cdc2 by SC-$\alpha\alpha\delta$9, a novel small molecule antisignaling agent identified in a targeted array library. *J Pharmacol Exp Ther* **287:**806–813.

Wang LM, Myers MGJ, Sun XJ, Aaronson SA, White M and Pierce JH (1993) IRS-1: Essential for insulin- and IL-4-stimulated mitogenesis in hematopoietic cells. *Science (Wash DC)* **261:**1591–1594.

Wipf P, Cunningham A, Rice RL and Lazo JS (1997) Combinatorial synthesis and biological evaluation of library of small-molecule Ser/Thr-protein phosphatase inhibitors. *Bioorg Med Chem* **5:**165–177.

Yee D, Paik S, Lebovic GS, Marcus RR, Favoni RE, Cullen KJ, Lippman ME and Rosen N (1989) Analysis of insulin-like growth factor I gene expression in malignancy: Evidence for a paracrine role in human breast cancer. *Mol Endocrinol* **3:**509–517.

The Journal of

PHARMACOLOGY
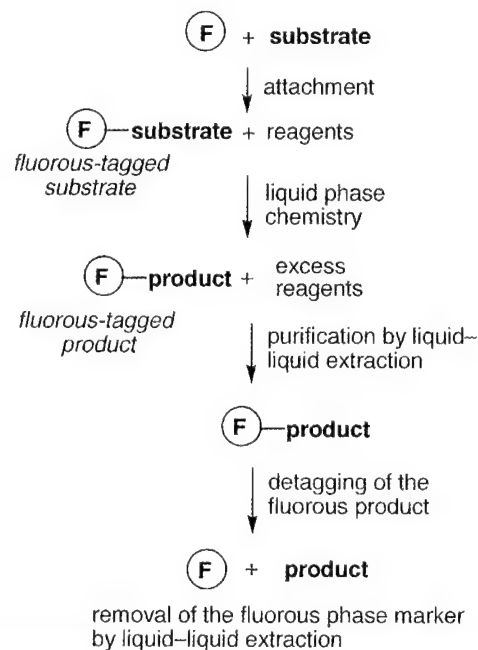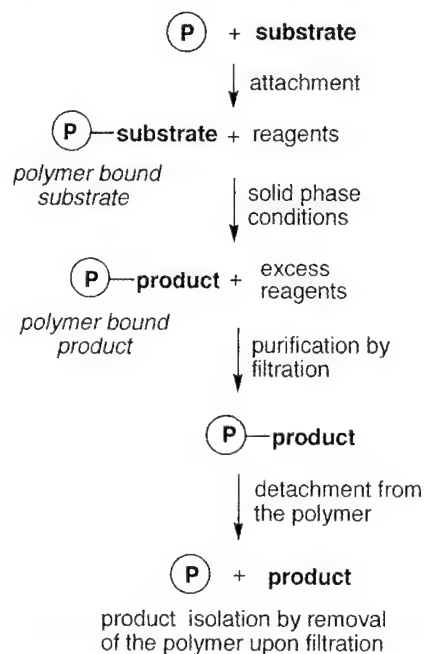
And Experimental Therapeutics

Solid Phase Synthesis vs. Fluorous Tag Strategies for Combinatorial Chemistry

A Publication of the American Society for Pharmacology and Experimental Therapeutics

Edited for the Society by S. J. Enna

Perspectives in Pharmacology

Combinatorial Chemistry and Contemporary Pharmacology

JOHN S. LAZO and PETER WIPF

Departments of Pharmacology and Chemistry, The Fiske Drug Discovery Laboratory and The Combinatorial Chemistry Center, University of Pittsburgh, Pittsburgh, Pennsylvania

Accepted for publication February 7, 2000   This paper is available online at http://www.jpet.org

ABSTRACT

Both solid- and liquid-phase combinatorial chemistry have emerged as powerful tools for identifying pharmacologically active compounds and optimizing the biological activity of a lead compound. Complementary high-throughput in vitro assays are essential for compound evaluation. Cell-based assays that use optical endpoints permit investigation of a wide variety of functional properties of these compounds including specific intracellular biochemical pathways, protein-protein interactions, and the subcellular localization of targets. Integration of combinatorial chemistry with contemporary pharmacology now represents an important factor in drug discovery and development.

This is an exceptionally exciting time in the field of pharmacology. The environment for the identification of new therapeutic targets and agents that interact with these targets has rapidly changed with the application of genetic tools and genomics. Extrapolation from the genomic sequencing of lower organisms suggests that there will be a 10-fold increase in the number of potential human therapeutic targets in the next several years with the completion of the Human Genome Project (Drews, 1996). This is leading to a fundamental transformation in pharmacology; no longer is there a dearth of molecular targets for small molecules. Rather, the emphasis is now on validating whether or not the targets are appropriate for therapeutic intervention, on generating large arrays of compounds that represent diverse portions of "chemical space", and developing methods to quickly assess the credentials of small molecules as target disrupters. We believe many of the tools and reagents that are being developed to facilitate this scientific activity will emerge as vital for future academic pharmacological research. Perhaps most important will be the exploitation of combinatorial chemistry libraries, which are becoming widely available. Although we cannot comprehensively review this broad topic here, the goal of this brief commentary is to portray some of the strategies and potentials of combinatorial chemistry libraries as they relate to pharmacological studies.

Discussion

Combinatorial Chemistry Strategies. Combinatorial chemistry has emerged because of genomics and new efficient biological screening strategies and is widely cited as a paradigm shift in the way that new small molecule lead structures will be identified (Choong and Ellman, 1996; Gold and Alper, 1997; Obrecht and Villalgordo, 1998). Traditionally, natural product extracts or industrial collections of randomly synthesized organic molecules were screened to discover "hits", which were then optimized in an iterative process by the synthesis of derivatives. Combinatorial synthesis (Curran and Wipf, 1997) is now supplementing traditional strategies at both the lead discovery and the lead optimization stage. Surveys of very recent combinatorial chemistry-derived structure activity relationships serve to underline the tremendous impact that this technology already has had on drug discovery in industry and academe (Dolle and Nelson, 1999).

Combinatorial synthesis assembles building blocks to make new molecules. Large libraries (>100,000) can be made by assembling all possible combinations of a set of building blocks, and new lead compounds can be identified by using techniques like split-mix synthesis (Gallop et al., 1994; Gordon et al., 1994; Nefzi et al., 1997) coupled with suitable tagging or deconvolution strategies (Nestler et al., 1994) (Fig. 1). Smaller discovery libraries (<10,000) can be made as individual components by rapidly advancing techniques of automated parallel synthesis (Hogan, 1996), and the further
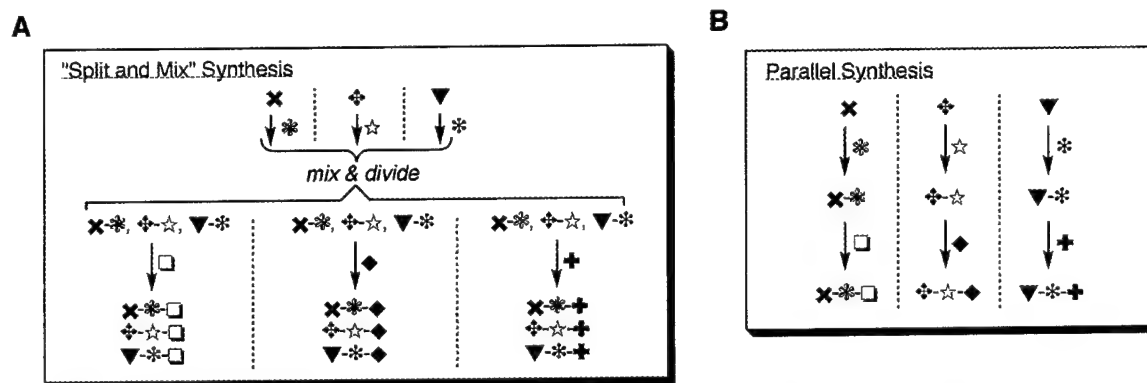

A

B

Fig. 1. Combinatorial chemistry strategies. A, aggregate libraries can be made by aggregate synthesis (split synthesis or solution synthesis of mixtures) or by mixing individual members of a library (>10^6 compounds, deconvolution necessary). B, libraries of individual compounds can be made by serial (that is, traditional) synthesis or parallel synthesis (automated solid support and solution) (<10^4 compounds, focused libraries, no encoding necessary, one compound/well).

optimization of a lead discovered in a combinatorial process follows naturally because the building blocks are already in place (Fig. 1). Focused (directed screening) or secondary libraries have a more narrowly defined structural focus and carve out structure-activity relationships for increasing potency and selectivity that are critical in a lead molecule. In this strategy, the synthesis of tailored building blocks is often the rate-limiting step, and the synthetic sequence can exceed eight steps and tolerate some low-yielding methodology; parallel purification techniques and other specialized combinatorial chemistry methods can be used. Most of the commercial automation vendors are now aggressively targeting these applications where sample size remains in the 100s or low 1000s. Ideally, products will be well characterized and of high purity, but very often an arbitrary purity cutoff of 80% or higher will suffice to limit the number of "false positive" hits. Lower purities, which often are the result of incomplete reactions, can be tolerated if the structure of the major side products is known.

The lead(s) may come from an existing program, from a screening hit from a discovery library or a compound database (including virtual libraries), from the literature or from a competitor's compound, or from a rational design structure-based approach. The integration of structure-guided design and combinatorial chemistry is referred to as the targeted diversity approach. The ArQule group has used this approach for the successful preparation of a library of HIV protease inhibitors (Hogan, 1997). Structurally complex natural products form a particularly attractive resource for targeted array design of exploratory libraries. For example, a library of dual-specificity phosphatase inhibitors was based on the structures of the natural product serine-threonine protein phosphatase inhibitors microcystin LR and calyculin A (Fig. 2) (Rice et al., 1997; Wipf et al., 1997).

Much of the efficiency of combinatorial synthesis strategies is due to improvements in the work-up of organic reactions by attachment of the substrate molecule to an insoluble resin, most often a polystyrene bead, 100 to 150 μm in diameter,
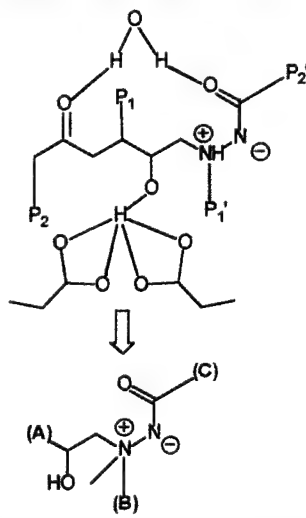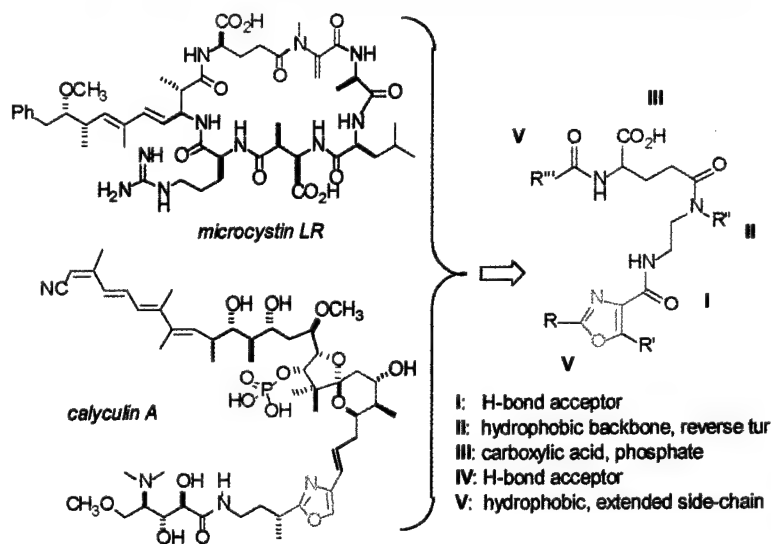

Fig. 2. Library scaffold design. This illustrates how a pharmacophore can be designed from natural products (for additional details, see Rice et al., 1997 and Wipf et al., 1997).

copolymerized with divinyl benzene. The technique of solid-phase organic synthesis (SPOS) is a logical extension toward small molecule synthesis of the methodology from solid-phase peptide (Jung, 1996) and oligonucleotide (Pirrung, 1997) synthesis where supported phase synthesis has emerged as the medium of choice for repetitive couplings of standard building blocks.

A central aim of SPOS is to overcome the unpredictable physical characteristics of synthetic intermediates and products by covalent attachment to a polymeric support. Purification is then facilitated by removal of excess reagents and by-products by filtration. This heterogeneous approach represents the most widely applied variant of the general idea to simplify isolation of pure compounds. Some of the advantages of SPOS include: excess reagents can be used; the reactions can be driven to completion; filtration can be used for rapid purification; automation is easily achieved; and relative site isolation. Among the limitations of SPOS are requirements for linkage or cleavage steps that may restrict the possible chemical reactions, restrained control of reaction stoichiometry, difficulty in purification after low-yielding steps, time-consuming conversion of solution-phase chemistry to solid-phase chemistry, and scale-up restrictions. In part because of the limitations of SPOS, alternative strategies have been developed that exploit the benefits of conducting liquid-phase polymer-supported synthesis in a homogeneous environment. In this approach, separation is accomplished via membrane ultrafiltration, precipitation, or crystallization. More recently, solution-phase methods have emerged to complement solid-phase techniques. To date, most of these methods are founded on acid-base chemistry and sequestration-enabling reagents (Gayo and Suto, 1997; Parlow et al., 1997; Siegel et al., 1997). The pioneering acid-base extraction work of Boger and coworkers (Boger et al., 1996), for example, clearly shows that hundreds to thousands of individual pure molecules can be made by solution synthesis, if the purification methods are simple enough. The use of fluorous tags provides organic compounds with sufficient affinity to perfluorinated solvents that are immiscible with water and standard organic solvents to allow selective purification via fluorous liquid-liquid extraction or fluorinated silica gel (Fig. 3) (Studer et al., 1997). Thus, the advantages of liquid-phase synthesis are that all organic reactions can be used, extensive purification and compound characterization is possible after every step, and large-scale syntheses are possible. Solution-phase parallel synthesis is, however, more labor and time intensive than SPOS, and automation is more difficult. In addition, driving reaction to completion is challenging and repeated chromatographic purification is often necessary.

An important aspect of any library synthesis is quality control. Both the identity and purity of the library samples has to be ascertained for all or a representative selection of compounds. Among the currently available methods, liquid chromatography-mass spectroscopy, which has almost become the universal standard, and high-throughput NMR are particularly valuable. IR is an excellent method for on-bead reaction control (Yan, 1998). Gel-phase NMR or magic angle spinning-NMR can also be used for assaying the structure of samples still attached to solid support.

Principles of Rapid Compound Analyses. Traditional pharmacological approaches using intact animals, ex vivo preparations, and cell-based or cell-free (in vitro) assays readily accommodate analysis of individual compounds. The compound libraries derived from combinatorial chemistry, however, demand high-throughput detection systems to optimize their utility. Mindful that the quantity of each element in the libraries is limiting and not always pure, cell-free, in vitro systems have been the primary screening tools either in a microtiter plate format (96, 384, or 1536 wells per plate) or in a solid or semisolid matrix. An excellent review describing the merits of different automation schemes and assay platforms has been provided elsewhere (Houston and Banks, 1997). It seems likely that the highly popular liquid workstations commonly found in pharmaceutical laboratories will begin to populate academic laboratories as the advantages of rapid screening are appreciated and their price decreases. The most popular format for cell-free high-throughput systems is the 96-well plate because of the availability of a multitude of detection systems. Disruption of enzyme activity or protein-protein interactions can be moni-
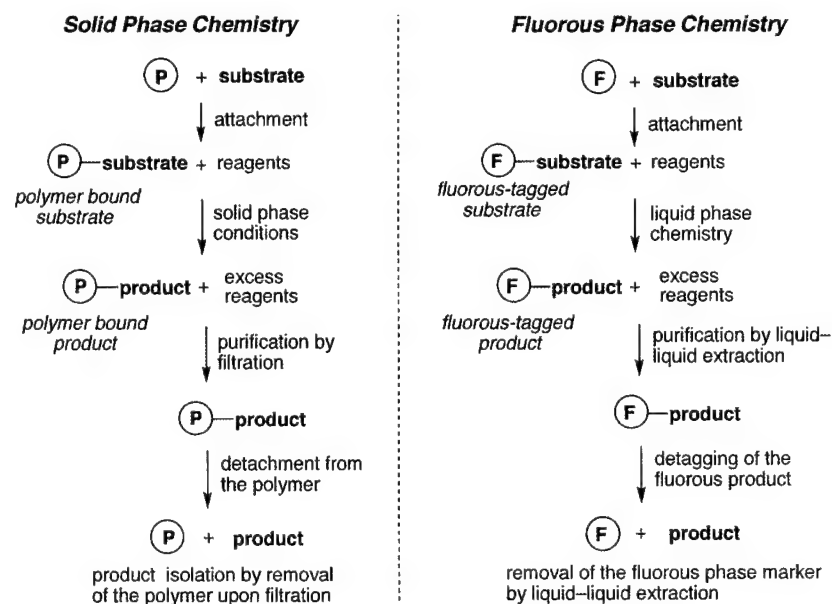

Fig. 3. Solid-phase synthesis versus fluorous tag strategies.

tored using a variety of endpoints including radioactivity, fluorescence, absorbance, surface plasmon resonance, and immunoreactivity. Of particular concern is the use of only small amounts of reagents, including the test samples, and a relatively rapid but robust assay system. The initial strategy used to evaluate the compounds usually seeks a qualitative or semiquantitative answer, namely do any of the compounds affect the system in a desirable manner. More refined studies of the nature of the activity are reserved to a time when purer compound and larger quantities are available. Thus, complete concentration-response curves, so highly desired by pharmacologists, often must wait. Reagent composition, such as the assay protein, is often designed for quick isolation and purification. Thus, recombinant fusion proteins with tags that facilitate purification, such as glutathione *S*-transferase or multiple histidines, are favored. Studies from several laboratories serve to illustrate how such a process would be implemented. Gray et al. (1999), for example, used a 96-well plate solution-phase phosphorylation assay and a combinatorial library synthesis approach with a purine scaffold to generate selective inhibitors of an important cyclin-dependent protein kinase, Cdk2. In another example, potential Cdc25 dual-specificity phosphatase inhibitors from a targeted array library were evaluated using 96-well microtiter plates and recombinant human enzyme fused to glutathione *S*-transferase (Rice et al., 1997). Targeting Cdc25 dual-specificity phosphatases normally demands the full-length protein substrate, namely a cyclin-dependent kinase, which would need to be made by recombinant techniques and phosphorylated. Thus, a more rapid and inexpensive approach was used with an artificial, commercially available, small-molecular-weight substrate, which adopted enhanced fluorescent intensity when dephosphorylated. All of the compounds in the library were easily and quickly examined against at least seven protein phosphatases to assess both activity and specificity. Once a potentially active compound was identified, the investigators obtained a more highly purified compound and expanded the evaluation by using complete concentration-response curves and determining the nature and kinetics of the inhibition (Rice et al., 1997). Iterating chemical library synthesis and biological screening should permit the identification of even more potent and efficacious compounds built on this lead structure.

More recently, cell-based systems have been developed that greatly expand the pharmacological questions that now can be addressed with combinatorial libraries. Many of the contemporary molecular targets are intracellular and, thus, demand that the test compounds enter cells to act. Cell-based assays permit interrogation of compounds for this property. Moreover, some targets, such as ion channels or transcription factors, inherently require cell-based functional assays to detect disruption. Cell-based assays also permit more information-rich, multiparameter readouts using live cells even in real time. Typically, cell-based assays rely on optical methods for detection (Gonzalez and Negulescu, 1998). Some of the more popular methods are listed in Table 1. A primary advantage of these optical readouts is that the endogenous background signal can be quite small, whereas the signal from the indicator can be very bright. These properties enable the high signal-to-noise and sensitivity required for high-throughput assays. Chemiluminescent assays use chemical reactions to generate light. The most established probes for intracellular detection are the bioluminescent substrate for luciferase, luciferin, which is often used in reporter gene constructs, and the Ca^{2+}-sensitive protein aequorin. Substrates for both of these systems can be delivered to intact cells. The primary advantage offered by luminescent indicators is the low background signal and, consequently, luminescence assays are very sensitive and have a large dynamic range. The low photon flux of the current luminescence systems, which is about 0.1 to 0.2 photons per second, however, restricts this method to large cell numbers and can require high intracellular expression that is often only obtained by transient transfection protocols (Gonzalez and Negulescu, 1998; González et al., 1999). In contrast to chemiluminescence, the photons in fluorescence systems are used to generate an excited state rather than a chemical reaction. The excited state is short-lived and can be repeatedly excited, yielding a bright signal. Thus, single cell assays are possible with spatial resolution sufficient for the investigators to determine the subcellular distribution of the fluorescence probe. Single-cell detection can also be quite useful because it allows separation of expressing cells and, thus, enrichment of the cell population for function transfectants. A potential problem with fluorescence is that the library compounds may have inherent fluorescence that causes false readings. A par-

TABLE 1
Cell-based optical detection methods

Methods	Detection Probes	Advantages	Disadvantages
Absorbance	X-gal (β-galactosidase substrate)	Simple methodology	Limited prospects for miniaturization
	Horseradish peroxidase	Easily used with antibodies	
Fluorescence Intensity	Fluo-3 (Ca indicator)	Bright signal, good for miniaturization	Autofluorescence
	Fluorescein di-β-D-galactopyranoside (β-galactosidase substrate)	Easily used with antibodies	Interference by compounds
	Cy3 and Cy5	Can be used for subcellular localization	
	Green fluorescent protein chimeras		
Luminescence	Luciferin	Very sensitive due to low background	Low proton flux requires longer read-out times
FRET	Coumarin-fluorescein-based FRET substrate (β-lactamase), Cameleons	Ratiometric output, detects protein-protein interactions and good for miniaturization	Sensitive to placement of probe and significant probe development

ticularly powerful fluorescence-based approach is fluorescence resonance energy transfer (FRET), which results when two fluorophores with appropriate spectral overlap are in close proximity either due to intra- or intermolecular interactions. For example, one can even use FRET to detect the conformation and metal binding of proteins, such as metallothionein, within cells (Pearce et al., 2000). Excited energy is transferred from the donor to the acceptor, which results in a decrease in donor intensity and a concomitant increase in acceptor intensity. The ratiometric detection of the changes in signals not only improves reproducibility and sensitivity but it also markedly reduces cell number, probe concentration, and optical path distance as variables. Restrictions of FRET are: the optimal spatial location or orientation of fluorescence probes is often not known; high levels of intracellular probe expression are required and sometime difficult to achieve except with transient transfection; and the spectral overlap between the emissions of the donor and acceptor can reduce the dynamic range of the assay. The power of FRET, especially for mapping the subcellular localization of targets and intracellular protein-protein interactions, makes it likely that its use with combinatorial libraries will increase as more probes are developed.

Conclusions

Most of the discussion in this commentary has focused on the generation and examination of small organic molecules, but obviously combinatorial libraries of peptides, nucleic acids, and oligosaccharides continue to be generated. The inherently higher molecular weight peptides, nucleic acids, and oligosaccharides can be evaluated with most of the in vitro assays, but cell-based assays are more problematic because of cellular entry barriers and susceptibility to catabolic processes. Expansion in the number, diversity, and general availability of small molecule, combinatorial chemical libraries seems likely to make these essential reagents for future pharmacological studies.

References

Boger DL, Tarby CM, Myers PL and Caporale LH (1996) Generalized dipeptidomimetic template: Solution phase parallel synthesis of combinatorial libraries. *J Am Chem Soc* **118:**2109–2110.

Choong IC and Ellman JA (1996) Solid-phase synthesis: Applications to combinatorial libraries. *Annu Rev Med Chem* **31:**309–318.

Curran DP and Wipf P (1997) Combinatorial definitions. *Chem Eng News* **75:**6–7.

Dolle RE and Nelson KH (1999) Comprehensive survey of combinatorial library synthesis. *J Comb Chem* **1:**235–282.

Drews J (1996) Genomic sciences and the medicine of tomorrow. *Nature Biotechnol* **14:**1516–1518.

Gallop MA, Barret RW, Dower WJ, Fodor SPA and Gordon EM (1994) Applications of combinatorial technologies to drug discovery. Background and peptide combinatorial libraries. *J Med Chem* **37:**1233–1251.

Gayo LM and Suto MJ (1997) Ion-exchange resins for solution phase parallel synthesis of chemical libraries. *Tetrahedron Lett* **38:**513–516.

Gold L and Alper J (1997) Keeping pace with genomics through combinatorial chemistry. *Nature Biotechnol* **15:**297.

Gonzalez JE and Negulescu PA (1998) Intracellular detection assays for high-throughput screening. *Curr Opin Biotechnol* **9:**624–631.

González JE, Oades K, Leychkis Y, Harootunian A and Negulescu PA (1999) Cell-based assays and instrumentation for screening ion-channel targets. *Drug Discovery Today* **4:**431–439.

Gordon EM, Barrett RW, Dower WJ, Fodor SPA and Gallop MA (1994) Applications of combinatorial technologies to drug discovery. Combinatorial organic synthesis, library screening strategies, and future directions. *J Med Chem* **37:**1385–1401.

Gray NS, Wodicka L, Thunnissen A-M WH, Norman TC, Kwon S, Espinoza FH, Morgan DO, Barnes G, LeClerc S, Meijer L, Kim S-H, Lockhart DJ and Schultz PG (1999) Exploiting chemical libraries, structure, and genomics in the search for kinase inhibitors. *Science (Wash DC)* **281:**533–538.

Hogan JC (1996) Directed combinatorial chemistry. *Nature (Lond)* **384:**17–19.

Hogan JC (1997) Combinatorial chemistry in drug discovery. *Nat Biotechnol* **15:**328–330.

Houston JH and Banks M (1997) The chemical-biological interface: Developments in automated and miniaturised screening technology. *Curr Opin Biotechnol* **8:**734–740.

Jung G (1996) *Combinatorial Peptide and Nonpeptide Libraries: A Handbook.* Weinheim, New York.

Nefzi A, Ostresh JM and Houghten RA (1997) The current status of heterocyclic combinatorial libraries. *Chem Rev* **97:**449–472.

Nestler HP, Bartlett PA and Still WC (1994) A general method for molecular tagging of encoded combinatorial chemistry libraries. *J Org Chem* **59:**4723–4724.

Obrecht D and Villalgordo JM (1998) Solid-Supported Combinatorial and Parallel Synthesis of Small-Molecular-Weight Compound Libraries. Pergamon Press Ltd., Oxford, UK.

Parlow JJ, Naing W, South MS and Flynn DL (1997) *In situ* chemical tagging: Tetrafluorophthalic anhydride as a "sequestration enabling reagent" (SER) in the purification of solution-phase combinatorial libraries. *Tetrahedron Lett* **38:**7959–7962.

Pearce LL, Gandley RE, Han W, Wasserloos K, Stitt M, Kanai AJ, McLaughlin MK, Pitt BR and Levitan ES (2000) Role of metallothionein in nitric oxide signaling as revealed by a green fluorescent fusion protein. *Proc Natl Acad Sci USA* **97:**477–482.

Pirrung MC (1997) Spatially addressable combinatorial libraries. *Chem Rev* **97:**473–488.

Rice RL, Rusnak JM, Yokokawa F, Yokokawa S, Messner DJ, Boynton AL, Wipf P and Lazo JS (1997) A targeted library of small molecule, tyrosine and dual specificity phosphatase inhibitors derived from a rational core design and random side chain variation. *Biochemistry* **36:**15965–15974.

Siegel MG, Hahn PJ, Dressman BA, Fritz JE, Grunwell JR and Kaldor SW (1997) Rapid purification of small molecule libraries by ion exchange chromatography. *Tetrahedron Lett* **38:**3357–3360.

Studer A, Hadida S, Ferritto R, Kim S-Y, Jeger P, Wipf P and Curran DP (1997) Fluorous synthesis: A fluorous-phase strategy for improving separation efficiency in organic synthesis. *Science (Wash DC)* **275:**823–826.

Wipf P, Cunningham A, Rice RL and Lazo JS (1997) Combinatorial synthesis and biological evaluation of a library of small-molecule Ser/Thr-protein phosphatase inhibitors. *Bioorg Med Chem* **5:**165–177.

Yan B (1998) Monitoring the progress and the yield of solid-phase organic reactions on resin supports. *Acc Chem Res* **31:**621–630.

Send reprint requests to: John S. Lazo, Department of Pharmacology, Biomedical Science Tower E-1340, University of Pittsburgh, Pittsburgh, PA 15261. E-mail: lazo+@pitt.edu

Identification of New Cdc25 Dual Specificity Phosphatase Inhibitors in a Targeted Small Molecule Array

Alexander P. Ducruet, [a] Robert L. Rice, [a] Kenji Tamura, [a] Fumiaki Yokokawa, [b] Shiho Yokokawa, [b] Peter Wipf [b] and John S. Lazo [a],*

[a]*Department of Pharmacology, the Combinatorial Chemistry Center and the Molecular Therapeutic/Drug Discovery Program of the University of Pittsburgh Cancer Institute, University of Pittsburgh, Pittsburgh, PA 15261, USA*
[b]*Department of Chemistry, the Combinatorial Chemistry Center and the Molecular Therapeutic/Drug Discovery Program of the University of Pittsburgh Cancer Institute, University of Pittsburgh, Pittsburgh, PA 15261, USA*

Abstract—Dual specificity protein phosphatases (DSPases) are key regulators of signal transduction, oncogenesis and the cell cycle. Few potent or specific inhibitors of DSPases, however, are readily available for these pharmacological targets. We have used a combinatorial/parallel synthetic approach to rigidify the variable core region and modify the side chains of 4-(benzyl-(2-[2,5-diphenyl-oxazole-4-carbonyl)-amino]-ethyl)-carbamoyl)-2-decanoylamino butyric acid (or SC-$\alpha\alpha\delta9$), which is the most active element in a previously described library of phosphatase inhibitors (Rice, R. L.; Rusnak, J. M.; Yokokawa, F.; Yokokawa, S.; Messner, D. J.; Boynton, A. L.; Wipf, P.; Lazo, J. S. *Biochemistry* 1997, *36*, 15965). Several analogues were identified as effective inhibitors of the protein tyrosine phosphatase (PTPase) PTP1B and the DSPases VHR and Cdc25B$_2$. Two compounds, FY3-$\alpha\alpha09$ and FY21-$\alpha\alpha09$, were partial competitive inhibitors of Cdc25B$_2$ with K_1 values of 7.6±0.5 and 1.6±0.2 μM, respectively. FY21-$\alpha\alpha09$ possessed only moderate activity against PTP1B. Consistent with its in vitro anti-phosphatase activity, FY21-$\alpha\alpha09$ inhibited growth in MDA-MB-231 and MCF-7 human breast cancer cell lines. FY21-$\alpha\alpha09$ also inhibited the G$_2$/M transition in tsFT210 cells, consistent with Cdc25B inhibition. Several architectural requirements for DSPase inhibition were revealed through modification of the side chain moieties or variable core region of the pharmacophore, which resulted in decreased compound potency. The structure of FY21-$\alpha\alpha09$ provides a useful platform from which additional potent and more highly selective phosphatase inhibitors might be generated. © 2000 Elsevier Science Ltd. All rights reserved.

Introduction

Phosphorylation and dephosphorylation by the concomitant actions of kinases and phosphatases are critical control mechanisms for numerous physiological functions.[2] More specifically, protein phosphorylation is the major component of signal transduction pathways, highly regulated processes by which cells convey information from the cell surface to their nucleus or other remote subcellular sites.[3,4] This information then controls such processes as cell growth and differentiation, metabolism, cell cycle regulation, cytoskeletal functions and even transformation.[2,5]

Phosphatases are generally divided into two main groups based on their enzymatic mechanism, structure

and substrate specificity. The protein phosphatases (PPases) hydrolyze phosphomonoester bonds found specifically on serine or threonine amino acid residues, while the protein tyrosine phosphatases (PTPases) are phosphotyrosine specific, removing the phosphomonoester from the phosphorylated tyrosine residue, returning it to the analogous initial alcohol.[4,5] A PTPase sub-class is the dual specificity protein phosphatases (DSPases), which are capable of hydrolyzing the phosphomonoester bonds on both phosphotyrosine and phosphoserine/threonine residues found on the same protein substrate.[5] While PTPases have extremely limited sequence similarity, they share the active site signature motif (I/V) HCXAGXGR(S/T)G, harboring the catalytic cysteine residue that plays an essential role in the phosphatase-mediated phosphotyrosine phosphomonoester bond cleavage.[6,7]

The PTPases have diverse biochemical and cellular roles. For example, PTP1B regulates both epidermal growth factor and insulin signaling pathways.[6,8–10]

*Corresponding author. Department of Pharmacology, Biomedical Science Tower E-1340, University of Pittsburgh, Pittsburgh, PA 15261, USA. Tel.: +1-412-648-9319; fax: +1-412-648-2229; e-mail: lazo@pop.pitt.edu

PTP1B can also reverse the transformation of cells by v-src, v-crk and v-ras when over-expressed in these cells.[11]

The DSPase VHR (vaccina human-related) regulates mitogenic signaling by specifically dephosphorylating members of the MAPK (mitogen-activated protein kinase) family, namely the extracellular regulated kinases ERK1 and ERK2.[5,12,13] The Cdc25 DSPases coordinate the cell cycle by dephosphorylating, and thereby activating, cell cycle dependent kinases. For example, Cdc25B and Cdc25C dephosphorylate $p34^{cdc2}$ (also known as cdkl) and permit entry into mitosis.[14–17]

Since members of the PTPase family appear to play an important role in cell signaling, cell cycle control and oncogenesis, specific inhibitors of these proteins would be highly desirable. Unfortunately, selective and potent inhibitors of PTPases are not currently available. Present crystallographic data, however, suggest that selective inhibitors may be obtainable as significant differences have been observed in the active site of Cdc25A, VHR and PTP1B phosphatases.[13,14,18] The shallow 6 Å pocket of VHR and the even shallower pocket of Cdc25A can accommodate both phosphotyrosine as well as phosphoserine/threonine residues.[13,14] In contrast, PTP1B possesses a deeper 9 Å catalytic pocket where only the more extended phosphotyrosine side chain, unencumbered by any adjacent phosphoserine/threonine, can reach the nucleophilic cysteine at the base of the catalytic pocket.[5,18] The structural differences present in these phosphatases should be exploitable in the selection of targeted inhibitors. Furthermore, inhibitors may be helpful in biochemically defining other unidentified intracellular functions.

We have used a previously described non-electrophilic phosphatase inhibitor, namely SC-ααδ99,[1] as a pharmacophore to synthesize a new targeted library of small molecules and examined each element for selective DSPase inhibition. Minimal structural changes in the pharmacophore resulted in significant differences in inhibitory properties. In addition, the hydrophobic domain of the core pharmacophore was essential for anti-phosphatase activity. We have defined a structure with enhanced selectivity for the dual specificity phosphatase Cdc25B$_2$. This compound, FY21-αα09, also blocked the proliferation of human breast cancer cells in vitro.

Results

Phosphatase inhibition by SC-αα09 enantiomers and R$_4$ analogues

Because we previously found that racemic SC-αα09 (Fig. 1B) was an inhibitor of dual specificity phosphatases,[1] we further examined the structural basis for inhibition by synthesizing and testing both the (R)-SC-ααδ9 and (S)-SC-ααδ9 enantiomers. Both enantiomers inhibited Cdc25B$_2$ phosphatase activity by approximately 85% at 100 μM (Table 1). At 3 μM, neither enantiomers had significant inhibitory activity.
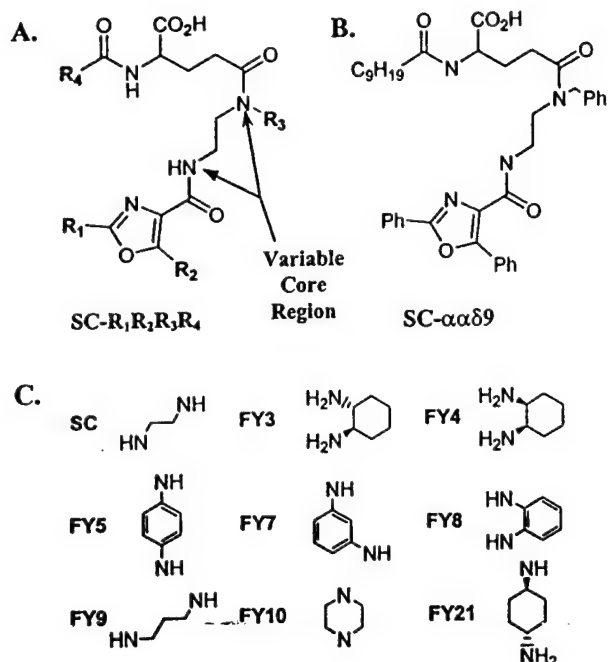

Figure 1. SC pharmacophore and variable core region substituents. general chemical structure for the founding SC pharmacophore series. −R$_n$ indicates the combinatorial sites on the pharmacophore and are sequentially listed after the core prefix: (A) the variable core region; (B) chemical structure of SC-ααδ9 (C) structure of variable core diamine linker substitutions.

Table 1. Inhibition of Cdc25B$_2$ phosphatase activity and lipophilicity of SC-ααδ9 analogues[a]

Compound	Cdc25B$_2$ (% Inhibition)		clog P value[b]	
	3 μM	100 μM	Carboxylate	Free acid
(R)-SC-ααδ9	3±3	85±2	1.2	4.9
(S)-SC-ααδ9	2±2	83±2	1.2	4.9
SC-ααδA	6±6	78±2	ND[c]	ND[c]
SC-ααδ15	11±9	76±3	3.6	8.4
SC-ααδ17A	13±10	78±3	4.3	8.9
SC-ααδ17B	7±7	79±4	4.4	9.0
SC-ααδ6III	7±7	13±2	−2.0	1.4
SC-ααδ4II	6±4	23±2	−1.8	1.9

[a]Each value is the percent inhibition from untreated control and the mean and SEM from three or more independent determinations.
[b]clog P values represent logarithms of the octanol–water partition coefficient and were calculated based on energy-minimized extended conformations by the method of Alkorta and Villar.[26]
[c]ND, not determined.

Previous observations lead us to speculate that the hydrophobic nonyl substituent of our SC pharmacophore was critical for phosphatase inhibition.[1] To investigate this hypothesis, we replaced the nonyl moiety (R$_4$) of the SC-ααδ9 core pharmacophore with hydrophobic substituents of variable length (Fig. 2). Compounds such as SC-ααδ15, which contain a pentadecyl side chain, had a greater clog P value than SC-ααδ9 but had similar Cdc25B$_2$ inhibitory activity as compared to that seen with SC-ααδ9 (Table 1). Similarly, SC-ααδ17A and SC-ααδ17B, which had greater

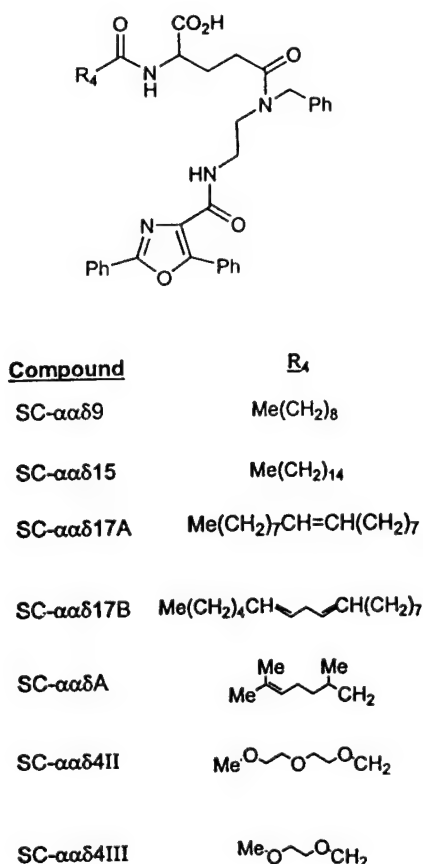| Compound	R_4
SC-ααδ9	$Me(CH_2)_8$
SC-ααδ15	$Me(CH_2)_{14}$
SC-ααδ17A	$Me(CH_2)_7CH=CH(CH_2)_7$
SC-ααδ17B	$Me(CH_2)_4CH \sim \sim CH(CH_2)_7$
SC-ααδA	(structure)
SC-ααδ4II	(structure)
SC-ααδ4III	(structure)

Figure 2. Chemical structures of SC-ααδ9 R_4 analogues.

clog P values than SC-ααδ15, maintained anti-Cdc25B$_2$ activity, while the ether-containing SC-ααδ6III and SC-ααδ4II, with the lowest clog P values of these compounds, had no inhibitory activity against Cdc25B$_2$ up to a concentration of 100 μM. These results demonstrated a critical role for hydrophobicity rather than just the length of the R_4 substituent for Cdc25B$_2$ phosphatase inhibition.

Phosphatase inhibition by modified core pharmacophore library members

Conformational rigidity can be achieved by replacing the flexible ethyldiamine portion of the original SC-ααδ9 pharmacophore with a series of cyclic diamantes (Figs. 1 and 3).

Specifically, cyclohexyldiamine, piperazine and phenyldiamine substructures were used to enhance rigidity of the variable core region and alter overall size. We also examined an extended alkyl linker, a propyldiamine substructure, to determine if the length of the linker was important. Because of the absence of stereospecificity in the parental SC structure, all congeners were synthesized as racemic mixtures. We found SC-ααδ > SC-αα09 > SC-α109 as inhibitors of Cdc25B$_2$ (Tables 1 and 2) revealing the importance of an aromatic moiety

on the C$_5$ oxazole (R_2) position and the R_3 amine. The importance of the R_2 aromatic moiety was further established with the full FY series, where -αα09 compounds were generally more inhibitory than the -α109 compounds (Table 2). When we examined the inhibition of Cdc25B$_2$ with 100 μM of the -αα09 series, we found that enzyme inhibition was moderately resistant to modification of the core pharmacophore structure (Table 2), although several cores, such as FY9 and FY10 exhibited decreased Cdc25 inhibitory activity. FY21-αα09 was the most effective inhibitor of Cdc25B$_2$ at 3 μM (Table 2), causing a 36% decrease in enzyme activity. In the -α109 series, no compound was as effective as FY21-αα09. Many congeners were similar to SC-α109, although notably, FY3-α109, FY5-α109, FY7-α109 and FY8-α109 exhibited 2- to 5-fold higher inhibitory activity against Cdc25B$_2$ than SC-α109. None of the compounds in the rigidified FY series, however, caused marked inhibition of VHR or PTP1B at 3 μM (Table 2). FY5-αα09 was the only compound with a distinct preference for VHR over Cdc25B$_2$ or PTP1B. FY3-αα09, FY8-αα09 and FY21-αα09 showed no significant in vitro preference for Cdc25B$_2$, VHR or PTP1B in these preliminary studies at 100 μM. A more comprehensive study of FY21-αα09, however, revealed that PTP1B (IC$_{50}$ = 41.4 μM) was approximately 4-fold less sensitive to the compound than Cdc25B$_2$ or VHR (IC$_{50}$s of 7.0 μM and 12.1 μM, respectively) (Fig. 4).

Inhibition kinetics of compounds

We next determined the kinetic characteristics of Cdc25B$_2$ inhibition with two of our most potent compounds, FY3-αα09 and FY21-αα09. We found that FY3-αα09 and FY21-αα09 were partial competitive inhibitors of Cdc25B$_2$, with K_i values of 7.6±0.5 μM and 1.6±0.2 μM, respectively (Fig. 5). Kinetic studies using 1 to 60 μM FY3-αα09 with VHR and rhPTP1B were most consistent with an S-parabolic noncompetitive inhibition model (data not shown), although higher FY3-αα09 concentrations presented a more mixed profile. The differences in the FY3-αα09 kinetic profiles seen with VHR, PTP1B and Cdc25B$_2$ may reflect the structural dissimilarities of these phosphatases.

Cell proliferation assays

Previous studies with the founding core library members indicated that only SC-ααδ9 caused marked, concentration-dependent inhibition of tumor cell growth in culture.[19] We found with the current FY series that only FY21-αα09 caused greater than 90% inhibition of MDA-MB-231 cell growth at 100 μM, while 100 μM of either FY8-αα09 or FY21-αα inhibited MCF-7 cell growth by greater than 90% (Fig. 6). Studies with tsFT210 cells indicated that a 6 h exposure to 100 μM FY21-αα09 partially blocked cell cycle progression at the G$_2$/M checkpoint while the biochemically inactive congener SC-αα09 did not cause any block (Fig. 7). FY21-αα09 at 100 μM was as effective inhibiting the G$_2$/M transition as the tubulin binder nocodazole at 1 μM. The G$_2$/M block observed with FY21-αα09 is consistent with intracellular inhibition of Cdc25B$_2$.
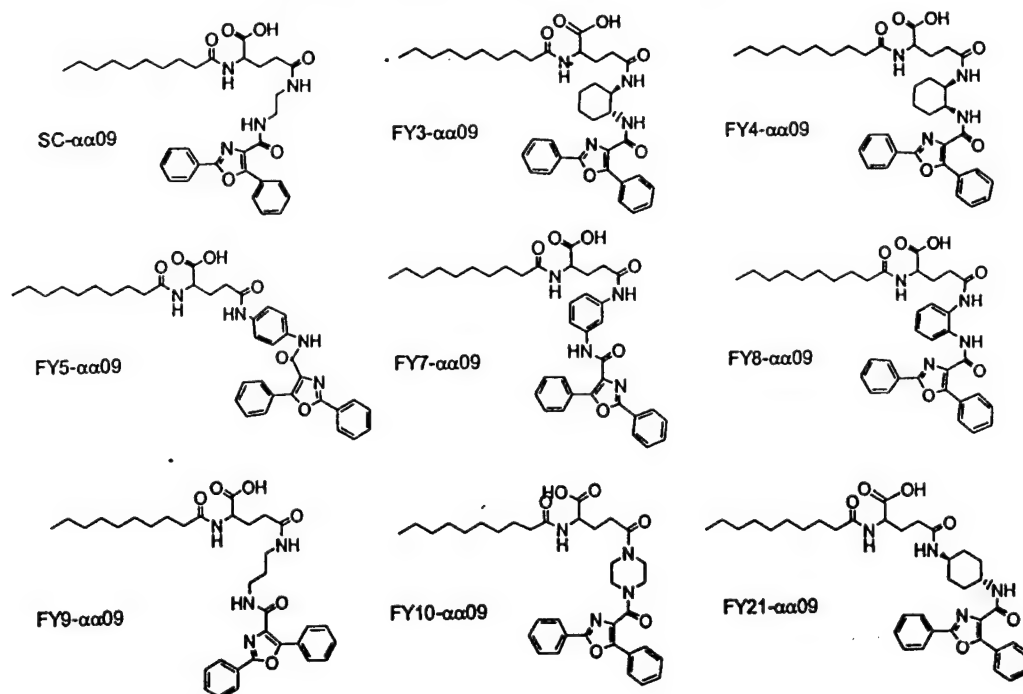
Figure 3. Chemical structures of representative analogues of the -αα09 series.

Table 2. Inhibition of dual specificity and tyrosine-specific phosphatase activity[a]

Compound	Cdc25B$_2$ (% Inhibition)		VHR (% Inhibition)		rhPTP1B (% Inhibition)	
	3 μM	100 μM	3 μM	100 μM	3 μM	100 μM
SC-αα09	2.1±1.3	57±8.0	3.0±0.7	6.4±3.6	−0.2±0.6	1.3±2.5
SC-α109	2.8±1.7	15±7.7	4.5±1.4	12±1.4	−0.6±0.7	−3.5±1.3
FY3-αα09	4.0±2.4	72±4.4	8.4±1.1	99± 0.4	4.5±1.2	89±2.1
FY3-α109	3.3±2.3	25±9.8	5.5±0.3	31±1.6	4.3±0.7	16±1.4
FY4-αα09	4.1±2.4	73±1.0	5.2±0.2	61±2.4	4.3±1.3	33±3.3
FY4-α109	1.4±1.0	19±7.1	1.3±0.3	42±0.8	−0.3±0.2	6.7±0.8
FY5-αα09	0.9±0.9	63±4.3	6.4±1.1	95±0.9	0.7±0.4	40±6.3
FY5-α109	3.3±3.0	48±3.3	1.1±2.1	65±1.2	0.8±0.4	23±5.5
FY7-αα09	17±4.4	80±3.5	10±0.5	73±3.3	1.9±0.8	17±1.0
FY7-α109	3.1±1.8	68±2.7	6.4±0.1	35±1.2	3.1±0.6	12±1.3
FY8-αα09	4.4±2.8	85±2.6	6.5±1.0	95±1.9	5.9±0.9	90±2.3
FY8-α109	1.1±0.6	44±8.8	1.7±0.6	87±2.4	3.8±0.9	69±2.4
FY9-αα09	0.1±0.1	51±5.4	2.2±0.9	9.0±1.0	0.3±0.9	3.2±1.4
FY9-α109	2.5±4.1	4.1±2.4	3.4±0.7	4.5±2.2	−0.3±0.5	−6.3±1.3
FY10-αα09	2.3±1.3	28±8.3	4.4±0.2	11±2.7	−0.4±0.3	−3.7±1.0
FY10-α109	3.2±3.2	16±6.9	2.6±2.1	8.3±3.0	0.5±0.3	−3.8±1.0
FY21-αα09	36±1.3	83±0.6	11±2.7	95±2.6	3.4±1.6	78±1.7

[a]Each value is the percent inhibition from untreated control and the mean and SEM from three or more independent determinations.

Discussion

The dual specificity and tyrosine specific phosphatases share low sequence homology except for conserved residues involved in phosphate binding and catalysis. Based on their crystal structures, Cdc25 and VHR appear to be more accommodating to substrates and less sterically hindered than PTP1B. Our structure–activity relationship results support this conclusion: several of the rigid compounds show marked preference for Cdc25 and VHR rather than PTP1B.

The crystal structure of Cdc25 reveals a hydrophobic region within 20–22 Å of the active site, suggesting that small molecules of a more hydrophobic nature may possess enhanced anti-phosphatase activity.[14] To test the hypothesis that the hydrophobic nonyl substituent in our founding pharmacophore was essential for phosphatase inhibition, we replaced the SC-ααδ9 nonyl moiety, which has an extended length of 22 Å, with various more hydrophobic substituents (Fig. 2). There seemed to be a parallel relationship between clog P values and inhibition of Cdc25B$_2$ phosphatase activity. Compounds with R$_4$ substituents of a more hydrophobic nature than the nonyl group found in SC-ααδ9 displayed an inhibitory profile against Cdc25B$_2$ similar to that of SC-ααδ9. On the other hand, compounds with R$_4$ substituents with more hydrophilic character and
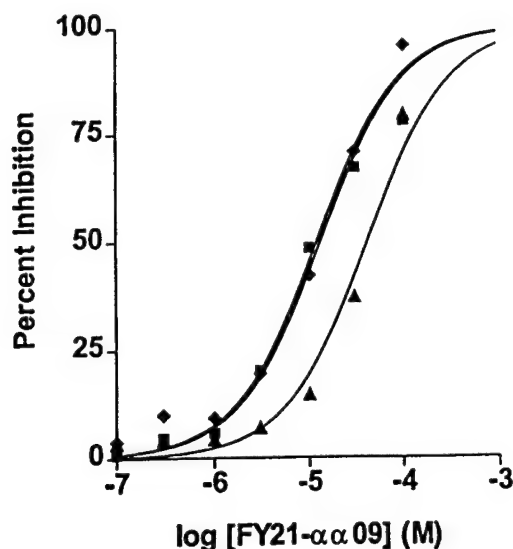
Figure 4. Inhibition of dual specificity and tyrosine-specific phosphatases by FY21-αα09. Concentration-dependent phosphatase inhibition by FY21-αα09 (representative results from one experiment). -■-, Cdc25B₂; -◆-, VHR; -▲-, PTP1B. Enzyme activities were determined as described in Experimental. Non-linear regressions were performed using GraphPad Prism 3.0.

Figure 5. Kinetic analysis of Cdc25b₂ inhibition by FY3-αα09 and FY21-αα09. Panel A: Lineweaver–Burk plot of Cdc25B₂ inhibition by FY3-αα09. -■-, 0 μM; -▼-, 0.1 μM; -●-, 1 μM; -□-, 10 μM -△-, 50 μM; and -▽-, 100 μM FY3-αα09. Panel B: Lineweaver–Burk plot of Cdc25B₂ inhibition by FY21-αα09. -■-, 0 μM -▼-, 5 μM; -◆-, 15 μM; -●-, 30 μM; and -□-, 60 μM FY21-αα09. Enzyme activities were determined as described in Experimental procedures and the data fit to the Michaelis–Mention equation. The best fit kinetic model was determined using EZ-Fit™.

therefore lower clog P values, such as the ether-containing SC-ααδ6III and SC-ααδ4II, demonstrated negligible Cdc25B₂ inhibitory activity at concentrations up to 100 μM. Because kinetic studies with SC-ααδ9 suggest that its mode of inhibition of Cdc25B₂ is most consistent with a competitive model, the importance of a hydrophobic moiety in the R₄ position of the pharmacophore suggested that the Cdc2SB₂ active site, with the exception of the phosphate binding site, is hydrophobic in nature.[1,20]

Rigidification of our basic SC pharmacophore model in our founding targeted array improved the inhibitory profile against DSPases. By replacing the ethyldiamine linker with a cyclohexyldiamine scaffold, such as in FY3-αα09, FY4-αα09 and FY21-αα09, we did not significantly alter the anti-Cdc25B₂ activity; these three compounds also efficiently inhibited VHR. FY4-αα09, however, demonstrated significant preference for the DSPases and did not inhibit PTP1B. Perhaps this is due to the less extended nature of FY4-αα09 as compared with the other cyclohexyldiamine congeners. FY21-αα09 was even more potent against DSPases at 100 μM compared with FY4-αα09, but it also inhibited PTP1B; at 3 μM, however, FY21-αα09 displayed a significant preference for Cdc25B₂. Perhaps this specificity for Cdc25B₂ depends on the previously reported shallow nature of the enzyme's active site relative to that of PTP1B.[14] In addition to rigidifying the pharmacophore, we also varied the substituents at the R₁ and R₂ positions. All the new compounds with anti-phosphatase activity displayed a strong preference for an aromatic moiety in the R₂ position. This may be due to the more hydrophobic nature of DSPase active sites and the documented second aryl phosphate binding site adjacent to the active site of PTP1B.[1,20,21]

In examining a subset of compounds, we found that the better in vitro inhibitors of DSPases were effective inhibitors of breast cancer proliferation. MDA-MB-231 cells were more selective and intrinsically less sensitive to the compounds tested than MCF-7 cells. Cell proliferation was inhibited in a clear concentration response manner, with FY21-αα09 being the most potent agent tested. The growth inhibition seen with several of the compounds, such as FY3-α109, which lacked significant anti-DSPase activity in vitro, seems most likely due to other activities. Cdc25 is the major regulator of the G₂/M checkpoint and blockage seen with FY21-αα09 is similar to that observed with other Cdc2S inhibitors.[22] Nonetheless, we recognize that the G₂/M block seen with FY21-αα09 could be the result of mechanisms other than inhibition of Cdc25. Additional studies are required to confirm our hypothesis about the mechanism of G₂/M arrest.
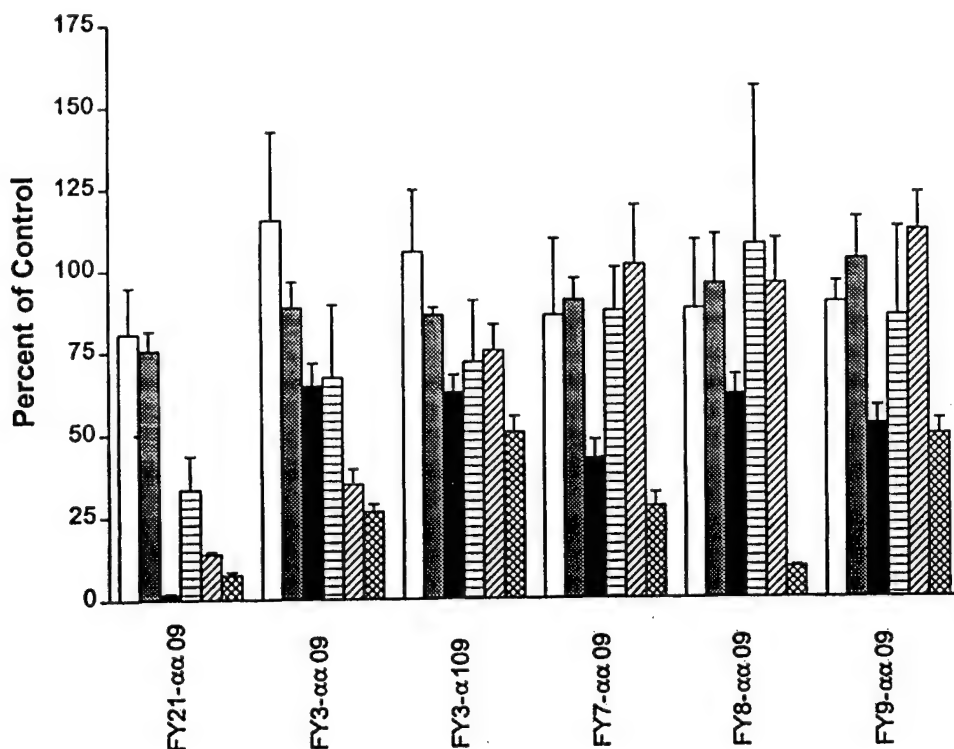
Figure 6. Antiproliferative effects of selected compounds on MDA-MB-231 and MCF-7 human breast cancer cells. Antiproliferative effect of compounds. MDA-MB-231 cells: 10 μM (□) 30 μM (▨) and 100 μM (■), MCF-7 cells: 10 μM (▤), 30 μM (▨) and 100 μM (▨). The antiproliferative effect of compounds was determined as described in Experimental procedures and results were normalized to vehicle treated controls. Error bars represent standard deviations (n = 6).
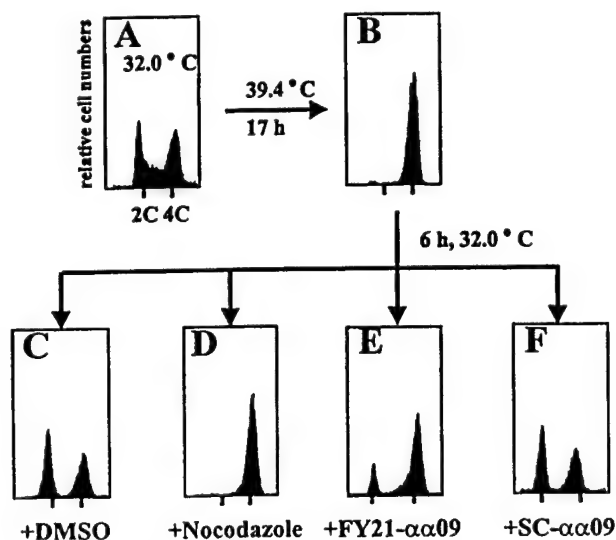
**Figure 7.** Inhibition of tsFT210 cell cycle progression at G₂/M by FY21-αα09. (A) tsFT210 cells were cultured at the permissive temperature of 32.0°C and then (B) incubated for 17 h at the non-permissive temperature of 34.9°C. Cells were released from cycle arrest by shifting to the 32.0°C medium. The cells were then incubated for 6 h in the presence of (C) DMSO vehicle, (D) 1 μM nocodazole, (E) 100 μM FY21-αα09 or (F) 100 μM SC-αα09. Fluorescence corresponding to 2C or 4C DNA content are represented by vertical bars.

With FY21-αα09, we have identified one of the most potent Cdc25B₂ inhibitors reported to date. Dysidiolide, which was reported to have an IC₅₀ of 9.4 μM against Cdc25A,[23] has more recently been found to lack potent inhibitory activity against this phosphatase.[24] A 3-α-azido-B-homo-6-oxa-4-cholesten-7-one derivative, compound 7 had an IC₅₀ of 2 μM for Cdc25A, although there is no information concerning its selectivity.[25] Although FY21-αα09 efficiently inhibited both DSPases and PTPases in vitro, unlike SC-ααδ9,[1] it exhibited some preference for the DSPases. As a partial competitive inhibitor, FY21-αα09 interacted with Cdc25B₂ in the vicinity of the active site though was unable to completely impede substrate binding. R₄ substituents in the original SC pharmacophore revealed the importance of a hydrophobic moiety for Cdc25B₂ inhibition and rigidification of the variable core region and modification of the side chain moieties of the pharmacophore suggests several structural requirements for DSPase inhibition. The structures of FY5-αα09, FY7-αα09 and FY21-αα09 should provide excellent platforms for future analogue development. Our results indicate that selective inhibition of DSPases and PTPases is indeed possible.

Experimental

Chemical compounds

We have previously described the general nomenclature system to be used for our phosphatase library elements.[1] The alphanumeric prefix provides a unique indicator of the core pharmacophore. Thus, the 'SC' prefix was used to designate the pharmacophore used in the founding

phosphatase inhibitor library (Fig. 1A). Replacement of the ethylenediamine in the founding pharmacophore with a *trans* cyclohexyl-1,2-diamine produced the FY3 series, *cis* cyclohexyl-1,2-diamine produced the FY4 series, *para*-phenyldiamine produced the FY5 series, *meta*-phenyldiamine produced the FY7 series, *ortho*-phenyldiamine produced the FY8 series, propyldiamine produced the FY9 series, piperazine produced the FY10 series and a *trans* cyclohexyl-1,4-diamine produced the FY21 series. The FY6 series utilizes ethylenediamine as the core structure. The four descriptors following the prefix indicate the chemical nature of the substituents on the four variable domains of the pharmacophore. The first descriptor always described the substituent (R_1) furthest from the assumed surrogate phosphate, a carbonyl moiety in both the SC and FY families. The closer the proximity of the substituent to the carbonyl, the further the descriptor was from the prefix. Greek letters indicate an aromatic moiety so that the addition of a phenyl was termed α, a phenethyl was β, benzyl was δ and a styryl was γ.[1] Alkyl chains were designated on the basis of carbon length with Roman numerals and

capital letters added if there was chain branching or the inclusion of non-carbon-based linkers. Thus, each compound has a unique name. For most compounds in this study the R_3 site was unsubstantiated and this was designated as 0. Compounds were resuspended in DMSO prior to use and stocks (powder and resuspended) were stored at −20 °C.

The general synthesis of compounds SC-ααδ9 and SC-αα09 has been previously described.[19] A slightly modified strategy was used for the synthesis of the new compounds SC-ααδ4II and SC-ααδ6III. DL-Glutamate (1) was selectively side-chain esterified with trimethylsilylchloride in allyl alcohol, *N*-protected with β,β,β-trichloroethoxycarbonyl chloride, and methylated to give Troc-Glu(allyl)-OMe (2b) in 28% overall yield (Scheme 1). After Pd(0)-catalyzed deallylation, the side-chain carboxyl terminus was extended by PyBroP-mediated coupling with BnNHCH₂CH₂NHAlloc, renewed Pd(0)-catalyzed deallylation and coupling with the oxazole segment to give 4. After deprotection of the *N*-terminus with zinc in acetic acid, EDCI-mediated coupling
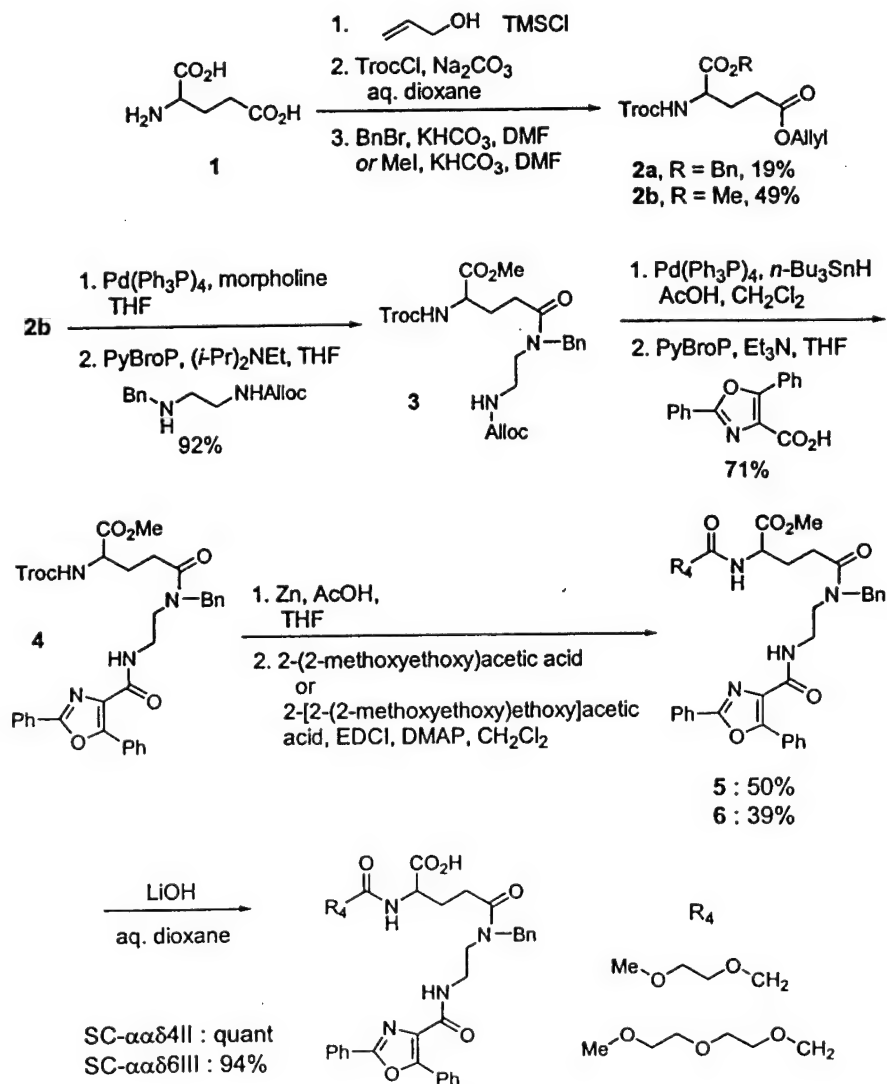
Scheme 1.

provided SC-ααδ4II and SC-ααδ6II in 5–10% overall yield from DL-glutamate.

For the synthesis of FY21-αα09, protected glutamate **2a** was acylated at the N-terminus after removal of the Troc group, deallylated and coupled to diamine **8** to give the segment **9** in 52% yield from **2a** (Scheme 2). Acidolytic cleavage of the Boc group and PyBroP-mediated coupling with oxazole **10** provided ester **11**, which was readily converted to the desired FY21-αα09.

Detailed experimental protocols for FY21-αα09, FY3-αα09, FY4-αα09, FY5-αα09, FY7-αα09, FY8-αα09, FY9-αα09, FY10-αα09, SC-ααδ17A, SC-ααδ17B, SC-ααδA, SC-ααδ4II, and SC-ααδ6III are listed below.

FY21-αα09

2-(2,2,2-Trichloroethoxycarbonylamino)-pentanoic acid 5-allyl ester 1-benzyl ester (2a). To a stirred suspension of 10 g (68 mmol) of D,L-glutamic acid (**1**) in 170 mL of allyl alcohol was added dropwise 21.6 mL (170 mmol) of chlorotrimethylsilane. The suspension was stirred at 22 °C for 22 h and concentrated in vacuo. The resulting oil was dissolved in 180 mL of dioxane. The resulting solution was treated with 237.9 mmol of aqueous sodium carbonate (25.21 g in 180 mL of H_2O) at 0 °C, stirred for 5 mm, and treated with 9.5 mL (69.3 mmol) of TrocCl. The reaction mixture was stirred at 0 °C for 10 mm and warmed to 22 °C, stirred for 17 h, concentrated in vacuo, poured into 300 mL of H_2O and washed with Et_2O. The aqueous layer was acidified to

pH 1 with concentrated HCl, salted out with NaCl, and extracted with EtOAc (3×). The resulting organic layer was dried (Na_2SO_4) and concentrated in vacuo to give 8.76 g of carboxylic acid as a yellow oil. To a solution of the resulting oil in 32 mL of DMF was added 3.87 g (38.7 mmol) of $KHCO_3$ and 3.4 mL (29 mmol) of benzyl bromide. The reaction mixture was stirred at 22 °C for 14 h, diluted with EtOAc, and washed with 10% HCl, H_2O, saturated aqueous $NaHCO_3$ and brine. The organic layer was dried (Na_2SO_4), concentrated in vacuo, and chromatographed on SiO_2 (hexanes:EtOAc, 6:1→5:1→4:1→3:1) to give 5.70 g (19% over three steps) of **2a** as a pale yellow oil: IR (neat) 3344, 2953, 1745, 1519, 1327, 1269, 1203 cm^{-1} H NMR (CDCl$_3$) δ 7.31 (m, 5H), 5.94–5.83 (m, 1H), 5.69 (d, 1H, J = 8.1 Hz), 5.34–5.21 (m, 2H), 5.19 (s, 2H), 4.71 (AB, 2H, J = 11.9 Hz), 4.57 (d, 2H, J = 4.7 Hz), 4.51–4.44 (m, 1H), 2.50–2.33 (m, 2H), 2.32–2.24 (m, 1H), 2.10–2.01 (m, 1H); ^{13}C NMR (CDCl$_3$) δ 172.2, 171.3, 154.2, 135.0, 131.9, 128.6, 128.3, 118.4, 95.3, 74.5, 67.4, 65.4, 53.5, 29.9, 27.2.

2-Decanoylamino-pentanedioic acid 5-allyl ester 1-benzyl ester (7). To a solution of 5.698 g (12.59 mmol) of **2a** in 16.5 mL of acetic acid and 24.7 mL of THF was added 16.455 g (251.73 mmol) of zinc dust. The suspension was stirred at 22 °C for 1 h. The reaction mixture was filtered through a Celite pad and the filtrate was concentrated in vacuo. The resulting residue was diluted with EtOAc and washed with saturated aqueous $NaHCO_3$ and brine. The organic layer was dried (Na_2SO_4) and concentrated in vacuo to give 2.68 g
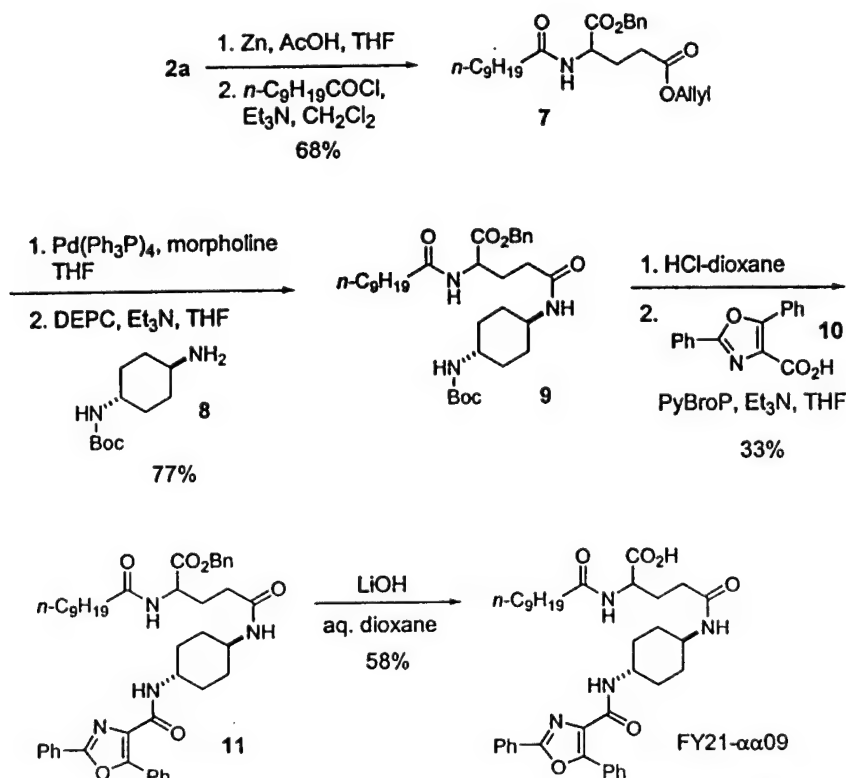
Scheme 2.

of free amine. The resulting residue was dissolved in 42 mL of CH_2Cl_2 and treated with 5.3 mL (38 mmol) of triethylamine and 3.9 mL (19 mmol) of decanoyl chloride at 0 °C. The reaction mixture was stirred at 0 °C for 15 mm and warmed to 22 °C, stirred for 12 h, concentrated in vacuo, diluted with EtOAc, and washed with 10% HCl, H_2O, saturated aqueous $NaHCO_3$ and brine. The organic layer was dried (Na_2SO_4), concentrated in vacuo, and chromatographed on SiO_2 (hexane:EtOAc, 5:1→3:1) to give 3.69 g (68% over two steps) of **9** as a yellow oil: IR (neat) 3293, 3063, 2924, 2855, 1740, 1649, 1534, 1453, 1379, 1175, 986, 930 cm^{-1}; ^{1}H NMR δ 7.26 (s, 5H), 6.68 (d, 1H, $J = 7.8$ Hz), 5.85–5.75 (m, 1H), 5.22 (d, 1H, $J = 17.3$ Hz), 5.14 (d, 1H, $J = 10.4$ Hz), 5.08 (s, 2H), 4.63–4.57 (m, 1H), 4.48 (d, 2H, $J = 5.6$ Hz), 2.38–2.28 (m, 2H), 2.2–2.1 (m, 3H), 2.0–1.9 (m, 1H), 1.55 (t, 2H, $J = 6.9$ Hz), 1.20 (bs, 12H), 0.82 (t, 3H, $J = 5.9$ Hz); ^{13}C NMR δ 173.0, 172.1, 171.6, 135.0, 131.7, 128.2, 128.1, 127.8, 117.9, 66.8, 64.9, 51.3, 36.0, 31.6, 29.9, 29.1, 29.0, 26.8, 25.3, 22.3, 13.8; MS (EI) m/z (relative intensity) 431 (M^+, 12), 319 (21), 296 (51), 142 (100), 124 (31), 91(91); HRMS (EI) m/z calcd for $C_{25}H_{37}NO_5$: 431.2672; found: 431.2673.

trans-1-Amino-4-*t*-butoxycarbonylamino-cyclohexane (8).

To a solution of 1.0 g (8.8 mmol) of *trans*-1,4-diaminocyclohexane in 30 mL of MeCN was added 1.93 g (8.85 mmol) of Boc$_2$O. The reaction was stirred at 22 °C for 12 h, concentrated in vacuo, poured into 50 mL of H_2O, and washed with Et$_2$O. The aqueous layer was acidified to pH 4 with 10% citric acid, salted out with NaCl, and extracted with EtOAc (3×). The resulting organic layer was dried (Na_2SO_4) and concentrated in vacuo to give 401 mg (21%) of **8** as a colorless solid: ^{1}H NMR (CDCl$_3$) δ 4.35 (br, 1H), 3.38 (br, 1H), 2.63–2.62 (m, 1H), 2.01–1.97 (m, 2H), 1.87–1.84 (m, 2H), 1.44 (s, 9H), 1.40 (m, 2H), 1.26–1.11 (m, 4H); HRMS (EI) m/z calcd for $C_7H_{13}N_2O_2$ (M-*t*-Bu): 157.0977; found: 157.0980.

4-[(*trans*-4-*t*-Butoxycarbonylamino-1-cyclohexyl)-carbamoyl]-2-decanoylamino-butyric acid benzyl ester (9).

To a solution of 518.1 mg (1.201 mmol) of 9 in 8.6 mL of THF was added 1.0 mL (12 mmol) of morpholine followed by 83 mg (0.072 mmol) of tetrakistriphenylphosphine Pd(0) under a nitrogen atmosphere at 22 °C. After stirring for 30 min, the reaction mixture was diluted with EtOAc and washed with 10% HCl and brine. The organic layer was dried (Na_2SO_4) and concentrated in vacuo to give 557.2 mg of carboxylic acid as a pale yellow solid. The carboxylic acid (50 mg, 0.13 mmol) and 27 mg (0.13 mmol) of diamine fragment 8 were dissolved in 0.85 mL of THF. To this solution was added 28 μL (0.20 mmol) of triethylaniine followed by 25 μL (0.17 mmol) of diethylphosphoryl cyanide (DEPC) at 0 °C. After stirring at 0 °C for 1 h and at 22 °C for 14 h, the reaction mixture was diluted with EtOAc, washed with 10% citric acid, H_2O, saturated aqueous $NaHCO_3$ and brine. The organic layer was dried (Na_2SO_4), concentrated in vacuo, and chromatographed on SiO_2 (hexanes:EtOAc, 1:4→EtOAc) to give 58.2 mg (77%) of **9** as an amorphous solid: ^{1}H NMR (CDCl$_3$) δ 7.35 (br, 5H), 6.54–6.52 (br, 1H), 5.93 (br,

1H), 5.22–5.12 (m, 2H), 4.56 (m, 1H), 4.37 (m, 1H), 3.70 (m, 1H), 3.41 (m, 1H), 2.24–2.17 (m, 5H), 1.19–1.15 (m, 5H), 1.59–1.53 (br, 4H), 1.44 (s, 9H), 1.26 (br, 12H), 0.90–0.86 (m, 5H).

2-Decanoylamino-4-({5-[2,5-diphenyl-oxazole-4-carbonyl]-*trans*-1,4-cyclohexyl}-carbamoyl)-butyric acid benzyl ester (11).

A mixture of 167 mg (0.284 mmol) of 9 in a HCl/dioxane solution was stirred at 0 °C for 5 min, warmed to 22 °C, stirred for 4 h, and concentrated in vacuo. The resulting residue and 75 mg (0.29 mmol) of oxazole segment 10 were dissolved in 0.95 mL of THF. To this solution was added 99 μl (0.71 mmol) of triethylamine followed by 238 mg (0.511 mmol) of PyBroP at 0 °C. After stirring at 0 °C for 1 h and at 22 °C for 12 h, the reaction mixture was diluted with EtOAc and washed with 10% HCl, H_2O, saturated aqueous $NaHCO_3$ and brine. The organic layer was dried (Na_2SO_4), concentrated in vacuo, and chromatographed on SiO_2 (hexanes:EtOAc, 1:1→1:2→1:3)to give 70 mg (33% over two steps) of 11 as a white solid: ^{1}H NMR (CDCl$_3$) δ 8.38–8.36 (m, 2H), 7.70–7.22 (m, 13H), 5.21–5.10 (m, 2H), 4.54–4.53 (m, 1H), 3.93–3.92 (m, 1H), 3.76 (m, 1H), 2.29–1.82 (m, 8H), 1.61 (br, 2H), 1.47–1.38 (m, 4H), 1.26 (br, 12H), 0.89–0.85 (m, 5H).

2-Decanoylamino-4-({5-[2,5-diphenyl-oxazole-4-carbonyl]-*trans*-1,4-cyclohexyl}-carbamoyl)-butyric acid (FY21-αα09).

To a solution of 23.6 mg (0.0321 mmol) of 11 in 0.24 mL of dioxane was added 0.385 mmol of aqueous lithium hydroxide (16.2 mg in 0.08 mL of H_2O) at 0 °C. The reaction mixture was stirred at 0 °C for 10 min and at 22 °C for 3 h, poured into 20 mL of 1120 and washed with Et$_2$O. The aqueous layer was acidified to pH 1 with 10% HCl, salted out with NaCl, and extracted with EtOAc (3×). The resulting organic layer was dried (Na_2SO_4) and concentrated in vacuo to give 12.1 mg (58%) of FY21-αα09 as a pale yellow solid: ^{1}H NMR (CDCl$_3$) δ 7.62–7.19 (m, 10H), 4.26–4.23 (m, 1H), 3.88 (m, 1H), 3.63–3.61 (m, 1H), 2.19–1.76 (m, 19H), 1.55 (m, 2H), 1.41–1.34 (m, 4H), 1.18 (br, 12H), 0.82–0.78 (m, 5H); MS (EI) m/z 626 ([M–H_2O]$^+$).

FY3-αα09

4-[(*trans*-2-*t*-Butoxycarbonylamino-1-cyclohexyl)-carbamoyl]-2-decanoylamino-butyric acid benzyl ester.

According to the procedure described for 9, 7(100 mg, 0.255 mmol) was converted to 4-[(*trans*-2-*t*-butoxycarbonylamino-1-cyclohexyl)-carbamoyl]-2-decanoylamino-butyric acid benzyl ester (162 mg, 30%) as an amorphous solid: ^{1}H NMR (CDCl$_3$) δ 7.38–7.28 (m, SH), 6.91–6.82 (m, 1H), 6.47–6.45 (m, 1H), 5.16–5.11 (m, 2H), 4.74–4.68 (m, 1H), 4.55–4.51 (m, IH), 3.51–3.50 (m, 1H), 3.34–3.31 (m, 1H), 2.24–1.97 (m, 8H), 1.73–1.61 (m, 4H), 1.39 (m, 9H), 1.25 (m, 16H), 0.88 (m, 3H).

2-Decanoylamino-4-({4-[2,5-diphenyl-oxazole-4-carbonyl]-*trans*-1,2-cyclohexyl}-carbamoyl)-butyric acid benzyl ester.

According to the procedure described for 11, 4-[(*trans*-2-*t*-butoxycarbonylamino-1-cyclohexyl)-carbamoyl]-2-decanoylamino-butyric acid benzyl ester was converted

to 2-decanoylamino-4-({4-[2,5-diphenyl-oxazole-4-carbonyl]-*trans*-1,2-cyclohexyl}-carbamoyl)-butyric acid benzyl ester (53.8 mg, 78%): ^{1}H NMR (CDCl$_3$) δ 8.34–8.32 (m, 2H), 8.11–8.10 (m, 2H), 7.51–7.14 (m, 11H), 6.68–6.57 (m, 1H), 6.41–6.38 (m, 1H), 5.05–4.86 (m, 2H), 4.43–4.36 (m, 1H), 3.81–3.74 (m, 2H), 2.17–1.18 (m, 8H), 1.65–1.32 (m, 8H), 1.24 (br, 12H), 0.87 (m, 3H).

2-Decanoylamino-44{4-[2,5-diphenyl-oxazole-4-carbonyl]-*trans*-1,2-cyclohexyl}-carbamoyl)-butyric acid (FY3-αα09). According to the procedure described for FY21-αα09, 2-decanoylamino-4-({4-[2,5-diphenyl-oxazole-4-carbonyl]-*trans*-1,2-cyclohexyl}-carbamoyl)-butyric acid benzyl ester was converted to FY3-αα09 (40.8 mg, 86%): ^{1}H NMR (CDCl$_3$) δ 8.30–8.28 (m, 2H), 8.09 (br, 2H), 7.60–7.36 (m, 6H), 4.31 (m, 1H), 3.93 (m, 1H), 3.80 (m, 1H), 2.50–1.83 (m, 8H), 1.52–1.43 (m, 8H), 1.23 (br, 12H), 0.87 (br, 3H); HRMS (EI) *m/z* calcd for C$_{37}$H$_{48}$N$_4$O$_6$: 644.3574; found: 644.3595.

FY4-αα09

4-[(*cis*-2-*t*-Butoxycarbonylamino-1-cyclohexyl)-carbamoyl]-2-decanoylamino-butyric acid benzyl ester. According to the procedure described for 9, 7(250 mg, 0.637 mmol) was converted to 4-[(*cis*-2-*t*-butoxycarbonylamino-1-cyclohexyl)-carbamoyl]-2-decanoylamino-butyric acid benzyl ester (159 mg, 42%): ^{1}H NMR (CDCl$_3$) δ 7.35 (br, 5H), 6.72 (m, 1H), 6.60 (m, 1H), 5.23–5.12 (m, 2H), 4.56 (m, 1H), 4.05 (m, 1H), 3.82 (m, 1H), 2.29–2.18 (m, 4H), 2.02 (m, 2H), 1.70–1.62 (m, 4H), 1.44 (br, 9H), 1.32–1.26 (m, 16H), 0.88 (m, 3H).

2-Decanoylamino-4-({4-[2,5-diphenyl-oxazole-4-carbonyl]-*cis*-1,2-cyclohexyl}-carbamoyl)-butyric acid benzyl ester. According to the procedure described for 11, 4-[(*cis*-2-*t*-butoxycarbonylamino-1-cyclohexyl)-carbamoyl]-2-decanoylamino-butyric acid benzyl ester was converted to 2-decanoylamino-4-({4-[2,5-diphenyl-oxazole-4-carbonyl}-*cis*-1,2-cyclohexyl}-carbamoyl)-butyric acid benzyl ester (41.2 mg, 41%): ^{1}H NMR (CDCl$_3$) δ 8.39–8.34 (m, 2H), 8.11–8.02 (m, 2H), 7.52–7.16 (m, 11H), 5.17–4.79 (m, 2H), 4.65–4.56 (m, 1H), 4.36 (1H), 4.16–4.09 (m, 1H), 2.24–1.54 (m, 16H), 1.19 (br, 12H), 0.86 (m, 3H).

2-Decanoylamino-4-({4-[2,5-diphenyl-oxazole-4-carbonyl]-*cis*-1,2-cyclohexyl}-carbamoyl)-butyric acid (FY4-αα09). According to the procedure described for FY2I-αα09, 2-decanoylamino-4-({4-[2,5-diphenyl-oxazole-4-carbonyl]-*cis*-1,2-cyclohexyl}-carbamoyl)-butyric acid benzyl ester was converted to FY4-αα09 (15.4 mg, quant.) as a pale yellow oil: ^{1}H NMR (CDCl$_3$) δ 8.67–8.21 (m, 2H), 8.04–7.98 (m, 2H), 7.45–7.19 (m, 6H), 4.33 (m, 1H), 4.01–3.97 (m, 2H), 2.11–1.47 (m, 16H), 1.16 (m, 12H), 0.78 (m, 3H); MS (EI) *m/z* 644 (M$^+$).

FY5-αα09

4-[(4-*t*-Butoxycarbonylamino-1-phenyl)-carbamoyl]-2-decanoyl-amino-butyric acid benzyl ester. According to the procedure described for 9,7 (247 mg, 0.631 mmol) was converted to 4-[(4-*t*-butoxycarbonylaznino-1-phenyl)-

carbamoyl]-2-decanoyl-amino-butyric acid benzyl ester (295 mg, 80%): ^{1}H NMR (CDCl$_3$) δ 7.70–7.63 (m, 2H), 7.58–7.30 (m, 7H), 6.48 (m, 2H), 5.21–5.11 (m, 2H), 4.65 (m, 1H), 2.37–2.18 (m, 4H), 1.97 (m, 1H), 1.72 (m, 1H), 1.61 (m, 2H), 1.51 (s, 9H), 1.25 (br. 12H), 0.87 (m, 3H).

2-Decanoylamino-4-({5-[2,5-diphenyl-oxazole-4-carbonyl]-1,4-phenyl}-carbamoyl)-butyric acid benzyl ester. According to the procedure described for 11,4-[(4-*t*-butoxycarbonylamino-1-phenyl)-carbamoyl}-2-decanoyl-amino-butyric acid benzyl ester was converted to 2-decanoylamino-4-({5-[2,5-diphenyl-oxazole-4-carbonyl]-1,4-pheyl}-carbamoyl)-butyric acid benzyl ester (22.4 mg, 12%) as a pale yellow oil: ^{1}H NMR (CDCl$_3$) δ 7.70–7.13 (m, 19H), 5.16 (m, 2H), 4.66 (m, 1H), 2.40–1.81 (m, 6H), 1.61 (m, 2H), 1.25 (br, 12H), 0.87 (m, 3H).

2-Decanoylamino-4-({5-[2,5-diphenyl-oxazole-4-carbonyl]-1,4-phenyl}-carbamoyl)-butyric acid (FY5-αα09). According to the procedure described for FY21-αα09, 2-decanoylamino-4-({5-[2,5-diphenyl-oxazole-4-carbonyl]-1,4-phenyl}-carbamoyl)-butyric acid benzyl ester was converted to FY5-αα09 (13.9 mg, 71%): ^{1}H NMR (CDCl$_3$) δ 7.62–7.24 (m, 14H), 4.64 (m, 1H), 2.50 (m, 1H), 2.19–1.89 (m, 5H), 1.55 (m, 2H), 1.19 (br, 12H), 0.83 (m, 3H); MS (EI) *m/z* 638 (M$^+$T), 620 ([M−H$_2$O]$^+$).

FY7-αα09

4-[(3-*t*-Butoxycarbonylamino-1-phenyl)-carbamoyl]-2-decanoyl-amino-butyric acid benzyl ester. According to the procedure described for 9, 7 (300 mg, 0.766 mmol) was converted to 4-[(3-*t*-butoxycarbonylamino-1-phenyl)-carbamoyl]-2-decanoyl-amino-butyric acid benzyl ester (194 mg, 43%) as a pale yellow oil: ^{1}H NMR (CDCl$_3$) δ 7.64 (br, 1H), 7.34 (br, 5H), 7.20 (m, 3H), 6.70 (m, 1H), 6.58 (m, 1H), 5.20–5.15 (m, 2H), 4.65 (m, 1H), 2.39–2.17 (m, 5H), 2.03 (m, 1H), 1.60 (br, 2H), 1.50 (br. 9H), 1.24 (br, 12H), 0.89 (m, 3H).

2-Decanoylamino-4-({4-[2,5-diphenyl-oxazole-4-carbonyl]-1,3-phenyl}-carbamoyl)-butyric acid benzyl ester. According to the procedure described for 11, 4-[(3-*t*-butoxycarbonylamino-1-phenyl)-carbamoyl]-2-decanoyl-amino-butyric acid benzyl ester was converted to 2-decanoylamino-4-({4-[2,5-diphenyl-oxazole-4-carbonyl]-1,3-phenyl}-carbamoyl)-butyric acid benzyl ester (92.7 mg, 79%): ^{1}H NMR (CDCl$_3$) δ 8.35 (m, 1H), 8.14–8.02 (m, 2H), 7.52–7.24 (m, 16H), 6.70 (m, 1H), 5.13 (m, 2H), 4.66 (m, 1H), 2.41–1.97 (m, 6H), 1.58 (m, 2H), 1.21 (br, 12H), 0.84 (m, 3H); HRMS (EI) *m/z* calcd for C$_{44}$H$_{48}$N$_4$O$_6$: 728.3574, found: 728.3552.

2-Decanoylamino-4-({4-[2,5-diphenyl-oxazole-4-carbonyl)-1,3-phenyl}-carbamoyl)-butyric acid (FY7-αα09). According to the procedure described for FY21-αα09, 2-decanoylamino-4-({4-[2,5-diphenyl-oxazole-4-carbonyl]-1,3-phenyl}-carbamoyl)-butyric acid benzyl ester was converted to FY7-αα09 (31.9 mg, quant.): ^{1}H NMR (CDCl$_3$) δ 8.24 (m, 1H), 8.04–7.95 (m, 2H), 7.44–7.19 (m, 11H), 4.50 (m, 1H), 2.51–2.44 (m, 2H), 2.20–1.98 (m, 3H), 1.76 (m 1H), 1.50 (m, 2H), 1.12 (br, 12H), 0.76 (m, 3H); MS (EI) *m/z* 620 ([M−H$_2$O]$^+$).

FY8-αα09

4-[(2-*t*-Butoxycarbonylamino-1-phenyl)-carbamoyl]-2-decanoyl-amino-butyric acid benzyl ester. According to the procedure described for 9, 7 (301 mg, 0.769 mmol) was converted to 4-[(2-*t*-butoxycarbonylamino-1-phenyl)-carbamoyl]-2-decanoyl-amino-butyric acid benzyl ester (239 mg, 53%) as a brown oil: ^{1}H NMR (CDCl$_3$) δ 7.57 (m, 1H), 7.48 (m, 1H), 7.34 (br, 5H), 7.19–7.06 (m, 2H), 6.54 (m, 1H), 5.16 (m, 2H), 4.63 (m, 1H), 2.43–2.19 (m, 4H), 2.04–1.82 (m, 2H), 1.60 (m, 2H), 1.49 (br, 9H), 1.25 (br, 12H), 0.88 (m, 3H).

2-Decanoylamino-4-({3-[2,5-diphenyl-oxazole-4-carbonyl]-1,2-phenyl}-carbamoyl)-butyric acid benzyl ester. According to the procedure described for 11, 4-[(2-*t*-butoxycarbonylamino-1-phenyl)-carbamoyl]-2-decanoyl-amino-butyric acid benzyl ester was converted to 2-decanoylamino-4-({3-[2,5-diphenyl-oxazole-4-carbonyl]-1,2-phenyl}-carbamoyl)-butyric acid benzyl ester (113 mg, 64%) as a pale yellow solid: ^{1}H NMR (CDCl$_3$) δ 8.36 (m, 1H), 7.95 (br, 2H), 7.42–7.15 (m, 16H), 6.67 (m, 1H), 5.03 (m, 2H), 4.58 (m, 1H), 2.47–1.89 (m, 6H), 1.50 (m, 2H), 1.09 (br, 12H), 0.86 (m, 3H).

2-Decanoylamino-4-{{3-[2,5-diphenyl-oxazole-4-carbonyl)-1,2-phenyl}-carbamoyl}-butyric acid benzyl ester (FY8-αα09). According to the procedure described for FY21-αα09, 2-decanoylamino-4-({3-[2,5-diphenyl-oxazole-4-carbonyl]-1,2-phenyl}-carbamoyl)-butyric acid benzyl ester was converted to FY8-αα09 (93.3 mg, 94%): ^{1}H NMR (CDCl$_3$) δ 8.23 (m, 1H), 7.99 (m, 2H), 7.40–7.05 (m, 11H), 4.37 (m, 1H), 2.52–1.69 (m, 6H), 1.38 (m, 2H), 1.10 (br, 12H), 0.77 (m, 3H); MS (EI) *m/z* 638 (M$^+$), 620 ([M−H$_2$O]$^+$).

FY9-αα09

4-[(3-*t*-Butoxycarbonylamino-propyl)-carbamoyl]-2-decanoylamino-butyric acid benzyl ester. According to the procedure described for 9, 7 (304 mg, 0.776 mmol) was converted to 4-[(3-*t*-butoxycarbonylamino-propyl)-carbamoyl]-2-decanoylamino-butyric acid benzyl ester (279 mg, 66%): ^{1}H NMR (CDCl$_3$) δ 7.36 (m, 5H), 6.72 (m, 1H), 5.16 (m, 2H), 4.56 (m, 1H), 3.29–3.11 (m, 4H), 2.27–2.15 (m, 4H), 1.99 (m, 1H), 1.73 (m, 2H), 1.63–1.57 (m, 3H), 1.44 (br, 9H), 1.26 (br, 12H), 0.88 (m, 3H).

2-Decanoylamino-4-{{4-[2,5-diphenyl-oxazole-4-carbonyl]-propyl}-carbamoyl)-butyric acid benzyl ester. According to the procedure described for 11, 4-[(3-*t*-butoxycarbonylamino-propyl)-carbamoyl]-2-decanoylamino-butyric acid benzyl ester was converted to 2-decanoylamino-4-({4-[2,5-diphenyl-oxazole-4-carbonyl]-propyl}-carbamoyl)-butyric acid benzyl ester (131 mg, 63%): ^{1}H NMR (CDCl$_3$) δ 8.37–7.33 (m, 15H), 6.79 (m, 2H), 5.16 (m, 2H), 4.58 (m, 1H), 3.53–3.32 (m, 4H), 2.32–2.17 (m, 6H), 1.87–1.73 (m, 4H), 1.23 (br, 12H), 0.86 (m, 3H).

2-Decanoylamino-4-({4-[2,5-diphenyl-oxazole-4-carbonyl]-propyl}-carbamoyl)-butyric acid (FY9-αα09). According to the procedure described for FY21-αα09, 2-decanoyl-amino-4-({4-[2,5-diphenyl-oxazole-4-carbonyl]-propyl}-

carbamoyl)butyric acid benzyl ester was converted to FY9-αα09 (169 mg, quant.) as a pale yellow oil: ^{1}H NMR (CDCl$_3$) δ 8.30–7.24 (m, 10H), 4.49 (m, 1H), 3.49–3.32 (m, 4H), 2.40 (m, 2H), 2.21 (m, 2H), 1.98 (m, 2H), 1.79 (m, 2H), 1.57 (m, 2H), 1.20 (br, 12H), 0.84 (m, 3H); MS (EI) *m/z* 604 (M$^+$), 586 ([M–H$_2$O]$^+$).

FY10-αα09

4-[(2-*t*-Butoxycarbonylamino-piperazine)-carbamoyl]-2-decanoyl-amino-butyric acid benzyl ester. According to the procedure described for 9, 7(300 mg, 0.766 mmol) and *tert*-butyl 1-piperazinecarboxylate (143 mg, 0.768 mmol) were converted to 4-[(2-*t*-butoxycarbonylamino-piperazine)-carbamoyl]-2-decanoyl-amino-butyric acid benzyl ester (366 Mg, 85%) as a yellow oil: ^{1}H NMR (CDCl$_3$) δ 7.36 (br, 5H), 6.65 (m, 1H), 5.17 (m, 2H), 4.59 (m, 1H), 3.57 (m, 2H), 3.43 (m, 4H), 3.29 (m, 2H), 2.35–2.05 (m, 5H), 1.70 (m, 1H), 1.61 (m, 2H), 1.47 (br, 9H), 1.26 (br, 12H), 0.88 (m, 3H).

2-Decanoylamino-4-{{3-[2,5-diphenyl-oxazole-4-carbonyl]-piperazine}-carbamoyl)-butyric acid benzyl ester. According to the procedure described for 11, 4-[(2-*t*-butoxycarbonylamino-piperazine)-carbamoyl]-2-decanoyl-amino-butyric acid benzyl ester was converted to 2-decanoylamino-4-({3-[2,5-diphenyl-oxazole-4-carbonyl}-piperazine}-carbamoyl)-butyric acid benzyl ester (160 mg, 68%): ^{1}H NMR (CDCl$_3$) δ 8.10–7.29 (m, 15H), 6.65 (m, 1H), 5.14 (m, 2H), 4.60 (m, 1H), 3.78–3.34 (m, 8H), 2.38–2.08 (m, 5H), 1.86 (m, 1H), 1.59 (m, 2H), 1.24 (br, 12H), 0.86 (m, 3H).

2-Decanoylamino-4-({3-[2,5-diphenyl-oxazole-4-carbonyl-piperazine-carbamoyl)-butyric acid (FY10-αα09). According to the procedure described for FY21-αα09, 2-decanoylamino-4-({3-[2,5-diphenyl-oxazole-4-carbonyl]-piperazine}-carbamoyl)-butyric acid benzyl ester was converted to FY10-αα09 (146 mg, quant.): ^{1}H NMR (CDCl$_3$) δ 8.05–7.24 (m, 10H), 4.42 (m, 1H), 3.62–3.43 (m, 8H), 2.53 (m, 2H), 2.20 (m, 2H), 2.02 (m, 2H), 1.53 (m, 2H), 1.20 (br, 12H), 0.84 (m, 3H); MS (EI) *m/z* 616 (M$^+$), 598 ([M−H$_2$O]$^+$).

SC-ααδ 17A

DL-2-(2,2,2-Trichloroethoxycarbonylamino)-pentanoic acid 5-allyl ester 1-methyl ester (2b). To a stirred suspension of 5.0 g (34 mmol) of DL-glutamic acid (1) in 85 mL of allyl alcohol was added dropwise 10.8 mL (85 mmol) of chlorotrimethylsilane. The suspension was stirred at 22 °C for 13 h and concentrated in vacuo. The resulting oil was dissolved in 90 mL of dioxane. This solution was treated with 118.9 mmol of aqueous sodium carbonate (12.61 g in 90 mL of H$_2$O) at 0 °C, stirred for 5 mm, and treated with 4.80 mL (34.7 mmol) of TrocCl. The reaction mixture was stirred at 0 °C for 10 mm and warmed to 22 °C, stirred for 16 h, concentrated in vacuo, quenched with 150 mL of H$_2$O and washed with Et$_2$O. The aqueous layer was acidified to pH 1 with concentrated HCl, salted out with NaCl, and extracted with EtOAc (3×). The resulting organic layer was dried (Na$_2$SO$_4$) and concentrated in vacuo to give

7.92 g of carboxylic acid as a yellow oil. To a solution of the resulting oil in 29 mL of DMF was added 3.50 g (35.0 mmol) of $KHCO_3$ and 1.60 mL (26.2 mmol) of iodomethane. The reaction mixture was stirred at 22 °C for 16 h, diluted with EtOAc, and washed with 10% HCl, H_2O, saturated aqueous $NaHCO_3$ and brine. The organic layer was dried (Na_2SO_4), concentrated in vacuo, and chromatographed on SiO_2 (hexanes:EtOAc, 5:1→4:1→3:1→2:1) to give 6.26 g (49% over three steps) of **2b** as a pale yellow oil: ^{1}H NMR (CDCl$_3$) δ 5.95–5.86 (m, 1H), 5.71 (d, 1H, J 7.2 Hz), 5.34–5.22 (m, 2H), 4.72 (AB, 2H, J = 13.9 Hz), 4.58 (d, 2H, J 5.8 Hz), 4.47–4.40 (m, 1H), 3.77 (s, 3H), 2.50–2.42 (m, 2H), 2.32–2.23 (m, 1H), 2.07–2.00 (m, 1H); MS (CI) m/z 376 ([M + 1]$^+$).

2-Oleoylamino-pentanedioic acid 5-allyl ester 1-methyl ester. To a solution of 947 mg (2.51 mmol) of **2b** in 3.3 mL of acetic acid and 4.9 mL of THF was added 3.29 g (50.271 mmol) of zinc dust. The reaction mixture was stirred at 22 °C for 1 h, filtered through a Celite pad, and the filtrate was concentrated in vacuo. The resulting residue was diluted with EtOAc and washed with saturated aqueous $NaHCO_3$ and brine. The organic layer was dried (Na_2SO_4) and concentrated in vacuo to give free amine. This amine (67.7 mg) was dissolved in 1.1 mL of CH_2Cl_2 and treated with 0.14 mL (1.02 mmol) of triethylamine and 0.17 mL (0.51 mmol) of oleoyl chloride at 0 °C. The reaction mixture was stirred at 0 °C for 15 min and warmed to 22 °C, stirred for 14 h, diluted with EtOAc, and washed with 10% HCl, H_2O, saturated aqueous $NaHCO_3$ and brine. The organic layer was dried (Na_2 SO$_4$), concentrated in vacuo, and chromatographed on SiO_2 (hexanes:EtOAc, 8:1→7:1→5:1) to give 110 mg (70%) of 2-oleoylamino-pentanedioic acid 5-allyl ester 1-methyl ester as a pale yellow oil: ^{1}H NMR (CDCl$_3$) δ 6.12 (d, 1H, J 7.7 Hz), 5.98–5.85 (m, 1H), 5.37–5.23 (m, 4H), 4.68–4.58 (m, 3H), 3.76 (s, 3H), 2.47–2.17 (m, 6H), 2.07–1.95 (m, 4H), 1.60 (m, 2H), 1.30 (brd, 20H, J = 10.5 Hz), 0.89 (m, 3H); MS (EI) m/z 465 (M$^+$).

4-[(2-Allyloxycarbonylamino-ethyl)-benzyl-carbamoyl]-2-oleoyl-amino-butyric acid methyl ester. To a solution of 110 mg (0.236 mmol) of 2-oleoylamino-pentanedioic acid 5-allyl ester 1-methyl ester in 1 mL of THF was added 0.20 mL (2.4 mmol) of morpholine followed by 27.3 mg (0.024 mmol) of tetrakistriphenylphosphine Pd(0) under nitrogen atmosphere at 22 °C. After stirring for 30 min, the reaction mixture was diluted with EtOAc, and washed with 10% HCl and brine. The organic layer was dried (Na_2SO_4), concentrated in vacuo. The resulting residue and 27.0 mg (0.115 mmol) of diamine segment were dissolved in 0.5 mL of THF. The solution was treated with 0.03 mL (0.18 mmol) of *N,N*-diisopropylethylamine and 0.070 g (0.15 mmol) of PyBroP at 0 °C, stirred for 1 h, warmed to 22 °C and stirred for 9 h. The reaction mixture was diluted with EtOAc, washed with 10% HCl, H_2O, saturated aqueous $NaHCO_3$ and brine. The organic layer was dried (Na_2SO_4), concentrated in vacuo, and chromatographed on SiO_2 (hexanes:EtOAc, 1:1→1:2) to give 169 mg (quant.) of 4-[(2-allyloxycarbonylamino-ethyl)-benzyl-

carbamoyl]-2-oleoyl-amino-butyric acid methyl ester: ^{1}H NMR (CDCl$_3$) δ 7.69–7.13 (m, 5H), 6.65 (m, 1H), 5.91–5.85 (m, 2H), 5.35–5.17 (m, 4H), 4.61–4.45 (m, 5H), 3.73–3.36 (m, 7H), 2.45–2.00 (m, 10H), 1.60 (m, 2H), 1.27 (br, 20H), 0.86 (m, 3H); MS (EI) m/z 641 (M$^+$).

2-Oleoylamino-4-(benzyl-{3-[2,5-diphenyl-oxazole-4-carbonyl]-ethyl}-carbamoyl)-butyric acid methyl ester. To a solution of 169 mg (0.263 mmol) of 4-[(2-allyloxycarbonylamino-ethyl)-benzyl-carbamoyl]-2-oleoyl-amino-butyric acid methyl ester in 2 mL of CH_2Cl_2 was added 0.031 mL (0.53 mmol) of acetic acid and 9 mg (0.008 mmol) of tetrakistriphenylphosphine Pd(0) followed by 0.092 mL (0.34 mmol) of tributyltin hydride under nitrogen atmosphere at 22 °C. After stirring for 30 min, the reaction mixture was diluted with EtOAc, washed with saturated aqueous $NaHCO_3$ and brine. The organic layer was dried (Na_2SO_4), concentrated in vacuo. The resulting residue and 70 mg (0.26 mmol) of oxazole fragment were dissolved in 1 mL of THF. To this solution was added 0.092 mL (0.66 mmol) of triethylamine followed by 0.221 g (0.473 mmol) of PyBroP at 0 °C. After stirring at 0 °C for 1 h and at 22 °C for 12 h, the reaction mixture was diluted with EtOAc, washed with 10% HCl, H_2O, saturated aqueous $NaHCO_3$ and brine. The organic layer was dried (Na_2SO_4), concentrated in vacuo, and chromatographed on SiO_2 (hexane:EtOAc, 2:1→1:1) to give 2-oleoylamino-4-(benzyl-{3-[2,5-diphenyl-oxazole-4-carbonyl]-ethyl}-carbamoyl)-butyric acid methyl ester (104 mg, 55%) as a pale yellow oil: ^{1}H NMR (CDCl$_3$) δ 8.37–8.35 (m, 2H), 8.10 (m, 2H), 7.52–7.13 (m, 6H), 5.31 (m, 2H), 4.70–4.60 (m, 3H), 3.68–3.52 (m, 7H), 2.13–1.95 (m, 10H), 1.64 (m, 2H), 1.26 (br, 20H), 0.90 (m, 3H); MS (EI) m/z 804 (M$^+$).

2-Oleoylamino-4-(benzyl-{3-[2,5-diphenyl-oxazole-4-carbonyl]-ethyl}-carbamoyl)-butyric acid (SC-ααδ17A). To a solution of 104 mg (0.129 mmol) of 2-oleoylamino-4-(benzyl-{3-[2,5-diphenyl-oxazole-4-carbonyl]-ethyl}-carbamoyl)-butyric acid methyl ester in 0.5 mL of dioxane was added 1.6 mmol of aqueous lithium hydroxide (65 mg in 0.2 mL of H_2O) at 0 °C. The reaction mixture was stirred at 0 °C for 10 min and at 22 °C for 1 h, poured into 50 mL of H_2O and washed with Et$_2$O. The aqueous layer was acidified to pH 1 with 10% HCl, salted out with NaCl, and extracted with EtOAc (3×). The resulting organic layer was dried (Na_2SO_4) and concentrated in vacuo to give SC-ααδ17A (28.1 mg, 28%) as a pale yellow oil: ^{1}H NMR (CDCl$_3$) δ 8.26–8.23 (m, 2H), 8.01 (m, 2H), 7.43–7.07 (m, 11H), 5.25 (m, 2H), 4.69–4.49 (m, 2H), 4.34–4.26 (m, 1H), 3.82–3.45 (m, 6H), 2.19–1.91 (m, 8H), 1.47 (m, 2H), 1.18 (br, 20H), 0.80 (m, 3H); HRMS (EI) m/z calcd for $C_{48}H_{60}N_4O_5$ ([M−H$_2$O]$^+$): 772.4564; found: 772.4540.

SC-ααδ17B

4-[(2-Allyloxycarbonylamino-ethyl)-benzyl-carbamoyl]-2-(2,2,2-trichloroethoxycarbonylamino)-butyric acid methyl ester (3). According to the procedure described for 4-[(2-allyloxycarbonylamino-ethyl)-benzyl-carbamoyl]-2-

oleoyl-amino-butyric acid methyl ester, **2b** (217 mg, 0.577 mmol) was converted to 4-[(2-allyloxycarbonyl-amino-ethyl)-benzyl-carbamoyl]-2-(2,2,2-trichloroeth-oxycarbonyl-amino)-butyric acid methyl ester (**3**, 294 mg, 92%) as an orange oil: ^{1}H NMR (CDCl$_3$) δ 7.68–7.11 (m, 5H), 6.08 (m, 1H), 5.91 (m, 1H), 5.32–5.19 (m, 2H), 4.8 1–4.40 (m, 5H), 3.80–3.65 (m, 5H), 3.40 (m, 2H), 2.61–2.31 (m, 6H); MS (EI) m/z 553 (M$^+$).

2-(2,2,2-Trichloroethoxycarbonylamino)-4-(benzyl-{3-[2,5-diphenyl-oxazole-4-carbonyl-ethyl}-carbamoyl)-butyric acid methyl ester (4).

According to the procedure described for 2-oleoylamino-4-(benzyl-{3-[2,5-di-phenyl-oxazole-4-carbonyl]-ethyl}-carbamoyl)-butyric acid methyl ester, 4-[(2-allyloxycarbonylamino-ethyl)-benzyl-carbamoyl]-2-(2,2,2-trichloroethoxycarbonyl-amino)-butyric acid methyl ester (**3**, 887 mg, 1.604 mmol) was converted to 2-(2,2,2-trichloroethoxy-carbonylamino)-4-(benzyl-{3-[2,5-diphenyl-oxazole-4-carbonyl]-ethyl}-carbamoyl)-butyric acid methyl ester (**4**, 819 mg, 71%) as a pale yellow oil: ^{1}H NMR (CDCl$_3$) δ 8.38–8.35 (m, 2H), 8.13–8.09 (m, 2H), 7.53–7.13 (m, 11H), 4.74–4.58 (m, 4H), 4.36 (m, 1H), 3.80–3.52 (m, 7H), 2.51–2.05 (m, 4H); MS (EI) m/z 716 (M$^+$).

2-Linoleylamino-4-(benzyl-{3-[2,5-diphenyl-oxazole-4-carbonyl]-ethyl}-carbamoyl)-butyric acid methyl ester.

To a solution of 143 mg (0.199 mmol) of 2-(2,2,2-tri-chloroethoxycarbonylamino)-4-(benzyl-{3-[2,5-diphenyl-oxazole-4-carbonyl]-ethyl}-carbamoyl)-butyric acid methyl ester in 0.3 mL of acetic acid and 0.5 mL of THF was added 0.260 g (3.98 mmol) of zinc dust. The reaction was stirred at 22 °C for 1 h. The mixture was filtered through a Celite pad and the filtrate was con-centrated in vacuo. The resulting residue was diluted with EtOAc and washed with saturated aqueous NaHCO$_3$ and brine. The organic layer was dried (Na$_2$SO$_4$) and concentrated in vacuo to give free amine. The resulting residue was dissolved in 0.1 mL of CH$_2$Cl$_2$ and treated with 0.3 mg (0.003 mmol) of DMAP, 9.3 μl (0.03 mmol) of linoleic acid and 6.2 mg (0.032 mmol) of EDCI at 0 °C. The reaction mixture was stirred at 0 °C for 15 min and warmed to 22 °C, stirred for 14 h, diluted with EtOAc, and washed with 10% HCl, H$_2$O, satu-rated aqueous NaHCO$_3$ and brine. The organic layer was dried (Na$_2$SO$_4$), concentrated in vacuo, and chro-matographed on SiO$_2$ (hexanes:EtOAc, 7:1→5:1) to give 67.7 mg (42%) of 2-linoleylamino-4-(benzyl-{3-[2,5-diphenyl-oxazole-4-carbonyl]-ethyl}-carbamoyl)-butyric acid methyl ester of as a colorless oil: ^{1}H NMR (CDCl$_3$) δ 8.37–8.35 (m, 2H), 8.13–8.07 (m, 2H), 7.52–7.13 (m, 11H), 5.33 (m, 4H), 4.70–4.51 (m, 3H), 3.75–3.52 (m, 7H), 2.76 (m, 2H), 2.45 (m, 2H), 2.23–1.99 (m, 8H), 1.55 (m, 2H), 1.26 (br, 14H), 0.88 (m, 3H); MS (EI) m/z 802 (M$^+$).

2-Linoleylamino-4-(benzyl-{3-[2,5-diphenyl-oxazole-4-carbonyl]-ethyl}-carbamoyl)-butyric acid (SC-ααδ17B).

According to the procedure described for SCααδ17A, 2-linoleylamino-4-(benzyl-{3-[2,5-diphenyl-oxazole-4-carbonyl]-ethyl}-carbamoyl)-butyric acid methyl ester (67.7 mg, 0.0843 mmol) was converted to SC-ααδ17B (66.4 mg, 99%) as a pale yellow oil: ^{1}H NMR (CDCl$_3$) δ

8.33–8.30 (m, 2H), 8.08 (m, 2H), 7.50–7.03 (m, 11H), 5.34 (m, 2H), 4.72–4.42 (m, 4H), 4.13–4.07 (m, 1H), 3.80–3.48 (m, 4H), 2.75 (m, 2H), 2.50–2.01 (m, 10H), 1.54 (m, 2H), 1.23 (br, 14H), 0.88 (m, 3H); HRMS (EI) m/z calcd for C$_{48}$H$_{59}$N$_4$O$_5$ (M–OH): 771.4485, found: 771.4487.

SC-ααδA

2-Citronellylamino-pentanedioic acid 5-allyl ester 1-methyl ester.

To a solution of 947 mg (2.51 mmol) of **2b** in 3.3 mL of acetic acid and 4.9 mL of THF was added 3.286 g (50.27 mmol) of zinc dust. The reaction was stirred at 22 °C for 1 h. The mixture was filtered through a Celite pad and the filtrate was concentrated in vacuo. The resulting residue was diluted with EtOAc and washed with saturated aqueous NaHCO$_3$ and brine. The organic layer was dried (Na$_2$SO$_4$) and con-centrated in vacuo to give free amine. The resulting residue (68.7 mg) was dissolved in 1.1 mL of CH$_2$Cl$_2$ and treated with 4.2 mg (0.034 mmol) of DMAP, 69 μL (0.38 mmol) of racemic citronellic acid and 79 mg (0.41 mmol) of EDCI at 0 °C. The reaction mixture was stirred at 0 °C for 15 mm and warmed to 22 °C, stirred for 14 h, diluted with EtOAc, and washed with 10% HCl, H$_2$O, saturated aqueous NaHCO$_3$ and brine. The organic layer was dried (Na$_2$SO$_4$), concentrated in vacuo, and chromatographed on SiO$_2$ (hexanes:EtOAc, 7:1→5:1) to give 83.9 mg (69%) of 2-citronellylamino-pentanedioic acid 5-allyl ester 1-methyl ester as a color-less oil: ^{1}H NMIR (CDCl$_3$) δ 6.19 (d, 1H, J=7.4 Hz), 5.95–5.86 (m, 1H), 5.34–5.23 (m, 2H), 5.09 (m, 1H), 4.66–4.57 (m, 3H), 3.75 (s, 3H), 2.48–1.97 (m, 9H), 1.68 (s, 3H), 1.60 (s, 3H), 1.38–1.36 (m, 1H), 1.26–1.20 (m, 1H), 0.99–0.93 (m, 3H); MS (EI) m/z 353 (M$^+$).

4-[(2-Allyloxycarbonylamino-ethyl)-benzyl-carbamoyl]-2-citronellyl-amino-butyric acid methyl ester.

According to the procedure described for 4-[(2-allyloxycarbonyl-amino-ethyl)-benzyl-carbamoyl]-2-oleoyl-amino-butyric acid methyl ester, 2-citronellylamino-pentanedioic acid 5-allyl ester 1-methyl ester (83.9 mg, 0.237 mmol) was converted to 4-[(2-allyloxycarbonylamino-ethyl)-benzyl-carbamoyl]-2-citronellyl-amino-butyric acid methyl ester (128 mg, quant.) as a brown oil: ^{1}H NMR (CDCl$_3$) δ 7.70–7.13 (m, 5H), 6.56 (m, 1H), 5.92–5.86 (m, 1H), 5.72 (br, 1H), 5.32–5.18 (m, 2H), 5.08 (m, 1H), 4.62–4.45 (m, 5H), 3.74–3.71 (m, 5H), 3.42–3.23 (m, 4H), 2.50–1.93 (m, 9H), 1.67 (s, 3H), 1.59 (s, 3H), 1.37–1.32 (m, 1H), 1.26–1.18 (m, 1H), 0.92 (m, 3H); MS (FAB) m/z 530 ([M + 1]$^+$).

2-Citronellylamino-4-(benzyl-{3-[2,5-diphenyl-oxazole-4-carbonyl]-ethyl}-carbamoyl)-butyric acid methyl ester.

According to the procedure described for 2-oleoyl-amino-4-(benzyl-{3-[2,5-diphenyl-oxazole-4-carbonyl]-ethyl}-carbamoyl)-butyric acid methyl ester, 4-[(2-allyl-oxycarbonylamino-ethyl)-benzyl-carbamoyl]-2-citro-nellyl-amino-butyric acid methyl ester (128 mg, 0.241 mmol) was converted to 2-citronellylamino-4-(benzyl-{3-[2,5-diphenyl-oxazole-4-carbonyl]-ethyl}-carbamoyl)-butyric acid methyl ester (152 mg, 92%) as a pale yellow oil: ^{1}H NMR (CDCl$_3$) δ 8.37 (m, 2H), 8.10 (m, 2H),

7.69–7.15 (m, 11H), 5.04 (m, 1H), 4.69–4.60 (m, 3H), 3.68–3.52 (m, 7H), 2.48–1.86 (m, 9H), 1.65 (s, 3H), 1.57 (s, 3H), 1.28–1.26 (m, 2H), 0.85 (m, 3H); MS (EI) m/z 692 (M$^+$).

2-Citronellylamino-4-(benzyl-{3-[2,5-diphenyl-oxazole-4-carbonyl]-ethyl}-carbamoyl)-butyric acid (SC-$\alpha\alpha\delta$A). According to the procedure described for SC$\alpha\alpha\delta$l7A, 2-citronellylamino-4-(benzyl-{3-[2,5-diphenyl-oxazole-4-carbonyl]-ethyl}-carbamoyl)-butyric acid methyl ester (152 mg, 0.219 mmol) was converted to SC-$\alpha\alpha\delta$A (87.1 mg, 58%): ^{1}H NMR (CDCl$_3$) δ 8.29 (m, 2H), 8.08 (m, 2H), 7.50–7.13 (m, 11H), 5.03 (m, 1H), 4.72–4.37 (m, 3H), 3.78–3.56 (m, 4H), 2.78–1.91 (m, 9H), 1.56 (s, 3H), 1.54 (s, 3H), 1.28–1.14 (m, 2H), 0.87 (m, 3H); HRMS (EI) m/z calcd for C$_{40}$H$_{46}$N$_4$O$_6$: 678.3417; found: 678.3441.

SC-$\alpha\alpha\delta$4II

2-[2-(2-Methoxyethoxy)acetyl]-amino-4-(benzyl-{3-[2,5-diphenyl-oxazole-4-carbonyl-ethyl}-carbamoyl)-butyric acid methyl ester (6). To a solution of 290 mg (0.404 mmol) of 2-(2,2,2-trichloroethoxycarbonylamino)-4-(benzyl-{3-[2,5-diphenyl-oxazole-4-carbonyl]-ethyl}-carbamoyl)-butyric acid methyl ester (4) in 0.53 mL of acetic acid and 0.79 mL of THF was added 529 mg (8.09 mmol) of zinc dust. The reaction was stirred at 22 °C for 1 h. The mixture was filtered through a Celite pad and the filtrate was concentrated in vacuo. The resulting residue was diluted with EtOAc and washed with saturated aqueous NaHCO$_3$ and brine. The organic layer was dried (Na$_2$SO$_4$) and concentrated in vacuo to give free amine. This amine (112 mg) was dissolved in 0.7 mL of THF and treated with 72 µL (0.52 mmol) of triethylamine, 26 µl (0.23 mmol) of 2-(2-methoxyethoxy)-acetic acid and 173 mg (0.372 mmol) of PyBroP at 0 °C. The reaction mixture was stirred at 0 °C for 1 h and warmed to 22 °C, stirred for 11 h, diluted with EtOAc, and washed with 10% HCl, H$_2$O, saturated aqueous NaHCO$_3$ and brine. The organic layer was dried (Na$_2$SO$_4$), concentrated in vacuo, and chromatographed on SiO$_2$ (hexanes:EtOAc, 1:1→1:4→1:5→EtOAc only) to give 68.2 mg (50%) of 6: ^{1}H NMR (CDCl$_3$) δ 8.36 (m, 2H), 8.11 (m, 2H), 7.52–7.13 (m, 11H), 4.69–4.60 (m, 3H), 4.00 (m, 2H), 3.68–3.47 (m, 11H), 3.35 (s, 3H), 2.48–1.83 (m, 4H); HRMS (EI) m/z calcd for C$_{36}$H$_{40}$N$_4$O$_8$: 656.2846; found: 656.2844.

2-[2-(2-Methoxyethoxy)acetyl]-amino-4-(benzyl-{3-[2,5-diphenyl-oxazole-4-carbonyl]-ethyl}-carbamoyl)-butyric acid (SC-$\alpha\alpha\delta$4II). According to the procedure described for SC-$\alpha\alpha\delta$17A, 2-[2-(2-methoxyethoxy)acetyl]-amino-4-(benzyl-{3-[2,5-diphenyl-oxazole-4-carbonyl]-ethyl}-carbamoyl)-butyric acid methyl ester (6, 68.2 mg, 0.104 mmol) was converted to SC-$\alpha\alpha\delta$4II (70.3 mg, quant.) as a pale yellow oil: ^{1}H NMR (CDCl$_3$) δ 9.28 (brs, 1H), 8.21 (m, 2H), 7.99 (m, 2H), 7.39–7.05 (m, 11H), 4.63–4.46 (m, 3H), 3.90 (m, 2H), 3.61–3.42 (m, 8H), 3.24 (s, 3H), 2.63–1.96 (m, 4H); HRMS (EI) m/z calcd for C$_{35}$H$_{38}$N$_4$O$_8$: 642.2690, found: 642.2702.

SC-$\alpha\alpha\delta$6III

2-2-[2-(2-Methoxyethoxy)ethoxy]acetyl}-amino-4-(benzyl-{3-[2,5-diphenyl-oxazole-4-carbonyl]-ethyl}-carbamoyl)-butyric acid methyl ester (5). According to the procedure described for 2-[2-(2-methoxyethoxy)acetyl]-amino-4-(benzyl-{3-[2,5-diphenyl-oxazole-4-carbonyl]-ethyl}-carbamoyl)-butyric acid methyl ester (6), 2-(2,2,2-trichloroethoxycarbonylamino)-4-(benzyl-{3-[2,5-diphenyl-oxazole-4-carbonyl]-ethyl}-carbamoyl)-butyric acid methyl ester (4) was converted to 2-{2-[2-(2-methoxyethoxy)ethoxy]acetyl}-amino-4-(benzyl-{3-[2,5-diphenyl-oxazole-4-carbonyl]-ethyl}-carbamoyl)-butyric acid methyl ester (5, 57.2 mg, 39%): ^{1}H NMR (CDCl$_3$) δ 8.37 (m, 2H), 8.11 (m, 2H), 7.51–7.13 (m, 11H), 4.73–4.60 (m, 3H), 3.98 (m, 2H), 3.71–3.50 (m, 15H), 3.33 (s, 3H), 2.50–2.02 (m, 4H); MS (EI) m/z 700 (M$^+$).

2-{2-[2-(2-Methoxyethoxy)ethoxy]acetyl}-amino-4-(benzyl-{3-[2,5-diphenyl-oxazole-4-carbonyl-ethyl}-carbamoyl)-butyric acid (SC-$\alpha\alpha\delta$6III). According to the procedure described for SC-$\alpha\alpha\delta$17A 5 (57.2 mg, 0.0816 mmol) was converted to SC-$\alpha\alpha\delta$6III (52.9 mg, 94%) as a pale yellow oil: ^{1}H NMR (CDCl$_3$) δ 8.80 (brs, 1H), 8.24 (m, 2H), 8.01 (m, 2H), 7.42–7.06 (m, 11H), 4.65–4.45 (m, 3H), 3.90 (m, 2H), 3.63–3.43 (m, 12H), 3.26 (s, 3H), 2.90–2.20 (m, 4H); HRMS (EI) m/z calcd for C$_{37}$H$_{42}$N$_4$O$_9$: 686.2952; found: 686.2958.

Plasmids and reagents

Plasmids pGEX2T-KG containing the GST-fusion of full length human Cdc25B$_2$ were previously described.[1] Recombinant human PTP1B was a gift from Dr. Zhong-Yin Zhang (Albert Einstein College of Medicine, Bronx, NY). To generate recombinant human VHR, we excised the coding sequence for VHR phosphatase from pT7-7-VHR (a gift from Dr. Jack E. Dixon, University of Michigan, Ann Arbor, MI) using Ned and EcoRI. The resulting DNA was ligated into the pMTL 22 vector. The pMTL 22-VHR plasmid was used to transform *DH5α Escherichia coli,* and the plasmid DNA was purified. The VHR phosphatase sequence from pMTL 22-VHR was excised with EcoRV and XhoI and ligated into the pGEX-4T3 plasmid, which had been digested with SmaI and XhoI. The pGEX-4T3 plasmids were used to transform *DH5αE. coli.* This clone was then used to produce the GST-VHR phosphatase protein as were all other recombinant fusion proteins by our previously published methods.[1]

Tyrosine specific phosphatase and dual specificity phosphatase assays

The activity of the GST-tagged dual specificity phosphatases and recombinant tyrosine specific phosphatase was measured in 96-well microtiter plates with *O*-methylfluorescein monophosphate (OMFP) (Sigma, St. Louis, MO) as the substrate in three to six independent experiments. The phosphatases catalyzed the metabolism of OMFP to the fluorescent product *O*-methylfluorescein

(OMF) (Sigma; St. Louis, MO). The reaction mixture (150 μl) consisted of 30 mM Tris (pH 7.0), 75 mM NaCl, 1 mM EDTA, 0.033% bovine serum albumin and 1 mM DTT for GST-VHR and rhPTP1B or 30 mM Tris (pH 8.0), 75 mM NaCl, 1 mM EDTA, 0.033% bovine serum albumin and 1 mM DTT for GST-Cdc25B$_2$. Substrate concentrations approximating the K_m were used: VHR, 10 μM; rhPTP1B, 200 μM; Cdc25B$_2$, 40 μM. Both the substrate and compounds were resuspended in DMSO and diluted in water; the final DMSO concentration remained at 7% for all assays. The inhibitory potential for each compound was monitored at 0, 3 and 100 μM reaction concentrations, and the reactions were initiated by the addition of ~0.025 μg of VHR, ~0.25 μg of rhPTP1B and ~0.10 μg Cdc25B$_2$. Reaction length varied with each phosphatase: 21 min for GST-VHR, 14 min for rhPTP1B and 60 min for Cdc25B$_2$. Fluorescent emissions from the hydrolysis of OMFP to OMF were measured at 25 °C during the entire course of the reaction using a Perseptive Biosystems Cytofluor II (Framingham, MA) with an excitation filter of 485 nm (20 nm band width) and an emissions filter of 530 nm (30 nm band width). The fluorescent emissions were converted to units of product formation using an OMF standard curve that was performed with each experiment. Spontaneous hydrolysis of OMFP to OMF as monitored in an enzyme free reaction was normalized to the OMF standard curve. Product formation with 0 μM inhibitor was also monitored and determined to be linear for all enzymes over the incubation period. Furthermore, the reaction was directly proportional to both the enzyme and substrate concentration.

Steady-state kinetics

Initial enzyme rates with five to eight inhibitor concentrations were determined using at least eight substrate (OMFP) concentrations between $K_m/2$ and 5^*K_m. The V_0 for each substrate concentration was determined and then fit to the Michaelis-Menten equation as previously described[1] using GraphPad Prism 3.0 (GraphPad Software, Inc., San Diego, CA). The best fit kinetic model and inhibition constants were obtained using EZ-Fit™ (Perrella Scientific, Amherst, NH).

Determination of clog P values

Computation of clog P, the calculated logarithm of the octanol–water partition coefficient, was performed on an Indigo2 R4400 workstation according to a previously published protocol.[26] Extended conformations of compounds were fully optimized using the semi-empirical method PM3. Charges and other parameters for the regression analysis were also obtained with the PM3 module on Spartan 5.0 (Wavefunction, Inc., Irvine, CA).

Cell culture and anti-proliferation studies

We used human MDA-MB-231 and MCF-7 breast cancer cells to determine the antiproliferative activity of several compounds.[19] Cells were plated at 2000 cells per well in RPMI-1640 culture medium containing 10% fetal bovine serum. After a 24 h incubation, 100 μM of selected compounds were added to the cells. The cells were then incubated with the compounds for 72 h and viable cell number was determined by our previously described method using 3-[4,5-dimethylthiazol-2-yl]-2,5-diphenyl tetrazolium bromide.[19] All results were normalized to vehicle treated control values.

For cell cycle studies, we used the previously described tsFT210 cells.[27] Cells were plated at 2×10^5 cells/mL and maintained at 32.0 °C until they were blocked at G$_2$ phase by incubation at 39.4 °C for 17 h. The synchronized cells were then released from G$_2$ blockage by reincubating at 32.0 °C and treated immediately with FY21-αα09, SC-ααδ, nocodazole or the DMSO vehicle to probe for G$_2$/M arrest. After a 6 h incubation, cells were harvested with phosphate buffered saline and stained with a solution containing 50 μg/mL propidium iodide and 250 μg/mL RNase A. Flow cytometry analyses were conducted with a Becton Dickinson FACS Star (Becton Dickinson, Franklin Lakes, NJ).

References and Notes

1. Rice, R. L.; Rusnak, J. M.; Yokokawa, F.; Yokokawa, S.; Messner, D. J.; Boynton, A. L.; Wipf, P.; Lazo, J. S. *Biochemistry* **1997**, *36*, 15965.
2. Tonks, N. K.; Neel, B. G. *Cell* **1996**, *87*, 365.
3. Hunter, T. *Cell* **1995**, *80*, 225.
4. Taing, M.; Keng, Y.-F.; Shen, K.; Wu, L.; Lawrence, D. S.; Zhang, Z.-Y. *Biochemistry* **1999**, *38*, 3793.
5. Denu, J. M.; Stuckey, J. A.; Saper, M. A.; Dixon, J. E. *Cell* **1996**, *87*, 361.
6. Flint, A. J.; Tigianis, T.; Barford, D.; Tonks, N. K. *Proc. Natl. Acad. Sci. USA* **1997**, *94*, 1680.
7. Stone, R. L.; Dixon, J. E. *J. Biol. Chem.* **1994**, *269*, 31323.
8. Brown-Shimer, S.; Johnson, K. A.; Hill, D. E.; Bruskun, A. M. *Cancer Res.* **1992**, *52*, 478.
9. Li, L.; Ernsting, B. R.; Wishart, M. J.; Lohse, D. L.; Dixon, J. E. *J. Biol. Chem.* **1997**, *272*, 29403.
10. Seely, B. L.; Staubs, P. A.; Reichart, D. R.; Berhanu, P.; Milarski, K. L.; Saltiel, A. R.; Kusari, J.; Olefsky, J. M. *Diabetes* **1996**, *45*, 1379.
11. Liu, F.; Hill, D. E.; Chernoff, J. *J. Biol. Chem.* **1996**, *271*, 31290.   Tanner, K.G.; Denu, J.M.
12. Todd, J. L.; ~~G., T. K.; M., D. J.~~ *J. Biol. Chem.* **1999**, *274*, 13271.
13. Yuvaniyama, J.; Denu, J. M.; Dixon, J. E.; Saper, M. A. *Science* **1996**, *272*, 1328.
14. Fauman, E. B.; Cogswell, J. P.; Lovejoy, B.; Rocque, W. J.; Holmes, W.; Montana, V. G.; Piwnica-Worms, H.; Rink, M. J.; Saper, M. A. *Cell* **1998**, *93*, 617.

15. Baldin, V.; Cans, C.; Superti-Furga, G.; Ducommun, B. *Oncogene* **1997**, *14*, 2485.

16. Gabrielli, B. G.; De Souza, C. P.; Tonks, I. D.; Clark, J. M.; Hayward, N. K.; Ellem, A. *J. Cell. Sci.* **1996**, *109*, 1081.

17. Gabrielli, B. G.; Clark, J. M.; McCormack, A. K.; Ellem, K. A. *J. Biol. Chem.* **1997**, *272*, 28607.

18. Stuckey, J. A.; Schubert, H. L.; Fauman, E. B.; Zhang, Z.-Y.; Dixon, J. E.; Saper, M. A. *Nature* **1994**, *370*, 571.

19. Wipf, P.; Cunningham, A.; Rice, R. L.; Lazo, J. S. *Bioorg. Med. Chem.* **1997**, *5*, 165.

20. Bergnes, G.; Gilliam, C. L.; Boisclair, M. D.; Blanchard, J. L.; Blake, K. V.; Epstein, D. M.; Pal, K. *Bioorg. Med. Chem. Lett.* **1999**, *9*, 2843.

21. Puius, Y. A.; Zhao, Y.; Sullivan, M.; Lawrence, D. S.; Almo, S. C.; Zhang, Z.-Y. *Proc. Natl. Acad. Sci. USA* **1997**, *94*, 13420.

22. Tamura, K.; Rice, R. L.; Wipf, P.; Lazo, J. S. *Oncogene* **1999**, *18*, 6989.

23. Gunasekera, S. P.; McCarthy, P. J.; Kelly-Borges, M. *J. Amer. Chem. Soc.* **1996**, *118*, 8759.

24. Blanchard, J. L.; Epstein, D. M.; Boisclair, M. D.; Rudolph, J. K.; D. *Bioorg. Med. Chem. Lett.* **1999**, *9*, 2537.

25. Peng, H.; Zalkow, L. H. *J. Med. Chem.* **1998**, *41*, 4677.

26. Alkorta, I.; O., V. H. *Int. J. Quant. Chem.* **1992**, *44*, 203.

27. Th'ng, J. P.; Wright, P. S.; Hamaguchi, J.; Lee, M. G.; Norbury, C. J.; Nurse, P.; Bradbury, E. M. *Cell* **1990**, *63*, 313.

Identification of New Cdc25 Dual Specificity Phosphatase Inhibitors in a Targeted Small Molecule Array

Alexander P. Ducruet,[a] Robert L. Rice,[a] Kenji Tanlura,[a] Fumiaki Yokokawa,[b] Shiho Yokokawa,[b] Peter Wipf[b] and John S. Lazo[a]

[a]Department of Pharmacology, the Combinatorial Chemistry Center and the Molecular Therapeutic/Drug Discovery Program of the University of Pittsburgh Cancer Institute, University of Pittsburgh, Pittsburgh, PA 15261, USA
[b]Department of Chemistry, the Combinatorial Chemistry Center and the Molecular Therapeutic/Drug Discovery Program of the University of Pittsburgh Cancer Institute, University of Pittsburgh, Pittsburgh, PA 15261, USA

FY21-αα09

Synthesis and Biological Evaluation of Deoxypreussomerin A and Palmarumycin CP₁ and Related Naphthoquinone Spiroketals

Peter Wipf,* Jae-Kyu Jung, Sonia R. Rodríguez and John S. Lazo

Departments of Chemistry and Pharmacology, University of Pittsburgh,

Pittsburgh, Pennsylvania 15260

Abstract: Oxidative cyclization of bis-naphthyl ethers allows concise total syntheses of palmarumycin CP1 and deoxypreussomerin A in 8-9 steps and 15-35% overall yield from 5-hydroxy-8-methoxy-1-tetralone (**8**). Polymer-bound triphenyl phosphine was found to be a superior reagent for the rapid preparation of a small library of palmarumycin analogs. Preliminary biological evaluation of naphthoquinone spiroketals against MCF-7 and MDA-MB-231 human breast cancer cells revealed several low-micromolar growth inhibitors.

Introduction

The novel antifungal metabolites preussomerins A-F were identified in 1990 by Gloer and coworkers during the course of an investigation of chemical agents involved in interspecies competition among coprophilous (dung-colonizing) fungi (Figure 1).[1] In addition to these early reports from *Preussia isomera* Cain samples, preussomerins were later also discovered in the endophytic fungus *Harmonerna dematioides* by Polishhook and coworkers.[2] Another report of an epoxy naphthalenediol spiroketal compound, bipendensin, was published in 1990 by Connolly.[3] The latter natural product was isolated in very small amounts from wood samples of the African tree *Afzelia bipendensis*. A compound having the same gross structure as bipendensin was isolated in 1994 from an unidentified *Coniothyium* fungus collected from forest soil on West Borneo, and was named palmarumycin C_{11} by Krohn and coworkers.[4]

Figure 1. Preussomerins isolated from *Preussia isomera*.

preussomerin A   preussomerin B   preussomerin C

preussomerin D   preussomerin E   preussomerin F
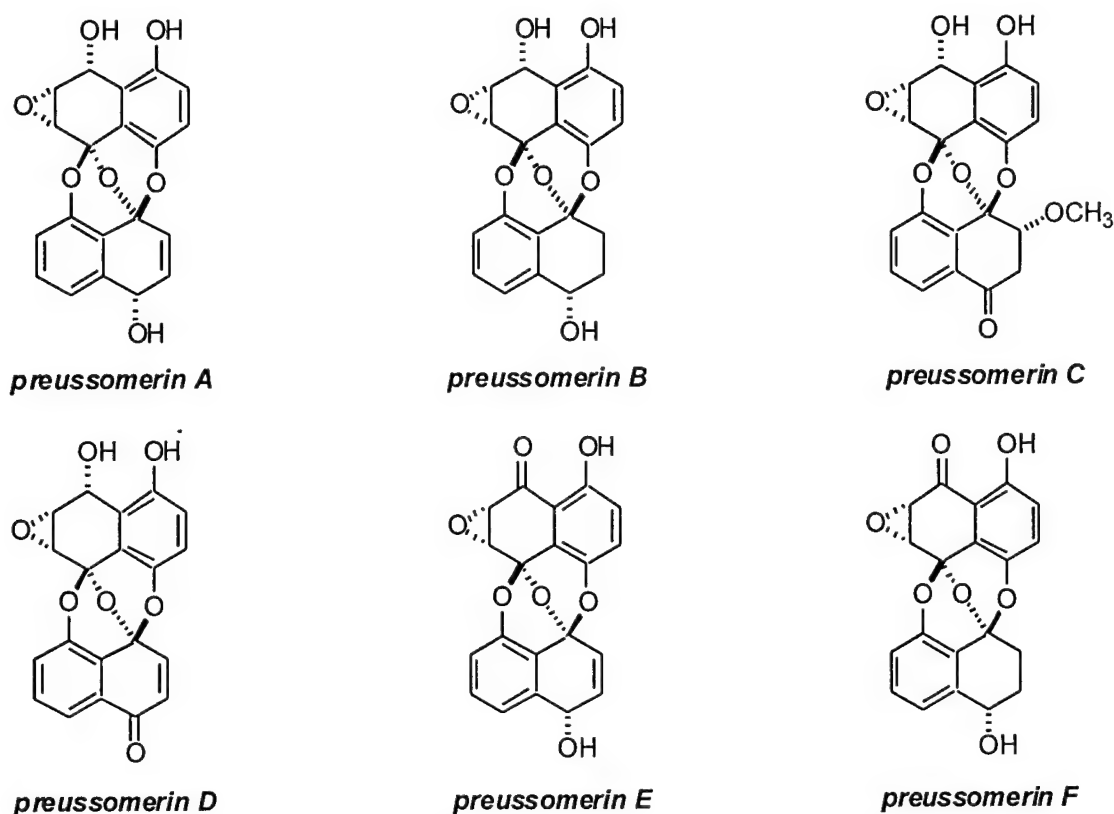
The absolute stereochemistry of preussomerins was assigned as shown in Figure 1 on the basis of the isolation of known (-)-regiolone as a degradation product.[1b] Although the ketal linkages were resistant to acid hydrolysis at room temperature, vigorous cleavage conditions (6 M HCl/ acetone, 1:1, 100 °C, 12 h) afforded (-)-regiolone[5] as the major product. Conservation of the stereochemistry at the C-1' position could be rationalized by a mechanism involving protonation at the C-2' position during the decomposition process followed by loss of the 9-OH proton and formation of an enol ether (Figure 2). Hydrolysis of the remaining ketal linkage would then account for the formation of regiolone without loss of stereochemical integrity at the hydroxylated benzylic carbon.

Figure 2. Acidic degradation of preussomerin A.

preussomerin A   hydrolysis   (-)-regiolone

Even though preussomerin A exhibited only low-micromolar cytotoxicity toward a mammalian cell line,[1b] a Merck group reported that preussomerins and deoxypreussomerins showed promising effects as novel ras farnesyl-protein transferase (FTPase) inhibitors.[6] Preussomerin G-I and deoxypreussomerin A and B, accompanied by preussomerin D, were isolated from the fermentation broth of an unidentified coelomycetes fungus collected in Bajo Verde, Argentina (Figure 3). IC$_{50}$'s of FTPase inhibitory activities of preussomerins, deoxypreussomerins and derivatives of preussomerin G range between 1-20 μM. Preussomerin G and preussomerin D were the most active. Interestingly, deoxypreussomerins, which possibly are biosynthetic precursors of preussomerins,[6] had equal or better activities than preussomerins H and I. Deoxypreussomerin A and B were also reported independently as antifungal agents and named palmarumycin C_2 and CP_2, respectively.[4,7]

Figure 3. Preussomerins and deoxypreussomerins isolated from a coelomycetes fungus.

preussomerin G

preussomerin H

preussomerin I

preussomerin D

deoxypreussomerin A
(palmarumycin C$_2$)

deoxypreussomerin B
(palmarumycin CP$_2$)

Preussomerin G reacted with strong nucleophiles in a highly stereospecific Michael fashion to give a quantitative yield of the C-3' adduct (Scheme 1). Presumably, steric hindrance makes the top face of preussomerin G inaccessible to nucleophiles, and thus Michael addition takes place exclusively from the more accessible α-face.

Additional naphthalenediol spiroketals of the palmarumycin family have been reported by Krohn and coworkers.[4,7,8] These metabolites were produced by two strains of the endophytic fungi *Coniothyrium palmarium* and an unidentified *Coniothyrium* species (Figures 4 and 5).

Scheme 1.

preussomerin G

R-SH

CD$_3$CN

R =
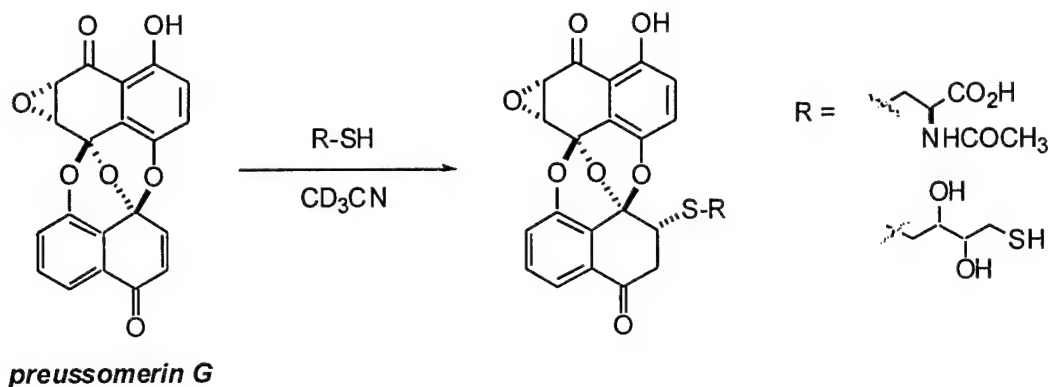
Figure 4. Palmarumycins from *Coniothyrium palmarium*

palmarumycin CP$_1$ palmarumycin CP$_3$ palmarumycin CP$_4$ palmarumycin CP$_{4a}$ palmarumycin CP$_5$
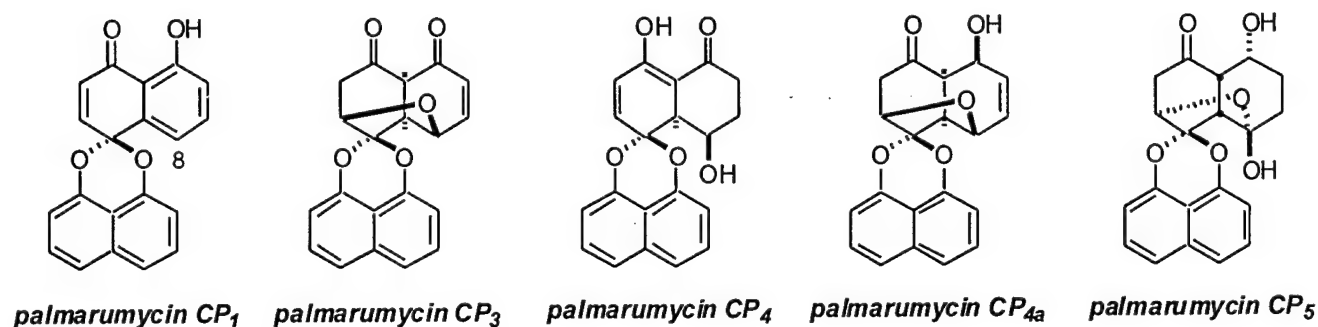
Palmarumycin CP$_3$, CP$_4$, C$_3$, C$_{10}$ and C$_{12}$ show high antifungal activity. Apparently, the introduction of an oxygen function into the 8-position significantly increases the antifungal effect. The chloroepoxide palmarumycin C$_4$ and palmarumycin C$_9$, isolated as an isomeric mixture of epoxides, completely inhibited germination and growth of garden cress. In most palmarumycins, only the relative configuration was elucidated, except for palmarumycin CP$_{4a}$ and CP$_5$. The absolute configurations of the latter compounds were elucidated by CD calculations. After computation of the CD spectra of six low energy conformers, Boltzmann-weighted addition and comparison of the resulting averaged spectrum with the experimental data allowed the assignment of the absolute configuration of palmarumycin CP$_{4a}$ and CP$_5$ as shown in Figure 4.[8]

Krohn and coworkers proposed a biosynthesis of palmarumycin CP$_1$ based on a 1,8-dihydroxynaphthalene or a suitable phenolic derivative precursor.[4,9] According to their hypothesis, coupling could occur via a phenol oxidation as often encountered in polyketide biosynthesis,[10] and the chlorinated palmarumycins could be derived from addition of chloride ions to epoxides. In order to probe this mechanism, palmarumycin CP$_2$ and palmarumycin C$_9$ were treated with methanolic hydrochloric acid (Scheme 2). As expected, formation of chlorinated palmarumycin C$_4$ from palmarumycin C$_9$ could be detected by TLC. For the reaction of palmarumycin C$_2$, an intermediate chlorohydrin was identified as the major isomer. This chlorohydrin slowly decomposed to palmarumycin C$_1$ upon standing in chloroform solution. Palmarumycin C$_2$ was recovered upon treatment with base. These experiments established a possible pathway to the chlorinated palmarumycins. They also

highlighted the unexpected stability of the naphthalenediol spiroketal that was not even affected by heating in acetic acid at 100 °C.[4]

Figure 5. Palmarumycins from an unidentified *Coniothyrium* species.

palmarumycin C₁   palmarumycin C₃   palmarumycin C₄   palmarumycin C₅

palmarumycin C₆   palmarumycin C₇   palmarumycin C₈   palmarumycin C₉

palmarumycin C₁₂   palmarumycin C₁₅   palmarumycin C₁₆
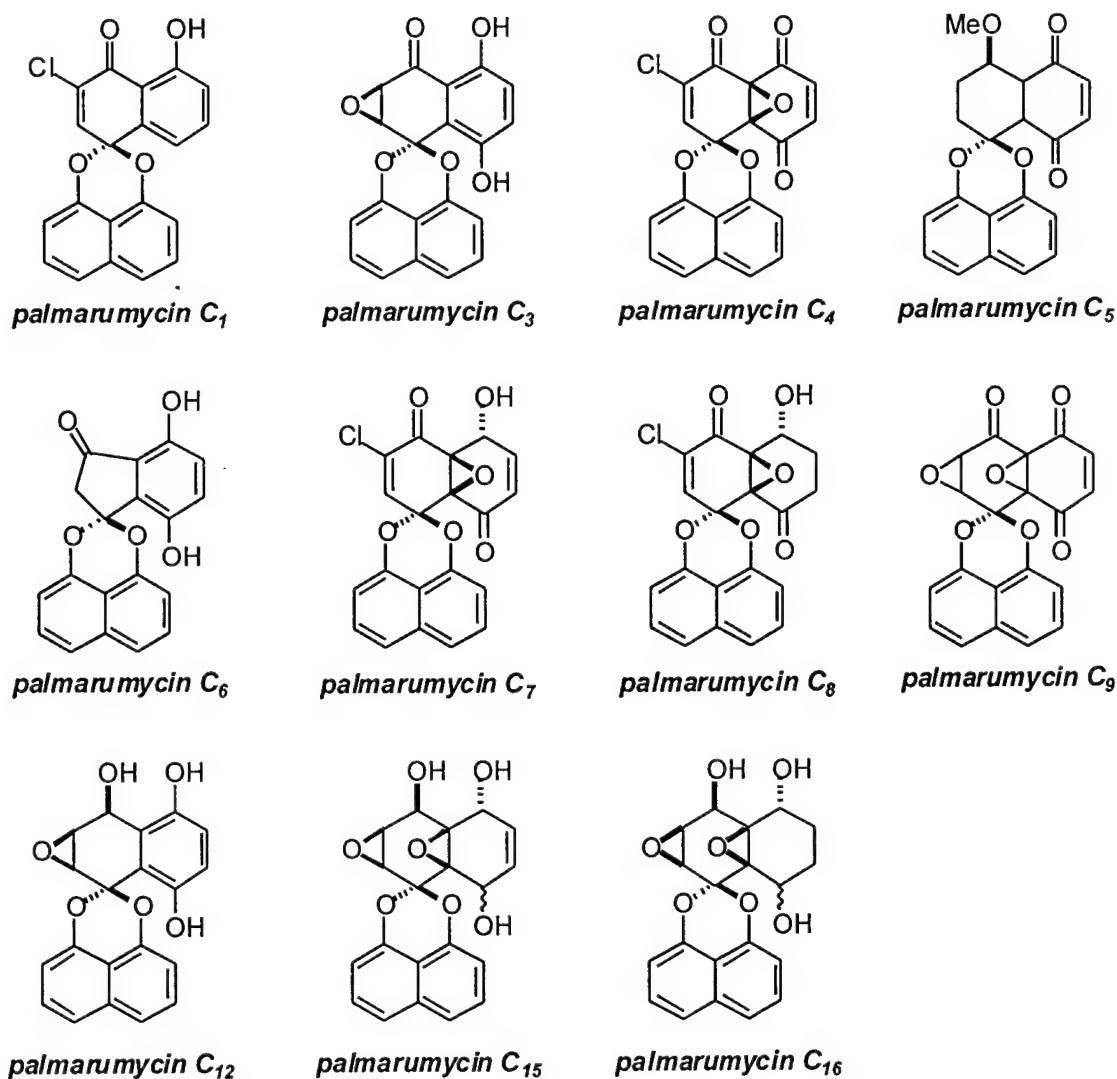
Interestingly, Krohn and coworkers isolated the open chain compound **1** from *Coniothyrium palmarum*.[11] This isolation offered the chance to probe the biosynthetic hypothesis involving phenol oxidation. Upon exposure to silver(II) oxide, the binaphthyl ether **1** cyclized to give quinone ketal **2** (Scheme 3). However, **2** could not be detected in the fermentation broth of *Coniothyrium palmarum*. It is possible that a total synthesis of palmarumycins based on the phenolic oxidation of binaphthyl ethers could be achieved as shown for **3**; however, no further studies along these lines have been reported. Taylor and coworkers also investigated a biomimetic cyclization approach with little success.[12]

Scheme 2.

palmarumycin C₉ → HCl → *palmarumycin C₄*

palmarumycin C₂ ⇌ HCl / base → → *palmarumycin C₁*

Scheme 3.

1 → Ag₂O, toluene, MeOH, 67% → **2**
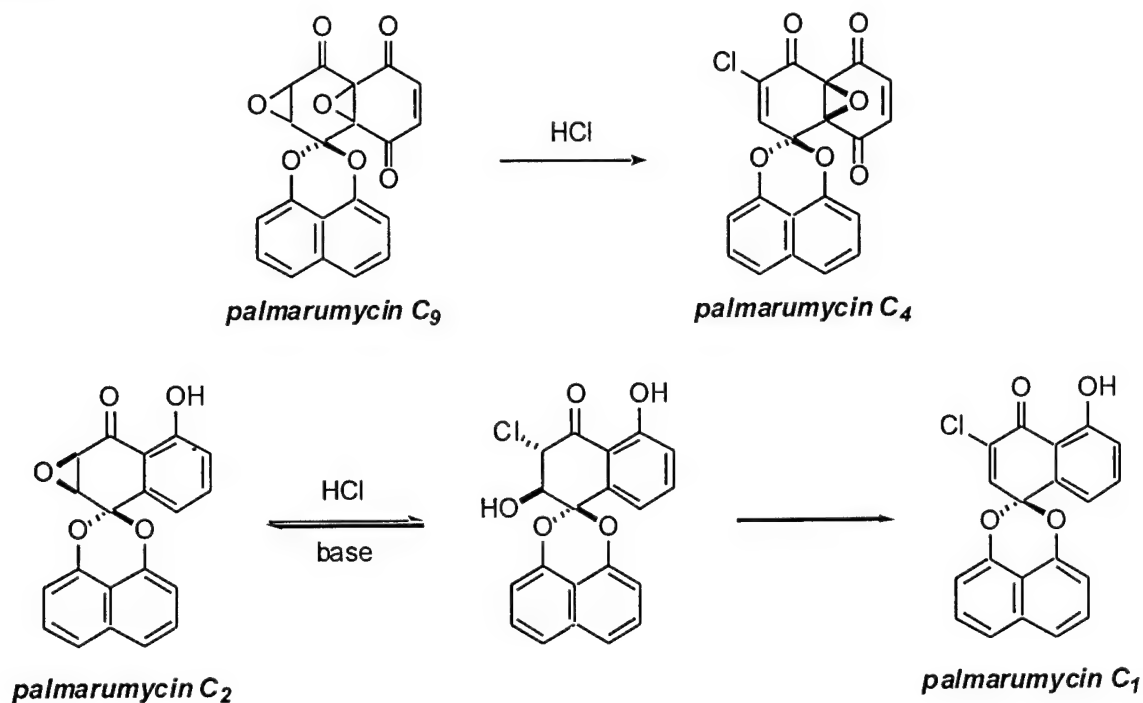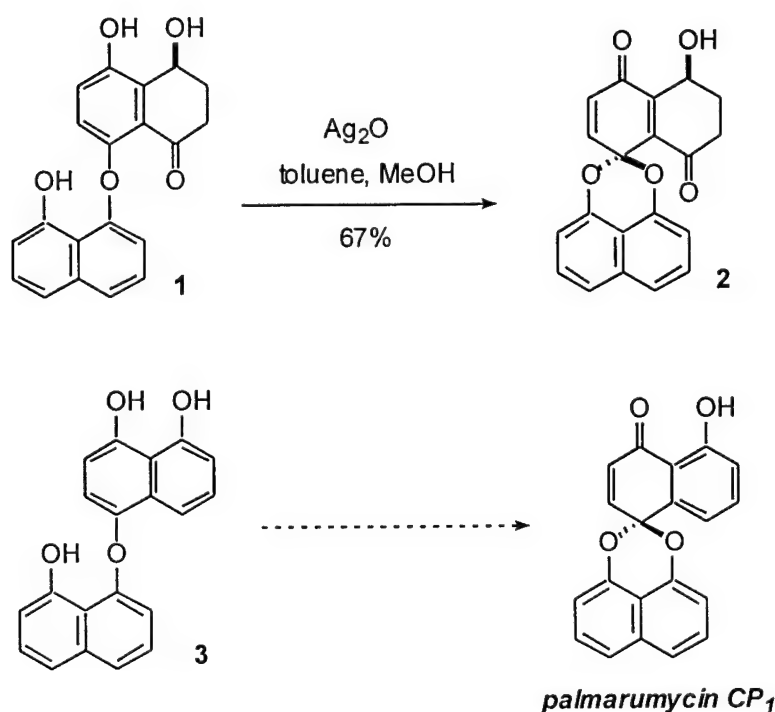
3 - - - → *palmarumycin CP₁*

Deoxypreussomerins and palmarumycins are structurally closely related to the more recently isolated diepoxins,[13] CJ-12,371 and CJ-12,372,[14] and spiroxins[15] (Figure 6).[16] Antimicrobial, antifungal, and some anticancer activities were identified for diepoxins and spiroxins. A Pfizer research group isolated the novel fungal metabolites CJ-12,371 and CJ-12,372 from a fermentation broth of an unidentified fungus N983-46. These compounds showed DNA gyrase inhibitory activity. The phospholipase D inhibitor Sch 53823 has the

same gross structure as palmarumycin C_{11}, however, the melting point and optical rotation are different, suggesting that palmarumycin C_{11} and Sch 53823 are stereoisomers.[16b]

Figure 6. Representative structurally related fungal metabolites.

diepoxin α

diepoxin η
(Sch 53516)
(palmarumycin C_{14})

diepoxin ζ
(Sch 53514)
(palmarumycin C_{13})
(cladospirone bisepoxide)

diepoxin σ
(Sch 49209)

CJ-12,371

spiroxin A

Sch 53823
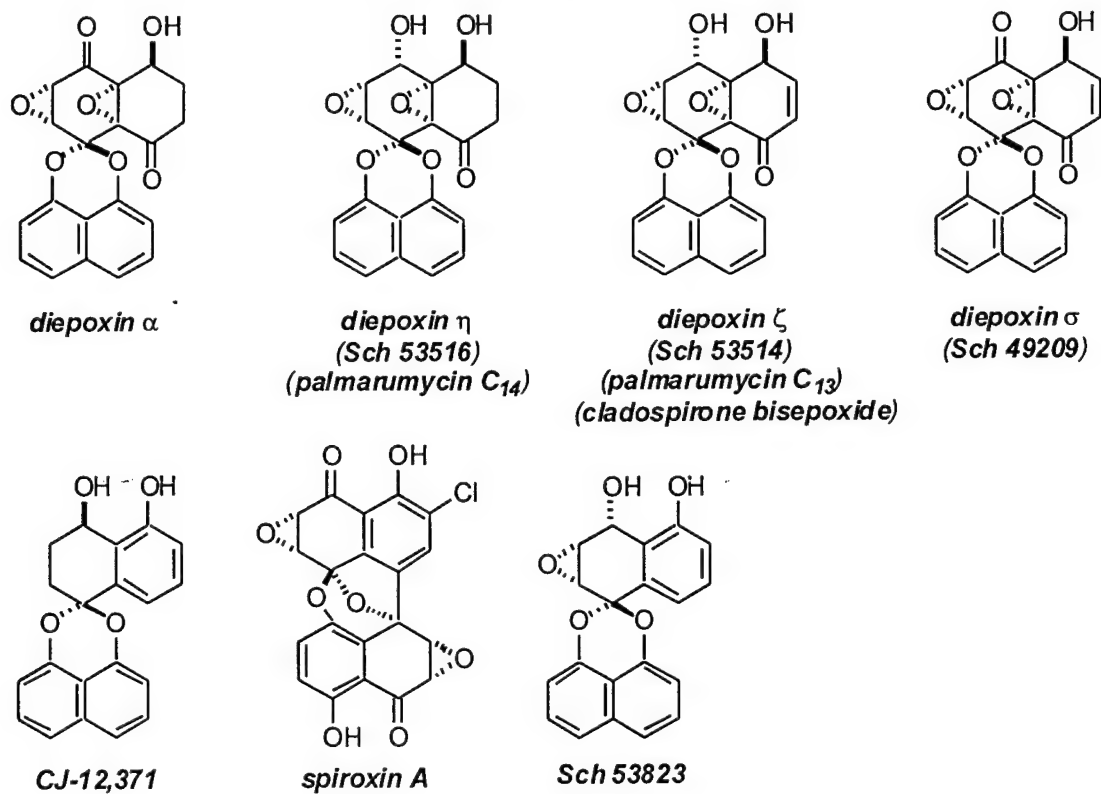
The combination of attractive biological activities and novel structural features in the spirobisnaphthalene family of natural products has attracted considerable interest from the synthetic organic community. In addition to pioneering total syntheses of palmarumycin CP_1 and deoxypreussomerin A,[12,17,18,19] innovative approaches toward diepoxin σ,[20] preussomerins G and I,[21] palmarumycin CP_2,[18,19] palmarumycin C_{11},[18] and CJ-12,371[18,19] have been reported since 1997.

Results and Discussion

In the course of our approaches toward the total synthesis of diepoxin σ,[20,22] we also devised a potential synthetic strategy toward palmarumycin CP1 and deoxopreussomerin A (Scheme 4).[17] Naphthalenediol spiroketal **4** was derived from a binaphthyl ether **5**, and dehydrogenation at C(5) and C(6) in **4** should by facilitated be the presence of the enone moiety. Compound **5** would be easily prepared by an Ullmann ether coupling reaction with 1-iodo-8-methoxynaphthalene (**7**)[23] and the tetraline derivative **6**.

Scheme 4.

palmarumycin CP₁
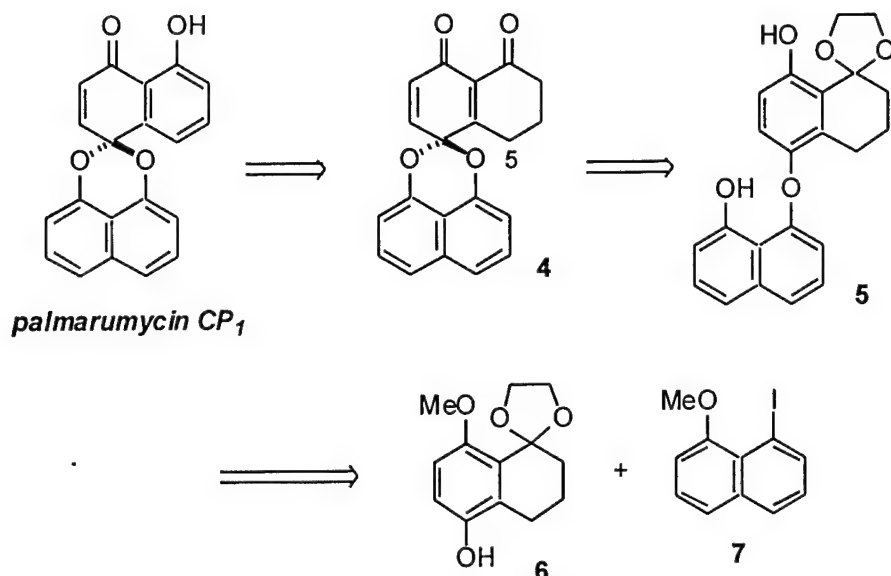
- -5-Hydroxy-8-methoxy- 1-tetralone (**8**) was prepared by a modified literature procedure (Scheme 5).[22,24] Attempts for an Ullmann ether coupling between **8** and 8-iodo-1-methoxynaphthalene (**7**) failed, quite likely due to the deactivating effect of the tetralone carbonyl group. Coupling with ketal **6** was more successful and resulted in a 78% yield of naphthyl ether **9** which was further converted to ketone **10**. While we failed to demethylate ketal **9** with NaSEt in DMF or with BBr₃, demethylation of ketone **10** using BBr₃ smoothly afforded compound **11** in 95% yield. The presence of a ketone function in **11** was likely to retard the subsequent oxidative cyclization which involves a very electron deficient transition state. Since the ketone function in **11** was unreactive to acetalization conditions, the phenolic hydroxyl groups were first acetylated, and ketal **13** was subsequently saponified to afford the oxidative cyclization precursor **5** in good overall yield (Scheme 6).

Scheme 5.
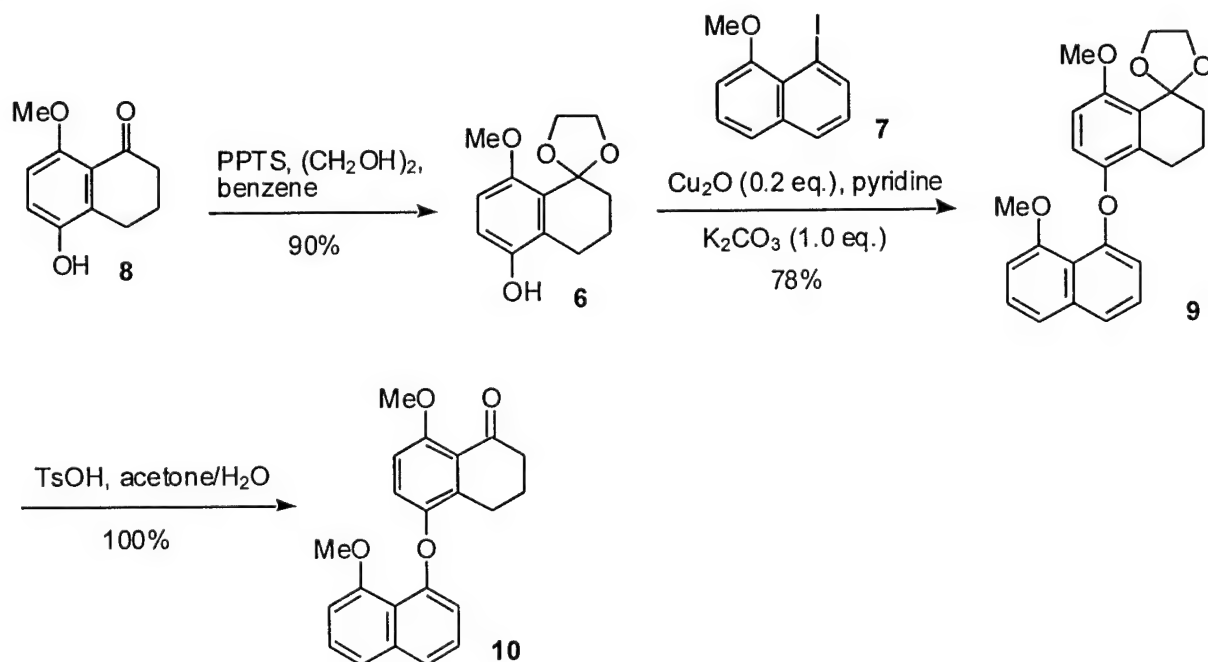
Scheme 6.
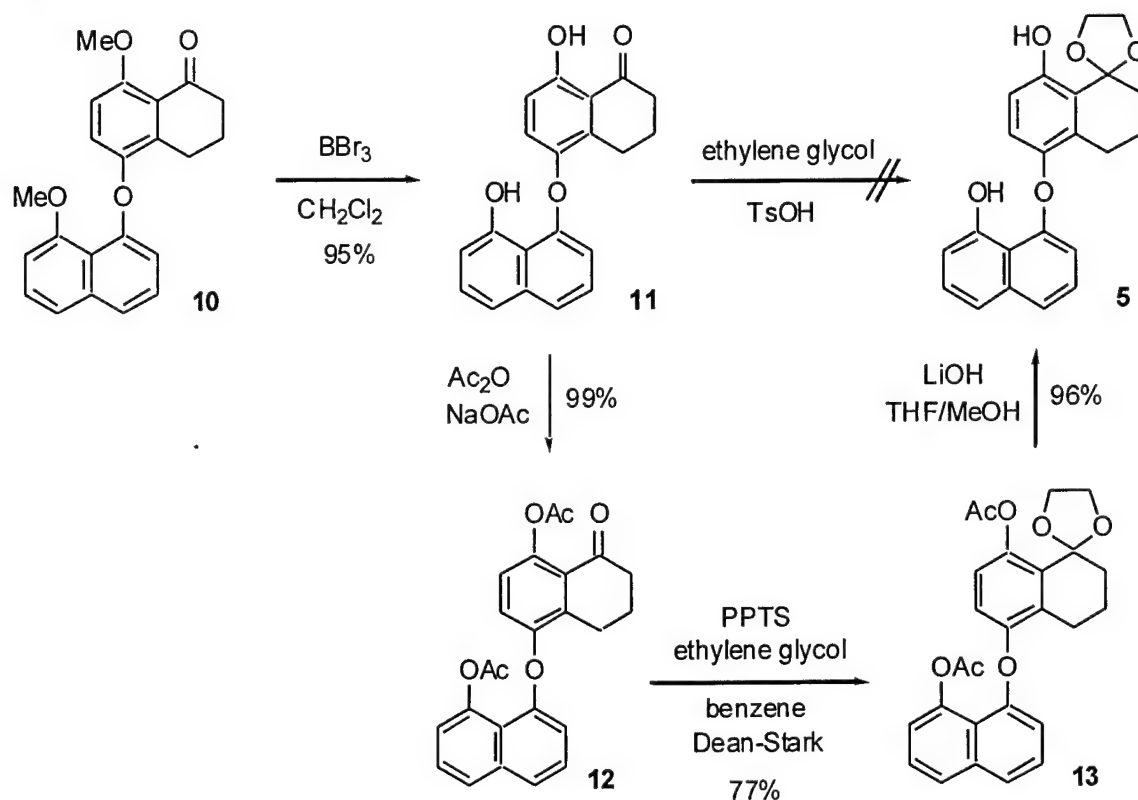
Oxidative cyclization of ketal **5** with PhI(OAc)$_2$ in trifluoroethanol afforded bisketal **14** in 75% yield (Scheme 7). Unfortunately, deprotection of **14** under acidic conditions led to complex mixtures.

Scheme 7.
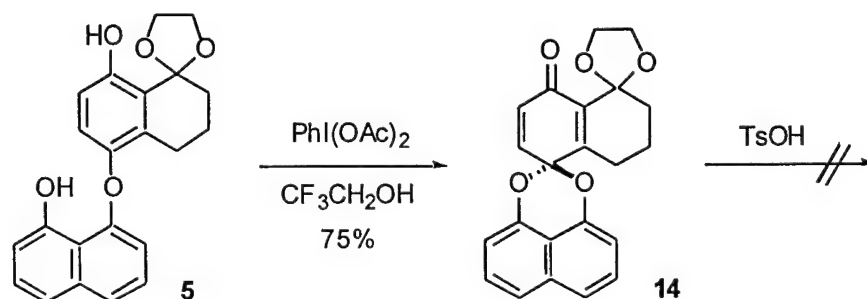
Diol **11** was quantitatively reduced to triol **15**, which was oxidatively cyclized using PhI(OAc)$_2$ in trifluoroethanol to afford naphthalenediol spiroketal **16** in 87% yield (Scheme 8). Further oxidation of the alcohol function of **16** was attempted with PCC and BaMnO$_4$ under buffered conditions but failed to provide the desired ketone in acceptable yields. In contrast, when **16** was treated with activated MnO$_2$ at room temperature, a clean conversion to the natural product palmarumycin CP$_1$ was effected (Scheme 9). For complete conversion of **16** to palmarumycin CP$_1$, a large excess (more than 50 equivalents) of MnO$_2$ was required, and a considerable amount of product remained adsorbed on MnO$_2$ and could not be recovered. When the reaction was performed in dry benzene at reflux, the amount of MnO$_2$ required for the complete conversion of **16** was decreased to ~10 equivalents, but the resulting

palmarumycin CP$_1$ was contaminated with a inseparable byproduct. We therefore resorted to a two-step protocol. Oxidation of **16** with Dess-Martin periodinane, purification of the intermediate ketone by column chromatography on SiO$_2$, and treatment with 10 equivalents of MnO$_2$ in dry methylene chloride for 2 days at room temperature afford the target molecule in 60% yield. Palmarumycin CP$_1$ was thus obtained in 35% overall yield in 8 steps from the known tetralone **8**.

Scheme 8.
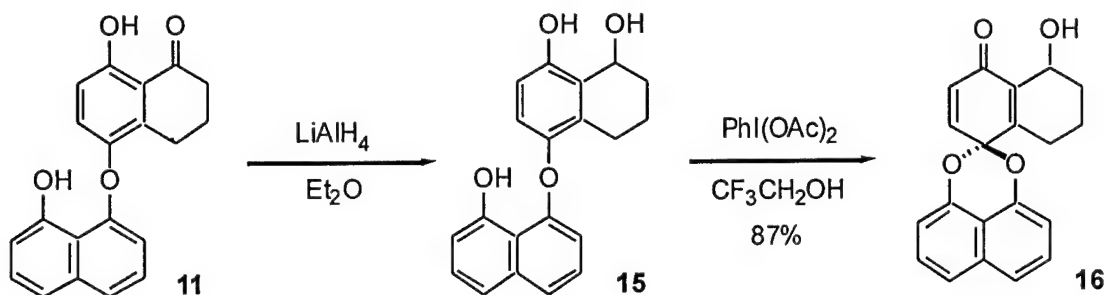
Scheme 9.
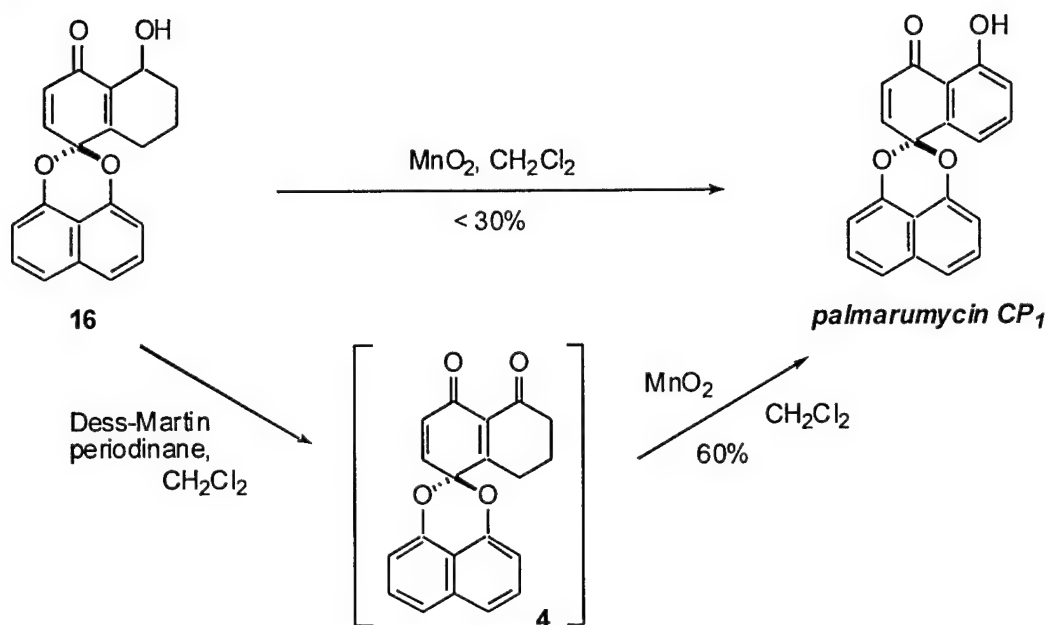
In consideration of the close structural similarity between palmarumycin CP$_1$ and the farnesyl-protein transferase inhibitor deoxypreussomerin A, an epoxidation reaction of palmarumycin CP$_1$ was attempted. However, treatment with hydrogen peroxide anion led to decomposition instead of epoxidation, and a mild epoxidizing agent, dimethyldioxirane also provided only decomposed products. Even after protection of the phenol function of palmarumycin CP$_1$ as the TBDMS ether, no synthetically useful epoxidation could be realized (Scheme 10). Therefore, we had to resort to earlier, more extensively protected synthetic intermediates.

Scheme 10.

palmarumycin CP₁
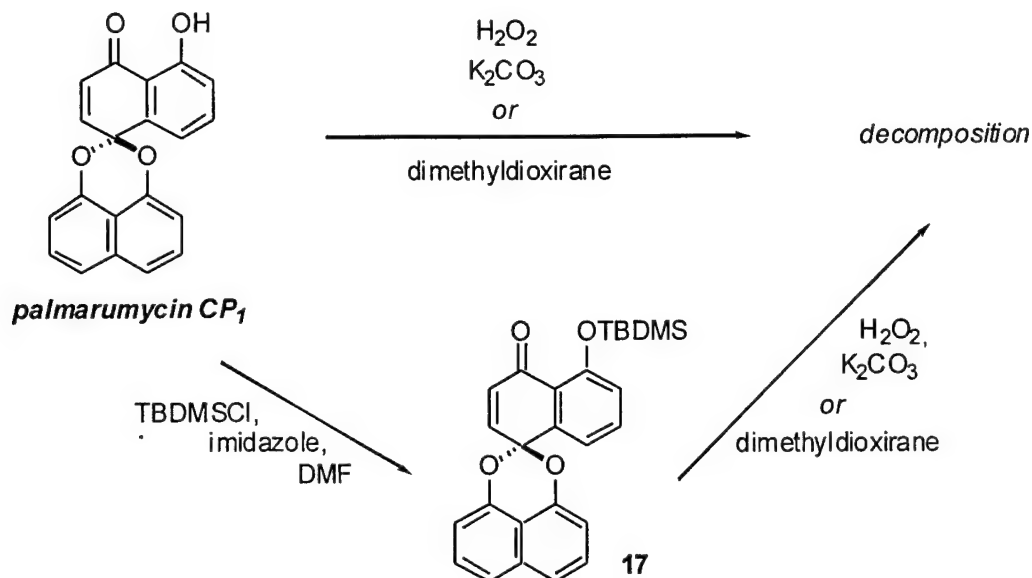
When compound 14 was treated with excess hydrogen peroxide anion, monitoring of the reaction progress was difficult due to the overlap of products with the starting material **14** on TLC. The reaction mixture was thus quenched before complete consumption of **14**. ^{1}H NMR analysis of the crude product showed that mono- and diepoxides were formed in a ratio of about 1:1 with ~10% remaining starting material (Scheme 11). This result demonstrated that a regioselective epoxidation of the disubstituted double bond of **14** in the presence of the internal tetrasubstituted double bond was unlikely to succeed.

Scheme 11.

inseparable mixture
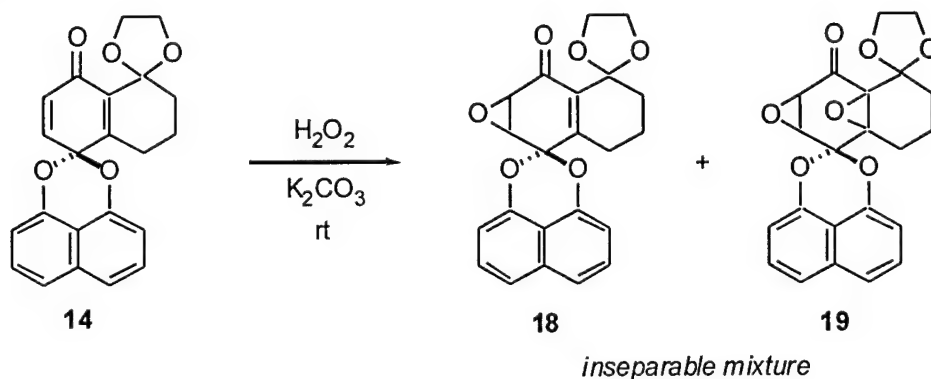
In contrast, treatment of allylic alcohol **16** with hydrogen peroxide anion resulted in the isolation of the desired monoepoxide **20** in 25% yield (Scheme 12). The relative configuration of the epoxide and the hydroxyl group was not determined. Peroxides and bases were screened to optimize the epoxidation reaction. When cumene hydroperoxide and NaH were used at -20 °C, the epoxidation yield increased to 47%. The two step oxidation protocol developed for the synthesis of palmarumycin CP₁ converted epoxy alcohol **20** to the desired natural product in 55% yield. (±)-Deoxypreussomerin A was thus synthesized in 15% overall yield and 9 steps from the known **8**.

Scheme 12.
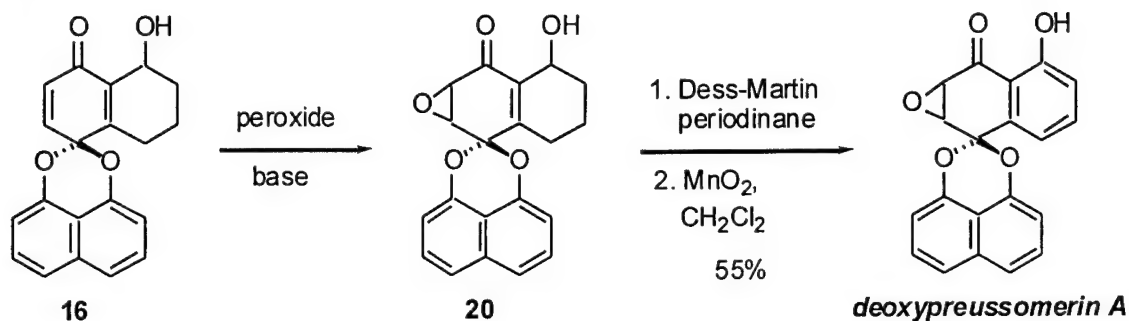
Peroxide	Base	Temperature	Yield of **20**
Hydrogen peroxide	K_2CO_3	rt	25%
t-Butyl hydroperoxide	NaOH	0 °C	31%
Cumene hydroperoxide	NaOH	0 °C	40%
Cumene hydroperoxide	NaH	0 °C	45%
Cumene hydroperoxide	NaH	-20 °C	47%

The successful development of efficient synthetic strategies for the preparation of palmarumycin CP_1 and deoxypreussomerin A allowed us to prepare analogs and investigate the biological SAR of this class of compounds in more detail. A small library of palmarumycin analogs was obtained by Mitsunobu reaction of the natural product using polystyrene-bound triphenylphosphine (Scheme 13). A total of 13 allylic and benzylic alcohols was used for the coupling, and yields and ease of purification were greatly improved by the use of the polymer-bound reagent. In the treatment of palmarumycin CP_1 with 2-furyl methanol, the ether product **28** was accompanied by the C-alkylated phenol **27** (Scheme 14). All other reactions produced a single isomer. In addition to these palmarumycin analogs, several diepoxin σ derivatives[20,22] were subjected to biological testing (Figure 7).

Scheme 13.

21, R = (E)-HC=CHPh
22, R = (E)-HC=CHMe
23, R = n-C_5H_{11}
24, R = (E)-CH_2HC=CHEt
25, R = (m)-MeOPh
26, R = Bn
27, R = 2-furyl
29, R = (E,E)-HC=C(Me)CH_2CH_2CH=CMe$_2$
30, R = 3-furyl
31, R = 2-pyridyl
32, R = 3-pyridyl
33, R = 4-pyridyl
34, R = HC=CH_2

Scheme 14.

palmarumycin CP₁
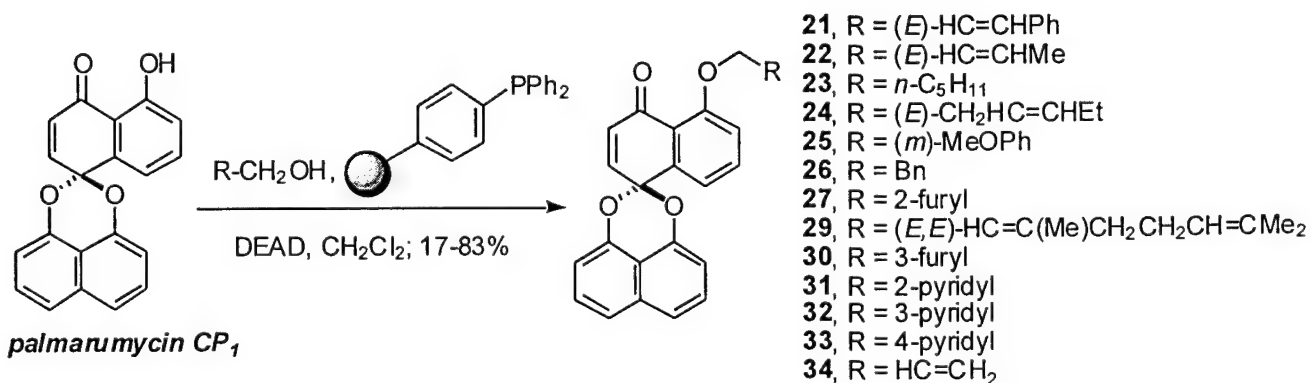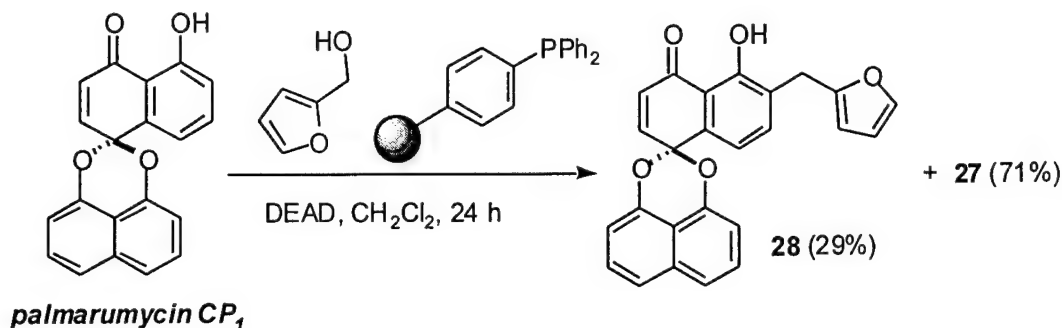
Figure 7. Deoxypreussomerin A and diepoxin σ analogs.

35   36   37   38   39   40
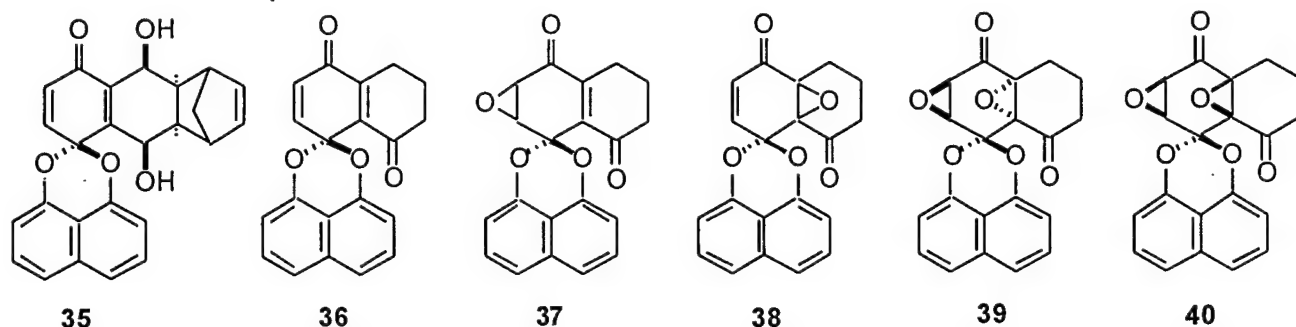
Two widely used human breast cancer cell lines were evaluated for their sensitivity to the cytotoxic effects of the naphthoquinone spiroketals. MCF-7 cells were originally derived from an adenocarcinoma of the breast and retain several characteristics of differentiated mammary epithelium including the ability to process estradiol via cytoplasmic estrogen receptors. MCF-7 cells express the tumor suppressor gene product p53, which is required for the programmed cell death or apoptosis caused by many agents.[25] MDA-MB-231 cells, which were also derived from an adenocarcinoma of the breast, are less differentiated than the MCF-7 cells and fail to express functional p53 or estrogen receptors. This class of tumor cells are important targets for new therapies, because loss of estrogen receptor expression is associated with poor patient prognosis.[26] All cells were tested for 72 h with six concentrations of compounds ranging from 0.1 to 30 μM to determine the concentration required for 50% growth inhibition (IC_{50}). We extrapolated to determine the IC_{50} for compounds with little cytotoxicity at 30 μM, the highest concentration tested. As indicated in Table 1, 45% of the compounds (10/22) had an IC_{50} <3 μM in both cell types. Half of the compounds showed no selectivity to either human tumor cell type, while 32% of the compounds were more cytotoxic to MCF-7 compared with MDA-MB-231 cells. This included **37**, which was 5-fold more cytotoxic to MCF-7 cells (IC_{50} 4.6 vs. 23 μM). The enhanced sensitivity of MCF-7 to these compounds may be due to the expression of p53 in these cells. The assay used in our studies, however, did not specifically measure apoptosis and this could be examined in the future. Studies to be published elsewhere indicate that at least one compound, **27**, can arrest mammalian cells in the G2/M phase of the cell cycle. The five fold enhanced sensitivity of MDA-MB-231 cells to **24** compared to MCF-7 cells is of interest, because the MDA-MB-231 cells lack both functional estrogen receptors and p53.

Table 1. IC_{50} values [μM] in 2 cancer cell lines.

Compound	MCF-7	MDA-MB-231
21	7.6	3.6
22	5.5	1.4
23	13.4	13.6
24	43.4	9.2
25	2.3	2.7
26	3.9	4.6
27	1.1	2.5
28	2	6.5
29	4.6	2
30	2	2
31	2	2.8
32	1.5	1.4
33	8	7.3
34	2	2.7
diepoxin σ	1.5	2
palmarumycin CP$_1$	0.9	2.4
35	1.3	2.1
36	3.8	6.4
37	4.6	23
38	1.3	3.4
39	4.6	8.2
40	2.8	2.9

Conclusions

Oxidative cyclization of bis-naphthyl ethers with hypervalent iodine reagents allows a ready access to structurally novel naphthoquinone spiroketal natural products. We have achieved concise total syntheses of palmarumycin CP1 and deoxypreussomerin A in 8-9 steps and 15-35% overall yield from 5-hydroxy-8-methoxy-1-tetralone (**8**). Polymer-bound triphenylphosphine was found to be a superior reagent for the rapid preparation of a small library of palmarumycin analogs. Preliminary biological evaluation of 22 naphthoquinone spiroketals against two human breast cancer cell lines revealed several potent and selective growth inhibitors. In view of this favorable profile, further biological studies of this series are continuing.

Experimental Part

General. All moisture-sensitive reactions were performed under an atmosphere of N_2 or Ar and all glassware was dried in an oven at 140 °C prior to use. THF and Et_2O were dried by distillation over Na / benzophenone under a nitrogen atmosphere. Dry CH_2Cl_2 was obtained by distillation from CaH_2. Dry DMF was obtained by distillation from alumina under reduced pressure. Dry CF_3CH_2OH was obtained by distillation from $CaSO_4$. Unless otherwise noted, solvents or reagents were used without further purification. NMR spectra were recorded at either 300 MHz / 75 MHz (^{1}H / ^{13}C NMR) or 500 MHz / 125 MHz (^{1}H / ^{13}C NMR) in $CDCl_3$ unless stated otherwise.

Antiproliferative Assay. The antiproliferative actions of our compounds were examined using a colorimetric assay described previously[27] with two human breast cancer cell lines: the p53 replete, estrogen-receptor positive MCF-7 and the p53 deficient, estrogen-receptor negative MDA-MB-231 cells (American Type Culture Collection, Manassas, VA). Briefly, cells were seeded (6000/well) in 96-well plates that contained Eagle's minimum essential medium (MCF-7) or RPMI-1640 medium (MDA-MB-231) and 10% fetal bovine serum and placed in a humidified 37 °C incubator maintained at 5% CO_2. Cells were allowed to attach overnight and treated with vehicle or compounds (0.1–30 μM) for 72 h. The medium was then replaced with serum free medium containing 0.1% of 3-[4,5-dimethylthiazol-2-yl]-2,5-diphenyl tetrazolium bromide. Plates were incubated for 3 h in the dark and the total cell number was calculated by colorimetric determination at 540 nm of the formazane metabolic product as previously described.[27]

5-Hydroxy-8-methoxy-1,2,3,4-tetrahydronaphthalene-1-spiro-2'-dioxolane (6). To a solution of **8** (4.8 g, 25 mmol) and ethylene glycol (3.1 g, 50 mmol) in benzene (700 mL) was added PPTS (0.3 g). The reaction mixture was heated at reflux for 30 h in a flask equipped with a Dean-Stark apparatus, washed with 5% $NaHCO_3$ solution (2x 200 mL) and brine (300 mL), dried (Na_2SO_4), and concentrated *in vacuo*. Chromatography on SiO_2 (hexanes/EtOAc, 2:1) gave 5.32 g (90%) of **6** as a solid: Mp 139 - 140 °C; IR (neat) 3359, 2928, 1583, 1468, 1327, 1244, 1159, 1118, 1064, 1008, 945, 924, 864, 794, 716 cm^{-1}; ^{1}H NMR δ 6.55 (d, 1 H, *J* = 8.8 Hz), 6.54 (d, 1 H, *J* = 8.8 Hz), 5.42 (s, 1 H, OH), 4.25 (t, 2 H, *J* = 6.6 Hz), 4.07 (t, 2 H, *J* = 6.6 Hz), 3.75 (s, 3 H), 2.57 (t, 2 H, *J* = 6.0 Hz), 1.93-1.80 (m, 4 H); ^{13}C NMR δ 152.6, 146.9, 128.3, 125.8, 115.2, 110.7, 108.1, 65.5, 56.6, 35.9, 24.0, 20.1; MS (EI) m/z (rel intensity) 236 (M$^+$, 94), 208 (100), 193 (19), 175 (11), 164 (19), 149 (11), 134 (20), 121 (10), 106 (10), 99 (20), 77 (10), 65 (9), 55 (13); HRMS (EI) calcd for $C_{13}H_{16}O_4$ 236.1049, found 236.1052.

8-Methoxy-5-(8'-methoxynaphthalene-1'-yloxy)-3,4-dihydro-2*H*-naphthalen-1-one (10). To a solution of **6** (4.72 g, 0.02 mol) and **7** (8.52 g, 0.03 mol) in degassed pyridine (150 mL) were added K_2CO_3 (2.76 g, 0.02 mol) and Cu_2O (286 mg, 0.002 mol). This reaction mixture was heated at reflux for 12 h under a nitrogen atmosphere. After addition of additional Cu_2O (286 mg, 0.002 mol) to the solution, heating was continued for 12 h. Pyridine was removed under reduced pressure and the residue was redissolved in EtOAc (300 mL). It was washed with water (100 mL) and brine (100 mL), dried (Na_2SO_4), and concentrated *in vacuo*. Chromatography on SiO_2 (hexanes/EtOAc, 2:1) gave 6.14 g (78%) of **9** as an oil. This oil was treated with TsOH (100 mg) in a mixture of acetone/water (7:1, 50 mL) for 7 h at room

temperature. The reaction mixture was concentrated *in vacuo* and the residue was diluted with EtOAc (300 mL), washed with water (2x 100 mL) and brine (100 mL), dried (Na_2SO_4), and concentrated *in vacuo*. Chromatography on SiO_2 (hexanes/EtOAc, 1:1) gave 5.44 g (100%) of **10** as a colorless solid: Mp 152 - 153 °C; IR(neat) 2952, 1696, 1581, 1484, 1387, 1272, 1245, 1183, 1095, 980, 838, 821, 759 cm^{-1}; ^{1}H NMR δ 7.59 (dd, 1 H, J = 8.2, 0.8 Hz), 7.45 (dd, 1 H, J = 8.2, 1.0 Hz), 7.37 (q, 2 H, J = 7.9 Hz), 6.87 (dd, 1 H, J = 7.6, 0.8 Hz), 6.81 (dd, 1 H, J = 7.6, 0.8 Hz), 6.72 (d, 1 H, J = 8.9 Hz), 6.67 (d, 1 H, J = 9.1 Hz), 3.84 (s, 3 H), 3.74 (s, 3 H), 3.05 (t, 2 H, J = 6.2 Hz), 2.67 (t, 2 H, J = 6.3 Hz), 2.11 (p, 2 H, J = 6.4 Hz); ^{13}C NMR δ 197.9, 156.2, 155.4, 152.7, 149.3, 137.6,136.4, 126.7, 126.4, 124.1, 123.1, 121.7, 120.7, 118.8, 115.9, 110.1, 106.1, 56.3, 56.0, 40.9, 24.1, 22.5; MS (EI) m/z (rel intensity) 348 (M+, 100), 319 (7), 305 (10), 291 (14), 261 (8), 218 (7), 189 (12), 174 (24), 158 (45), 127 (34), 115 (29), 101 (10), 77 (15), 63 (8); HRMS (EI) Calcd for $C_{22}H_{20}O_4$ 348.1361, found 348.1361.

8-Hydroxy-5-(8'-hydroxynaphthalen-1'-yloxy)-3,4-dihydro-2*H*-naphthalen-1-one (11). To a solution of **10** (3.92 g, 11.3 mmol) in CH_2Cl_2 (120 mL) was added a 1 M solution of BBr_3 in CH_2Cl_2 (40 mL, 40 mmol) at −78 °C. The reaction mixture was warmed to room temperature, stirred for 12 h, poured into ice water (200 g) and extracted with CH_2Cl_2 (2x 300 mL). The combined organic layers were washed with brine (200 mL), dried (Na_2SO_4) and concentrated *in vacuo*. Chromatography on SiO_2 (hexanes/EtOAc, 8:1) gave 3.44 g (95%) of **11** as a colorless solid: Mp 165 - 166 °C; IR (neat) 3403, 2947, 1624, 1449, 1387, 1343, 1289, 1213, 1167, 1024, 808, 749 cm^{-1}; ^{1}H NMR δ 12.46 (s, 1 H, OH), 9.02 (s, 1 H, OH), 7.50-7.32 (m, 4 H), 7.18 (t, 1 H, J = 8.0 Hz), 6.98 (dd, 1 H, J = 7.2, 1.1 Hz), 6.93 (d, 1 H, J = 8.9 Hz), 6.40 (d, 1 H, J = 7.7 Hz), 2.85 (t, 2 H, J = 6.0 Hz), 2,70 (t, 2 H, J = 6.3 Hz), 2.06 (p, 2 H, J = 6.4 Hz); ^{13}C NMR δ 204.7, 161.1, 155.4, 154.0, 141.8, 137.2, 137.1, 131.1, 128.1, 125.5, 123.1, 119.3, 117.4, 117.1, 114.9, 111.0, 107.4, 38.7, 23.6, 22.1; MS (EI) m/z (rel intensity) 320 (M$^+$, 100), 287 (6), 263 (10), 247 (7), 177 (9), 159 (25), 144 (38), 131 (29), 115 (34), 103 (15), 89 (10), 77 (23), 65 (14); HRMS (EI) Calcd for $C_{20}H_{16}O_4$ 320.1049, found 320.1044.

Acetic acid 8-(4'-acetoxy-5'-oxo-5',6',7',8'-tetrahydro-naphthalen-1'-yloxy)-naphthalen-1-yl ester (12). To a solution of **11** (487 mg, 1.52 mmol) in acetic anhydride (2 mL) was added sodium acetate (100 mg). The reaction mixture was heated to 95 °C, stirred for 4 h and cooled to room temperature. The mixture was poured into ice water (100 g), stirred for 1 h and extracted with ethyl acetate (100 mL). The ethyl acetate layer was washed with brine (50 mL), dried (Na_2SO_4) and concentrated *in vacuo*. Chromatography on SiO_2 (hexanes/EtOAc, 2:1) gave 607 mg (99%) of **12** as an oil: IR (neat) 3059, 2951, 1765, 1686, 1601, 1573, 1460, 1367, 1258, 1202, 1115, 1025, 898, 825, 760, 735 cm^{-1}; ^{1}H NMR δ 7.77 (d, 1 H, J = 7.9 Hz), 7.58 (d, 1 H, J = 8.0 Hz), 7.50 (t, 1 H, J = 8.0 Hz), 7.29 (t, 1 H, J = 7.7 Hz), 7.18 (t, 1 H, J = 7.4 Hz), 7.16 (d, 1 H, J = 7.6 Hz), 6.97 (d, 1 H, J = 8.7 Hz), 6.58 (dd, 1 H, J = 7.7, 0.7 Hz), 2.91 (t, 2 H, J = 5.7 Hz), 2.62 (t, 2 H, J = 6.2 Hz), 2.40 (s, 3 H), 2.19 (s, 3 H), 2.07 (p, 2 H, J = 6.4 Hz); ^{13}C NMR δ 196.3, 170.3, 170.0, 153.1, 150.8, 146.8, 146.0, 138.3, 137.1, 126.6, 126.4, 126.3, 126.2, 125.8, 123.3, 123.1, 120.0, 119.4, 111.8, 40.1, 23.8, 22.0, 21.2, 21.1; MS (EI) m/z (rel intensity) 404 (M$^+$, 23), 362 (30), 320 (100), 202 (10), 149 (21), 115 (12), 91 (33), 69 (18), 57 (28); HRMS (EI) calcd for $C_{24}H_{20}O_6$ 404.1260, found 404.1266.

8-Hydroxy-5-(8'-hydroxynaphthalene-1'-yloxy)-1,2,3,4-tetrahydronaphthalene-1-spiro-2''-dioxolane (5). To a solution of **12** (240 mg, 0.593 mmol) and ethylene glycol (1.10 g, 17.79 mmol) in benzene (20 mL) was added PPTS (75 mg, 0.297 mmol). The reaction mixture was heated at reflux for 62 h in a flask equipped with a Dean-Stark apparatus, cooled to room temperature, diluted with benzene (100 mL), washed with 5% $NaHCO_3$ solution (2x 50 mL) and brine (50 mL), dried (Na_2SO_4), and concentrated *in vacuo*. Chromatography on SiO_2 (hexanes/EtOAc, 1:1) gave 205 mg (77%) of **13** as an oil. To a solution of **13** (175 mg, 0.39 mmol) in degassed THF/MeOH (15 mL, 2/1) was added lithium hydroxide monohydrate (41 mg, 0.98 mmol) at 0 °C. The reaction mixture was stirred for 2 h in an ice bath, neutralized with saturated ammonium chloride solution and extracted with ethyl acetate (2x 100 mL). The combined organic layers were washed with brine (100 mL), dried (Na_2SO_4), and concentrated *in vacuo*. Chromatography on SiO_2 (hexanes/EtOAc, 2:1) gave 137 mg (96%) of **5** as a solid: Mp 174 - 175 °C; IR (neat) 3405, 3318, 3057. 2959, 2904, 1608, 1581, 1469,1402, 1365, 1301, 1253, 1220, 1182, 1157, 1121, 1035, 944, 928, 878, 818, 759 cm^{-1}; ^{1}H NMR δ 9.18 (s, 1 H, OH), 8.43 (s, 1 H, OH), 7.46-7.34 (m, 3 H), 7.17 (t, 1 H, J = 8.0 Hz), 7.10 (d, 1 H, J = 8.8 Hz), 6.96 (dd, 1 H, J = 7.2, 1.1 Hz), 6.85 (d, 1 H, J = 8.8 Hz), 6.45 (d, 1 H, J = 7.6 Hz), 4.34-4.17 (m, 4 H), 2.68 (t, 2 H, J = 6.3 Hz), 1.99-1.95 (m, 2 H), 1.91-1.83 (m, 2 H); ^{13}C NMR δ 155.5, 154.8, 154.2, 143.3, 137.0, 133.5, 127.8, 125.7, 124.4, 122.6, 120.6, 119.1, 116.1, 114.9, 110.6, 109.8, 107.3, 63.9, 31.3, 23.5, 19.2; MS (EI) m/z (rel intensity) 364 (M$^+$, 100), 320 (55), 159 (11), 144 (24), 131 (14), 115 (22), 77 (7), 55 (8); HRMS (EI) calcd for $C_{22}H_{20}O_5$ 364.1311, found 364.1311.

1-Oxo-1,4,5,6,7,8-hexahydronaphthalene-4-spiro-2'-naphtho[1'',8''-de][1',3']dioxin-8-spiro-2'''-dioxolane (14). To a suspension of **5** (58 mg, 0.159 mmol) in trifluoroethanol (20 mL) was added PhI(OAc)$_2$ (62 mg, 0.191 mmol). The reaction mixture was stirred for 2 h at room temperature and $NaHCO_3$ (32 mg, 0.382 mmol) was. The resulting mixture was concentrated *in vacuo* and the residue was diluted with EtOAc (50 mL), washed with water (30 mL) and brine (30 mL), dried (Na_2SO_4), and concentrated *in vacuo*. Chromatography on SiO_2 (hexanes/EtOAc, 4:1) gave 43 mg (75%) of **14** as an oily solid: IR (neat) 3059, 2949, 2897, 1680, 1651, 1608, 1584, 1412, 1396, 1302, 1271, 1144, 1096, 1052, 1031, 949, 825, 814, 757 cm^{-1}; ^{1}H NMR δ 7.52 (d, 2 H, J = 8.1 Hz), 7.43 (t, 2 H, J = 7.9 Hz), 6.93 (d, 2 H, J = 7.1 Hz), 6.76 (d, 1 H, J = 10.3 Hz), 6.08 (d, 1 H, J = 10.4 Hz), 4.41-4.36 (m, 2 H), 4.08-4.04 (m, 2 H), 2.75-2.65 (m, 2 H), 1.95-1.85 (m, 4 H); ^{13}C NMR δ 182.4, 154.1, 146.8, 136.4, 134.1, 134.0, 130.6, 127.6, 121.2, 112.9, 109.7, 105.9, 92.8, 66.1, 35.6, 24.5, 19.5; MS (EI) m/z (rel intensity) 362 (M$^+$, 100), 319 (39), 306 (16), 262 (15), 234 (9), 204 (10), 178 (16), 131 (13), 115 (17), 99 (13), 84 (22), 55 (13); HRMS (EI) calcd for $C_{22}H_{18}O_5$ 362.1154, found 362.1160.

(±)-8-Hydroxy-1-oxo-1,4,5,6,7,8-hexahydronaphthalene-4-spiro-2'-naphtho[1'',8''-de][1',3']dioxin (16). To a solution of **11** (1.51 g, 4.72 mmol) in Et$_2$O (70 mL) was added in portions solid LiAlH$_4$ (358 mg, 9.44 mmol) at 0 °C. The solution was stirred for 2 h at 0 °C, warmed to room temperature and stirred for an additional 2 h. The reaction mixture was carefully quenched with 5% sodium bisulfate solution in an ice bath. After adding 40 mL of 5% sodium bisulfate solution, the product was extracted with Et$_2$O (2x 150 mL). The combined ether layers were washed with brine (100 mL), dried (Na_2SO_4) and concentrated *in vacuo*. The resulting solid was added to dry trifluoroethanol (150 mL) and stirred until a fine

suspension was obtained. After addition of PhI(OAc)$_2$ (1.67 g, 5.19 mmol), the mixture was stirred for 30 min at room temperature, NaHCO$_3$ (1.0 g, 12 mmol) was added. The solution was concentrated *in vacuo* and the resulting residue was diluted with EtOAc (300 mL), washed with water (100 mL) and brine (100 mL), dried (Na$_2$SO$_4$), and concentrated *in vacuo*. Chromatography on SiO$_2$ (hexanes/EtOAc, 2:1) gave 1.32 g (87%) of **16** as a yellow solid: Mp 199 - 200 °C; IR (neat) 3434, 2945, 1673, 1642, 1630, 1600, 1409, 1374, 1263, 1080, 944, 757 cm^{-1}; ^{1}H NMR δ 7.54 (d, 2 H, J = 8.0 Hz), 7.45 (td, 2 H, J = 7.4, 2.2 Hz), 6.95 (td, 2 H, J = 7.6, 0.7 Hz), 6.90 (d, 1 H, J = 10.4 Hz), 6.19 (d, 1 H, J = 10.4 Hz), 4.82 (t, 1 H, J = 4.9 Hz), 3.31 (bs, 1 H, OH), 2.78-2.51 (m, 2 H), 1.98-1.90 (m, 3 H), 1.82-1.72 (m, 1 H); ^{13}C NMR δ 185.8, 151.6, 146.8, 139.3, 135.6, 134.1, 129.1, 127.7, 127.6, 121.3, 112.9, 109.8, 109.7, 92.6, 62.7, 29.6, 24.2, 17.7; MS (EI) m/z (rel intensity) 320 (M$^+$, 100), 304 (30), 265 (35), 247 (21), 235 (10), 219 (11), 197 (18), 169 (24), 160 (32), 144 (35), 133 (35), 115 (50), 103 (16), 88 (13), 77 (28), 63 (17); HRMS (EI) Calcd for C$_{20}$H$_{16}$O$_4$ 320.1049, found 320.1039

8-Hydroxy-1-oxo-1,4-dihydronaphthalene-4-spiro-2'-naphtho[1",8"-de][1',3']dioxin (palmarumycin CP$_1$).

To a solution of **16** (32 mg, 0.1 mmol) in CH$_2$Cl$_2$ (5 mL) was added Dess-Martin periodinane (64 mg, 0.15 mmol) at room temperature. The reaction mixture was stirred for 2 h and diluted with EtOAc (30 mL). It was washed with 5% NaHCO$_3$ solution (10 mL) and brine(15 mL), dried (Na$_2$SO$_4$), and concentrated *in vacuo*. Chromatography on SiO$_2$ (hexanes/EtOAc, 2:1) gave 32 mg of a yellow residue which was treated with MnO$_2$ (Aldrich, 85% activated, 102 mg, 1 mmol, dried over P$_2$O$_5$ just before use) in dry CH$_2$Cl$_2$ (5 mL) for 2 d at room temperature. The reaction mixture was filtered through celite and washed with CH$_2$Cl$_2$ (10 mL). The combined solutions were concentrated *in vacuo*. Chromatography on SiO$_2$ (hexanes/EtOAc, 4:1) gave 19 mg (60%) of palmarumycin CP$_1$ as a yellow solid; Mp 170 °C (dec.); IR (neat) 3053, 1659, 1602, 1449, 1409, 1372, 1341, 1269, 1237, 1110, 1073, 942, 822, 746 cm^{-1}; ^{1}H NMR δ 12.17 (s, 1 H, OH), 7.67 (t, 1 H, J = 8.0 Hz), 7.58 (d, 2 H, J = 8.5 Hz), 7.47 (t, 2 H, J = 7.9 Hz), 7.46 (d, 1 H, J = 7.8 Hz), 7.14 (dd, 1 H, J = 8.2, 1.1 Hz), 7.02 (d, 1 H, J = 10.9 Hz), 6.98 (d, 2 H, J = 7.7 Hz), 6.37 (d, 1 H, J = 10.9 Hz); ^{13}C NMR δ 188.8, 161.9, 147.2, 139.7, 138.8, 136.7, 134.2, 129.8, 127.7, 121.4, 119.7, 119.4, 113.8, 113.0, 109.9, 92.9; MS (EI) m/z (rel intensity) 316 (M$^+$, 100), 288 (12), 287 (19), 259 (8), 175 (11), 114 (45), 88 (11), 63 (9); HRMS (EI) Calcd for C$_{20}$H$_{12}$O$_4$ 316.0736, found 316.0730.

(±)-2,3-Epoxy-8-hydroxy-1-oxo-1,2,3,4-tetrahydro-naphthalene-4-spiro-2'-naphtho[1",8"-de][1',3']dioxin [(±)-deoxypreussomerin A].

To a solution of **16** (54.5 mg, 0.17 mmol) in THF (5 mL) was added cumene hydroperoxide (157 μL, 0.85 mmol) and NaH (60%, 6.5 mg, 0.17 mmol) at -20 °C. The reaction mixture was stirred for 4 h at -20 °C, and diluted with EtOAc (40 mL) and brine (5 mL). The separated organic layer was washed with an additional brine(20 mL), dried(Na$_2$SO$_4$), and concentrated *in vacuo*. Chromatography on SiO$_2$ (hexanes/EtOAc, 3:1) gave 27 mg (47%) of monoepoxide **20**. To a solution of this epoxide in CH$_2$Cl$_2$ (4 mL) was added Dess-Martin periodinane (51 mg, 0.12 mmol) at room temperature. The reaction mixture was stirred for 2 h, diluted with EtOAc (30 mL), washed with 5% NaHCO$_3$ solution (10 mL) and brine (15 mL), dried (Na$_2$SO$_4$), and concentrated *in vacuo*. Chromatography on SiO$_2$ (hexanes/EtOAc, 2:1) gave 27 mg of a yellow residue which was treated with MnO$_2$ (Aldrich, 85% activated, 82 mg, 0.8 mmol, dried over P$_2$O$_5$ just before use) in dry CH$_2$Cl$_2$ (5 mL) for 37 h at room temperature. The mixture was filtered through

celite and washed with CH_2Cl_2 (10 mL). The combined solutions were concentrated *in vacuo*. Chromatography on SiO_2 (hexanes/EtOAc, 3:1) gave 14.5 mg (26% from **16**) of (±)-deoxypreussomerin A as a colorless solid: Mp 200 - 201 °C; IR (neat) 3050, 1651, 1605, 1455, 1409, 1380, 1330, 1266, 1239, 1173, 1110, 1061, 963, 920, 878, 820, 809, 759, 720 cm^{-1}; ^{1}H NMR δ 11.37 (s, 1 H, OH), 7.65 (t, 1 H, J = 8.0 Hz), 7.60 (d, 1 H, J = 8.6 Hz), 7.57 (d, 1 H, J = 8.0 Hz), 7.53 (t, 1 H, J = 8.3 Hz), 7.45 (t, 1 H, J = 7.4Hz), 7.44 (d, 1 H, J = 7.9 Hz), 7.19 (dd, 1 H, J = 7.6, 0.8 Hz), 7.14 (dd, 1 H, J = 8.6, 0.8 Hz), 6.92 (dd, 1 H, J = 7.6, 0.7 Hz), 4.09 (d, 1 H, J = 4.1 Hz), 3.68 (d, 1 H, J = 3.9 Hz); ^{13}C NMR δ 196.6, 161.9, 146.9, 146.7, 137.8, 136.9, 134.2, 127.9, 127.7, 121.5, 121.4, 120.1, 119.1, 112.8, 112.3, 110.2, 109.4, 96.0, 53.3; MS (EI) m/z (rel intensity) 332 (M+, 100), 316 (28), 303 (11), 287 (19), 173 (15), 145 (23), 132 (12), 114 (27), 89 (13), 74 (14), 63 (12), 57 (7); HRMS(EI) Calcd for $C_{20}H_{12}O_5$ 332.0685, found 332.0688.

General procedure for Mitsunobu reactions. (*E*)-8-(3-Phenyl-allyloxy)-1-oxo-1,4-dihydronaphthalene-4-spiro-2'-naphto[1",8"-de][1',3']dioxin (21). A solution of palmarumycin CP$_1$ (7.4 mg, 0.023 mmol), diphenylphosphino-polystyrene (82.1 mg, 1.41 mmol/g, 0.116 mmol) and cinnamyl alcohol (15.5 µL, 0.118 mmol) in dry CH_2Cl_2 (0.4 mL) was stirred for 30 min at room temperature and cooled to 0 °C. DEAD (18.0 µL, 0.114 mmol) was added to the reaction mixture at 0 °C and stirring was continued for 24 h at room temperature. The reaction mixture was washed with 5% aqueous KOH solution (0.5 mL), followed by 5% HCl (0.5 mL). The methylene chloride extract was filtered, the resin was washed further with CH_2Cl_2 (2x 0.5 mL) and the solvent was concentrated. Chromatography on SiO_2 (hexanes/EtOAc, 9:1) gave 1.8 mg (24%) of palmarumycin CP$_1$ and 5.0 mg (52%) of **21** as a colorless oil: ^{1}H NMR δ 7.70 (t, 1 H, J = 8.0 Hz), 7.60-7.56 (m, 3 H), 7.50-7.45 (m, 4 H), 7.37-7.20 (m, 4 H), 6.99 (d, 2 H, J = 7.3 Hz), 6.93 (bs, 1 H), 6.87 (d, 1 H, J =10.5 Hz), 6.49 (dt, 1 H, J = 5.2, 16.0 Hz), 6.31 (d, 1 H, J = 10.5 Hz), 4.93 (d, 2 H, J = 5.2 Hz); HRMS(EI) Calcd for $C_{29}H_{20}O_4$ 432.1362, found 432.1362.

(*E*)-8-(But-2-enyloxy)-1-oxo-1,4-dihydronaphthalene-4-spiro-2'-naphto[1",8"-de][1',3']dioxin (22). According to the general procedure, palmarumycin CP$_1$ (2.4 mg, 0.008 mmol), diphenylphosphino-polystyrene (28.2 mg, 1.41 mmol/g, 0.040 mmol), 2-buten-1-ol (3.3 µL, 0.038 mmol) and DEAD (6.0 µL, 0.038 mmol) in dry CH_2Cl_2 (0.2 mL) provided after 24 h 2.5 mg (88%) of **22** as a colorless oil: ^{1}H NMR δ 7.68 (t, 1 H, J = 8.0 Hz), 7.60-7.55 (m, 3 H), 7.49 (d, 1 H, J = 7.7 Hz), 7.46 (d, 1 H, J = 8.2 Hz), 7.17 (d, 1 H, J = 8.6 Hz), 6.98 (d, 2 H, J = 7.4 Hz), 6.85 (d, 1 H, J = 10.5 Hz), 6.29 (d, 1 H, J = 10.5 Hz), 6.03 (dq, 1 H, J = 15.3, 6.5 Hz), 5.85-5.75 (m, 1 H), 4.69 (d, 2 H, J = 5.4 Hz), 1.80 (d, 3 H, J = 6.2 Hz); HRMS(EI) Calcd for $C_{24}H_{18}O_4$ 370.1205, found 370.1214.

8-Hexyloxy-1-oxo-1,4-dihydronaphthalene-4-spiro-2'-naphto[1",8"-de][1',3']dioxin (23). According to the general procedure, palmarumycin CP$_1$ (2.0 mg, 0.006 mmol), diphenylphosphino-polystyrene (31.3 mg, 1.41 mmol/g, 0.044 mmol), hexyl alcohol (4.0 µL, 0.031 mmol) and DEAD (5.0 µL, 0.032 mmol) in dry CH_2Cl_2 (0.1 mL) provided after 43 h 1.3 mg (50%) of **23** as a colorless oil: ^{1}H NMR δ 7.66 (t, 1 H, J = 8.3 Hz), 7.57-7.50 (m, 3 H), 7.48-7.42 (m, 2 H), 7.14 (d, 1 H, J = 8.3 Hz), 6.96 (d, 2 H, J = 7.5 Hz), 6.82 (d, 1 H, J = 10.4 Hz), 6.26 (d, 1 H, J = 10.4 Hz), 4.10 (t, 2 H, J = 5.9 Hz), 2.30-1.20 (m, 11 H).

(*E*)-8-(Hex-3-enyloxy)-1-oxo-1,4-dihydronaphthalene-4-spiro-2'-naphto[1",8"-de][1',3']dioxin (24). According to the general procedure, palmarumycin CP$_1$ (2.1 mg, 0.007

mmol), diphenylphosphino-polystyrene (23.9 mg, 1.41 mmol/g, 0.034 mmol), *trans*-3-hexen-1-ol (4.2 μL, 0.034 mmol) and DEAD (5.2 μL, 0.033 mmol) in dry CH_2Cl_2 (0.1 mL) provided after 67 h 1.3 mg (43%) of **24** as a colorless oil: ^1H NMR δ 7.68 (t, 1 H, J = 8.3 Hz), 7.60-7.45 (m, 5 H), 7.16 (d, 1 H, J = 8.4 Hz), 6.97 (d, 2 H, J = 7.5 Hz), 6.85 (d, 1 H, J = 10.5 Hz), 6.28 (d, 1 H, J = 10.4 Hz), 5.66-5.60 (m, 1 H), 5.45-5.30 (m, 1 H), 4.15 (t, 2 H, J = 6.9 Hz), 2.7-2.6 (m, 2 H), 2.4-2.3 (m, 2 H), 1.00 (t, 3 H, J = 6.4 Hz).

8-(3-Methoxy-benzyloxy)-1-oxo-1,4-dihydronaphthalene-4-spiro-2'-naphto[1'',8''-de][1',3']dioxin (25).

According to the general procedure, palmarumycin CP_1 (2.0 mg, 0.006 mmol), diphenylphosphino-polystyrene (22.8 mg, 1.41 mmol/g, 0.032 mmol), 3-mehoxybenzyl alcohol (4.0 μL, 0.032 mmol) and DEAD (5.0 μL, 0.032 mmol) in dry CH_2Cl_2 (0.1 mL) provided after 45 h 1.6 mg (67%) of **25** as a colorless oil: ^1H NMR δ 7.68-7.54 (m, 4 H), 7.45 (t, 2 H, J = 7.7 Hz), 7.24-7.10 (m, 4 H), 6.97 (d, 2 H, J = 7.5 Hz), 6.9-6.8 (m, 2 H), 6.30 (d, 1 H, J = 10.4 Hz), 5.29 (s, 2 H), 3.86 (s, 3 H).

8-(2-Phenyl-ethoxy)-1-oxo-1,4-dihydronaphthalene-4-spiro-2'-naphto[1'',8''-de][1',3']dioxin (26).

According to the general procedure, palmarumycin CP_1 (2.0 mg, 0.006 mmol), diphenylphosphino-polystyrene (23.4 mg, 1.41 mmol/g, 0.033 mmol), phenethyl alcohol (3.8 μL, 0.032 mmol) and DEAD (5.0 μL, 0.032 mmol) in dry CH_2Cl_2 (0.2 mL) provided after 24 h 1.0 mg (33%) of **26** as a colorless oil: ^1H NMR δ 7.67-7.1 (m, 12 H), 6.98 (d, 2 H, J = 7.5 Hz), 6.86 (d, 1 H, J = 10.5 Hz), 6.30 (d, 1 H, J = 10.6 Hz), 4.33 (t, 2 H, J = 7.0 Hz), 3.27 (t, 2 H, J = 7.0 Hz).

8-(Furan-2-ylmethoxy)-1-oxo-1,4-dihydronaphthalene-4-spiro-2'-naphto[1'',8''-de][1',3']dioxin (27) and 7-(furan-2-ylmethyl)-8-hydroxy-1-oxo-1,4-dihydronaphthalene-4-spiro-2'-naphto[1'',8''-de][1',3']dioxin (28).

According to the general procedure, palmarumycin CP_1 (2.1 mg, 0.007 mmol), diphenylphosphino-polystyrene (22.5 mg, 1.41 mmol/g, 0.032 mmol), furfuryl alcohol (2.8 μL, 0.032 mmol) and DEAD (5.0 μL, 0.032 mmol) in dry CH_2Cl_2 (0.2 mL) provided after 5 d 2.0 mg (71%) of **27** and 1.0 mg (29%) of **28** as colorless oils. **27**: ^1H NMR δ 7.70-7.45 (m, 6 H), 7.29-7.26 (m, 2 H), 7.05-6.95 (m, 2 H), 6.86 (d, 1 H, J = 10.5 Hz), 6.55 (bs, 1 H), 6.41 (bs, 1 H), 6.28 (d, 1 H, J = 10.5 Hz), 5.23 (s, 2 H). **28**: ^1H NMR δ 12.67 (s, 1 H), 7.61 (d, 2 H, J = 8.2 Hz), 7.62-7.44 (m, 4 H), 7.11 (d, 1 H, J = 8.8 Hz), 7.00-6.92 (m, 3 H), 6.35 (d, 1 H, J = 10.4 Hz), 6.26 (t, 1 H, J = 2.4 Hz), 5.91 (d, 1 H, J = 3.2 Hz), 4.26 (s, 2 H).

(*E,E*)-8-(3,7-Diemthyl-octa-2,6-dienyloxy)-1-oxo-1,4-dihydronaphthalene-4-spiro-2'-naphto[1'',8''-de][1',3']dioxin (29).

According to the general procedure, palmarumycin CP_1 (2.0 mg, 0.006 mmol), diphenylphosphino-polystyrene (23.1 mg, 1.41 mmol/g, 0.033 mmol), geraniol (5.6 μL, 0.032 mmol) and DEAD (5.0 μL, 0.032 mmol) in dry CH_2Cl_2 (0.2 mL) provided after 29 h 2.1 mg (83%) of **29** as a colorless oil: ^1H NMR δ 7.67 (t, 1 H, J = 8.2 Hz), 7.59-7.55 (m, 3 H), 7.50-7.44 (m, 2 H), 7.16 (d, 1 H, J = 8.2 Hz), 6.98 (d, 2 H, J = 7.4 Hz), 6.85 (d, 1 H, J = 10.5 Hz), 6.28 (d, 1 H, J = 10.5 Hz), 5.56 (t, 1 H, J = 6.0 Hz), 5.10 (bs, 1 H), 4.79 (d, 2 H, J = 6.2 Hz), 2.11 (bs, 4 H), 1.78 (s, 3 H), 1.69 (s, 3 H), 1.62 (s, 3 H).

8-(Furan-3-ylmethoxy)-1-oxo-1,4-dihydronaphthalene-4-spiro-2'-naphto[1'',8''-de][1',3']dioxin (30).

According to the general procedure, palmarumycin CP_1 (2.0 mg, 0.006 mmol), diphenylphosphino-polystyrene (23.4 mg, 1.41 mmol/g, 0.033 mmol), 3-furanmethanol (2.8 μL, 0.032 mmol) and DEAD (5.0 μL, 0.032 mmol) in dry CH_2Cl_2 (0.2 mL) provided after 3 d 1.2 mg (50%) of **30** as a colorless oil: ^1H NMR δ 7.63-7.45 (m, 5 H), 7.42-

7.35 (m, 3 H), 7.16 (d, 1 H, J = 8.2 Hz), 6.89 (d, 2 H, J = 7.4 Hz), 6.77 (dd, 1 H, J = 10.5, 1.3 Hz), 6.51 (bs, 1 H), 6.20 (dd, 1 H, J = 10.5, 1.3 Hz), 5.08 (s, 2 H); HRMS(EI) Calcd for $C_{25}H_{16}O_5$ 396.0998, found 396.0997.

8-(Pyridin-2-ylmethoxy)-1-oxo-1,4-dihydronaphthalene-4-spiro-2'-naphto[1'',8''-de][1',3']dioxin (31). According to the general procedure, palmarumycin CP$_1$ (2.2 mg, 0.007 mmol), diphenylphosphino-polystyrene (29.7 mg, 1.41 mmol/g, 0.042 mmol), 2-pyridylcarbinol (3.4 μL, 0.035 mmol) and DEAD (5.5 μL, 0.035 mmol) in dry CH_2Cl_2 (0.2 mL) provided after 4 d 0.2 mg (9%) of palmarumycin CP$_1$ and 1.2 mg (43%) of **31** as a colourless oil: ^{1}H NMR δ 8.50 (bs, 1 H), 8.16 (bs, 1 H), 7.88 (bs, 1 H), 7.77-7.50 (m, 4 H), 7.51-7.45 (m, 3 H), 7.4-7.3 (m, 1 H); 6.99 (d, 2 H, J = 7.7 Hz), 6.92 (bd, 1 H, J = 10.5 Hz), 6.33 (d, 1 H, J =10.5 Hz), 5.42 (bs, 2 H); HRMS(EI) Calcd for $C_{26}H_{17}NO_4$ 407.1158, found 407.1139.

8-(Pyridin-3-ylmethoxy)-1-oxo-1,4-dihydronaphthalene-4-spiro-2'-naphto[1'',8''-de][1',3']dioxin (32). According to the general procedure, palmarumycin CP$_1$ (2.1 mg, 0.007 mmol), diphenylphosphino-polystyrene (23.8 mg, 1.41 mmol/g, 0.034 mmol), 3-pyridylcarbinol (3.3 μL, 0.033 mmol) and DEAD (5.2 μL, 0.033 mmol) in dry CH_2Cl_2 (0.2 mL) provided after 5 d 0.3 mg (14%) of palmarumycin CP$_1$ and 0.9 mg (29%) of **32** as a colorless oil: ^{1}H NMR δ 8.8-8.5 (m, 2 H), 8.29 (d, 1 H, J = 7.9 Hz), 7.74-7.40 (m, 8 H), 7.25-7.20 (m, 1 H), 6.97 (d, 1 H, J = 7.1 Hz), 6.88 (d, 1 H, J = 10.5 Hz), 6.30 (d, 1 H, J = 10.4 Hz), 5.32 (s, 2 H); HRMS(EI) Calcd for $C_{26}H_{17}NO_4$ 407.1158, found 407.1152.

8-(Pyridin-4-ylmethoxy)-1-oxo-1,4-dihydronaphthalene-4-spiro-2'-naphto[1'',8''-de][1',3']dioxin (33). According to the general procedure, palmarumycin CP$_1$ (2.0 mg, 0.006 mmol), diphenylphosphino-polystyrene (22.4 mg, 1.41 mmol/g, 0.032 mmol), 4-pyridylcarbinol (7.6 mg, 0.069 mmol) and DEAD (5.0 μL, 0.032 mmol) in dry CH_2Cl_2 (0.2 mL) provided after 7 d 0.6 mg (30%) of palmarumycin CP$_1$ and 0.5 mg (17%) of **33** as a colorless oil: ^{1}H NMR δ 8.9-8.5 (m, 2 H), 8.10 (bs, 1 H), 7.78-7.1 (m, 7 H), 7.00 (d, 2 H, J = 7.4 Hz), 6.94 (d, 1 H, J = 10.5 Hz), 6.34 (d, 1 H, J = 10.5 Hz), 5.40 (bs, 1 H), 4.80 (bs, 2 H).

8-Allyloxy-1-oxo-1,4-dihydronaphthalene-4-spiro-2'-naphto[1'',8''-de][1',3']dioxin (34). According to the general procedure, palmarumycin CP$_1$ (2.1 mg, 0.007 mmol), diphenylphosphino-polystyrene (23.5 mg, 1.41 mmol/g, 0.033 mmol), allyl alcohol (2.3 μL, 0.034 mmol) and DEAD (5.2 μL, 0.033 mmol) in dry CH_2Cl_2 (0.2 mL) provided after 3 d 0.6 mg (33%) of palmarumycin CP$_1$ and 1.8 mg (71%) of **34** as a colorless oil: ^{1}H NMR δ 7.69 (t, 1 H, J = 8.1 Hz), 7.62-7.56 (m, 2 H), 7.49 (d, 1 H, J = 7.5 Hz), 7.46 (d, 1 H, J = 8.3 Hz), 7.17 (d, 1 H, J = 8.3 Hz), 6.98 (d, 2 H, J = 7.0 Hz), 6.86 (d, 1 H, J = 10.5 Hz), 6.29 (d, 1 H, J = 10.7 Hz), 6.20-6.06 (m, 1 H), 5.68 (dd, 1 H, J = 17.2, 1.5 Hz), 5.38 (dd, 1 H, J = 10.8, 1.5 Hz), 4.77-4.74 (m, 2 H); HRMS(EI) Calcd for $C_{23}H_{16}O_4$ 356.1049, found 356.1064.

References and Notes

1. (a) Weber, H. A.; Baenziger, N. C.; Gloer, J. B. *J. Am. Chem. Soc.* **1990**, *112*, 6718. (b) Preussomerins A-F: Weber, H. A.; Gloer, J. B. *J. Org. Chem.* **1991**, *56*, 4355.

2. Polish J. D.; Dombrowski, A. W.; Tsou, N. N.; Salituro, G. M.; Curotto, J. E. *Mycologia* **1993**, *85*, 62.

3. Connolly, J. D. *4th International Symposium and Pakistan-US. Binational Workshop on Natural Products Chemistry*, Karachi, Pakistan, January **1990**. (b) Connolly, J. D.: *Structural elucidation of some natural products. In Studies in Natural Products Chemistry*, Vol 9. *Ed.*, Atta-ur-Rahman, pp. 256-258, Elsevier Science Publishers B. V., Amsterdam, **1991**.

4. Krohn, K.; Michel, A.; Florke, U.; Aust, H.-J.; Draeger, S.; Schulz, B. *Liebigs Ann. Chem.* **1994**, 1099.

5. Talapatra, S. L.; Karmacharya, B.; Shambhu, C. D.; Talapatra, B. *Phytochemistry* **1988**, *27*, 3929.

6. Singh, S. B.; Zink, D. L.; Liesch, J. M.; Ball, R. G.; Goetz, M. A.; Bolessa, E. A.; Giacobbe, R. A.; Silverman, K. C.; Bills, G. F.; Pelaez, F.; Cascales, C.; Gibbs, J. B.; Lingham, R. B. *J. Org. Chem.* **1994**, *59*, 6296.

7. Krohn, K.; Michel, A.; Flörke, U.; Aust, H.-J.; Draeger, S.; Schulz, B. *Liebigs Ann. Chem.* **1994**, 1093.

8. Krohn, K.; Beckmann, K.; Flörke, U.; Aust, H.-J.; Draeger, S.; Schulz, B.; Busemann, S.; Bringmann, G. *Tetrahedron* **1997**, *53*, 3101.

9. See also: Bode, H. B.; Wegner, B.; Zeeck, A. *J. Antibiot.* **2000**, *53*, 153.

10. (a) Herbert, R. B. *The Biosynthesis of Secondary Metabolites*, 2nd ed., Chapman and Hall, London, **1989**. (b) O'Hagen, D. *The Polyketide Metabolites*, Ellis Horwood, New York, **1991**.

11. Krohn, K.; Beckmann, K.; Aust, H.-J.; Draeger, S.; Schulz, B.; Busemann, S.; Bringmann, G. *Liebigs Ann./Recueil* **1997**, 2531.

12. Ragot, J. P.; Alcaraz, M.-L.; Taylor, R. J. K. *Tetrahedron Lett.* **1998**, *39*, 4921.

13. (a) Schlingmann, G.; West, R. R.; Milne, L.; Pearce, C. J.; Carter, G. T. *Tetrahedron Lett.* **1993**, *34*, 7225. (b) Schlingmann, G.; Matile, S.; Berova, N.; Nakanishi, K.; Carter, G. T. *Tetrahedron* **1996**, *52*, 435.

14. Sakemi, S.; Inagaki, T.; Kaneda, K.; Hirai, H.; Iwata, E.; Sakakibara, T.; Yamauchi, Y.; Norcia, M.; Wondrack, L. M. *J. Antibiot.* **1995**, *48*, 134.

15. McDonald, L. A.; Abbanat, D. R.; Barbieri, L. R.; Bernan, V. S.; Discafani, C. M.; Greenstein, M.; Janota, K.; Korshalla, J. D.; Lassota, P.; Tischler, M.; Carter, G. T. *Tetrahedron Lett.* **1999**, *40*, 2489.

16. For related compounds, see also: (a) Thiergardt, R.; Rihs, G.; Hug, P.; Peter, H. H. *Tetrahedron* **1995**, *51*, 733. (b) Chu, M.; Patel, M.; Pai, J.-K.; Das, P. R.; Puar, M. S. *Bioorg. Med. Chem. Lett.* **1996**, *6*, 579. (c) Chu, M.; Truumees, I.; Patel, M.; Das, P. R.; Puar, M. S. *J. Antibiot.* **1995**, *48*, 329. (d) Chu, M.; Truumees, I.; Patel, M. G.; Gullo, V. P.; Pai, J.-K.; Das, P. R.; Puar, M. S. *Bioorg. Med. Chem. Lett.* **1994**, *4*, 1539. (e) Chu, M.; Truumees, I.; Patel, M. G.; Gullo, V. P.; Puar, M. S.; McPhail, A. T. *J. Org. Chem.* **1994**, *59*, 1222. (f) Soman, A. G.; Gloer, J. B.; Koster, B.; Malloch, D. *J. Nat. Prod.* **1999**, *62*, 659.

17. Wipf, P.; Jung, J.-K. *J. Org. Chem.* **1998**, *63*, 3530.

18. Ragot, J. P.; Steeneck, C.; Alcaraz, M.-L.; Taylor, R. J. K. *Perkin Trans. 1* **1999**, 1073, and ref. 12.

19. Barrett, A. G. M.; Hamprecht, D.; Meyer, T. *Chem. Commun.* **1998**, 809.

20. (a) Wipf, P.; Jung, J.-K. *Angew. Chem. Int. Ed. Engl.* **1997**, *36*, 764. (b) Wipf, P.; Jung, J.-K. *J. Org. Chem.* **1999**, *64*, 1092.

21. Chi, S.; Heathcock, C. H. *Org. Lett.* **1999**, *1*, 3.

22. Wipf, P.; Jung, J.-K. *manuscript in preparation.*

23. A modified experimental variant of the method of Graybill, B. M.; Shirley, D. A. *J. Org. Chem.* **1966**, *31*, 1221, was used. See ref. 22.

24. Newhall, W. F.; Harris, S. A.; Holly, F. W.; Johnston, E. L.; Richter, J. W.; Walton, E.; Wilson, A. N.; Folkers, K. *J. Am. Chem. Soc.* **1955**, *77*, 5646.

25. Foster, B. A.; Coffey, H. A.; Morin, M. J.; Rastinejad, F. *Science* **1999**, *286*, 2507.

26. Osborne, C. K. *Breast Canc. Res. Treatm.* **1998**, *51*, 227.

27. Vogt, A.; Rice, R. R.; Settineri, C. E.; Yokokawa, F.; Yokokawa, S.; Wipf, P.; Lazo, J. S. *J. Pharmcol. Exp. Ther.* **1998**, *287*, 806.

stimulation of HUVEC cells in vitro (IC_{50} values less than 0.04 μM). We evaluated the effects of PD166285 in vivo to determine if the compound would have antitumor activity or simply be extremely toxic due to its relatively non-specific inhibition of several tyrosine kinases. In vivo, PO administration of PD166285 on days 1–9 post-tumor implant produced good antitumor activity against mammary adenocarcinoma 16/C and M5076 (murine reticulum cell sarcoma) tumor models. Tumor growth delays in these sensitive models with treatment on days 1–9 ranged from 7.3 to 17.7 days. PD166285 was also active against advanced stage 16/C where it produced tumor growth delays of 13.6 and 10.4 days at 20 and 10 mg/kg/dose, respectively. There were 6/6 partial tumor regressions at both dose levels. Gross toxicity at less than maximum tolerated dose levels was limited to a 12% body weight loss. These data demonstrate that a broadly active tyrosine kinase inhibitor can produce good in vivo antitumor activity at tolerated doses suggesting that compounds of the "broadly active" class may have therapeutic potential.

#4780   Phase I and pharmacologic study with the novel farnesyltransferase inhibitor (FTI) R115777. Schellens, J.H.M., de Klerk, G., Swart, M., Palmer, P.A.*, Bol, C.J.*, van 't Veer, L.J., Tan, H*, ten Bokkel Huinink, W.W., Beijnen, J.H. The Netherlands Cancer Institute, *AMC, Amsterdam, *Janssen Research Foundation.

The FTI R115777 represents a new class of anticancer agent that may alter Ras signal transduction in tumor. The objectives were to determine the MTD and dose-limiting toxicity (DLT) of chronic twice daily dosing (bid) of R115777 in patients (pts) with incurable solid tumors. One pt was recruited per dose-level, and up to 6 pts in case of DLT. Doses have been escalated from 50 to 500 mg bid in 7 steps. 11 pts were entered: 8 males and 3 females with median age of 57 yrs (range 38-78). Tumor types were colorectal (7), pancreas (2), NSCLC (1) and ovarian (1) cancer. 9 pts received prior chemotherapy. Main toxicity observed was skin hypersensitivity CTC grade 3 (1 pt at 150 mg), leuko- and lymphocytopenia grade 2 (1 pt at 300 mg) and febrile neutropenia and thrombocytopenia grade 4 (= DLT in 1 pt at 500 mg). 4 pts are still on study, 1 pt for 21+ weeks. Hints of activity were seen in metastatic pancreatic cancer (SD after 21+ wks) and colorectal cancer (50% reduction of CEA in 2 patients). After oral intake R115777 peak plasma concentrations were reached after 2-4 h. Little accumulation occurred and steady-state levels were maintained throughout the dosing period that correspond to an in vitro pharmacologically active range. Although interpatient variability was significant, dose-linear PK is indicated. Currently, Ras mutations are determined in pt's tumor material by ASO-PCR. Recruitment continues at 500 mg bid to determine DLT and MTD.

#4781   Biological effects of cRaf1 kinase inhibitors. Wood, E.R., Crosby, R.M., Davenport, E.A., Gilmer, T.M., Hunter, B.N., Keith, B.R., Lee, A.V., McDonald, O.B., Mullin, R.J., Rusnak, D.W., and Lackey, K.E. Glaxo Wellcome, Inc., Research Triangle Park, NC 27709-3398

The protein kinase cRaf1 is implicated in the formation and progression of a variety of human cancers. Inhibition of cRaf1 activity may result in the direct regression of human tumors or may synergize with existing cytotoxic drugs. We used a series of potent, selective kinase inhibitors to determine the biological consequences of cRaf1 inhibition. We analyzed a variety of cRaf1-driven cellular processes including cell proliferation, anchorage-independent growth and cell survival in reduced serum. Inhibitors of cRaf1 affect all aspects of tumor cell proliferation, but the potency of the inhibitors depends upon the phenotype that is measured. Presumably, this reflects the relative contribution of cRaf1 activity to the measured phenotype. As expected, inhibition of cRaf1 results in down regulation of mitogen-activated protein kinase (MAPK) activity. Cell cycle analysis revealed that cRaf1 inhibitors block the cell cycle in the G2 phase. Continued exposure to the inhibitors resulted in the induction of apoptosis. We analyzed the effects of cRaf1 inhibitors on tumor growth in vivo using a ras-transformed rat fibroblast cell line growing as a subcutaneous xenograft in nude mice. cRaf1 inhibitors reduced the rate of tumor growth in this model.

#4782   Dual G1 and G2/M phase inhibition by SC-$\alpha\alpha\delta$9, a Cdc25 phosphatase inhibitor identified in a novel combinatorial library. Tamura, K., Rice, R.L., Wipf, P. and Lazo, J.S. Departments of Pharmacology (K.T, R.L.R., J.S.L.) and Chemistry (P.W.). University of Pittsburgh, Pittsburgh, PA 15261.

The Cdc25 family of dual specificity phosphatase has a central role in controlling cell cycle progression and has been implicated in the etiology of cancer. We previously reported the generation of a novel combinatorial library of small molecules designed as phosphatase inhibitors. One member of the targeted array library, SC-$\alpha\alpha\delta$9, was identified as the most potent synthetic inhibitor of Cdc25 phosphatases. In the present study, we show that SC-$\alpha\alpha\delta$9 inhibited cell cycle progression at both G1 and G2/M in tsFT210 cells, which express a temperature-sensitive Cdc2 mutant. Furthermore, SC-$\alpha\alpha\delta$9 increased the phosphorylation level of Cdc2 in tsFT210 cells in a concentration-dependent manner, suggesting that SC-$\alpha\alpha\delta$9 affected Cdc25 activity in vivo. Closely related chemical analogs that lacked Cdc25 inhibitory activity failed to block cell cycle progression and did not affect Cdc2 phosphorylation. Thus, SC-$\alpha\alpha\delta$9 could be a useful pharmacological tool to clarify the role of Cdc25 phosphatase dependent pathways. In addition, the SC-$\alpha\alpha\delta$9 pharmacophore could also serve as a platform in the further development of novel anticancer agents.

#4783   The novel cyclin dependent kinase inhibitors, GW5181 and GW9499 regulate cell cycle progression and induce tumor-selective cell death. Walker, D.H., Luzzio, M., Veal, J., Dold, K., Edelstein, M., Parker, P., Rusnak, D., Emerson, D., Miller, C., Onori, J., Bramson, H.N., Harris, P., Hunter, R., Dickerson, S., and Kuyper, L. Depts of Cancer Biology. Chemistry and Molecular Biochemistry, Glaxo Wellcome Inc., RTP, NC 27709.

We have characterized the cell-based and in vivo activities of two novel cyclin dependent kinase inhibitors GW5181 and GW9499 in both normal diploid fibroblasts and several tumor cell lines. Both compounds induce a cell cycle arrest in normal cells, inhibiting DNA synthesis resulting in the accumulation of cells in both the G1 and G2 phases of the cell cycle. This cell cycle arrest is consistent with the ability of these compounds to inhibit CDK activities. These compounds show a selective killing effect on several tumor cell lines. with IC_{50} values for cell kill greater than 5-fold lower in some tumor cells as compared to normal cells. We have further characterized the growth curves of both normal diploid fibroblasts and RKO colon carcinoma cells and demonstrate that it is possible to kill RKO cells in vitro under the same conditions that simply slow the proliferation of HDF cells, indicating a potential therapeutic window for cytotoxicity. Consistent with this effect, these compounds inhibit the growth of RKO colon carcinoma cells grown as xenografts in nude mice. These results support the possibility that inhibitors of cyclin dependent kinases may be potential antitumor agents.

#4784   Biochemical characterization of the drug-protein interaction between radicicol and members of the Hsp90 family of proteins. Schulte, T.W., Akinaga, S., Agatsuma, T., Murakata, T., Sugimoto, S., Nakano, H., Simen, B., Argon, Y., Toft, D., Neckers, L., Sharma, S. National Cancer Institute, Bethesda, MD, Kyowa Hakko Kogyo Co., Ltd., Japan, Mayo Graduate School, Rochester, MN, University of Tennessee, Memphis, TN, University of Chicago, Chicago, IL.

The Hsp90 family of proteins consists of Hsp90α and β, Grp94 and Trap-1 (Hsp75). Since a number of oncogenic proteins such as p185^{erbB2}, v-src, Raf-1 and mutant p53 depend on Hsp90 family members for stability and function, Hsp90 inhibitors are being studied as potential anti-cancer agents. Using two different approaches to immobilize radicicol, we have studied binding of the drug to N-terminal Hsp90 point mutants expressed by in vitro translation. The results point to important drug contacts with amino acids inside the N-terminal ATP/ADP binding pocket region and show slight differences when compared to geldanamycin binding. Radicicol binds more strongly to Hsp90 than to Grp94. Binding of radicicol to Grp94 requires both the N-terminal ATP/ADP binding domain as well as the adjacent negatively charged region. Radicicol also specifically binds to Trap-1, which has more homology to the bacterial HtpG than to Hsp90 and Grp94 and binds to TNFR1 and Rb. The use of immobilized radicicol and mutants of Hsp90 family proteins allows for a more detailed analysis of drug protein interactions between Hsp90 inhibitors and their targets.

#4785   Novobiocin and other coumarin antibiotics bind to Hsp90 and cause the degradation of Hsp90-dependent signaling proteins. Marcu, M.G., Schulte, T.W., and Neckers, L.M. Medicine Branch, NCI, Rockville, MD 20850.

Hsp90 interacts with and stabilizes several tyrosine and serine/threonine kinases, including p185^{erbB2} (Her2/neu), v-src, and src family kinases, and raf-1. Additionally, association with Hsp90 is required for the stability and dominant negative function of mutated p53. Two unrelated natural products, geldanamycin (GA) and radicicol (RD), bind specifically to Hsp90, disrupting its association with, and destabilizing, the client proteins described above. GA and RD display promising anti-tumor activity in animal models, and a GA derivative is about to enter human clinical trial. GA and RD bind to an atypical nucleotide binding pocket in the amino terminus of Hsp90 which shares significant homology with the ATP binding domain of bacterial DNA gyrase B. Since the nucleotide binding site of gyrase B is the target of the coumarin antibiotics, we investigated whether these drugs could also interact with Hsp90 and affect its chaperone activity. Novobiocin (NB)-Sepharose affinity purifies Hsp90 from a cell lysate and binding of solid phase novobiocin to Hsp90 is competed by excess soluble drug, as well as by chlorobiocin, coumermycin A, and ATP. NB competes with GA for binding to Hsp90 and binds to an amino terminal Hsp90 fragment containing the nucleotide binding domain. Thus, the coumarin antibiotics bind to Hsp90 at a site overlapping the GA/ATP binding site. NB, at clinically achievable levels, depleted the Hsp90-dependent proteins p185^{erbB2}, raf-1, v-src, and mutated p53. NB may be a clinically well-tolerated alternative to achieve depletion of Hsp90-associating oncogenic kinases and other signaling proteins on which cancer cells depend for proliferation and survival.

MOLECULAR BIOLOGY 32: Interactive Pathways among Cancer-associated Genes

#4786   The von Hippel-Lindau (VHL) gene is involved in cross-talk between cell-ECM and cell-cell signaling. Davidowitz, E.J., Schoenfeld, A.S. and Burk, R.D. Albert Einstein College of Medicine. Bronx, NY 10461.

contribute to CDK inhibition in LNCaP. Induction of p21 by low doses of flavopiridol protects LNCaP cells from cytotoxicity of microtubule-active drugs. Flavopiridol diminished Bcl-2 phosphorylation, a marker of the mitotic arrest, by either preventing mitotic arrest or by enhancing mitotic slippage. No cytoprotection was observed in PC3M. Therefore, a simple comparison of LNCaP and PC3M cells may provide an initial view on an experimental therapeutic in the prostate cancer model.

#367   A DEREGULATION IN PROTEIN KINASE C WAS ASSOCIATED WITH CISPLATIN RESISTANCE. S. Mohanty, and Alakananda Basu, *Institute for Cancer Res, Fort Worth, TX, and Univ of North Texas Health Sci Ctr, Fort Worth, TX*

Acquisition of resistance by tumor tissue to cisplatin is the major problem in cancer chemotherapy. We have shown previously that cellular sensitivity to cisplatin is influenced by the protein kinase C (PKC) signal transduction pathway. In this study, we have investigated how PKC signal transduction pathway is affected when cells acquire resistance to cisplatin. The levels of PKCα, -δ, -ϵ, -μ, -ι and -ζ were almost equivalent in parental and cisplatin-resistant HeLa cells (HeLa/CP). Prolonged cellular exposure to PKC activators, such as phorbol-12, 13-dibutyrate (PDBu), caused down-regulation of PKCα, -δ and -ϵ in HeLa cells. A similar treatment with PDBu, however, failed to induce down-regulation of PKCδ in HeLa/CP cells. Bryostatin 1, a non-tumor promoter and a partial agonist of PKC, induced a biphasic down-regulation of PKCδ in both cisplatin-sensitive and -resistant HeLa cells. Bryostatin 1 also elicited a similar biphasic concentration response on cisplatin -induced cell death. PKC activators caused a 2- to 3-fold increase in sensitivity of HeLa/CP cells to cisplatin. These results suggest that a defect in PKCδ regulation may be associated with cellular resistance to cisplatin and that PKC signal transduction pathway may be intervened to reverse cisplatin resistance. (Supported by a grant CA71727 from NCI.)

#368   INSULIN/IGF-I RECEPTOR-MEDIATED SIGNAL TRANSDUCTION PATHWAY REGULATES G₁ PHASE-DEPENDENT BCL-2 EXPRESSION AND TUMOR CHEMORESISTANCE. Q. P Dou, G Gao, and X Zhang, *H Lee Moffitt Cancer Ctr & Res Inst, Tampa, FL, and Univ of South Florida, Tampa, FL*

We tested the hypothesis that some apoptosis regulators are periodically expressed in human tumor cells, which confers the cell cycle-dependent chemoresistance. Indeed, we found that levels of the cell death inhibitor Bcl-2 mRNA and protein were very high in the mid to late G_1 phase, but dramatically decreased in S, G_2 and M phase of the cell cycle in all the tested tumor and transformed cells. In contrast, levels of the apoptosis inducer Bax protein remained relatively unchanged during the cell cycle in most of the cell lines. The Bcl-2 protein level in the mitochondria-containing fraction of G_1 cells was also higher than that in an S phase cell preparation, while an increased level of cytosolic Bcl-2 protein was observed in S phase cells. The mitochondrial Bcl-2 was associated with Bax under non-apoptotic conditions. During anticancer drug-induced apoptosis, the level of mitochondrial Bcl-2 protein was decreased. Furthermore, cells containing a high G_1 population and a high Bcl-2 protein level were much more resistant to chemotherapy-induced apoptosis than the cells containing a high S population and a low Bcl-2 level. Constitutive overexpression of Bcl-2 in Jurkat T cells partially inhibited the G_1 to S transition and completely blocked the S phase-associated chemosensitivity. Finally, addition of insulin or IGF-I into serum-starved cells significantly induced expression of Bcl-2 protein, primarily in nuclear/mitochondrial compartments, which was blocked by a specific antibody to the IGF-I receptor. Addition of an IGF-I analog, which exhibits greater growth promoting activity than IGF-I, induced Bcl-2 expression to a much higher level than IGF-I. Our studies have demonstrated that chemosensitivity and apoptotic commitment of human tumor cells are mediated by their cell cycle-dependent Bcl-2 expression and localization, which are in turn regulated by an insulin/IGF-I receptor-mediated signal transduction pathway(s).

#369   QUINIDINE INHIBITS HISTONE DEACETYLASE 1 (HDAC1) ACTIVITY IN MCF-7 HUMAN BREAST CANCER CELLS. Qun Zhou, M. Moniwa, J.R Davie, and J.S Strobl, *Univ of Manitoba, Winipeg, Canada, and West Virginia Univ, Morgantown, WV*

Evidence from our laboratory that quinidine (Q,90uM) acts as an anti-tumor agent in MCF-7 cells includes G1 cell cycle arrest, hyperacetylation of histone H4 and cell apoptosis. the profile of Q actions in MCF-7 cells indicates it is an HDAC inhibitor. Q affected a variety of G1 cell cycle regulatory proteins. Q decreased cyclin D1 levels 5.7-fold by 12 hr, and CDK4 levels 4.3-fold by 24 hr. Levels of cyclin dependent kinase inhibitors, p21(WAF1) increased 10-fold by 12 hr, and p27 increased 3.1-fold by 48 hr, but p16 levels did not change. Hyperphosphorylated Rb decreased 9-fold by 24 hy,but low levels of hypophosphorylated Rb(pRb) persisted at least 48 hr in Q-treated cells. Q decreased whole cell E2F1 levels 2.5-fold by 24 hr, and increased E2F1 bound to pRb 1.5-fold by 24 hr. HDAC1 protein levels decreased 4-fold by 24 hr in Q-treated cells. The cell-free HDAC1 activity measured in avian erythrocyte nuclear matrix was inhibited 60% by Q. The results show that Q is a HDAC1 inhibitor and is a potential lead compound for development of more potent HDAC1 inhibitors as breast cancer chemotherapeutic agents. Supported by WVU School of Medicine Research Grant. Apply for AACR Young Investigator Awards, the originial abstract and payment are sent by mail.

#370   HSP70 STIMULATES CELL PROLIFERATION AND IS CYTOPROTECTIVE AGAINST HEAT AND VINCRISTINE TOXICITY IN MCF-7 CELLS. Jill A Barnes, David J Dix, Barbara W Collins, and James W Allen, *National Res Council, US Environmental Protection Agency, RTP, NC, and US Environmental Protection Agency, RTP, NC*

Heat-shock proteins (HSPs) play important roles in regulating cell growth and protecting cells from adverse effects of heat and chemical stress. In many types of cancer, elevated HSP70 levels are associated with poor prognosis and resistance to chemotherapeutic agents. In the present study, we used a tetracycline-controlled gene expression system in human MCF-7 breast cancer cells to evaluate the effects of HSP70 overexpression on cell growth and resistance to hyperthermia and vincristine toxicity. HSP70 overexpressing cells exhibited faster doubling times as compared with non-overexpressing (control) cells (39 vs. 53 hrs.). Following hyperthermia treatment (43°C for 30 or 60 min.), control cells underwent dose-dependent decreases in cell number which were not observed in HSP70 overexpressing cells. Ethidium bromide and acridine orange staining of heat-treated cells also revealed significant reductions in cell viability (p<.05) and increases in death (p<.05) and apoptosis in control vs. HSP70 overexpressing cells. A cytokinesis-block micronucleus assay with kinetochore staining was used to measure chromosome damage induced by vincristine. Again, cytoprotection in HSP70 overexpressing cells was evident; lower frequencies of vincristine-induced chromosome loss were observed in overexpressing vs. control cells. Overall, the data in this study provide further evidence linking HSP70 expression with increased cell proliferation and resistance to toxic effects from heat and chemotherapeutic agents. *(This abstract does not necessarily reflect EPA policy.)*

#371   VITAMIN K ANALOGS INHIBIT CDC25B AND DISRUPT CDC25B2 SUBCELLULAR DISTRIBUTION. Katharine Pestell, E C Southwick, C Wilcox, and J S Lazo, *Univ of Pittsburgh, Pittsburgh, PA*

We have synthesized a small library of vitamin K analogs that are inhibitors of human recombinant Cdc25B. A close correlation was seen between the IC_{50} for *in vitro* Cdc25B inhibition and the cytotoxicity measured after a 96h exposure with a tetrazolium-based assay. The most and least potent *in vitro* inhibitors of Cdc25B were Compounds 5 (2-[2-mercaptothanol]-3-methyl-1,4-napthoquinone) and 22, with IC_{50} values of 3.8 and 200 μM, respectively. We have also examined the action of these compounds on Cdc25B subcellular localization, because of critical role the process has in regulating Cdc25 activity. CHO cells stably expressing green fluorescent protein (GFP), GFP-Cdc25 B_2 or GFP-Cdc25B_3 fusion proteins were synchronised at G_1, S or G_2 phase of the cell cycle and incubated with vitamin K analogs for 1 h. Synchronisation was achieved by incubation for 52 hours in isoleucine deficient medium (G_1 phase cells) then 19 hours in 400μM mimosine followed by 6 or 8 hours in standard medium (S and G_2 phase cells respectively). Localisation of GFP and Cdc25 B_3 was diffuse throughout the cell during the whole cell cycle. In contrast Cdc25 B_2 was diffuse throughout the cell in S and G_2 phase cells but there was bright punctate cytoplasmic staining in untreated G_1 phase cells. Treatment of cells with Compound 5, and to a lesser extent with Compound 7, eliminated the punctate cytoplasmic staining in G_1 phase cells, however this was seen in some S and G_2 phase cells. No change was seen in GFP or Cdc25 B_3 localization. Treatment with Compounds 15, 22 or 24 resulted in no difference in Cdc25B_2 subcellular localization. In conclusion, we have identified compounds that affect the spatial localization of Cdc25B_2 and this redistribution in Cdc25B_2 subcellular localization may contribute to the cytotoxicity of these compounds.

#372   THE ABILITY OF CRYPTOPHYCIN-52 TO BLOCK AND KILL H116 CELLS IN G₂M OF THE CELL CYCLE IS MEDIATED THROUGH A DOWN-REGULATION OF CYCLIN B1 PROTEIN. Alexander Nakeff, Joseph E Media, Balanehru Subramanian, and Frederick A Valeriote, *Josephine Ford Cancer Ctr, Henry Ford Health System, Detroit, MI*

Cryptophycin-52 (CP-52) is the synthetic analog of CP-1, discovered in our anti-cancer drug screen of blue-green algae (1), that demonstrated increased therapeutic efficacy and is presently in clinical trials (2). Although its activity is consequent to its strong tubulin binding (3), we have demonstrated that its mechanism of action is broader (4). Applying an algorithm developed in our laboratory using H116 human colon adenocarcinoma cells, we defined the H116 clonogenic CP-52 concentration-time response relationship. Exposing exponentially-growing H116 cells to LD$_{90}$ concentrations of CP-52 for 24 hr resulted in their complete blockage in G$_2$M phase of the cell cycle with a complete disappearance of cyclin B1 demonstrated by dual parameter flow cytometry. Loss of cyclin B1 was not observed when comparable cytotoxic doses of either taxol or CP-15 (an inactive analog)which also resulted in a reversible G$_2$M cell cycle block leading to polyploidization. Wash-out experiments following exposure to CP-52 indicated that the G$_2$M block and the drug-specific inhibition of cyclin B1 could not be reversed, even at C-52 doses as low as 1 pg/ml. The G$_2$M block eventually lead to phase-specific apoptosis as measured by flow cytometric analysis (APO-BUdr kit) that may account for the phase-specific cytotoxicity of CP-52. Our data indicate that CP-52 exhibits multiple sites of action, including blocking and eventually killing of H116 cells in G$_2$M phase of the cell cycle through its action on decreasing target cell cyclin B1 protein levels. *1. Moore et al, Cur. Pharmaceut. Design 2:317, 1996; 2. Wagner et al, Cancer Chem.Pharm.43:115, 1999; 3. Smith & Zhang, J. Biol. Chem 271:6192, 1996; 4. Chen et al, Int. J. Cancer 77:869. 1998.*

performed. Although multiple vaccinations with G207 alone showed a significant growth inhibition of both treated and untreated tumors in bilaterally established tumor model, none of the animals was responded completely. In contrast, multiple vaccinations with dvIL-12/G207 mediated complete response in both treated and untreated tumors in 20% of the animals. By the G207/rIL-12 combination, complete response was shown in 67% of the animals. These results indicate that local or systemic administration of IL-12 significantly enhances the antitumor activity of multiple in situ cancer vaccinations with HSV.

#2994 EXPRESSION OF THE INTERFERON REGULATORY TRANSCRIPTION FACTOR ICSBP INDUCES POTENT IMMUNITY AGAINST LEUKEMIA. Ming Deng, and G Q Daley. Whitehead Institute, Cambridge, MA

The BCR/ABL fusion protein induces human Chronic Myeloid Leukemia (CML). Interferon α (IFN-α) prolongs the chronic phase of the disease and has become a mainstay of CML treatment. However, the precise mechanism by which IFN-α alters the natural history of CML is unclear. IFN-α signaling is mediated by Interferon Regulatory Factors (IRFs), a family of transcription factor proteins implicated in anti-proliferative and immunomodulatory effects. Mice deficient in the IFN Consensus Sequence Binding Protein (ICSBP) develop a CML-like myeloproliferative disease (Holtschke et al., Cell 87:307, 1996). To examine whether ICSBP acts as a tumor suppressor gene, we tested whether ICSBP expression would antagonize the transformation of IL-3 dependent BaF3 cells by BCR/ABL. BaF3 cells expressing BCR/ABL (Ba-P210) proliferate in the absence of IL-3 and induce a rapidly fatal leukemia in syngeneic hosts. Overexpression of ICSBP in Ba-P210 (Ba-P210-ICSBP) had little demonstrable effect on proliferation, factor independence, or resistance to radiation-induced apoptosis in vitro. However, Ba-P210-ICSBP cells failed to induce leukemia in immunocompetent hosts, but remained leukemogenic in immunodeficient hosts. Furthermore, immunocompetent mice exposed to Ba-P210-ICSBP cells survived rechallenge with the parental Ba-P210 cells, suggesting that ICSBP expression in Ba-P210 cells induced potent immunity against Ba-P210 cells. Irradiated Ba-P210 cells failed to generate protective immunity, indicating a critical role for ICSBP expression. Relatively little is know about the function of ICSBP, and we are presently investigating the mechanisms by which ICSBP alters the immune response to BCR/ABL-transformed cells, including utilizing cDNA arrays to identify cytokines and other immunomodulatory molecules whose expression is modified by ICSBP. We are also examining whether ICSBP expression will induce protective immunity against other leukemia cells and solid tumor cell lines to determine whether ICSBP gene transfer might be harnessed for the immunotherapy of malignancy.

#2995 POLYVALENT HUMAN MELANOMA ANTIGEN GENE VACCINE PROPHYLACTIC & THERAPEUTIC EFFICACY AGAINST MELANOMA PROGRESSION. Kahoko Hashimoto, S. Fujii, M. Tanaka, Y. Kaneda, and D. Hoon, John Wayne Cancer Institute, Santa Monica, CA, and Osaka Univ, Osaka, Japan

Malignant melanoma has been shown to be immunogenic and responds to active-specific immunotherapy. The expression of immunogenic tumor-associated antigens (TAA) are very heterogeneous within melanoma lesions and amongst different lesions. A gene based delivery platform for active-specific immunotherapy was developed in the form of a polyvalent gene vaccine (PGV) for therapeutic and prophylactic control of melanoma progression. In a pre-clinical murine model two highly expressed immunogenic melanoma TAA (GP100 & TRP2) genes were expressed in a plasmid vector and assessed for their efficacy as a PGV. The HVJ (hemagglutinating virus Japan) fusion anionic liposome was used as an in vivo delivery system of TAA gene containing plasmids. This in vivo delivery system provides consistent transfection and efficient expression (2-3 wks) in target cells. Various sites of delivery of TAA genes were investigated. Both intramuscular and intranasal site injections (2 to 3X challenges) could induce high titers of IgG antibodies and delayed-type hypersensitivity to recombinant human GP100 and TRP-2 in mice rapidly, and consistently. A B16 mouse melanoma model was used to assess the efficacy of the PGV. In experiments with mice bearing B16 melanoma tumors treated 3X with PGV showed significant inhibition of tumor growth progression and prolonged survival compared to non-treated control mice. In experiments where mice were immunized with PGV 3X followed by B16 tumor challenge had significant enhanced disease-free and overall survival compared to mice challenged with HVJ-liposome plasmid control or non-treatment. These pre-clinical studies demonstrate the therapeutic and prophylactic efficacy of PGV using GP100 and TRP-2 to control malignant melanoma progression. The effector mechanism was shown to involve both T helper 1 and 2 antigen-specific responses.

#2996 ERADICATION OF PRIMARY TUMORS AND INDUCTION OF SYSTEMIC IMMUNITY BY AN INTRALESIONAL INJECTION OF BACULOVIRUS SYSTEM-MEDIATED INTERFERON-BETA GENE THERAPY. Weixin Lu, Z Dong, and I J Fidler. U T M D Anderson Cancer Ctr, Houston, TX

Baculovirus vector systems can efficiently express high levels of biologically active proteins in insect cells. Since insect cells are heterologous to mammalian hosts and interferon-beta (IFN-β) is a potent immune modulator, we hypothesize that delivering IFN-β into tumor lesions using this vector system will induce a potent antitumor immune response resulting in eradication of the tumors. We tested this hypothesis in a syngeneic C3H/HeN mouse UV-2237 fibrosarcoma model. High5 (H5) insect cells infected with the recombinant baculovirus-encoding mouse IFN-β gene (Bac-IFN-β) produced 2×10^4 units IFN-β activity/10^6 cells/48 h. A single injection of 2×10^6 Bac-IFN-β-infected H5 cells into subcutaneous UV-2237 fibrosarcoma tumors (5–6 mm in diameter) completely eradicated the tumors, prevented the development of spontaneous lung metastasis, and conferred tumor-specific immunity against subsequent challenge by UV-2237 cells. The therapy was less effective in nude mice. Immunohistochemical analysis revealed that tumors injected with H5-IFN-β contained more macrophages and CD4$^+$ and CD8$^+$ cells than control tumors injected with control H5 cells or with saline. These data demonstrate that intralesional injection of H5-IFN-β into UV-2237 fibrosarcoma can eradicate primary tumors and induce systemic immunity.

#2997 DNA VACCINE FOR COLORECTAL CANCER. Lindy G Durrant, Ian Spendlove, and Vanessa Potter. Univ of Nottingham, Nottingham, United Kingdom

DNA vaccination has been shown to induce sustained production of CTL, helper T cell and antibody responses. It is therefore an attractive approach for the treatment of colorectal cancer. CD55 is a complement regulatory protein overexpressed by the majority of solid tumors. The CDRH2, CDRH3 and CDRL1 regions of a human anti-idiotypic antibody 105AD7 have recently been shown to mimic a discontinuous epitope on CD55 domains 1 and 2. The antibody can therefore stimulate both antibody and T cell responses that recognize tumor cells expressing CD55. A recently completed neoadjuvant trial recruited 75 patients and demonstrated infiltration of helper T cells and NK cells associated with enhanced tumor cell apoptosis in immunized as compared to unimmunized patients. However no significant infiltration of CTLs were seen. To determine if this was the result of poor presentation of the CTL epitopes by the 105AD7 protein it was reconfigured as a DNA vaccine. The variable regions of 105AD7 were joined by flexible linkers of varying length to form either scFvs or diabodies. The CDRH3 was also configured as a minigene. In contrast to 105AD7 protein, all three DNA constructs stimulated CTL responses with the diabody giving the strongest responses. Both the scFv and the diabody DNA constructs also stimulated anti-CD55 IgG2a antibody responses and secretion of γIFN indicative of a Th1 response. The diabody was again superior. These results suggest that anti-idiotypic immunization may be even more effective using dimeric DNA vaccines.

PHARMACOLOGY AND EXPERIMENTAL THERAPEUTICS 36: The Cycle of Drug Discovery

#2998 IDENTIFICATION OF CDC25 DUAL SPECIFICITY PHOSPHATASE INHIBITORS IN A TARGETED SMALL MOLECULE ARRAY. Alexander P Ducruet, R L Rice, K Tamura, F Yokokawa, S Yokokawa, P Wipf, and J S Lazo. Univ of Pittsburgh, Pittsburgh, PA

The Cdc25B dual specificity protein phosphatases (DSPases) are key cell cycle regulators, yet few potent or specific inhibitors have been identified. Using a combinatorial/ parallel synthetic approach, we rigidified the variable core region and modified the side chains of SC-$\alpha\alpha\delta$59, a previously described anti-phosphatase pharmacophore. Structure activity relationship studies with the new targeted array revealed that in vitro anti-phosphatase activity was dependent on both the variable core region and the side chain substituents. Several analogs with conformationally constrained core regions were effective inhibitors of the DSPases VHR and Cdc25B$_2$ and the protein tyrosine phosphatase (PTPase) PTP1B. Two compounds, FY3-$\alpha\alpha$09 and FY21-$\alpha\alpha$09, were partial competitive inhibitors of Cdc25B$_2$ with K, values of 7.6 $\pm$ 0.5 μM and 1.6 $\pm$ 0.2 μM, respectively, while showing only moderate activity against PTP1B. FY21-$\alpha\alpha$09 inhibited growth of MDA-MB-231 and MCF-7 human breast cancer cell lines and blocked the G$_2$/M transition in synchronized tsFT210 cells, consistent with Cdc25B inhibition. The structure of FY21-$\alpha\alpha$09 provides an improved pharmacophore platform from which additional potent and more selective Cdc25 phosphatase inhibitors might be generated.

#2999 HIGHLY POTENT PEPTIDE ANTAGONISTS OF THE P53-HDM2 PROTEIN-PROTEIN INTERACTION. Carlos Garcia-Echeverria, P Chene, M J J Blommers, and P Furet, Novartis Pharma Inc., CH-4002 Basel, Switzerland

The disruption of the p53-hdm2 interaction is an attractive approach for cancer therapy because it opens the possibility to regulate the threshold of the wild-type p53 response with therapeutic agents. As part of our efforts to discover compounds able to block the binding of hdm2 to p53, we have attempted to establish a pharmacophore model for this protein-protein interaction. Together with the determination of the amino acid specificities of hdm2's binding pockets, this work has resulted in the identification of highly potent peptide antagonists. Combining molecular modeling selected conformational constrains and functional groups able to establish additional electrostatic and van der Waals interactions with the hdm2 protein, we have been able to dramatically boost the hdm2 binding affinity of Ac-Phe-Met-Asp-Tyr-Trp-Glu-Gly-Leu-NH$_2$, which has been reported by us and others as the minimal sequence retaining micromolar affinity for this protein (IC_{50} = 8.9 $\pm$ 0.6 μM). The new peptide Ac-Phe-Met-Aib-Pmp-6-Cl-Trp-Glu-